Development of a polyzwitterionic hydrogel coating for RO membranes by concentration polarization-enhanced in situ click reaction which can be applied in modules

Dissertation

Zur Erlangung des akademischen Grades eines Doktors der Naturwissenschaften

Doctor rerum naturalium

– Dr. rer. nat. –

Vorgelegt von

Soraya Laghmari El Moussati

geboren auf Teneriffa

Fakultät für Chemie

Universität Duisburg-Essen

2020

DOI: 10.17185/duepublico/73233
URN: urn:nbn:de:hbz:464-20211108-150041-8

Disputation: 27.10.2020

Referents: Prof. Dr. Mathias Ulbricht

Prof. Dr. -Ing. Stefan Panglisch

Chairman: Prof. Dr. Stefan Rumann

This work presented here was performed from December 2016 until July 2020 at Lehrstuhl für Technische Chemie II of Prof. Dr. M. Ulbricht in the faculty of chemistry at the University of Duisburg-Essen.

I declare that this dissertation represents my own work, except where it is stated by references. I only used the materials and references named and this work was not submitted to any other university before.

Essen, July 2020

Soraya Laghmari El Moussati

Widmung

Für meine Eltern

Danksagung

An dieser Stelle möchte ich mich bei einer Reihe von Menschen bedanken, die zum Erfolg dieser Doktorarbeit beigetragen haben.

Zunächst gilt mein Dank besonders meinem Doktorvater Prof. Dr. Mathias Ulbricht für die Bereitstellung dieser interdisziplinären und industrienahen Aufgabenstellung. Die fachlichen Anregungen, die stete Diskussionsbereitschaft und das entgegengebrachte Vertrauen waren sehr wertvoll für das Gelingen dieser Arbeit.

Herrn Prof. Dr. Stefan Panglisch danke ich für die freundliche Übernahme des Koreferats und außerdem für die Bereitstellung der Öl-Emulsionen, mit denen essentielle Versuche durchgeführt wurden. Mein Dank gilt ebenfalls Prof. Dr. Stefan Rumann für die Übernahme des Prüfungsvorsitzes.

Dem Projektträger Karlsruhe und dem Bundesministerium für Bildung und Forschung danke ich für die Finanzierung dieses Projekts, da diese Arbeit ein Teil des WEISS Forschungsprojekts ist. In diesem Zuge bedanke ich mich bei Frau Dr. Angela Ante, Herrn Hubrich, Herrn Dr. Fitzke, Herrn Prof. Geißen und Herrn Robin für die spannende und interessante Zusammenarbeit während der gemeinsamen Projekttreffen. Ein großer Dank gilt auch Franziska Blauth vom IUTA e.V. für die kompetente Unterstützung bei der Modulmodifizierung.

Ebenfalls bedanke ich mich bei Herrn Bochmann, Herrn Dr. Hagemann, Herrn Meya und Frau Römer für die Durchführung zahlreicher Analysen. Weiterhin danke ich allen Kollegen und Mitarbeitern des Lehrstuhls für Technische Chemie II. Besonders hervorzuheben sind Tobias Kallweit, Inge Danielzik, Roswitha Nordmann, Claudia Schenk und Dr. Jackelyn Aragon-Gomez für deren technische und administrative Unterstützung.

Vor allem danke ich meinen Masterstudenten und wissenschaftlichen Hilfskräften Nikolai Adler, Nadine Al-Akkad, Seden Caglar, Didem Denizer, Tharsiha Kandasamy, Celina Kersting, Rabia Mutlu und Ingo Schwarzrock, deren tatkräftige Unterstützung im Labor einen wertvollen Beitrag zu dieser Arbeit geleistet haben.

Für die fachlichen Diskussionen und die gute Arbeitsatmosphäre möchte ich ebenfalls Philipp Jahn, Dr. Patrick May und Dr. Janina Gaalken namentlich hervorheben. Besonders möchte ich

Sanae Gassa für die gemeinsamen Mittagessen, das immer offene Ohr und die gesamte schöne Arbeitszeit danken.

Der größte Dank geht an Mama und Papa. Ihr standet mir nicht nur während der Promotion, sondern auch in allen anderen Lebenslagen unermüdlich zur Seite. Ihr habt mich unterstützt, mich ermutigt und an mich geglaubt. Außerdem habt ihr mich gelehrt, wie man auch herausfordernde Situationen meistert. Eure bedingungslose Liebe hat mir Selbstvertrauen gegeben und mich zu dem Menschen gemacht, der ich bin. Auch meinen Geschwistern Uafa, Kamal und Najim Laghmari El Moussati danke ich ganz besonders für die gemeinsamen tollen Momente, eure wertvollen Ratschläge und, dass ich immer auf euch zählen kann.

Abstract

Although vast research efforts have been contributed to control fouling, it remains a problem in membrane filtration processes. While the most reports on surface modifications are focusing on flat-sheet membranes conducted in laboratory scales, only a few focalize the scale-up of the modification to membrane modules in industrial scale due to their complex configuration and the associated limited accessibility. A promising method overcoming this challenge, is the concentration polarization-enhanced in situ coating of membranes during filtration where the barrier properties of the membrane and the arising concentration polarization is exploited allowing the selective modification of membranes.

The main focus of this work was therefore to develop a polyzwitterionic anti-fouling hydrogel coating for RO TFC membranes by CP-enhanced in situ thiol-based click reaction. The gradual transfer of this modification method from dead-end to modules in cross-flow was to be demonstrated. This was done with the aim of integrating modified RO modules into a cooling circuit of the steel industry to purify and allow the reuse of cooling water, as in Germany approx. 77 % of water is used for product cooling. Therefore, a critical evaluation of the separation performance of established membranes was done first by analyzing fouling with real cooling water. The cross-linking of the zwitterionic copolymer with the cross-linker 1,4-Dithiothreitol (DTT) via thiol-ene Michael addition click reaction was then studied in the bulk via in situ rheology. In a further step, the in situ cross-linking reaction was examined during dead-end filtration. The modification was then transferred to flat-sheet membranes in cross-flow. In the last step, an up-scaling to spiral-wound RO modules was accomplished and were then implemented in a cooling circuit of the steel industry where pilot scale tests were done.

During the fouling tests (dead-end short-term and cross-flow long-term experiments), the membrane BW30 exhibited a very high fouling resistance and showed no irreversible fouling towards real cooling water from the steel industry. This membrane was therefore chosen for the membrane modification tests. By means of rheology, the influence of different parameters (polymer concentration, pH value, acrylate/crosslinker ratio) on the bulk hydrogel formation could be investigated. By this, optimal parameters for the composition of reaction solution for the modification experiments in dead-end could be established. A pH value of 9 and an acrylate/crosslinker ratio of 1:1 turned out to be optimal conditions for the formation of a

hydrogel with elastic properties in a short time. For a gelation time of 10 min, a critical concentration of 12 wt% was determined under these conditions which was to be correlated with the membrane surface concentration during modification. During dead-end modification, influencing factors, such as polymer concentration, flux and stirring rate on gel formation were identified. A basic understanding of hydrogel formation was gained. It was found that the hydrogel formation undergoes two processes. At polymer concentrations up to 0.03 wt%, the reactants are filtered below the critical concentration in a gel-particulate state towards the membrane so that only thin hydrogel layers are formed. From a bulk concentration of 0.04 wt%, the reaction solution is concentrated above the required critical concentration, resulting in the formation of a three-dimensional hydrogel layer.

It was also shown that the filtration conditions, especially the flux, are determining for the initiation of a crosslinking reaction via CP and the formation of the hydrogel on the membrane surface. Under the selected conditions (0.06 wt%, pH 9, acrylate/cross-linker ratio of 1:1), the flux must be > 18 LHM for a crosslinking reaction to take place. If these conditions are fulfilled, the hydrogel formation will occur within the first few minutes. The membrane surface concentration c_m for successful modifications calculated via film model turned out to be significantly lower than the critical concentration c_{crit} of 12 wt% calculated via rheology. This is primary caused by the fact that the gel point as an evaluation criterion is not representative for the reaction taking place at the membrane surface. Hence, rheology cannot be used to predict a priori conditions that lead to a certain coating effect, but it can be used to support the understanding of hydrogel formation. For the antifouling experiments, the cooling water from the steel industry was not a suitable test system due to low level of contaminants so that synthetic oil/water emulsions were used instead. However, it was found that membranes modified at even subcritical conditions (0.02 and 0.03 wt%), possess superior antifouling properties compared to unmodified membranes.

For the modification of membranes in spacer-filled channels, operated in cross-flow, conditions were applied from dead-end experiments which led to thick and homogeneous hydrogel layers. Different from dead-end, the selected conditions led only to thin hydrogel layers at subcritical conditions which is attributable to changed boundary conditions caused by the spacer. However, it could be shown that such membranes have outstanding antifouling properties towards crude oil emulsions compared to unmodified membranes. By enhancing

the flux for the modification, a clearly pronounced hydrogel layer could be formed on the membrane surface. Even though, the formation of the hydrogel layer was not homogeneously formed over the entire membrane area, the overall charge neutrality could be improved significantly. Thus, it could be demonstrated that also under cross-flow conditions, the crosslinking reaction can be controlled and adjusted mainly via flux even though a spacer is used. Finally, the general feasibility of coating SWMs and the application of such modules for the treatment of cooling water of the steel industry could be proven. The antifouling effect of the modified modules was shown for a number of different experiments in the initial phase of the field tests. However, the modification effect of the coated modules could not be demonstrated in the later stages due to severe irreversible iron oxide particle, organic and oil fouling caused by fluctuating cooling water composition, insufficient feed pre-treatment, production conversion and defects at the plant.

Content

List of figures

List of tables

List of equations

List of abbreviations

^{1}H-NMR	^{1}H-nuclear magnetic resonance
AIBN	Azobisisobutyronitrile
ATR-FTIR	Attenuated total reflection - Fourier transform - infrared spectroscopy
ATRP	Atom transfer radical polymerization
BFI	Betriebsforschungsinstitut
CA	Contact angle
CDI	Capacitive deionization
CFV	Cross-flow velocity
Copo	Copolymer
Conv	Conventional
CP	Concentration polarization
CPM	Concentration polarization modulus
CSL	Cationic surface linker
DEW	Deutsche Edelstahlwerke
DG	Modification degree
DLS	Dynamic light scattering
DMAc	Dimethylacetamide
DMAEMA	N,N-(dimethylamino)ethyl methacrylate
DOM	Dissolved organic matter
DTT	1,4-Dithiothreitol
EA	Elemental analysis
EDX	Energy dispersive X-ray
EfOM	Effluent organic matter
EPS	Extracellular polymer substances
EtOH	Ethanol
FRP	Free radical polymerization
FRR	Flux recovery ratio
HEMA	Hydroxyethyl methacrylate
IEP	Isoelectric point
IFAK	Institut für Automation und Kommunikation
IMS	Integrated membrane system
IP	Interfacial polymerization
IUTA	Institut für Energie- und Umwelttechnik e.V.
KOH	Potassium hydroxide
LHM	L/hm^2
LHMbar	L/hm^{2}bar
LTE	Long-term experiment
MAC	Methacryloyl chloride
MBT	Methylene blue test
MED	Multi-distillation
MF	Microfiltration
Mod	Modified
MPD	m-phenylenediamine

MSFD	Multi-flash distillation
MW	Molecular weight
NF	Nanofiltration
NaOH	Sodium hydroxide
NOM	Natural organic matter
OLC	Overlap concentration
PA	Polyamide
PDI	Polydispersity index
PDMAEMA-co-PHEMA	Polydimethylaminoethylmethacrylate-co-polyhydroxyethylmethacrylate
PDMAEMA-co-PMAEMA	Polydimethylaminoethylmethacrylate-co-polymethacryloylethylmethacrylate
PES	Poly(ether sulfone)
PIP	Piperazine
PMMA	Poly(methyl methacrylate)
PPD	p-phenylenediamine
PSBMA-co-PMAEMA	Polysulfobetaineethylmethacrylate-co-polymethacryloylethylmethacrylate
PTMAEMA-co-PMAEMA	Polytrimethylaminoethylmethacrylate-co-polymethacryloylethylmethacrylate
PVA	Poly(vinyl alcohol)
Re	Reynolds
RO	Reverse osmosis
SBMA	Sulfobetaine methacrylate
Sc	Schmidt
SDI	Silt density index
SEC	Size exclusion chromatography
SEM	Scanning electron microscopy
Sh	Sherwood
STE	Short-term experiment
SWM	Spiral wound module
TFC	Thin-film composite
TGA	Thermogravimetric analysis
TMC	Trimesoyl chloride
TMP	Transmembrane pressure
TOC	Total organic carbon
UDE	Universität Duisburg-Essen
UF	Ultrafiltration
VCD	Vapour compression distillation
WP	Water permeance
XPS	X-ray photoelectron spectroscopy
XRD	X-ray diffraction
ZLD	Zero liquid discharge
ZP	Zeta potential

List of symbols

A	Membrane surface area	[m^2]
A´	Cell-specific constant	[-]
C	Molarity	[mol/L]
c_p	Solute concentration in the permeate	[g/L]
c_m	Solute concentration at membrane surface	[g/L]
c_b	Solute concentration in the bulk	[g/L]
d_h	Hydrodynamic diameter of membrane channel	[m]
D_i	Solution diffusion coefficient of component i	[m^2/s]
$\triangle P$	Applied pressure difference	[bar]
$\triangle \pi$	Osmotic pressure difference	[bar]
δ	Boundary layer thickness	[m]
ϵ_{Sp}	Porosity of spacer	[-]
G^*	Complex shear modulus	[Pa]
G´´	Loss modulus	[Pa]
G´	Storage modulus	[Pa]
h_{dry}	Hydrogel layer thickness in dry state	[m]
h_{Sp}	Height of spacer	[m]
h_{wet}	Hydrogel layer thickness in wet state	[m]
i	*Vanthoff* factor	[-]
J_v	Permeate water flux through membrane	[L/hm^2]
K	Mark-Houwink factor	[-]
K_c	Constant for cake filtration mechanism	[-]
k_B	Boltzmann constant	[J/K]
k_i	Mass transfer coefficient of component i	[m/s]
L_i	Water mass transfer coefficient of component i	[m/s]
M	Molar mass	[g/mol]
M_w	Mass weighted molecular mass	[g/mol]
M_n	Number weighted molecular mass	[g/mol]
$(O/N)_{observed}$	Molar ratio of oxygen to nitrogen	[-]
Q_F	Feed flow	[L/h]
Q_P	Permeate flow	[L/h]
Q_c	Concentrate flow	[L/h]
R	Ideal gas constant	kgm^2/s^2mol K]
R_{in}	Intrinsic rejection	[%]
R_{obs}	Observed rejection	[%]
r_h	Hydrodynamic radius	[m]
r_t	Radius of stirred batch cell	[m]
ρ	Density	[kg/m^3]
T	Absolute temperature	[K]
τ	Shear stress	[Pa]
V_h	Hydrodynamic volume	[m^3]
ν	Kinematic viscosity	[m^2/s]
v	Cross-flow velocity	[m/s]
ω	Angular frequency	[s^{-1}]

w_{ch}	Width of membrane channel	[m]
γ	Shear rate	[s^{-1}]
μ or η	Dynamic viscosity	[Pas]
θ	Incidence angle	[°]
ζ	Zeta potential	[mV]

1 Introduction

1.1 Motivation

Water is not only the fundament of life, it is also the basis of all economic activities. The biggest amount of the worldwide water demand can be assigned to the agriculture, followed by industry and the energy sector.[1] However, in industrialized countries, such as Germany over 80 % of the water consumption is due to the industry. Around 77 % of this water is used for process and product cooling.[2]

An example is steel production and processing with a water requirement of 2.3 billion m^3/a for cooling circuits. The water cycles as well as the cooling water matrix are very complex in such circuits due to process contamination i.e. by particles and oil and the addition of conditioning chemicals like corrosion inhibitors and biocides. Furthermore, salting appears to be a big problem because of the recirculation and evaporation in the cooling circuits. In order to maintain the tolerable concentration of salts, 2 – 3 % of the circulation water has to be removed and replaced by fresh water which requires up to 200 m^3/h of blowdown water for a typical steel plant.[3]

This kind of “desalination” does not represent a resource-saving and sustainable manner, particularly with respect to the growing worldwide water stress. According to the water exploitation index which is the relation between the water abstraction to the renewable water resources and thus an indicator for the water stress, around 14 countries of the world are suffering from water stress. This number does not include Germany as the index is below the critical value of 20 %. However, water stress is a regionally limited problem which can vary within the country.[4] Since in Germany the prolonged droughts lately lead to the decrease of groundwater and river level, water scarcity could also become a problem in Germany soon leading to an increasing demand for water. A direct consequence for the steel industry would be the restriction of water uptake for cooling purposes.

The reuse of cooling water would be a starting point to increase the availability of the water resource. Membrane technology, especially reverse osmosis (RO) is considered to be a key technology when it comes to the reuse of water which has to meet strict reuse standards such as industrial cooling water.[5] Hence, integrating RO into the cooling circuits of the steel industry offer the opportunity to purify the cooling water and close the water cycles more efficiently.

But the implementation of RO in such a circuit cannot be realized easily due to the previous mentioned complex composition of cooling water. The application of RO in an Italian cooling circuit of the steel industry was investigated in 2015 by Colla *et al.* showing that RO cannot be applied without feed pre-treatment due to a high potential of membrane fouling.[6]

Membrane fouling is defined as a process where solutes or particles deposit on the membrane surface or into the pores such that membrane performance is deteriorated.[7] Since RO membranes are able to retain all relevant substances including monovalent ions, they are at the same time susceptible to all types of fouling which results in a severe performance decline. This goes along with a reduction of membrane life-time and consequently results in higher technical risks and costs. Other approaches to mitigate the fouling potential besides feed pre-treatment is the optimization of operating conditions or the surface modification of the membranes.[8, 9] The latter can effectively enhance anti-fouling properties of RO membranes by tailoring surface hydrophilicity and other membrane characteristics, such as roughness and charge to reduce the interactions between membrane surface and foulants.[10]

While the most reports on surface modifications are focusing on flat-sheet membranes conducted in laboratory scales, only a few focalize the scale-up of the modification to membrane modules in industrial scale because usually such modifications are easier to apply to flat-sheet membranes than to more complex module configurations. A novel, promising method is the in situ coating of membranes during filtration where the barrier properties of the membrane are utilized allowing the selective modification of membranes in modules. The basic feasibility of the in situ modification of spiral-wound RO modules was demonstrated but with another focus than antifouling improvement.[11-13]

Therefore, in this work the development of an anti-fouling coating by in situ modification of polyamide RO membranes during filtration which is applicable in ready to use membrane elements is aimed. Hence, individual coatings in combination with an up-scalable modification method enables the possibility to customize a modular coating that can be adapted to a certain application.

1.2 WEISS project – Aims

The work of this dissertation was part of the cooperative project “WEISS” which was funded by the Federal Ministry of Education and Research within the funding initiative “WavE” with the reference number: 02WAV1411. The WEISS project concerns the integration of different water-use processes into one system along with a substance flow analysis in order to build up an optimization model for the water-use network of a steel plant. The overall goal was to halve the blow-down water amount of a steel plant (project partner DEW[1]) by removing salts and solids from the make-up water and the establishment of an appropriate chemicals dosing by combining innovative process approaches in one pilot plant (Figure 1).

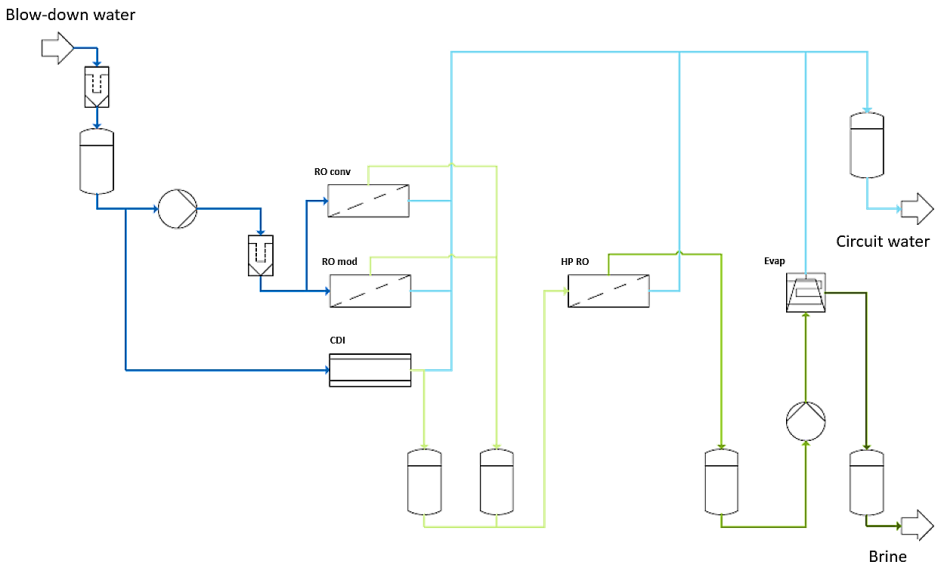

Figure 1: Simplified flow chart of the pilot plant of the project.[14]

The blow-down water undergoes several steps starting with a pre-filtration by a 5 µm MF filter for the removal of rough particles and solids. Afterwards, the desalination is carried out in a first desalination step by means of a conventional RO (project partner SMS[2]), in parallel by modified RO membranes with a novel anti-fouling coating (project partner UDE) and by a capacitive deionization (project partner BFI[3]) as a competitive process. The latter removes the salt from the water by applying an electrical potential difference over two electrodes where the removed anions are stored in the positively polarized anode and the removed cations in the negatively polarized cathode.[15] The produced permeates are recycled back to the circuit

[1] Deutsche Edelstahlwerke, Hagen
[2] SMS Simag Group, Hilchenbach
[3] Betriebsforschungsinstitut GmbH, Düsseldorf

water while the concentrate is narrowed down by a high pressure RO (project partner Wehrle[4]) and an evaporation step (project partner FOEN[5]) to meet zero liquid discharge. Due to the complex structure of the cooling circuits the goal could only be realized by an accompanying development of a simulation tool for the whole water circuit (project partner TU Berlin[6] and IFAK[7]).

The development of modified RO membranes with a novel anti-fouling coating is the main focus in this work. A critical evaluation of the separation performance of established membranes by analyzing fouling with real cooling water was done first, followed by the development of an in situ modification for RO flat-sheet membranes and the transfer of the modification to spiral-wound RO modules. In the last step, these coated modules were implemented in the cooling circuit of the steel industry where pilot scale tests were done.

[4] Wehrle Umwelt GmbH, Emmendingen
[5] Fontaine Engineering und Maschinen GmbH, Langenfeld
[6] Technische Universität Berlin, Institut für Umweltverfahrenstechnik, Berlin
[7] Institut für Automation und Kommunikation e.V., Magdeburg

2 Theoretical background

2.1 Steel industry

One of the largest energy- and water intensive process industries is the steel sector, in which iron ore concentrate is reduced to iron and converted to various steel products, and steel scrap is recycled to new ones. Integrated steel plants include blast furnaces, rolling mills, casting units, coke ovens, wire drawing machines, rod mills and other iron working units. A central plant without coke ovens and blast furnaces is defined as steel processing plant.[6, 16]

2.1.1 Cooling water for plant and product cooling

The production of steel and steel products requires large quantities of water, typically 180 – 200 m^3 of water per ton of steel produced. However, different steel plants use different amounts of water, depending on access to water, primarily determined by geography and local regulations. The tremendous amounts of water are used generally for waste transfer, dust control and cooling. However, most of the water is used for cooling purposes.[17, 18] The main purpose of cooling water systems is the control of temperature by transferring heat from the hot process into the cooling water in order to carry the heat away. By this, the cooling water heats up and has to be cooled by rejecting heat into the atmosphere while evaporating inside cooling towers before it can be used again, or it has to be replaced by fresh water.[19] Cooling can be divided into direct and indirect cooling. The latter refers to the process where the water does not have contact with the product, e.g. machine or oven cooling while the first is referred to product contact, e.g. contact with hot rolling or coils.[20]

2.1.2 Potential problems

Due to the tremendous use of cooling water, wastewater having specific characteristics is generated in huge quantities. It may contain solids, oil and grease, biodegradable organics, sludge, toxic materials, acid and alkali and other organics. Conductivity, total dissolved solids (TDS), hardness, pH, alkalinity and saturation index are the critical parameters for cooling water.[18, 21] All these key water chemistry properties have a direct impact on the three main problems of cooling water systems leading to three sides of cooling water triangle; corrosion, scale and microbial contamination (Figure 2).

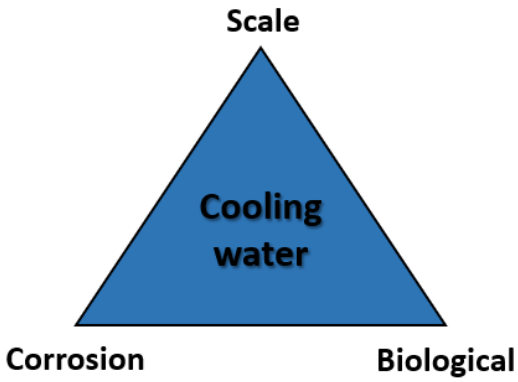

Figure 2: Cooling water triangle representing critical contaminants.

The manufacture of common metals used in cooling systems involves the removal of oxygen from the natural ore. Cooling water systems are an ideal environment for corrosion which is the reversion of the metal to the original oxide state. Additionally, minerals such as calcium carbonate, calcium phosphate, and magnesium silicate can precipitate to form scale deposits when exposed to conditions commonly found in cooling water systems as a consequence of high insolubility in water. Moreover, cooling water systems provide an ideal environment for microbial organisms to grow and multiply causing deposit problems in heat exchange installations. If not controlled properly, microbial growth strongly contributes to corrosion, fouling, and scale formation. Different species of clams, mussels, and other marine organisms can attach to the piping, leading to a reduction of water flow and an increase in corrosion. These problems can have a direct, negative impact on the entire operation and process, if it is not controlled properly.[19]

All these mentioned problems, usually a combination of them, result in costly unscheduled downtime, reduced capacity, increased water usage, high operation and maintenance costs, expensive parts replacements, and acid cleaning operations which reduce the life of the cooling system.[21]

2.1.3 Water re-use strategies

Water is often recycled in a closed loop inside the steel mill but as the quality of wastewater from some processes is not high enough for further usage, it is important to develop advanced treatments, enabling its reuse and increase the water recycling rate.[6]

Conventional pre-treatments represented by basic sedimentation/clarification combined with flocculant treatment may be effective to remove the fine colloidal suspended solids, organic matter and microorganisms from the water but it is not effective in removing salts which may cause scaling in reuse systems.[2] Therefore, RO is effective in the removal of both monovalent and divalent ions that cannot be removed by conventional physicochemical treatment. But, even when the efficiency of RO is very high, pre-treatment is usually necessary, due to the wastewater nature causing membrane fouling.[22] Fouling is usually induced by organic pollutants as well as by microorganisms, colloidal materials and salts (membrane fouling is described in detail in chapter 2.4). These deposits can lead to a tremendous decrease of flux and consequently to a reduction in efficiency.

Therefore, RO can be efficient when it is combined with conventional pre-treatments (e.g. disinfection, addition of coagulant, media filtration, etc.) along with unconventional pre-treatments such as microfiltration (MF) and ultrafiltration (UF) which will be further discussed in chapter 2.5. The feasibility of the application of RO in the steel industry was shown by *Colla et al*. by exactly this approach.[6] MF and UF could effectively reduce turbidity and the silt density index, providing eligible feed for the sequent RO. Thus, through the implementation of a recycling system including RO, waste or cooling water from the steel industry can be treated effectively and consequently reused. [2, 6]

2.2 Reverse osmosis

Compared to other pressure driven based membranes, the RO membrane acts as a semi-permeable barrier and its structure is denser, allowing only particular species (water) to pass through the membrane while contaminants such as monovalent ions (salts) are partially or completely retained. Salt rejection as high as 98 – 99.5 % can be achieved depending on the membrane used. Because of the denser membrane structure, the resistance of the membrane mass transfer is higher. Thus, the applied pressure must be higher and must also overcome the osmotic pressure in order to get a considerable amount of flux through the membrane.[23] A comparison between the separating capacity of pressure driven membrane processes: reverse osmosis (RO, NF) and membrane filtration (MF, UF) is given below in Figure 3.

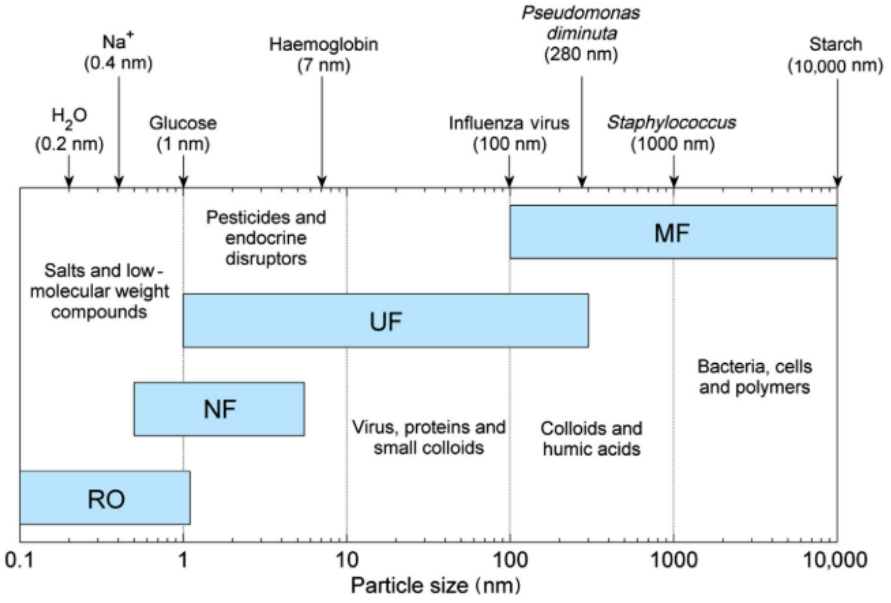

Figure 3: Particle size retention for pressure driven membrane processes.[24]

Actually, osmosis is the flow of solvent through a semi-permeable membrane, from a dilute solution to a concentrated solution (Figure 4, left side). This flow results from the driving force which is the difference in chemical potential for the solvent between the two solutions. The movement of the pure solvent through the membrane generates a pressure named "osmotic pressure". In contrast, the reverse osmosis membrane transports liquid against natural direction of osmosis, while the salts are retained and concentrated onto the membrane surface (Figure 4, right side). It is operated by achieving a hydrostatic pressure on the side of higher concentration that overcomes the osmotic pressure of the solution to induce a flow of clean water to the low concentration side.[25]

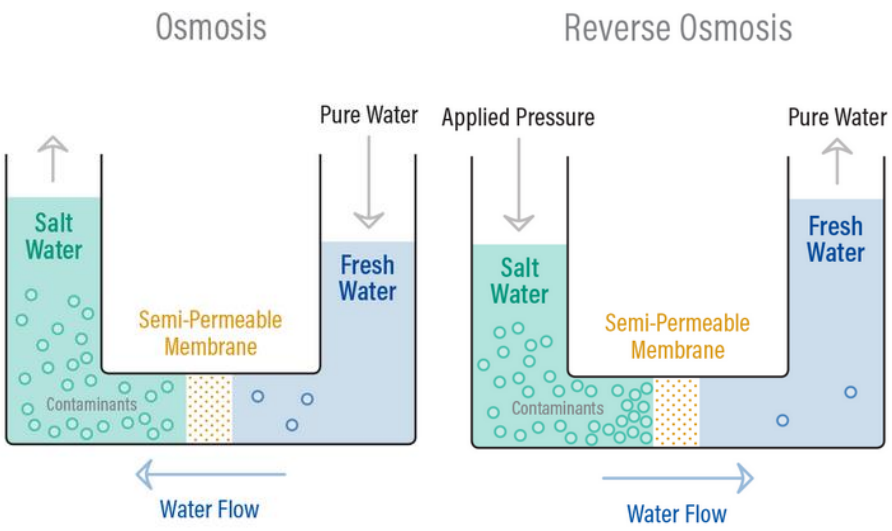

Figure 4: Normal osmosis (left) and reverse osmosis system (right).[26]

2.2.1 Thin-film composite RO membranes

The first historic discovery of *Loeb* and *Sourirajan* was an asymmetric reverse osmosis (RO) membrane in 1961.[27] A major breakthrough in the field of membrane-based separations was the invention of a new type of membrane, a thin film composite (TFC), first reported in the early 1978 by *Cadotte* who decided to use a microporous asymmetric membrane (a Loeb-Sorirajan type of membrane) with many other properties, such as surface charge, hydrophilicity, etc. to support a thin polyamide (PA) selective layer, prepared by interfacial polymerization (IP) which is responsible for salt separation.[28]

Currently, the most commercially available RO membranes are asymmetric thin-film composite (TFC) membranes (including polyamide, aryl-alkyl polyetherurea and polyester) and integrally skinned asymmetric membranes also referred to as Loeb-Sourirajan membranes (including cellulose acetate, diacetate, triacetate or their blend).[29] Figure 5 shows schematically a typical cross-sectional view of these two types of asymmetric membrane. The most widely-used thin-film composite membrane consists of highly cross-linked aromatic PA (with thickness varying from around 10 nanometers to several hundreds of nanometers) based on a porous support layer. Ideally, PA layer is formed via typical interfacial polymerization process using two monomer systems; m-phenylenediamine (MPD) in water and trimesoyl chloride (TMC) in organic solvent (usually, n-hexane). There are a number of combinations for the choice of amine and acid chloride monomers. Valuable aromatic polyamines include phenylenediamine such as m-phenylenediamine (MPD), p-phenylene-

diamine (PPD) and piperazine (PIP). Using latter one will produce semi-aromatic PA NF thin-film-composite (TFC) membranes while using MPD and PPD will produce full-aromatic PA RO TFC membranes.[30] Compared to integrally skinned cellulose acetate, TFC PA membranes dominate the membrane markets and are used in industrial separation processes.[31]

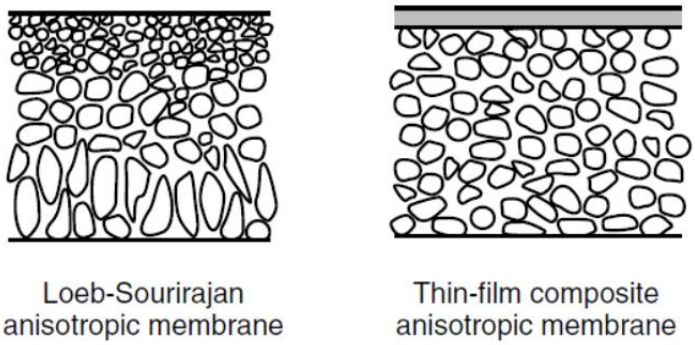

Figure 5: Principal types of anisotropic membranes due to their structure.[29]

The PA perm-selective dense layer provides the separation properties for the TFC membranes. Due to its high crosslinking, PA layer is reported to determine the fluxes and selectivity, while the porous sub-layer ensures mechanical strength.[29] Production of composite membranes contains preparation of the porous sub-layer (typically by phase inversion), which is then laminated by dip-coating, in situ polymerization, interfacial polymerization or plasma polymerization on the top of the sub-layer. The interfacial polymerization method has been proven to be commercially more successful.[32]

The main advantage of the composite membrane over the integrally skinned asymmetric membrane is that the material for the top skin layer and for the porous sublayer can be separately optimized in order to achieve desired membrane performance. Thus, composite membranes offer more flexibility. Furthermore, PA TFC membranes, can tolerate a wider range of the pH (4 – 11) and the temperature. Generally, PA and polyurea composite membranes typically have higher water permeance along with high salt and organic rejection.[33]

However, PA TFC membranes suffer from poor resistance to continuous exposure to oxidizing agents. They also tend to be highly susceptible to damage by chlorine that is a common disinfectant and oxidizing biocide in water and wastewater treatment, which causes degradation of the amide group. PA TFC membranes, similar to other membrane types, are fouled on long-term application, which causes serious decline in flux and process efficiency as

a whole therefore, higher pressure and more energy are needed to achieve the desired throughput. A number of attempts have been made to modify the PA TFC membranes to improve their applicability (mechanical, chemical and biological stability) and functionality (permeability and selectivity). The different strategies for modifying the surface of TFC RO membranes will be discussed in chapter 2.6.

Preparation

The available literature reports on PA thin films formed in a typical interfacial polymerization reaction between trimesoyl chloride and m-phenylenediamine, see Figure 6.

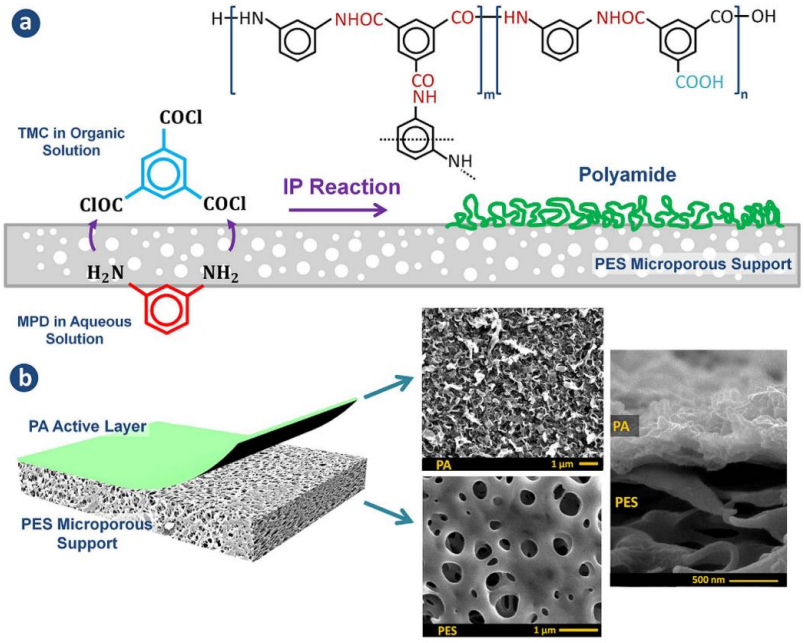

Figure 6: (a) Interfacial polymerization reaction between MPD and TMC at the surface of a microporous PES support and the chemical formula of the PA layer. **(b)** Structure of the synthesized TFC membranes with the top and cross-sectional morphologies.[34]

Typically, the preparation of PA TFC membranes starts with soaking of a porous support into an aqueous solution of diamine monomer for a certain time. During this step, the pores at the top and near to the surface of support are almost filled with the aqueous monomer. The excess diamine is removed from the surface and the membrane is then immersed in the organic solution of the acid chloride monomer for a definite short time. Many organic solvents are tested; however, n-hexane is the most frequent solvent used for PA synthesis on different supports. Since water and hexane are not miscible, an interface is formed at the boundary of the two phases. Polycondensation of diamine and tri-acid chloride will take place at the interface, resulting in a very thin layer of PA. Some of the acyl chlorides do not react with

amines, but they are hydrolyzed to form carboxyl groups, which always gives the PA layer an anionic charge at neutral pH ranges. In addition, it is reported that a less cross-linked, more permeable layer may be formed under the surface layer and fills the pores of the support membrane.[29] The process is schematically presented in Figure 7.

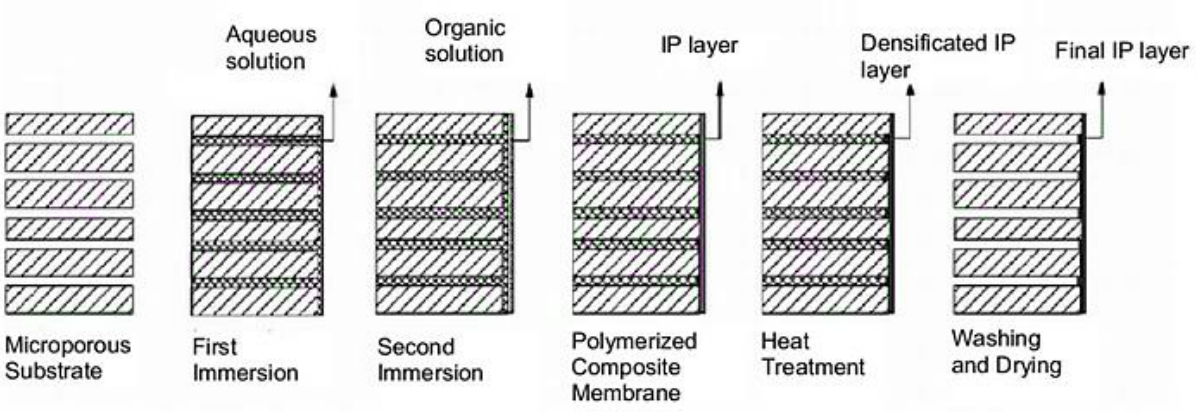

Figure 7: Preparation process of TFC membranes by conventional IP technique.[35]

Interfacial polymerization takes place predominantly in the organic phase side of the interface and not in the aqueous phase side since the acid chloride has negligible solubility in water while the diamine is soluble in organic solvents. Therefore, the amine monomer diffusivity is strongly affected by the nature of solvent (density and surface tension), the reactant concentration and the phase miscibility. It governs the PA growth rate and thus, the performance of the thin-film which is strongly correlated to the morphology, thickness and the density of the film. It is better to use a large excess of diamine over acid chloride (typically about 20:1), in order to drive partitioning and diffusion of the diamine into the organic phase.[32] After crossing the interface, the first diamine monomers meet a relatively high concentration of acyl chlorides and react to form amide bonds on both ends. Subsequent diamines will enter the reaction zone that now contains acyl chloride terminated oligomers as well as acyl chloride monomers. As the reaction progresses, diamines start coupling these oligomers forming larger polymeric molecules. High molecular weight polymers are formed over time because of the increasing probability that new diamine monomers crossing the interface will react with polymer chains rather than triacyl chloride monomers. In addition, the presence of the polymer film becomes an additional barrier for the diamines that now have to diffuse through the newly formed polyamide matrix to reach unreacted acyl chloride monomers and oligomers. So, polyamide chains continue to grow until the solubility limit is reached and precipitation of the polymer occurs. Eventually, the film reaches a certain

thickness that significantly reduces the flux of diamines, and the reaction effectively stops.[36] *Freger,* for example, describes the film formation process as a succession of different kinetic regimes; incipient film formation, slowdown, diffusion limited growth.[37] One problem that often occurs in the interfacial polymerization is the formation of an ultra-thin layer with a large number of defects, which results in poor membrane performance (very high flux with very low separation).

Impact of the support's characteristic

Reverse osmosis membrane separation is determined by the characteristic of the membrane used in the process. These properties depend on the chemical nature of the membrane material as well as its physical structure. Properties of the ideal RO membrane include that it is resistant to chemical and microbial attack and are mechanically and structurally stable over long operating periods, and have the desired separation characteristics for each particular system.[33]

Recently support materials used for polyamide composite membranes have been made from polymers like polysulfone, polyethersulfone, polycarbonate, polyphenylene oxide, polyetherimide, polypropylene, and others by phase inversion techniques. Polysulfone has found to be an optimum material as a support due to its stability in acidic conditions, fair thermal, chemical, mechanical, and anti-bacterial stability, resistance to compaction and its reasonable flux. In some applications, polysulfone was replaced with less hydrophobic comparable polymer material which is polyethersulfone. However, thin film composite membranes based on polysulfone or polyethersulfone are found to have limited stability in organic solvents.[38]

2.2.2 Transport mechanism

A lot of theories describe the mass transport through the PA RO membranes. Researchers assume that solvent or solute transport occurs through the interstitial spaces of the polymer chains. They postulated that the layer consists of polymer nodules (clusters of polymer macromolecules) and nodule aggregates. Thus, transport can occur through chain segment displacements in the polymer nodules (interstitial spaces) and through spaces between nodule aggregates (defect pores).[39]

However, there are two general models used to describe the mass transport through membranes as depicted in Figure 8. One is pore-flow model, in which permeation occurs by the pressure-driven convective flow through the pores and separation is based on the exclusion of permeants from the pores of MF and UF due to size exclusion. If the size of the permeants is greater than the biggest pore diameter of the membrane, then exclusion occurs. Two typically used equations for calculating the flux through the pores are the Hagen-Poiseuille and Kozeny-Carman equation. The first one fits when the pores are cylindrical with uniform radius and length. Solute molecules are simulated as rigid spheres and the solute concentration is assumed to be so small that there is no interaction inside the pores of the membrane.[40, 41] The Kozeny-Karman equation applies for pores which are irregular and assumed to be interstices between close-packed spheres.[42] The separation can also be achieved based by a geometric exclusion of solute particles bigger than the membrane pore size. The steric exclusion mechanism is similar to a sieving mechanism thereby causing an additional separation.

The other mechanism is the solution-diffusion model described by *Lonsdale et al*. in which permeants first dissolve in the membrane and then diffuse through the membrane by a concentration gradient (RO and pervaporation).[43]

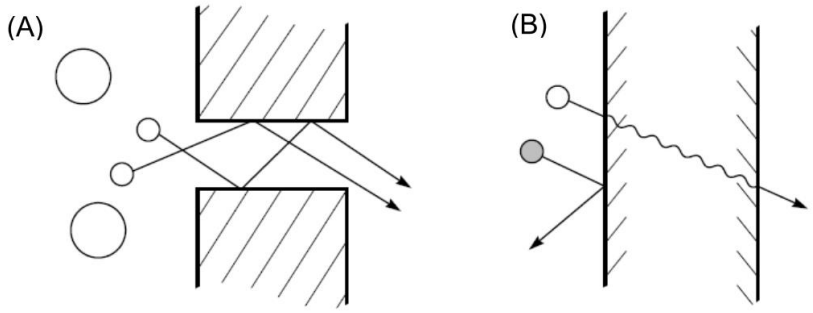

Figure 8: Schematic illustration of (A) the pore flow and (B) solution-diffusion mechanism.[29]

Pore flow cannot exist in RO membranes as the pores are too small, so the solution-diffusion model is the only valid mechanism along with any possible contribution from the membrane surface charge. The transport of molecules occurs by the driving forces, such as gradient in pressure, temperature and concentration. The overall driving force can be expressed as chemical potential gradient and the flux can be described by the simple equation (1), where J_i is the volumetric water flux, $\frac{d\mu_i}{dx}$ is the chemical potential of the component i and L_i is the

membrane permeance which can be defined as a proportional coefficient related to the intrinsic barrier properties:[29]

$$J_i = -L_i \frac{d\mu_i}{dx} \quad (1)$$

The driving force for the transport through RO membranes is the applied pressure and the governing equation for the solution-diffusion transport is therefore:[44]

$$J_i = L_i(\Delta p - \Delta\pi) \quad (2)$$

where $\triangle$p is the applied pressure difference and $\triangle\pi$ is the osmotic pressure difference between the feed and permeate solution. The osmotic pressure can be described with the following *Van´t Hoff* equation:

$$\Delta\pi = iCRT \quad (3)$$

C is the molarity of the ions present in the solution, R is the ideal gas constant, T is the ambient temperature and i is the *Vanthoff* factor which is the quotient of the colligative properties of the solutes and the colligative properties if the solute were nonelectrolyte. Osmotic pressure values for given solutions are represented in Table 1. A large osmotic pressure value in the feed solution reduces the driving force of the separation process through the membrane.

Table 1: Osmotic pressure values for different solutions.[45]

Solute	Concentration (mg/L)	Osmotic Pressure (bar)
NaCl	2,000	1.7
NaCl	35,000	27.4
Brackish water	2,000-5,000	1-2.7
Seawater	32,000	23.4

According to the solution-diffusion model, the transport of solvent and solute are independent so that the water and solute transport occur in three steps; sorption to the upstream side of the membrane, diffusion through the membrane and desorption from the downstream side of the membrane (permeate surface). When the water molecule is absorbed onto the membrane surface, the concentration gradient of water across the membrane causes the water molecules to diffuse down the concentration gradient to the permeate side of the membrane. Then the water molecules desorb from the membrane to the bulk permeates. The same holds true for the solutes.

The solution-diffusion model predicts that separation occurs because of the difference in solubility and diffusivity of different permeants (solvent and solute) in the membrane. Thereby

the solute concentration in the permeate is lower than in the feed. The adsorption occurs through different interactions such as hydrophobic or van der Waals interactions, hydrogen bonding and by electrostatic effects.[25, 46]

There is a further separation mechanism which is charged-based and is called *Donnan* exclusion. This charge-based exclusion mechanism is due to slightly charged nature of the most NF and RO membranes. Solutes with opposite charges to the membrane surface (counter-ions) are electrostatically attracted due to coulomb interactions, while solutes with the same charges (co-ions) are repelled. At the membrane surface, a distribution of co-ions and counter-ions will occur, called the *Donnan* potential, resulting in salt retention.[47, 48] As the feed concentration increases, the concentration of counter-ions at the membrane surface increases causing a shield effect which decreases the repulsion of co-ions resulting in a lower salt rejection. The effect is mainly controlled by the counter-ion concentration having the highest valence in the system. The *Donnan* potential and thus salt rejection becomes lower with higher concentration of divalent counter-ions.[48, 49] In this context, another important mechanism, called dielectric exclusion, contributes to the separation effect.[50, 51]

2.2.3 Geometric configuration

There are four commercially available membrane modules such as plate and frame, tubular, hollow fibre and spiral-wound.[24] But, the most commercially available modules are hollow fibre and spiral wound modules.[52] The comparison of the different module designs are given in Table 2.

Table 2: Comparison between different membrane modules.[53]

	Spiral wound element	Tubular high price	Tubular low price	Plate and frame system	Hollow wide fiber system	Hollow fine fiber	Ceramic
Membrane density [m2/m3]	high	low		average	average	very high	low
Plant investment	low	high	low	high	very high	medium	very high
Tendency to fouling	average	low		average	low	very high	medium
Cleanability	good	good		good	low	none	good
Variable costs	low	high	low	average	average	low	high
Change of membrane only, see note 1	no	yes	no	yes	no	no	yes
Flow demand	medium	high	medium	medium	high	low	very high
Prefilter other demands (see also table 26)	≤ 50 µm. no fibers	sieve		≤ 100 µm. few fibers	≤ 100 µm. few fibers	≤ 5 µm extreme pretreatment	sieve

Costs of supporting materials including housing, power consumption in pumping and the ease of replaceability are the factors for the selection, design and operation of membrane modules. Other key properties are high packing density, low operating and maintenance costs and good control of concentration polarization (CP) and membrane fouling. [54]

Plate-and-frame modules are the simplest device for packing flat sheet membranes. They can be constructed in different sizes and shapes. Small lab-scale devices holding small and single membrane coupons and industrial-scale systems holding more than thousand membranes.[24] On the contrary, tubular membranes are located on the inside of a tube which is the supporting layer for the membrane where the flow is usually inside out. Hollow fibre membranes are similar to tubular systems only the inner diameter is smaller; typically, less than 2 mm. But the cartridges can contain several hundred of fibres. The feedwater passes at the outside and goes through the membrane, while permeate is handled inside the lumen.[23]

Most RO membrane installations use flat sheet membranes in a spiral wound module configuration due to a good balance in terms of permeability, packing density, ease of operation and maintenance, lower replacement costs and higher pressure applications.[24] A schematic representation of a spiral wound module is shown in Figure 9 (a). It consists of several flat sheet membranes which are glued together in pairs on three sides with a permeate spacer inside, forming an envelope. The open side of the envelopes is connected to the porous permeate tube which collects the permeate from all membrane leaves. The envelopes are wound around the permeate tube forming the spiral shape with feed spacers between each envelope. As can be seen from Figure 9 (b), alternating feed and permeate channels are formed. In operation, the feed travels through the flow channel tangentially/axially across the length. The permeate will pass through the permeate spacer and will be collected in the permeate tube leaving the element. The retentate is concentrated, leaving the element at the end of the element.[55]

Single RO module elements are typically operated with a recovery of 5 to 15 %.[23] Though, larger membrane areas per unit volume are preferred for full-scale applications.

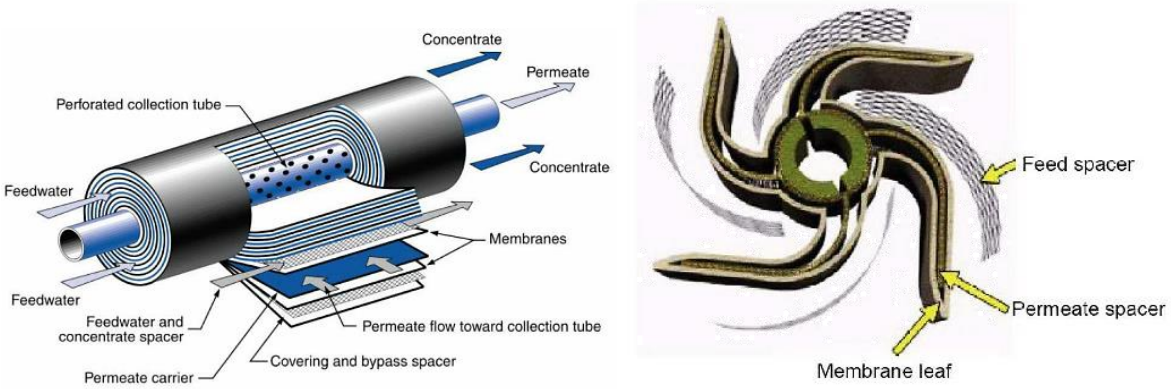

Figure 9: Schematic illustration of a spiral-wound reverse osmosis membrane element (left) and a cross-cut of such an element.[56]

However, the spiral-wound configuration has also some disadvantages such as susceptibility to fouling and difficult module cleaning. Additionally, the flow complexity reflected in continuous permeation of water and rejection of salt along the radial direction of the module leads to a variation of process parameters along the feed channel such as decline in transmembrane pressure, decreasing axial velocity, increasing bulk salt concentration and increasing CP that could probably result in membrane fouling.[23, 57, 58] Therefore, the analysis of flow hydrodynamics is a precondition for the prediction of the salt concentration variation and membrane performance. The film theory model is a wide-spread theory describing the transport perpendicular to the flow direction in the channel (discussed in chapter 2.3).[59, 60] Such theories can help to optimize spiral wound modules.

The function of the feed spacer is to separate the adjacent membrane envelopes and to allow good mixing of the feed by providing a flow path for the feed and concentrate stream along the leaves and by creating eddies. Thereby, high mass transfer rates are possible and consequently CP will be reduced (see chapter 2.3). Despite, feed spacers can contribute to an increase in feed channel pressure drop and to biofouling due to the attachment and growth of microbes on it. Commercially available feed spacers have a diamond shaped geometry with varying thicknesses ranging from 26 mil to 44 mil (1 mil = $2.54 \cdot 10^{-5}$ m).[61]

2.2.4 Applications

RO has become the mainstream of membrane desalination technology. It was originally conceived of as a method of producing potable water from sea or brackish water.[5] Hence, the first successful RO plant used brackish water as feed was installed in the late 1960s. In the

following decades, membrane permeability was much improved and RO membranes were then applied for seawater desalination. From the early 1960s to the beginning of the 2000s, the membrane productivity (flux) and salt rejection have much improved. The fluxes of currently available commercial membranes are an order of magnitude higher than the RO membranes of 1960s.[32, 62] Figure 10 shows a typical development path for Dow products.

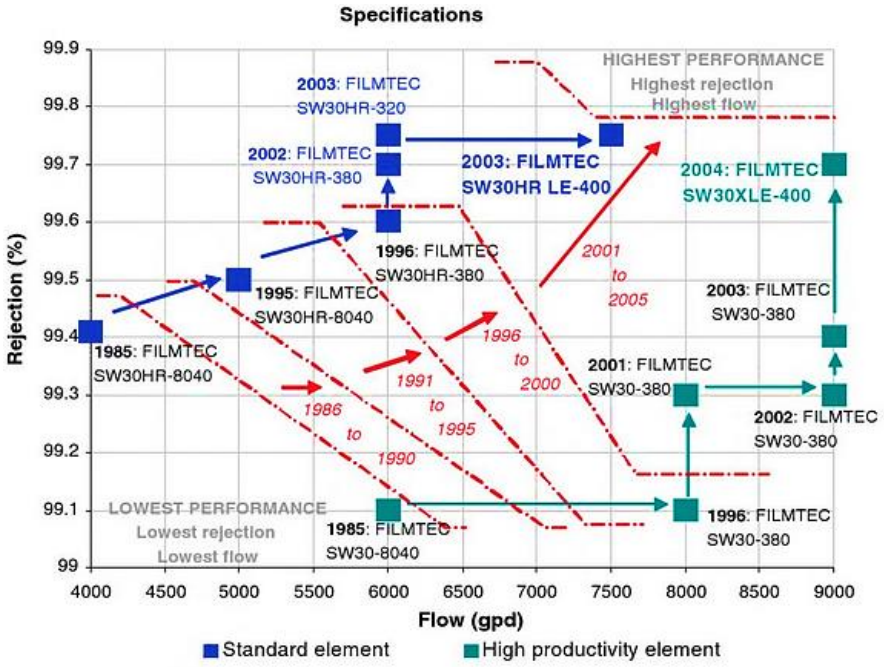

Figure 10: Progress in membrane performance from 1980´s – 2000´s.[62]

In general, desalination technologies can be divided into membrane processes, such as the mentioned RO and thermal processes like Multi-Stage Flash Distillation (MSFD), Multi-Effect distillation (MED), and Vapour Compression Distillation (VCD). Despite the fact, that thermal desalination can deal more saline waters and deliver higher permeate quality than RO, currently more than half of the desalination capacity worldwide (53%) is based on RO, far more than traditional processes like MSFD (25 %) and MED (8 %).[23, 63] The driving force behind the impressive progress becomes obvious when the energy requirements of RO are compared to the requirements of some traditional desalination techniques. The RO technology has proved to be the lowest energy consuming technique compared to other desalination processes. It consumes about a half of the energy used in thermal processes. Additional advantages of RO desalination systems are ease of operation, flexibility in capacity expansion, operation at ambient temperature and short construction periods.[64]

The RO technology is also being applied on a large scale in municipal, domestic, agricultural and industrial wastewater treatment. Probably the most promising field are re-use

applications such as industrial process and cooling water recycle due to stringent industrial and municipal discharge standards.[5] Specific technologies have been successfully applied in different kind of industries.[65-68] Also, the feasibility of the application of RO in the steel industry was shown by *Colla et al.* [6] (cf. chapter 2.1).

Another increasing attractive application area for RO membranes is the treatment of oil-containing process water. However, the use of RO membranes is currently still limited due to high fouling potential of these waters. Process water containing oil may arise i.e. from refineries, petrochemical plants and metal processing industry.[69] These oil containing waters can be divided into stable and unstable emulsions and waters with directly precipitable oil components.[70] Coagulation, flotation and biological water treatment are used as established treatment techniques. However, these techniques are only of limited suitability for the treatment of stable emulsions.[69] Membrane filtration of emulsions is based on the classification combined with selective moistening, e.g. for the separation of oil in water emulsions with a hydrophilic membrane with a pore size smaller than the droplet size of the emulsion. But there are some difficulties in the implementation, such as a broad droplet size distribution, instability of the emulsion and partially the solubility of oil in water. Hence, combined membrane processes consisting of MF, UF and NF/RO are required to maintain an appropriate separation efficiency,[71] otherwise there is a great risk of spreadable fouling which is discussed thoroughly in chapter 2.4.2.

2.3 Concentration polarization model

There are two basic membrane filtration principles; dead-end and cross-flow filtration. Dead-end describes the configuration where the feed flows perpendicular to the membrane surface while the rejected material, the concentrate/retentate, accumulates on the membrane surface. One major drawback of this configuration is the formation of a filter cake at the surface during the filtration. Membranes can also be operated in cross-flow mode where the feedwater flows tangentially to the membrane surface. By this, the feed is separated into a permeate and concentrate stream. The permeate contains solutes passing the membrane, while the retentate contains solutes and particles rejected by the membrane. The cross-flow configuration generates turbulences and thus preventing large molecules from clogging the membrane and forming a filter cake at the surface. Since RO is most often available in spiral wound modules, it is operated mainly in cross-flow mode.[30, 72]

Membrane life-time and permeate flux are primarily affected by the phenomena of CP and fouling at the membrane surface.[73] However, CP is not considered as fouling, even though it is also responsible for the flux decline. It is different because fouling involves the deposition of foulants as an immobile solid phase on the membrane surface whereas the phenomenon of CP disappears once the filtration process is stopped; it is therefore considered to be totally reversible.[5, 74, 75]

CP is a natural consequence of the selectivity of a membrane. During the filtration process, both, solutes and solvent are transported to the membrane surface by convective transport. When the solvent passes through the membrane, the solutes will accumulate adjacent to the membrane surface due to the difference in the permeability between the solvent and solute. As the back-diffusion of solutes is slower than the convective transport towards the membrane, the concentration of solutes gradually enhances near the membrane, resulting in a boundary layer δ near the membrane surface (Figure 11).

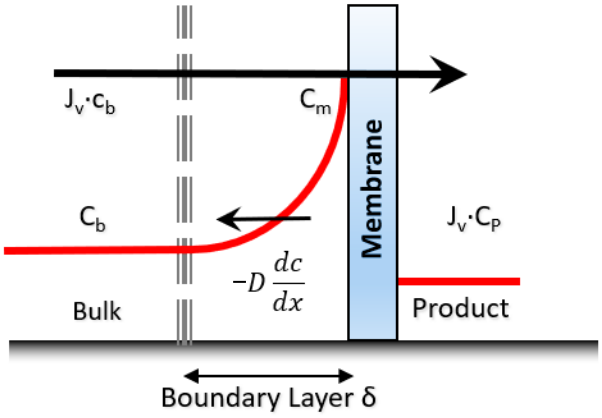

Figure 11: Schematic illustration of the concentration polarization phenomenon occurring during filtration.

Therefore, the concentration of the solutes near the membrane surface c_m is higher than the concentration in the bulk solution c_b and the ratio of c_m and c_b is called the concentration polarization factor (CPF) or modulus (CPM). During the process, the retained solutes diffuse back to the bulk solution due to the concentration gradient. Once the rate of back diffusion balances the rate of accumulation near the membrane surface, a steady state is reached.[5, 76]

The boundary layer consists of suspended solids, particles and solutes, which cause an increased resistance. Additionally, the boundary layer leads to an increase in osmotic pressure of the feed ($c_m > c_b$), and thus a decrease in driving force for water transport (cf. equation (2)), resulting in a lower flux. The increased salt concentration at the membrane surface increases the driving force for salt transport across the membrane leading to a higher salt flux (lower rejection) and a deteriorated permeate quality.[23] The most detrimental CP effect lies in the increased risk of precipitation of sparingly soluble salts by reaching the limit of solubility in the boundary layer and the precipitation on the membrane surface thus leading to fouling.[77]

Typically, reverse osmosis systems have CPF values ranging from 1.2 to 2, although these values are strongly dependent on the fluid mechanics of the filtrated solution and operating conditions. Values lower than 1.2 is recommended for RO systems.[29, 78, 79]

An increased cross flow velocity, a greater diffusion coefficient of the solutes, and a higher temperature are factors that enhance the back diffusion and therefore reducing CP whereas an increased filtration pressure or permeate flux increases the CP. The use of a spacer is also advantageous because it creates turbulences near the membrane surface, thus decreasing the CP.[75, 80, 81]

2.3.1 Film theory

Several theoretical models have been developed to describe the CP phenomenon during membrane filtration. The models involve the solution of the diffusion convection differential mass balance equation with appropriate boundary conditions and simplified presumptions.[82] The most widely used mathematical analysis of concentration polarization is the simple stagnant film model reported by Michaels in 1968.[83] This model assumes a stagnant film where mass transfer is described by a one-dimensional steady-state mass balance:[29]

$$J_v c - D_i \frac{dc}{dx} = J_v c_p \qquad (4)$$

where J_v is the permeate flux, c is the solute concentration in the boundary layer, D_i is the solution diffusion coefficient of the solute i (cf. equation (18)), dc/dx is the salt concentration gradient along the distance x from the membrane surface and c_p is the solute concentration in the permeate, meaning that the convective transport of solutes to the membrane surface is equal to the sum of the back-diffusion of the solute away from the membrane plus the permeate flux.

Integrating equation (4) over the boundary layer thickness δ with the boundary conditions of $c = c_b$ at $x = 0$ and $c = c_m$ at $x = \delta$ leads to the following equation:[29, 82]

$$CP = \frac{c_m - c_p}{c_b - c_p} = \exp\left(\frac{J_v}{k_i}\right) \qquad (5)$$

where c_m, c_p and c_b are the solute concentrations at the membrane surface, in the permeate and in the feed bulk. k_i is the mass transfer coefficient and defined as the ratio of the solution diffusion coefficient D_i and the boundary layer thickness δ.

If the rejection is 100% the degree of CP becomes:[30]

$$CP = \frac{c_m}{c_b} = \exp\left(\frac{J_v}{k_i}\right) \qquad (6)$$

Equation (5) can also be expressed by means of membrane rejection. The observed rejection R_{obs} is based on solute bulk concentration and is directly accessible:

$$R_{obs} = 1 - \frac{c_p}{c_b} \qquad (7)$$

whereas the real intrinsic rejection R_{in} is the solute concentration at the membrane surface and is given by:

$$R_{in} = 1 - \frac{c_p}{c_m} \quad (8)$$

Using these rejection values R_{obs} and R_{in} instead of concentrations, the CP expression takes the form:[82]

$$\ln\left(\frac{R_{obs}}{1 - R_{obs}}\right) = -\frac{J_v}{k_i} + \ln\left(\frac{R_{in}}{1 - R_{in}}\right) \quad (9)$$

2.3.2 Estimation of mass transfer coefficient in the CP layer

The theoretical expression of the mass transfer coefficient k is borrowed from heat transfer and was adopted in membrane separation.[84] Therefore, k is the most uncertain parameter in the theoretical determination of CP and cannot be readily determined by applying equation (5). However, several empirical models have been developed to estimate the mass transfer coefficient depending on system geometry and on flow parameters. Hence, it has to be distinguished between dead-end and cross-flow mode. One of the most widely used methods to determine k is the velocity variation method with film model where the change in observed rejection R_{obs} with varying flow rate Q for cross-flow (stirring rate ω for dead-end) for the same solution is measured. The effect of flow rate on k_i is assumed to obey the following relation:[82, 85]

$$k_i = A' \cdot Q^b \quad (10)$$

where the factor A´ is a cell-specific constant and the exponent b is a value that has to be chosen in advance based on the flow regime.

By combining equation (9) and (10) the following relation is given:[82]

$$\ln\left(\frac{R_{obs}}{1 - R_{obs}}\right) = -\frac{1 \cdot J_v}{A' \cdot Q^b} + \ln\left(\frac{R_{in}}{1 - R_{in}}\right) \quad (11)$$

As can be seen, a linear relation between the observed rejection expression $\ln\left(\frac{R_{obs}}{1-R_{obs}}\right)$ and $\frac{J_v}{Q^b}$ exists. By plotting these experimental values, the intrinsic rejection R_{in} and the cell-specific constant A´ can be determined graphically from the intercept and the slope, respectively.

The mass transfer coefficient k_i can also be estimated from a dimensionless correlation using the Sherwood number; for dead-end mode generally expressed as equation (12) for a stirred filtration cell and for cross-flow mode as equation (13):[86-88]

$$Sh = \frac{k_i \cdot \boldsymbol{r_t}}{D_i} = A \cdot Re^b \cdot Sc^c = A \cdot \left(\frac{\rho \cdot \boldsymbol{\omega} \cdot \boldsymbol{r_t^2}}{\mu} \right)^b \cdot \left(\frac{\mu}{\rho \cdot D_i} \right)^c \quad (12)$$

$$Sh = \frac{k_i \cdot \boldsymbol{d_h}}{D_i} = A \cdot Re^b \cdot Sc^c = A \cdot \left(\frac{\rho \cdot \boldsymbol{v} \cdot \boldsymbol{d_h}}{\mu} \right)^b \cdot \left(\frac{\mu}{\rho \cdot D_i} \right)^c \quad (13)$$

where Sh is the Sherwood number, Re is the Reynolds number, Sc is the Schmidt number, ω is the stirring rate, r_t is the radius of the stirred filtration cell in dead-end, v is the cross-flow velocity in cross-flow, d_h is the hydraulic diameter, μ is the dynamic viscosity of the solvent, ρ is the density of the solvent (transport properties of the fluids) and A is a numerical constant characterizing the flow channel geometry.

There is a number of empirical correlations in the literature for both configuration modes and it is assumed that these correlations can provide a reasonable estimation of the mass transfer. The most frequently used correlation in stirred batch cells is the one provided by Colton and Smith:[89]

$$Sh = 0.285 \cdot Re^{0.567} \cdot Sc^{0.33} \quad (14)$$

For the cross-flow mode it is additionally dependent on the spacer geometry and the flow condition (laminar or turbulent flow) thus leading to many different correlations.[86, 88, 90] The calculation of CP and mass transfer coefficient k under the operated conditions in this work is briefly described in chapter 4.7.2.

2.4 Membrane fouling

2.4.1 Introduction

Membrane fouling is a pervasive problem for all pressure-driven membrane processes (MF, UF, NF and RO) across a broad range of water treatment that restricts process efficiency by reducing water flux temporary or permanently, deteriorating product water quality, membrane lifecycle and increasing energy consumption and operational costs.[23, 76, 91]

There is no universally accepted definition for fouling.[5] But generally, fouling is the accumulation of undesired deposits on the membrane surface or inside the membrane pores, causing decrease of flux and salt rejection. It is a complicated phenomenon which involves more than one type of foulant with various surface characteristics, different mechanisms under different circumstances.[47, 92, 93] Fouling is roughly affected by the following factors: [94, 95] feedwater composition (concentration, pH, charge, etc.), process conditions (TMP, flux, etc.) and membrane properties (hydrophobicity, roughness, porosity, etc.) which will be further discussed in chapter 2.5. From the thermodynamic point of view, the driving force for the fouling is the reduction of Gibbs free energy, as foulants, water and membranes are regarded as thermodynamic systems and every system strives to minimize the Gibbs free energy.[96]

As foulants on the membrane surface or within the pores build up, the mass transfer resistance of the membrane to water transport increases and consequently decreases the membrane productivity. Membrane fouling results in a decrease in flux when the system is operated at constant pressure or in an increase in TMP to maintain a particular flux.[97, 98] But it is often characterized in terms of flux decline at a fixed transmembrane pressure, as shown in Figure 12.[99] The only mass transfer resistance to pure water filtration is caused by the membrane itself, called the membrane resistance, which is constant. The extent depends on the membrane thickness and various morphological features such as the tortuosity (which is the ratio of selective pore length to selective layer thickness).

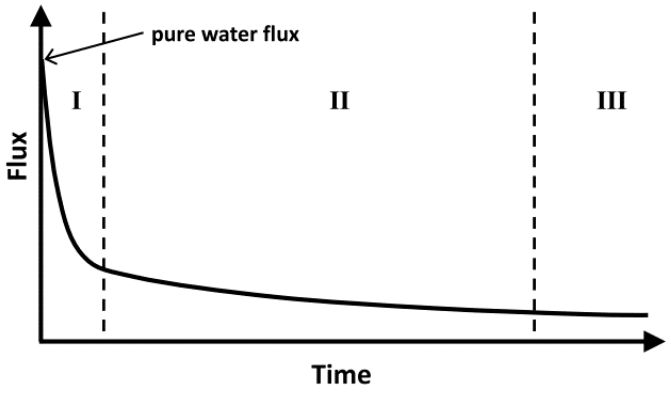

Figure 12: Schematic representation of the three stages of flux decline [99]

If foulants deposit on the membrane surface, an additional resistance arises on water passage, the fouling resistance, which reduces the permeate flux very rapidly (I). Then, the flux typically decreases gradually (II) before a steady state is reached (III).[98] Studies showed that higher initial flux favours more severe membrane fouling as a result of increased permeate drag force, enhanced CP, leading to a denser fouling layer.[10]

Generally, there are two fouling mechanisms in terms of the fouling places that are commonly observed in membrane developments which are fouling at the surface (adsorption, gel and cake formation) and in the pores (pore blockage). As far as RO membranes are concerned, the formation of a fouling layer on the membrane surface is the dominant fouling mechanism due to the dense membrane structure.[100, 101]

Flux decline caused by membrane fouling may be generally classified as reversible or irreversible. Reversible fouling can be easily removed after rinsing or flushing steps. For porous membranes, reversible fouling can be removed by backwashing (does not apply for non-porous membranes such as NF/RO membranes). Irreversible fouling is caused by strongly adhering films on the surface or adhering foulants in the pores and cannot be removed by physical rinsing, due to the interactions between foulants and membrane surfaces but rather by chemical reagents or the membrane has to be replaced.[75, 91] The cleaning frequency is determined by the severity level of fouling which in turn depends on recovery rate of the system, characteristics of feed water and pre-treatment processes.[100]

According to the intrinsic characteristics of foulants, membrane fouling can be classified into four categories: colloidal (particulate) fouling, inorganic fouling (scaling), organic fouling, and biofouling[5, 10, 93] schematically represented in Figure 13. However, organic fouling and

biofouling are in fact two kinds of fouling which are synergistic because biofouling is based on organic fouling and cannot be considered completely independent.[102] Also, most of inorganic fouling (scaling) belongs to colloidal fouling and is mostly discussed in the same context. Also, some high molecular weight organic compounds are also defined partially as colloidal foulants due to many of the same characteristic features.[97, 103] Each of the fouling type will be discussed briefly in the following section.

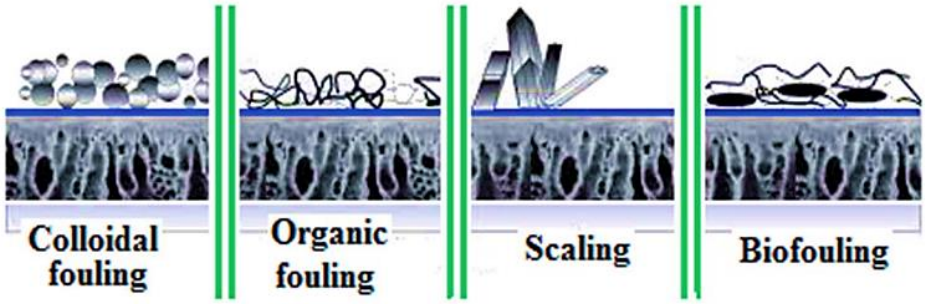

Figure 13: Schematic representation of fouling types: colloidal fouling, organic fouling, scaling and biofouling.[104]

2.4.2 Fouling types

Colloidal fouling

Colloids are fine suspended particles which have been classified by *Rudolfs* and *Balmat* in 1952 in the following categories:[5, 105]

Settleable solids: > 100 µm
Supra colloidal solids: 1 µm to 100 µm
Colloidal solids: 0.001 µm to 1 µm
Dissolved solids: < 10 Å

The behaviour of "real" colloids is determined mainly by their small size (0.001 – 1 µm) making the colloids inherently prone to cause RO membrane fouling whereas particles in the molecular size range can easily diffuse away from the membrane surface via molecular diffusion. Also, larger particles can be removed from the surface via shear-induced diffusion or lateral migration.[76] The common colloidal foulants are silt and clay, precipitated crystals, colloidal silica and sulfur, precipitated iron and aluminium compounds but also polysaccharides, proteins, carbohydrates, fats, oils and greases, and various surfactants as

well as some natural organic matters. These foulants can be divided into two groups, i.e., inorganic foulants and organic macromolecules.[5, 93, 94, 97]

Generally, the mechanisms of membrane fouling by colloids is due to initial pore blockage followed by cake formation. But for non-porous membranes (NF/RO), colloidal fouling is only due to the accumulation of particles on the membrane surface, which results in the formation of a cake layer. Once the cake is formed, the cake layer will control the further transport. Van der Waals forces and electrostatic interactions are the main interactions between the inorganic colloidal foulants and the membrane.[96, 97]

The main transport mechanisms of colloids from the feed bulk to and from the membrane surface are convection, Brownian diffusion, shear-induced diffusion, inertial lift, gravitational settling and lateral migration, which strongly depend on colloid size and concentration. Other important factors influencing the particle fouling are colloid shape, charge and deformability as well as interactions with ions of the colloids and operating parameters such as shear rate and transmembrane pressure (TMP).[97, 106]

Scaling

Inorganic foulants tend to precipitate onto the membrane surface or in the pores when they exceed the equilibrium solubility product and become supersaturated resulting in scaling.[75, 93] The hydrolysis, a pH change or oxidation can accelerate the deposition of inorganic salts during membrane filtration. Inorganic foulants mainly include substances such as calcium sulfate and -carbonate, magnesium carbonate, barium sulfate, silica, aluminium silicate minerals and ferric oxide/hydroxide colloids.[5, 76, 91]

The precipitation mechanism is as follows; first, the nucleation stage is reached by inorganic ions which exceed the equilibrium solubility product and then undergo surface (heterogeneous) or bulk (homogeneous) crystallization. The lateral growth of the scale deposit on the membrane surface is defined as heterogeneous surface crystallization. However, bulk crystallization is the process when crystal particles are formed in the bulk phase through homogeneous crystallization due to convective transportation and deposit on the membrane surface as a scale layer.[76, 93] According to a study heterogeneous surface crystallization is the dominant mechanism in unstirred batch membrane filtration, while for cross-flow operation, both mechanisms play a role in the scale layer formation.[93, 107]

Organic fouling

Organic fouling is caused by organic matter that are typically humic substances, polysaccharides, proteins, carbohydrates, nucleic, amino and organic acids and oils. All these foulants can be classified into two categories: non-migratory foulants and spreadable foulants, according to their typical fouling behaviours, adhesion and spread.[91, 93]

Non-migratory foulants, include organic colloids, dissolved organic matter (DOM) and biomacromolecules that deposit on membrane surfaces by adsorption and form a stable cake layer. DOM can be further classified into two different categories according to their origins: natural organic matter (NOM) derived from drinking water sources such as surface and sea water and synthetic organic compounds (SOC) (or effluent organic matter (EfOM)) added by consumers and disinfection by-products in water and wastewater treatment.[91, 97] The fouling mechanism includes the adsorption on the membrane surface and the formation of a gel or cake layer.[76]

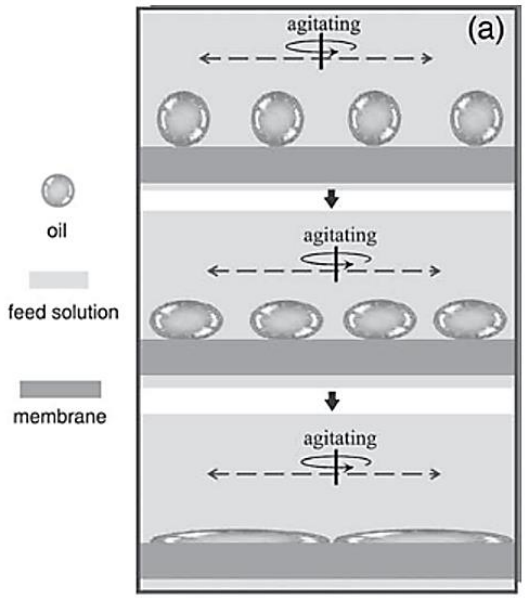

Figure 14: Schematic representation of spreadable foulants such as oil.[108]

Spreadable foulants such as oils do attach, spread and coalesce on the membrane surface forming a continuous oil film. Oil as a typical type of spreadable foulant, appears as free oil, emulsified oil and dissolved oil. Oil is strongly hydrophobic and due to the hydrophobic interactions between oil and the membrane, oil deposits easily onto the membrane surface. It is also much more unstable compared to e.g. proteins, ascribed to easy deformation and coalescence (cf. Figure 14). The concentration of oil and the presence of surfactants can

additionally influence the fouling behaviour by altering the size and charge of oil droplets which are decisive characteristics for the emulsion stability.[91]

Biofouling

Proliferative foulants, also referred to as biofoulants cover two key components; bacteria and the extracellular polymeric substances (EPS) which are developed by bacteria during the metabolism process along with fungi, algae, viruses. The EPS are mainly made up of polysaccharides, proteins, glycoproteins, lipoproteins or lipids and nucleic acids. The biofoulants can adhere to the membranes and cause the formation of a biofilm which is a microbial environment by creating complex layers of these microorganisms integrated in the EPS. Biofouling is inherently more complicated than other membrane fouling types because microorganisms can grow, proliferate and relocate on the membrane surface.[76, 93, 109, 110]

Biofouling is one of the main factors contributing to flux decline and loss of salt rejection of RO membranes. It was shown that a complete coverage of an RO membrane with a biofilm takes about three days.[5] The formation of a biofilm could be generally divided into three phases:[93]

1) Bacteria attachment
2) Reproduction/Proliferation
3) Detachment

The most important stage in biofilm formation is the bacteria attachment which is a dynamic process consisting of bacteria approaching and adhering to the membrane surface. During the reproduction step, the attached microorganisms consume nutrients provided in the water and go through proliferation, excreting EPS and making the biofilm structure stronger and act as a barrier to protect bacteria from biocides. The detachment is the final stage where the bacteria leaves the completed biofilm due to the absence of nutrients. Then, the bacteria colonise new sites repeating the process.[91, 93]

2.5 Combating fouling

Membrane fouling is a ubiquitous problem for all pressure-driven membrane processes across a broad range of water treatment that restricts process efficiency by reducing water flux. It is an inevitable phenomenon that can be minimized but not eliminated as it will always occur to some extent due to Gibbs free energy.[23, 96] Hence, membrane cleaning is a crucial step in order to remove the fouling layer from the membrane surface, to guarantee stable operation of the membrane system and to improve permeate flux and salt rejection.[76] But after a long period of operation and harsh fouling, cleaning may not restore the membrane performance successfully. The time between the cleaning cycles becomes shorter and thus irreversible fouling increases. In order to achieve less cleaning and thus longer membrane lifetime along with reduced operational costs, a variety of fouling control strategies such as optimization of process conditions and module design, feed pre-treatment and manipulation of membrane properties have been studied.[111, 112] These strategies, including membrane cleaning, are briefly described in the following subchapters.

2.5.1 Membrane cleaning

Membrane cleaning has been used extensively to restore fouled membranes. If transmembrane pressure or permeate flow vary between 10 and 15 % with respect to the initial values, then cleaning cycles are recommended to be conducted. The cleaning frequency is also important to a successful operation. It depends on the concentration of existing foulants, varying from weekly to yearly cleaning; too frequent cleaning can stress the membrane tremendously, while infrequent cleaning can lead to irreversible fouling, allowing the accumulation of non-removable foulants on the membranes. Overall operational conditions that can affect cleaning efficiency include cross-flow velocity, cleaning time and temperature.[76, 113] Cleaning procedures for RO membranes can be divided roughly into two main classes: physical and chemical cleaning.[5]

Methods for physical cleaning use mechanical forces to disturb and remove foulants from the membrane surface. In practice, flushing with water is the most frequent method used. These techniques can be quite effective in unblocking large colloidal foulants from certain types of RO modules mechanically due to pressure change causing expansion of the membrane and disturbing accumulated foulants. Additional turbulences cause further disruption of the

boundary layer leading to the detachment of foulants.[5] Physical cleaning can also involve other techniques like sponge ball cleaning, depressurization at high velocities, or osmotic backwashing. However, sponge ball cleaning is limited to the tubular configuration and can be used only in the absence of turbulence promotors like spacers or other internal obstructions.[5, 114]

If the foulant interacts strongly with the membrane, physical cleaning is not sufficient, although it exhibits great promise for the mitigation of foulants. Therefore, chemical cleaning is the most frequent cleaning method, especially for RO membranes by removing impurities by means of chemical agents. The cleaning agents should be able to dissolve the majority of the fouling material from the surface through the reaction with the foulant in order to weaken the cohesion forces between the foulants, and the adhesion between the foulants and the membrane surface making foulants easy to be removed. But it should not damage the membrane, thus maintaining membrane properties. The cleaning agent should also be low in costs, safe to handle, showing the ability to be removed with water. The possible reactions between foulant and cleaning agent are: hydrolysis, peptization, saponification, solubilization, dispersion (suspension), and chelation.[76]

Generally, there are five commonly used chemical agents; acids (nitric, phosphoric, hydrochloric, sulfuric, citric acids), alkali (sodium hydroxide), metal chelating agents, surfactants (surface-active agents, including anionic, cationic, non-ionic, and amphoteric electrolytes) and enzymes. In addition to the five main categories, disinfectants (O_3), oxidants (H_2O_2, $KMnO_4$, sodium hypochlorite), or sequestration agents (EDTA) are often used.[10, 76, 93]

Finding appropriate materials as cleaning agents, depends mainly on membrane material and type of foulant. For example, acids are effective in removing inorganic scale, while alkaline solutions are more effective in removing organic fouling and biofouling by hydrolysis and by enhancing electrostatic interactions between the negatively charged foulants and the membrane surface. Organic foulants can also be removed with detergents or surfactants that solubilize macromolecules by forming micelles around them.[10, 93]

In practice, a combination of chemical and physical cleaning is conducted, where the former contributes to loosening of the foulant layer by a chemical reaction between the foulants in the fouling layer and the cleaning agent while the latter releases the foulants from the membrane surface by shear forces.[115]

2.5.2 Optimization of process conditions and module design

Operational conditions, hydrodynamic parameters and the type of module design can be used in a way that reduces fouling. Operational conditions such as periodic rapid depressurization of the membrane results in osmotic flow from the permeate side to the retentate side, that leads to the floatation of solids away from the membrane surface. It was also reported that periodic reversal of feed flow direction reduces flux decline between cleaning cycles. Changing the flow configuration and doing the filtration in cross-flow mode instead of dead-end can also prevent foulants from attaching on the membrane surface by creating turbulences and eddies.[5]

Hydrodynamic parameters that can be manipulated in order to control fouling are inlet pressure, cross-flow velocity, recovery and temperature. Pressure affects fouling indirectly through an effect on flux rate, thus on concentration polarization. More severe fouling occurs at higher water fluxes because more water permeates through the membrane and at the same time greater amount of foulants are brought towards the membrane surface due to convection. In consequence, the concentration of foulants on the membrane surface increases along with higher adsorption and more severe CP. Further, greater hydrodynamic permeation drag force towards the membrane surface overcomes the opposing electrostatic repulsive force resulting in foulant deposition. In contrast, at low permeate flux, the repulsive electrostatic forces can be high enough to prevent foulant adsorption on the membrane.[76, 91]

Another hydrodynamic factor affecting the membrane fouling is the cross flow velocity over the membrane surface. An increase in cross flow velocity leads to a decrease of the CP by raising the mass transfer and enhancing back-diffusion of foulants, thus mitigating membrane fouling and improving flux behaviour.[116]

Another important physical parameter which can strongly affect membrane fouling is the temperature. This can be expressed in terms of the Schmidt number (Sc = v/D) because a higher temperature leads to a reduction of feed viscosity and an increase of solution diffusion coefficient, leading to an improvement of back diffusion of solutes and consequently to less CP. Therefore, lower values of Sc usually lead to less fouling. But that is dependent on the type of foulant.[10]

Membrane architecture such as module design (e.g., hollow fibre or spiral wound) and assemblies (turbulence promotors, feed spacer, etc.) have been shown to affect fouling.

Turbulence promotors reduce CP and therefore fouling by increasing friction factor and bulk velocity which are commonly used in tubular modules. Usually, they take the form of rigid spherical balls, static mixers and spiral wires. Thin channel systems such as spiral wound modules often employ mechanical spacers which have the same function.[5, 98]

2.5.3 Feed pre-treatment

High-quality feed water is required to ensure reliable RO operation due to fouling propensity of RO membranes. Pre-treatment can reduce fouling potential by removing foulant precursors, altering the physical, chemical, and biological properties of the feed water in order to increase membrane life and maintain performance level. The degree of feedwater pre-treatment used, and the choice of treatment method will depend on type of water source (surface water, brackish water, seawater, and industrial water), feed water characteristics, RO module design, expected recovery rate and tolerated degree and frequency of membrane cleaning.[5, 10]

Pre-treatments can be divided into two groups: conventional pre-treatments and unconventional pre-treatments. Conventional pre-treatments consist of a combination of chemical treatment (disinfectant addition, coagulation, activated carbon adsorption, acid addition and antiscalant addition) and conventional filtration (media and cartridge filtration) to achieve a conditioned feed suitable as RO feed.[76]

In contrast, membrane filtration as unconventional pre-treatment technique, especially UF and MF, is becoming more popular since it could save a lot of space and can be operated on a continuous basis, at higher permeate fluxes and recovery rates compared to conventional treatment technologies while producing higher quality of feed for subsequent RO. Furthermore, UF/MF pre-treatment could be more economical for long-term operation, which is achieved by reducing energy consumption, use of chemicals, cleaning frequencies as well as replacement of the RO. Due to smaller pore sizes than MF membranes and higher fluxes than NF membranes, UF membranes represent a balance between contaminant removal and productivity.[10, 93]

However, the combination of conventional pre-treatment techniques e.g. coagulation and unconventional membrane pre-treatment known as integrated membrane systems (IMS), is

the most efficient since colloids and suspended particles often pass through conventional filtration pre-treatment and can be removed by subsequently installed MF or UF membrane systems while other foulants can be removed through coagulation and thus fouling of subsequent UF/MF will be greatly reduced.[2] Figure 15 shows the flow diagram of a typical RO pre-treatment process that is common in RO plants.[93]

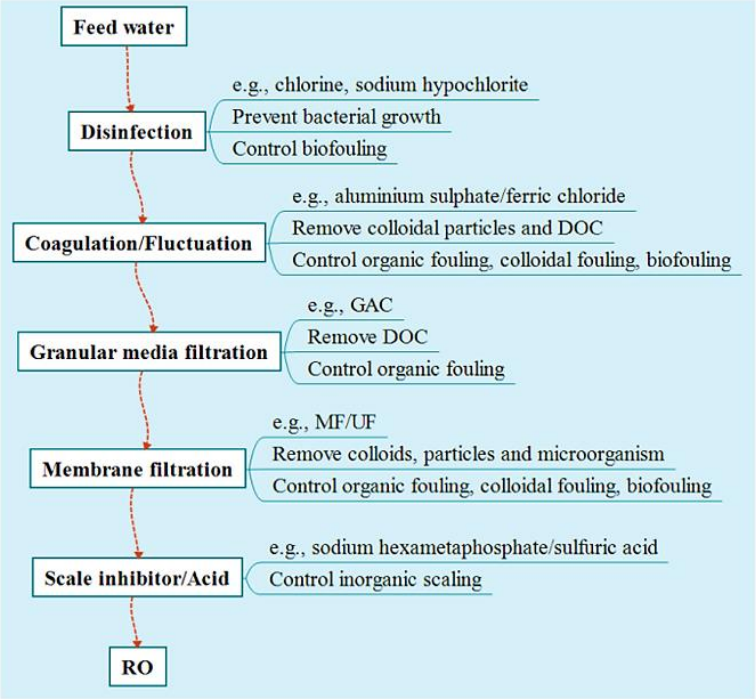

Figure 15: Schematic diagram of an RO pre-treatment process.[93]

2.5.4 Manipulation of membrane properties

In RO membrane filtration systems, fouling is caused by the interaction between the membrane surface and fouling material and depends strongly on membrane surface morphology and physiochemical properties such as hydrophilicity, charge, roughness and surface functional groups, especially interacting with foulants.[10]

One of the most important contributors to fouling in RO membranes is the surface roughness. Membranes with larger surface roughness, such as MPD-based PA TFC membranes, have higher fouling tendency, because of the increased total surface area which is in contact with the fouling material and because foulants can accumulate in valleys, shielding the foulant from cross-flow shear forces that normally act to remove the foulants. Additionally, increased roughness may lead to uneven boundary layer or flow distribution over the surface.[91, 98]

An important consideration for the reduction of membrane fouling is the electrostatic charge of the membrane. The reduction of foulant deposition onto the membrane can be achieved when the surface and the foulant have the same charge due to electrostatic repulsion forces between the foulants and the membrane. Thin film composite RO and NF membranes have ionizable groups in the polyamide layer and exhibit a negative surface charge under typical operating pH conditions (> pH 4 to 5). Enhancing the negative charge of such a membrane surface would increase electrostatic repulsion of anionic foulants and decrease the deposition of such compounds. Since most of the proteins are negatively charged under such conditions, a negative surface charge of the membrane has a beneficial effect on protein separation at neutral pH. Also, most of the colloidal particles such as NOM are negatively charged. However, not all foulants are negatively charged. Existing negatively charged NOM and metal cations can form insoluble complexes, depositing on the membrane surface.[76, 117]

After all, it is accepted and already demonstrated that membranes with smooth and hydrophilic surface with similar charge to the foulant seem to possess better anti-fouling property. Therefore, a great deal of research efforts has been devoted to the development of robust antifouling membranes to induce these characteristics leading to fouling-resistant membranes.[10, 101]

There are several ways to increase membrane surface smoothness as well as hydrophilic property, such as modification of PA during IP, incorporation of novel materials and surface modification.[118, 119] Surface modification with novel materials which is a promising field used to reduce membrane fouling will be discussed in detail in the next chapter 2.6. The modification of the PA layer during IP is not included in the following discussion. The following chapter is about physical and chemical surface post-modification of polyamide TFC RO membranes after synthesis of them.

2.6 Membrane modification

2.6.1 Modification types

Virtually all types of fouling are caused or at least initiated by foulant adsorption. Therefore, passive antifouling strategies intent to prevent the initial adsorption of foulants on the membrane surface without affecting the intrinsic features of the foulants. Thus, relying on manipulating the physicochemical and topological structures of the membrane surface in order to weaken the interactions between membrane and foulants. Whereas active strategies intent to eliminate proliferative fouling by destroying the chemical structure and inactivating the cells.[91] But the focus in the following discussion will be on passive strategies.

Passive antifouling strategies can be further classified into fouling-resistant and fouling-release strategies, cf. Figure 16. The prevention of the adsorption of foulants onto the membrane surface is the main target of fouling-resistant strategies whereas fouling-release strategies intent to drive the attached foulants away from the membrane surface by low shear forces. The incorporation of both, fouling-resistant and fouling-release domains leads to amphiphilic membranes.[91]

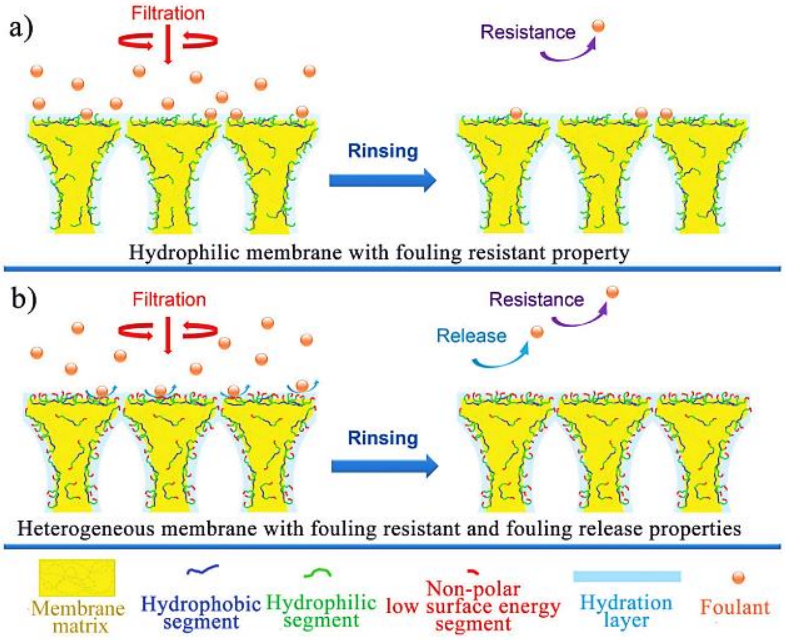

Figure 16: Schematic representation of fouling types: **(a)** hydrophilic fouling-resistant domains and **(b)** fouling-resistant and fouling-release domains.[91]

Hydrophilic approach

The repulsion of water molecules away from the hydrophobic membrane surface is a spontaneous process with increasing entropy while the foulant molecules tend to adsorb onto the membrane surface, dominating the boundary layer. Lack of hydrogen bonding interactions in the boundary layer between the membrane interface and water is the major reason for hydrophobic membrane fouling.[76] Most of the commercial membranes such as polyvinylidenefluoride (PVDF), polyethersulfone (PES), polysulfone (PS), polypropylene (PP), polyacrylonitrile (PAN) polyamide (PA) and polyethylene (PE) are made from hydrophobic polymers with high chemical, mechanical and thermal stability making these membranes prone to adsorption of various substances.[117]

Therefore, membranes possess better antifouling properties if they have smooth and hydrophilic surfaces with same charge to the foulant. Furthermore, hydrophilic functional groups that were hydrogen bond acceptors but not hydrogen bond donors and that were electrically neutral were most fouling-resistant because protein, microorganisms, and many other foulants are hydrophobic in nature.[98, 101]

The main target of a hydrophilic surface structure is to inhibit the interactions between membrane and fouling material and prevent the attachment of foulants onto the membrane surface, known as fouling-resistant approach. Hydrophilic surfaces are hypothesized to form the hydrogen bonds with surrounding water molecules to form a thin water boundary layer between the membrane and feed solution having a high surface tension. This makes it difficult for hydrophobic solutes to access the water boundary and break the orderly structure because energy would be required to remove the water layer. In this way, hydrophobic-hydrophobic forces between membrane and foulant are mitigated.[76, 91]

Additionally, surface-bound long-chain hydrophilic polymers were very effective in preventing adsorption of macromolecules onto the membrane surface due to the steric repulsion mechanism because adsorption of foulants (e.g., proteins) leads to a restriction of free mobility of the polymer due to compression of the extended polymer structure. This will create entropy loss, making the protein adsorption entropically unfavourable. Some of the most widely used antifouling materials are poly(ethylene glycol) (PEG)-based, zwitterionic, glycomimetic, and peptidomimetic polymers.[91, 101, 108]

Hydrophobic approach

Even though hydrophilic membrane surfaces are able to resist fouling caused by spreadable foulants, foulants such as oils, are prone to coalesce, spread and migrate to form a continuous fouling layer on the surface. Thus, spreadable fouling cannot be simply mitigated by hydrophilic modification. Therefore, a novel strategy of developing fouling release membrane surfaces has been proposed by constructing surfaces with non-polar low surface energy segments. The concept of fouling release was originally adapted from coatings against marine fouling inspired by natural lotus wax, a self-cleaning surface with low surface-energy, suggesting that the fouling release property of surfaces is most directly affected by the critical surface energy as well as wettability.[91]

Non-polar low surface energy segments, such as fluorine-containing segments and silicone-segments can equip the surface with a permanent fouling release ability. Fluorinated polymeric materials have unique properties, such as excellent chemical/thermal stability in diverse environments, superior weathering resistance, high hydrophobicity/oleophobicity. Rather than preventing foulants from adhering onto the surface, this strategy strives to weaken the interfacial bonds between foulants and membrane so that attached foulants are easier to remove from the surfaces at low hydrodynamic shear forces, known as fouling-release approach.[91, 108]

Amphiphilic approach

In many applications, either fouling-resistant nor fouling-release domains are not sufficient to generate membranes with excellent performances since membrane fouling is often caused by various foulants leading to different fouling types. Therefore, the coexistence of hydrophilic and non-polar hydrophobic domains leading to amphiphilic surfaces, is essential for constructing a substantial antifouling membrane surface. Wooley and co-workers have initiated the preparation of amphiphilic copolymer coatings by in situ phase separation and cross-linking of hyper-branched fluoropolymers (HBFP) and linear PEG networks.[91, 120, 121]

In the dynamic operation, the hydrophilic domains form a compact hydration layer, hindering the non-specific interactions between the fouling material and membrane surface while ensuring a high water permeation. The non-polar hydrophobic microdomains with intrinsic low surface energy inhibit the migration, spreading and coalescence of the oil droplets, or in

case of bioactive substances, impede the accumulation of proteins or bacteria. Moderate shear forces remove the oil droplets or bio-foulants from surface and drive them back to the feed bulk solution.[108] A variety of amphiphilic copolymers consisting of hydrophilic segments (e.g., PEG, polyzwitterions) and non-polar, low surface energy segments (e.g., fluorinated or silicon-based domains) have been explored as amphiphilic antifouling coatings.[91]

2.6.2 Modification methods

Generally, surface modification of polyamide TFC RO membranes can be conducted via physical or chemical techniques. In physical modification, the material interacts with the PA layer of RO membranes and attach onto the surface by van der Waals interactions, hydrogen bonding, or electrostatic interactions. The coating process is usually done by immersion into a coating solution followed by the removal of residual solvent by evaporation at certain temperature to construct the coating layer. As a result, these modifications are easier to apply to flat-sheet membranes than to membrane modules due to their complex configurations.[100]

Membrane modification by chemical means can be done through surface grafting, divided in grafting-to and grafting-from, which is one of the favourable methods to alter membrane surface. Here, the materials are connected to the surface of RO membranes by covalent bonds and have a better chemical and structural stability. The grafting-to method includes grafting the already formed polymers onto the membrane with binding or coupling sites, while the grafting-from technique includes a surface-initiated polymerization process in which the polymer chains grow on the membrane surface from functional monomers.[91, 122]

Here again, the application of both techniques, grafting-to and grafting-from is limited because many membranes (e.g., PVDF, PSf and PES) do not have sufficient functional groups for surface polymerization with antifouling monomers and have to be pre-functionalized to introduce the reactive sites. Therefore, various techniques such as UV irradiation or plasma treatment are essential to functionalize the membrane surface before the surface grafting process which limit its industrial application to membrane modules.[91]

Due to the mentioned problems, it is not surprising that most reports on surface modifications are focusing on flat-sheet membranes conducted in laboratory scales, rather than focalizing the scale-up of the modification to membrane modules in industrial scale.

A promising method overcoming the existing problems, is the in situ coating of membranes during filtration where the barrier properties of the membrane are utilized allowing the selective modification of membranes in modules. The in situ formation of polydopamine-based layers is a typical example where ultra-thin layers (< 10 nm) are obtained by chemical reaction leading to the deposition of a firmly adhering material.[98] The layer-by-layer technique (LbL) also enables a gradual build-up of a coating with thicknesses ranging from 10 to 100 nm but only limited to polyelectrolytes.[123]

A novel and promising surface-selective coating was developed by *Quillitzsch et al.* in which a thin polyzwitterionic hydrogel could be obtained by in situ cross-linking copolymerization. For this purpose, a special initiator system was developed with a novel macromolecular co-initiator, adsorbing on the surface of UF membranes and causing the decomposition of ammonium persulfate (APS), whereby initiator radicals only form on the membrane surface-selectively. The modification is carried out in two steps; i) surface-selective adsorption of macromolecular co-initiator which is retained by the separation layer of the membrane, ii) contact with a solution containing the monomers and APS. Also, the application on Inge Multibore PES capillary membranes leading to improved organic fouling resistance was demonstrated.[124]

Another important approach is the in situ concentration polarization-enhanced polymerization first proposed by *Freger et al*. At a critical filtration rate, the CP leads to the surpass of the critical concentration of reactants in the boundary layer near the membrane surface which is needed for the polymerization.[125] By using this relation, a radical graft copolymerization was triggered onto the membrane surface for a monomer mixture during the filtration process. Furthermore, the transfer to spiral-wound modules was demonstrated but with focus on boron rejection through defect blocking rather than membrane fouling.[11, 13]

The click chemistry, as another important in situ modification method; it refers to selective reactions for the synthesis of combinatorial libraries and modular platforms through the combination of different building blocks by heteroatom links (C-X-C), first defined by Sharpless and co-workers. [126, 127] The click chemistry has drawn increasing attention in membrane field since Kang *et al.* synthesized PVDF graft copolymers via click azide-alkyne cycloaddition reaction.[128] Compared with conventional chemical membrane modification techniques, click chemistry provides a more accurate and controllable modular platform, performed under

extremely mild conditions with the advantages of high yields and the use of environmentally friendly solvents allowing the scale-up of the modification to membrane modules in industrial scale.[126]

2.6.3 Zwitterionic hydrogels as novel materials for surface modification

Over recent years, zwitterionic polymers as a new type of fouling-resistant material have attracted increasing attention because of their formidable antifouling properties towards non-migratory foulants such as proteins and bacteria. Zwitterionic materials are biologically inspired by zwitterionic phosphatidylcholine (PC) headgroups available in phospholipid bi-layer of cell membranes. They possess both anionic and cationic groups leading to overall charge neutrality.

The cationic group generally consists of a quaternary ammonium while the anionic groups can consist of phosphate, carboxylate or sulfonate. According to whether the charged groups are located on the side chain of the same or different monomer unit, zwitterionic polymers can be classified into polybetaines and polyampholytes. Typical polybetaines are poly (2-methacryloyloxyethyl phosphorylcholine) (PMPC), poly(carboxybetaine methacrylate) (PCBMA) and poly (sulfobetaine methacrylate) (PSBMA), illustrated in Figure 17.

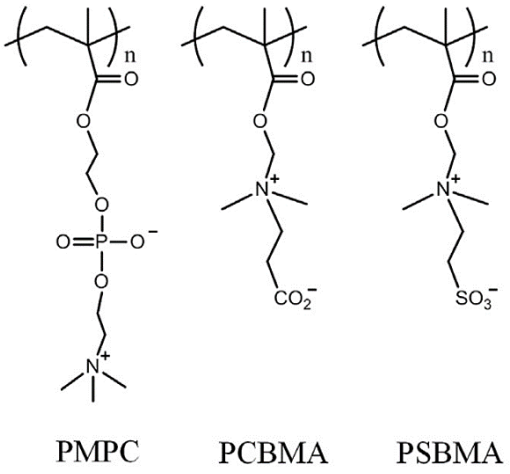

Figure 17: Representative structures of zwitterions: PMPC, PCBMA, PSBMA.[96]

Due to equally balanced cationic and anionic groups, zwitterionic polymers have a total neutral charge, whereas polyelectrolyte polymers always possess a net charge. Additionally, self-association of zwitterionic polymers exists as a result of the formation of ion pairs between intra- and inter-zwitterionic groups as can be seen from Figure 18.

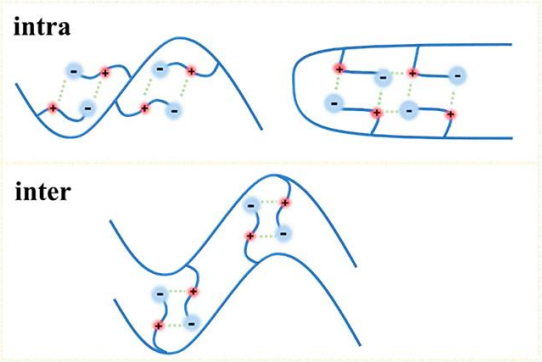

Figure 18: Different interaction modes between polymeric zwitterions.[129]

This leads to the anti-polyelectrolyte behaviour of zwitterionic polymers. That means, that zwitterionic polymer chains shrink in water but expand in salt solution, making them to have a higher solubility in salt solution than in pure water because the addition of salts screen out intra- and inter-zwitterionic electrostatic interactions by breaking ionic pairs and causing the dissociation and extension of these polymer chains (cf. Figure 19). However, the extent of chain conformation changes and associations for zwitterionic polymers strongly depend on charge distribution and ionic strength.[129]

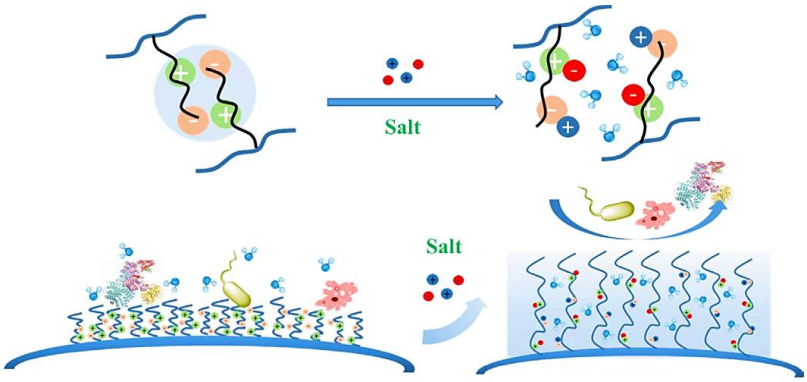

Figure 19: Anti-polyelectrolyte effect of zwitterionic polymers and antifouling property in response to salt.[129]

There are two major antifouling mechanisms for zwitterionic polymers. The first antifouling mechanism is strongly linked to the formation of a hydration layer near the surface. More precisely, water is attached to hydrophilic materials through hydrogen bonding, while it binds to zwitterionic materials through ionic solvation. Accordingly, higher energy is required to remove water from zwitterionic polymers compared to other hydrophilic materials.[76] The hydration shell formed by zwitterionic polymers is denser and thicker compared with PEG and its derivates since zwitterionic molecule chains consist of equally charged units. Therefore, each unit carries a positive and negative charged group, integrated with at most eight water

molecules via electrostatic interactions, while PEG molecular chains consist of repeat units -CH_2CH_2O-. And each unit carries an oxygen atom integrated with one water molecule via hydrogen bonding interactions, as can be seen from Figure 20. Additionally, the dipole array of water molecules in the hydration shell formed via electrostatic interactions with zwitterions, is closer to free water, which means that zwitterionic materials possess superior antifouling properties compared to PEG-based materials towards biological macromolecule foulants and are more biocompatible.[76, 96]

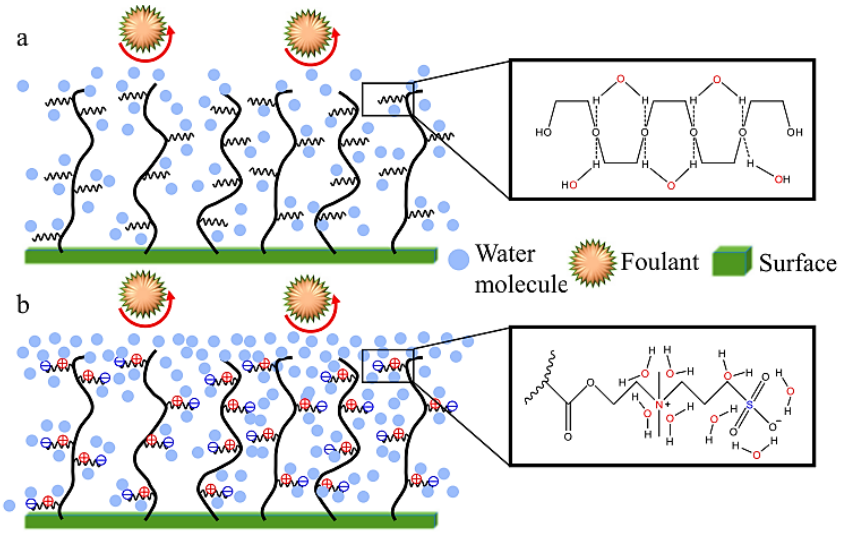

Figure 20: Schematic illustration of the formation of hydration shell. **(a)** Each unit of PEG material is integrated with one water molecule. **(b)** Each unit of zwitterionic material is integrated with eight water molecules.[96]

The second mechanism is the steric hindrance effect which is the same as for other hydrophilic polymers and was already discussed in 2.6.1. Carboxybetaine (CB) and sulfobetaine (SB) are the two most frequently used zwitterionic moieties for (co)polymerization. These membranes were found to be exceptionally resistant to fouling.[5, 129]

So, one can conclude, that the density and thickness of hydration shell, along with steric hindrance is strongly linked to the density and charge distribution of zwitterionic materials which is the unique characteristic compared to other hydrophilic materials.[96]

By combining zwitterionic properties with hydrogels, a novel type of antifouling material can be obtained. Hydrogels are three-dimensional cross-linked polymers whose hydrophilic structure enables them to take up water in their networks to a multitude of their own mass without dissolving. That means, that hydrogels swell in water and collapse when dried. Different types of cross-linking and interactions in the network along with high molecular weight and low mobility of the polymers are the reasons why hydrogels remain water-

insoluble and thus do not change their composition.[130, 131] Physical cross-linking includes entanglements and junction while chemical cross-linking includes covalent links, as can be seen from Figure 21.[132] The mesh size ξ is defined as the distance between two crossing points.

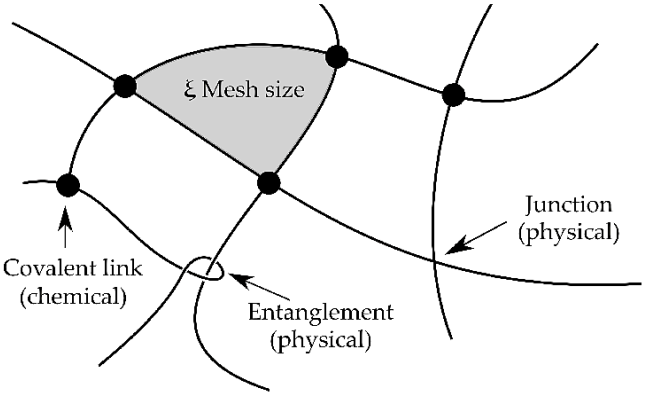

Figure 21: Schematic of cross-links and mesh-size in a hydrogel network.[132]

Due to a high mechanical stability combined with a low hydraulic resistance, hydrogels are particularly attractive as membrane coatings. Ideally, the flux of such membranes is hardly reduced compared to unmodified membranes.[133]

Zwitterionic hydrogels are usually incorporated onto membrane surfaces through free radical polymerization due carbon-carbon double bonds existing in their corresponding monomers.[96] A more promising method is the thiol-based addition to carbon-carbon multiple bonds which is a typical kind of click reaction. The well-known *thiol-ene* Michael addition,[134] as a specific base-catalyzed click reaction between a thiol and an alkene to form a thioether under relatively facile reaction conditions, has been successfully employed by numerous researchers and is also used in this work. As depicted in Figure 22, the reaction path is as follows: First, a proton from the thiol is abstracted to generate a thiolate anion and the corresponding conjugate acid. In turn, the thiolate anion, as a strong nucleophile, initiates the addition of the anion across the electron-deficient beta-carbon of the *ene* group forming an intermediate carbon-centered anion. This acts as a strong base and abstracts a hydrogen from the conjugate acid to finally form the thioether. [134]

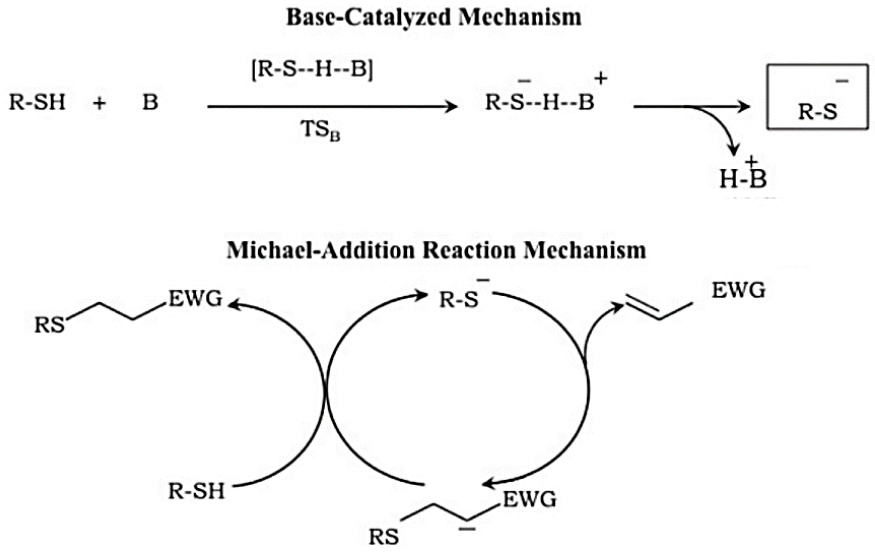

Figure 22: Reaction pathway of the base-catalyzed thiol-ene Michael addition.[134]

Thus, the *thiol-ene* Michael addition click reaction can be effectively used to modify and alter membrane surfaces with tailor-made homogenous and thin polyzwitterionic hydrogel networks, in which the structure and architecture is freely selectable, possessing excellent antifouling properties.

3 Scope of the work

3.1 Concept

Although vast research efforts have been undertaken to control fouling, it remains a challenge in membrane filtration processes, especially due to lack of simple but scalable surface modifications. Therefore, it is still significant to develop RO membranes with good anti-fouling properties with consistent water flux and salt rejection by simple surface modification techniques. The combination of click chemistry with the innovative approach of CP-enhanced in situ reaction, is a promising novel modification method to provide RO membranes with antifouling properties that can be defined much more flexible.

Thus, the main objective of this work is the development of a polyzwitterionic anti-fouling hydrogel coating for RO TFC membranes by CP-enhanced in situ thiol-based click reaction. The coating is carried out under filtration conditions where the barrier properties of the membrane are utilized allowing the selective modification of membranes. The main idea is to exploit the arising concentration polarization during filtration so that the critical reactant concentration (c_{crit}), to trigger the reaction of a two-component system, is reached on the membrane surface yielding a hydrogel layer with anti-fouling properties. By this, the applicability in ready to use membrane elements is enabled, schematically illustrated in Figure 23.

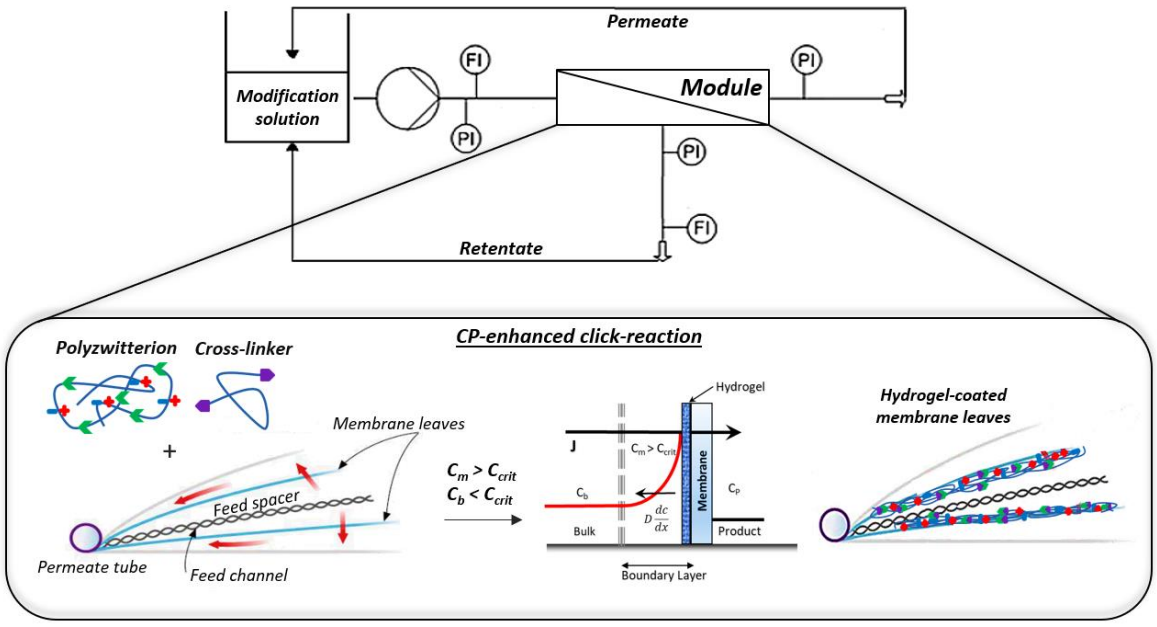

Figure 23: Schematic illustration of the in situ concentration polarization-enhanced click reaction applied to modules.

The two-component system consists of a self-synthesized zwitterionic copolymer with a second functionality (methacryl as *ene* group) that reacts in situ with the cross-linker DTT having a complementary reactivity (*thiol* group) in a *thiol-ene* Michael addition click reaction, depicted in Figure 24.

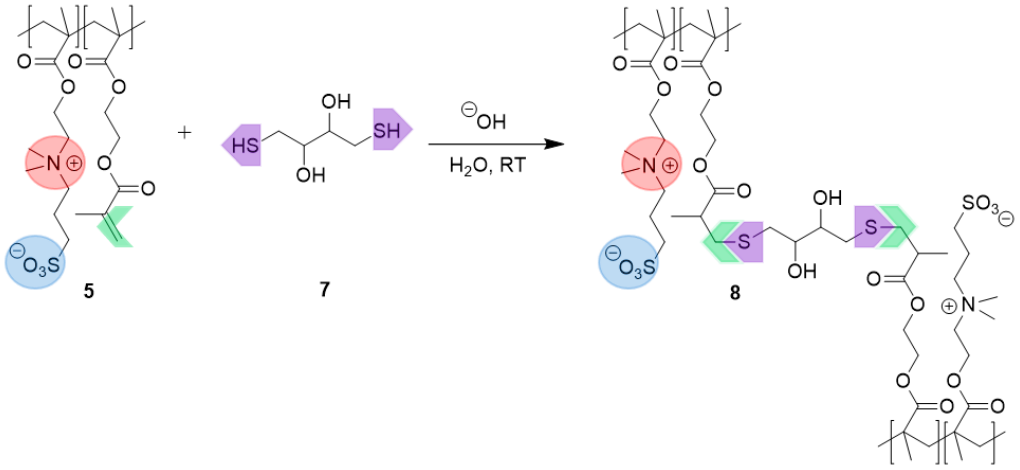

Figure 24: Reaction of the zwitterionic copolymer PSBMA-*co*-PMAEMA with DTT to a hydrogel.

The synthesis of the zwitterionic copolymer is based on preliminary works for the development of a modular platform for polymer systems and established methods for their preparation.[135] The synthesis generally takes place in three steps, according to Figure 25:

- Copolymerization
- Polymer-analogues functionalization for the introduction of **cross-linkable groups**
- Polymer-analogous functionalization for the introduction of **zwitterionic groups**

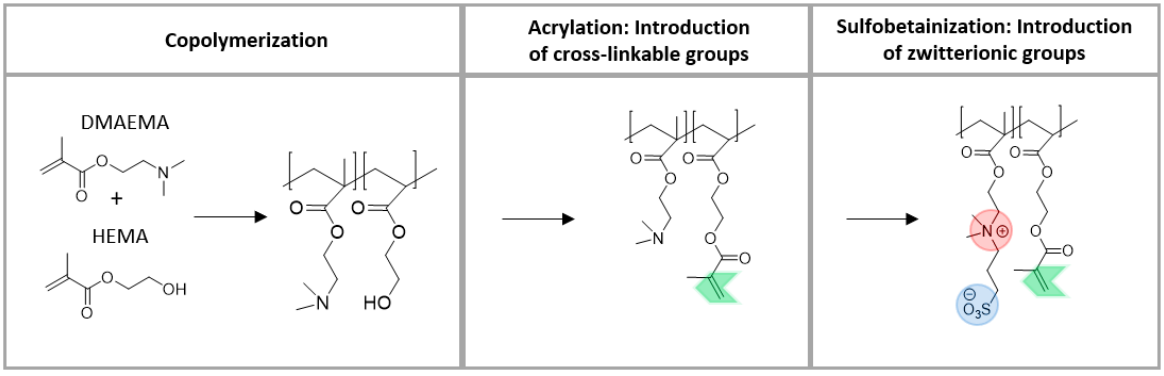

Figure 25: Overview of the synthesis platform.

Since RO TFC membranes are negatively charged due to carboxylic groups in the PA layer, a cationic surface linker is required, cf. Figure 26. The linker acts as adhesion promoter by adsorbing onto the membrane via electrostatic interactions (polyvalent ionic bonding onto

the membrane), enabling the click reaction with the hydrogel. The cationic surface linker is obtained from slight variations of the above-mentioned synthesis; DMAEMA and HEMA are functionalized only up to the second stage (acrylation), followed by quaternization of the amino group.

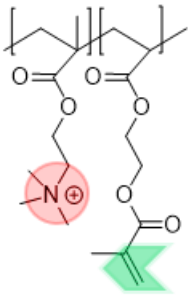

Figure 26: Structure of cationic surface linker PTMAEMA-co-PMAEMA.

3.2 Aims

The main objectives of this dissertation are as follows:

1. Critical evaluation of the separation performance of established membranes by analyzing fouling with real cooling water

a) Membrane pre-screening of commercial RO TFC membranes by analysis of membrane performance and characterization of membrane surface
b) Analysis of fouling potential of real cooling water (fouling prediction, short-term and long-term experiments, critical flux measurements)

2. Development of an in situ modification for RO flat-sheet membranes in dead-end

a) Synthesis and characterization of polymeric building blocks used for hydrogel coating of RO membranes
b) Analysis of critical concentration and free bulk gelation kinetics for “click” cross-linking as well as mechanical properties via in situ rheology
c) Identification of influencing parameters and successful modification conditions for in situ CP-enhanced hydrogel coating method and analysis of antifouling properties of coated membranes towards real cooling water and oil emulsions
d) Variation and influence of filtration parameters in order to control hydrogel formation and estimation of CPM during modification

e) Stability test of hydrogel-coated membranes under acid, basic and enzymatic cleaning conditions

3. Transfer of modification in dead-end to flat-sheet membranes in cross-flow mode

a) Analysis of the influences of cross-flow velocity and filtration rate on modification degree
b) Evaluation of antifouling properties of hydrogel-coated membranes towards oil emulsion

4. Up-scaling of modification to spiral-wound RO modules and pilot scale tests

a) Modification of a small TW30-2521 module
b) Destructive opening of coated module to evaluate the success of modification
c) Modification of two BW30-4040 modules
d) Implementation of coated modules into a cooling circuit of the steel industry, performance of pilot scale tests and autopsy of the elements after field tests

3.3 Work plan

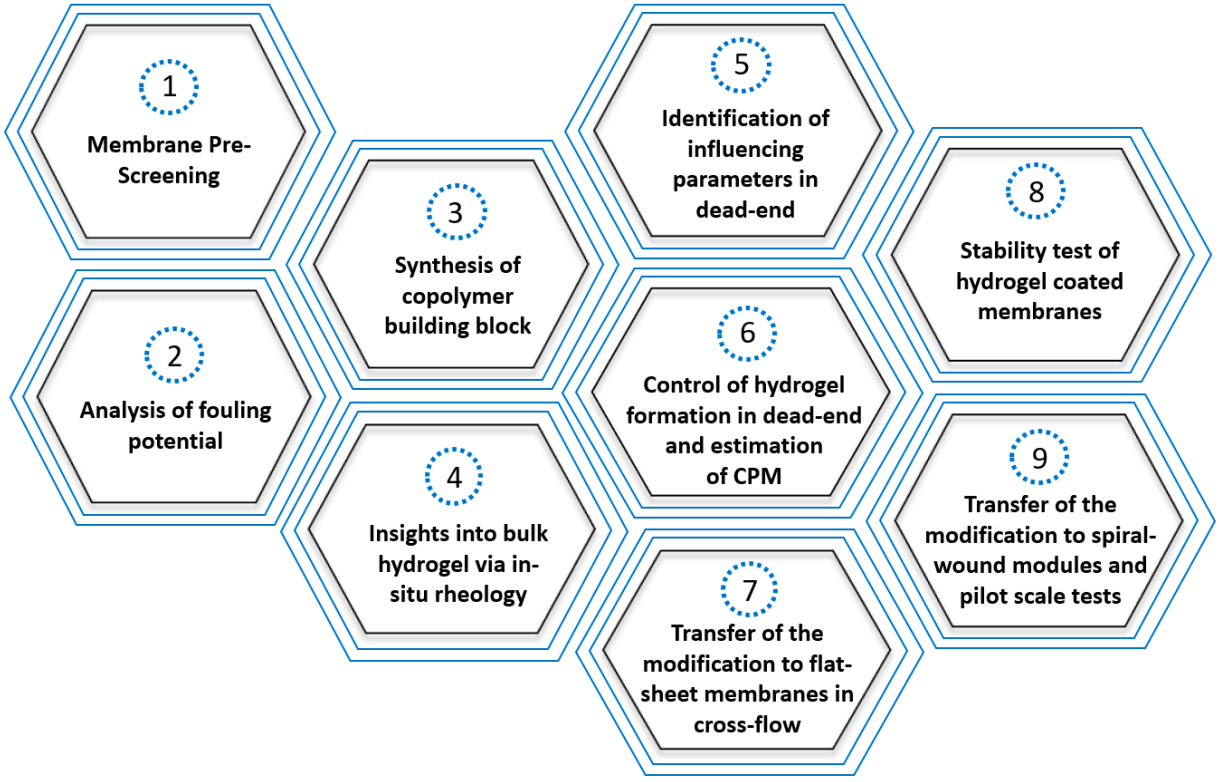

Figure 27: Representation of all work packages.

The results in this thesis are presented in nine chapters according to the work packages in Figure 27. Note: Since the whole work was part of a project and tied to the projects´ time schedule, the modification of spiral-wound modules had to be prioritized very soon. Therefore, the transfer to the modules and pilot scale tests ⑨ were brought forward and done before transferring the modification to flat-sheet membranes in cross-flow ⑦.

In the first chapter different commercially available reverse osmosis membranes (application: industry and sea water desalination) were purchased and investigated. A screening was carried out to evaluate the suitability of these membranes. First, the membranes were examined with regard to membrane performance (permeance and rejection). Structure characterization was completed by ATR-FTIR, zeta, contact angle and SEM measurements. In the second chapter fouling analysis was done by analyzing the feed composition. The critical indicators for scaling, particle and organic fouling were investigated in order to predict the fouling type. Subsequently, filtration experiments were performed by concentrating real cooling water from steel industry. The decline in flux was measured and the fouled membrane surfaces were examined in detail by means of SEM, ATR-FTIR, zeta, contact angle and EDX measurements. Long-term stability and critical flux were also analyzed in cross-flow experiments.

In the third chapter, the synthesized zwitterionic cross-linkable copolymer was characterized. First, composition and chemical structure were investigated via NMR spectroscopy. Molecular weight was determined via SEC and hydrodynamic size was obtained by means of DLS measurements. Finally, viscosity and overlap concentration were examined by rheological investigation of variously concentrated polymer solutions. In the fourth chapter, the cross-linking of zwitterionic copolymer with cross-linker 1,4-dithiothreitol (DTT) via thiol-ene Michael addition click reaction was first studied in the bulk via in situ rheology. The gelation and complete gelation time was determined in dependence of polymer concentration, pH and acrylate/cross-linker ratio. From these experiments, the optimal conditions (pH and acrylate/cross-linker ratio), the reactants´ critical concentration and mechanical properties (storage modulus and damping factor) were identified. These results were aimed to serve as basis for the modification experiments in chapter six.

In the fifth chapter, the in situ cross-linking reaction of the zwitterionic copolymer with DTT during dead-end filtration was examined. Experiments were done without stirring, at different

stirring rates and polymer concentrations in order to gain an elementary understanding for the hydrogel formation. By this, influencing parameters and modification conditions should be identified. Antifouling properties of hydrogel-coated membranes were then analyzed towards real cooling water from steel industry and synthetic oil/water emulsions. In the sixth chapter, a deeper analysis of different influencing parameters on the hydrogel formation was done by doing experiments first at different filtration rates and defined modification conditions. Through suitable combination of composition of solution and filtration rate, the local surface concentration c_m could be increased to exceed the reactants´ critical concentration. The concentration polarization modulus (CPM) and the membrane surface concentration c_m during modification were estimated via film model. After that, experiments were carried out at a constant filtration rate (above critical concentration) at different filtration times in order to adjust the hydrogel thickness. The results were then compared to the rheological data. Membranes that show change in performance were additionally characterized by ATR-FTIR, zeta, SEM and AFM measurements.

It was also of great interest to transfer the modification from vertical filtration in dead-end to the case of narrow filtration channels with spacers, operated in cross-flow mode which are representative for conditions in spiral wound membrane modules. Therefore, in chapter seven optimal conditions from dead-end modification experiments (obtained in chapter six) leading to a coating with good antifouling properties were transferred and optimized to flat-sheet membranes in cross-flow mode. Different cross-flow velocities and filtration rates were tested along with stability tests and recycling of the modification solution. Again, membranes showing change in performance were analyzed by ATR-FTIR, zeta and SEM measurements. Finally, the antifouling properties of hydrogel-coated membranes were investigated in comparison to unmodified ones by performing fouling experiments with crude oil emulsions.

In the eighth chapter, the stability of hydrogel-coated RO membranes (low and high degree of modification) was investigated under cleaning conditions in dead-end mode (acid, basic, enzymatic cleaning) specified by the membranes´ manufacturer. The removal of coating was evaluated primarily based on the flux recovery and a mass balance via TOC measurement. Finally, membranes were additionally characterized by ATR-FTIR and SEM measurements.

In chapter nine, suitable conditions from dead-end modification experiments (obtained in chapter five) leading to a coating with low flux loss and good antifouling properties were

transferred and upscaled to spiral wound modules in two steps. First, a small module (TW30-2521) was modified, followed by the modification of a bigger module (BW30-4040). After the modification of TW30-2521, a destructive opening was carried out to evaluate the success of the modification by means of SEM, ATR-FTIR and XPS measurements. After modifying the modules BW30-4040, they were implemented in a cooling circuit of the steel industry in which pilot scale tests were performed. Subsequently, a membrane module autopsy was carried out via deposit and membrane analysis in order to evaluate the occurring fouling during field tests.

4 Experimental

4.1 Materials

4.1.1 Flat-sheet membranes and spiral-wound modules

Note: Unless otherwise stated, water refers to ultrapure Milli-Q water produced using the Millipore RO system.

One target of this work was to evaluate the separation performance of different flat-sheet membranes and to identify suitable conditions for the modification of selected ones. For these purposes, the following flat-sheet RO membranes were used:

- RO98pHt (Alfa Laval) – Industrial wastewater
- BW30 (Dow Filmtec) – Brackish water
- Lewabrane (Lanxess) – Sea- and brackish water
- AK (GE Osmonics) – Brackish water
- SE (GE Osmonics) – Industrial wastewater
- CE (GE Osmonics) – Brackish water

All these membranes are thin-film composite polyamide (TFC PA) membranes with the exception of CE from GE Osmonics which is a cellulose acetate membrane. The PA membranes consists of an approx. 100 nm thick PA layer, which acts as a separation layer. The separation layer is supported by an asymmetric microporous mostly polysulfone layer and a non-woven reinforcing fabric which provides the membrane with mechanical stability. PA membranes are stable against organic solvents and can be applied in a wide pH range (3 - 11). The disadvantage of PA membranes is the low chemical chlorine resistance as amide nitrogen and aromatic rings of the PA are highly sensitive to free chlorine and can be easily attacked by it.[28, 76]

The ultimate goal of this work was to transfer the modification to spiral-wound elements. For the transfer from flat-sheet membranes to modules, it is important to scale-up the process in two steps. For that purpose, two spiral-wound elements of different sizes were used; one smaller module TW30-2521 and a larger module BW30-4040 from Dow Filmtec. The element characteristics are summarized below.

Table 3: Element specification of the modified modules.

Characteristics	Dow Filmtec TW30-2521	Dow Filmtec BW30-4040
Active membrane area [m^2]	**1.2**	**7.2**
Thickness of spacer [mm]	0.71 (28 mil)	0.86 (34 mil)
Applied pressure [bar]	15.5	15.5
Permeate flow [L/h]	51	379
Salt (NaCl) rejection [%]	99.5	99.5

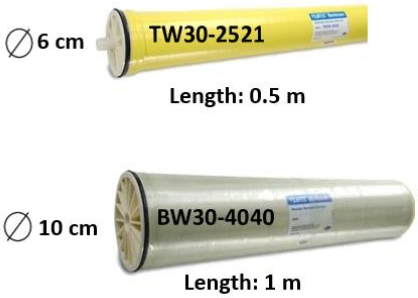

4.1.2 Materials used for hydrogel coating

The following table lists all chemicals used for the hydrogel coating.

Table 4: List of used chemicals.

Chemicals	Company
Azobis(isobutyronitrile) (AIBN)	Sigma-Aldrich
Chloroform	Fisher Chemicals
Deuterated water (D2O)	Deutero GmbH
1,4-Dithiothreitol (DTT)	TCI Chemicals
2-(Dimethylamino)ethylmethacrylat (DMAEMA)	Sigma-Aldrich
Diethyl ether	Fisher Chemicals
Ethanol	Fisher Chemicals
2-(Hydroxyethyl)methacrylate (HEMA)	Sigma-Aldrich
Inhibitor-Remover	Sigma-Aldrich
Iodomethane	Sigma-Aldrich
Isopropanol	Fisher Chemicals
Potassium chloride (KCl)	Bernd Kraft
Potassium hydroxide (KOH)	Bernd Kraft
Methacryloylchloride (MAC)	Sigma-Aldrich
Sodium chloride (NaCl)	Bernd Kraft
1 M Sodium hydroxide (NaOH)	Bernd Kraft
Hydrochloric acid	Bernd Kraft
1,3-Propanesultone	Sigma-Aldrich
Sodiumlaurylsulfate (SDS)	Sigma-Aldrich
Triethylamine (TEA)	Sigma-Aldrich
Tetrahydrofuran (THF)	Fisher Chemicals

4.2 Synthesis of zwitterionic copolymer and cationic surface linker

4.2.1 Free radical copolymerization

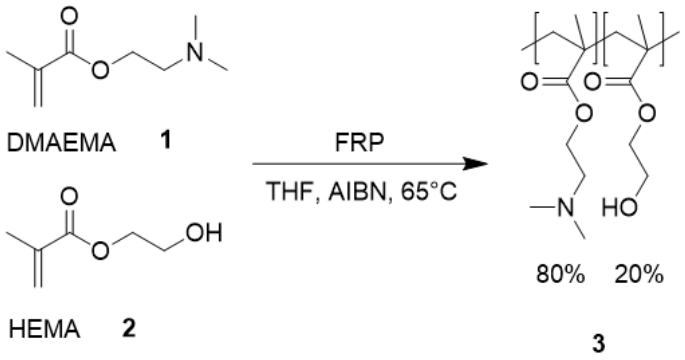

Figure 28: Synthesis of PDMAEMA-co-PHEMA.

First, 26.23 mL (0.156 mol) of DMAEMA and 4.72 mL (38.807 mmol) of HEMA were dissolved in 78 mL of THF in a three-neck round bottom flask. Then, 0.128 g (0.778 mmol) of AIBN was added after degassing the monomer solution with argon for around 20 min. The reaction was performed at 56 °C under reflux. After 48 h, the yellow viscous solution was cooled to room temperature, transferred to a dropping funnel and finally precipitated in diethyl ether. The supernatant was decanted and the remained solid was dried in a vacuum oven at 40 °C over night. Around 16 g of the copolymer PDMAEMA-co-PHEMA (**p**oly**d**i**m**ethyl**a**mino-**e**thyl**m**eth**a**crylate-co-**p**oly**h**ydroxy**e**thyl**m**eth**a**crylate) was obtained. NMR-spectroscopy was chosen to characterize the composition and SEC was used to measure the molecular weight.

4.2.2 Acrylation

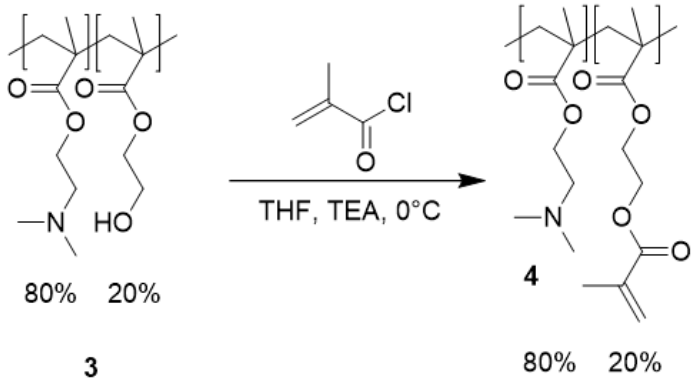

Figure 29: Synthesis of PDMAEMA-co-PMAEMA.

First, 5.109 g of PDMAEMA-co-PHEMA was transferred to a 500 mL one-neck round bottom flask and dissolved in 168 mL THF. After adding 1.21 mL (0.894 mol) of TEA, the solution was cooled to 0 °C with an ice bath and stirred for 1 h. Consequently, 6.58 mL (67.36 mmol) of MAC was dissolved in 66 mL THF and was added dropwise to the solution within 1 h. The white solution was further cooled at 0 °C for 1 h and then stirred at room temperature for 48 h. Subsequently, 100 mL of water was added in order to quench the reaction and the solvent was removed by rotary evaporator. 110 mL 1 M NaOH solution was added until the pH turned 11 and the copolymer precipitated completely. The supernatant solution was washed with chloroform in a separating funnel. The aqueous phase was discarded while the organic phase was put at a rotary evaporator to remove the solvent. The copolymer PDMAEMA-co-PMAEMA (**p**oly**d**i**m**ethyl**a**mino**e**thyl**m**eth**a**crylate-co-**p**oly**m**eth**a**cryloyl**e**thyl**m**eth**a**crylate) was obtained and dried in a vacuum oven at 40 °C over night.

4.2.3 Sulfobetainization

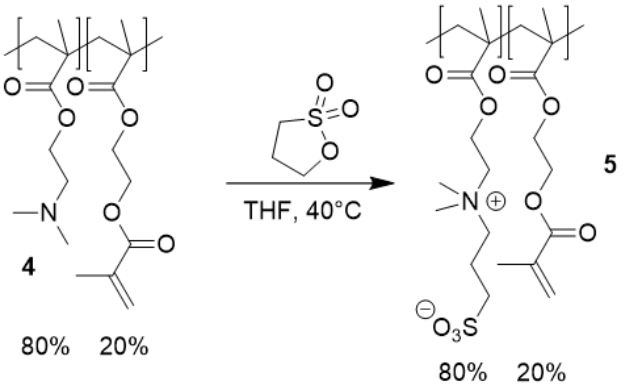

Figure 30: Synthesis of PSBMA-co-PMAEMA.

5.95 g of PDMAEMA-co-PMAEMA was dissolved in 360 mL THF and heated up to 40 °C. Then, 1,3-Propanesultone was liquefied in a warm water bath in order to add 3.77 mL (42.9 mmol) of it to the reaction solution. After 48 h, 200 mL of water was added to the opaque solution. THF was removed again by rotary evaporator and the remaining aqueous solution was purified by dialysis (cut-off: 12 – 14 kDa) for 3 days changing the water daily. The solid zwitterionic copolymer PSBMA-co-PMAEMA (**p**oly**s**ulfo**b**etaineethyl**m**eth**a**crylate-co-**p**oly**m**eth**a**cryloyl-**e**thyl**m**eth**a**crylate) was finally obtained after freeze-drying and characterized via NMR-spectroscopy.

4.2.4 Quaternization

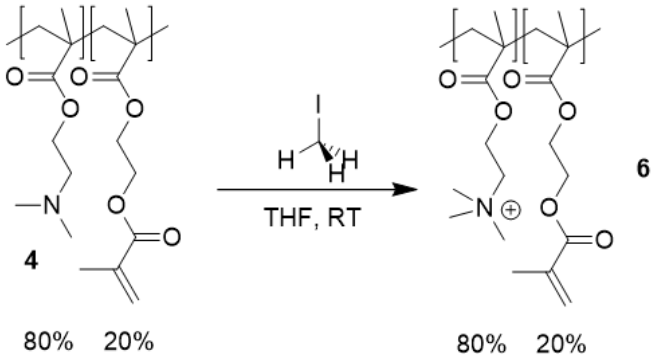

Figure 31: Synthesis of PTMAEMA-co-PMAEMA.

5.3 g of PDMAEMA-co-PMAEMA was dissolved in 40 mL THF. Then, 2.4 mL (38.5 mmol) of Iodomethane was additionally added and stirred at room temperature for 48 h. After adding 100 mL of water, THF was removed by a cooling trap. The purification of the remaining aqueous solution was done by dialysis and analogous to 4.2.3. Finally, PTMAEMA-co-PMAEMA (**p**oly**t**ri**m**ethyl**a**mino**e**thyl**m**eth**a**crylate-co-**p**oly**m**eth**a**cryloyl**e**thyl**m**eth**a**crylate) was obtained and characterized by NMR-spectroscopy.

4.3 In situ hydrogel coating of membranes

4.3.1 In situ hydrogel coating of flat-sheet membranes in dead-end

For the modification, the flat-sheet membrane BW30 (Dow Filmtec) and Lewabrane (Lanxess) were used. First, 48 mm coupons were cut to size and washed for 1 h in EtOH/water solution (30/70 vol.%) and for further 24 h in pure water. The membranes were mounted into a stainless-steel dead-end batch cell with an integrated magnetic stirrer (cf. Figure 32) and were first compacted with pure water for 4 h at 10 bar in order to receive the initial water permeance (J_0). The weight of the collected permeate was measured on a digital scale connected to the computer. Values were tracked at one-second intervals allowing the calculation of flux and permeance.

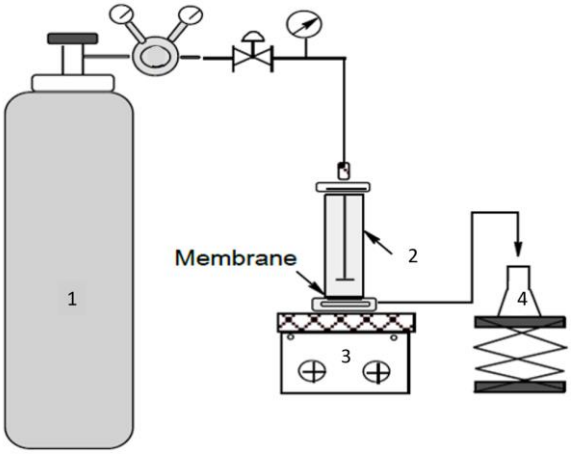

Figure 32: Schematic of the filtration set-up containing gas bottle (1), dead-end batch cell with membrane (2), magnetic stirring plate (3) and permeate collect vessel (4).

In order to attach the zwitterionic copolymer onto the negatively charged TFC RO membrane the adsorption of the cationic surface linker PTMAEMA-co-PMAEMA was carried out first by dissolving 30 mL of the linker in water (500 mg/L) and placing it into the cell. The adsorption was done at a stirring rate of 300 rpm and for 1 h. Once it was finished, the linker solution was removed, and the membrane was rinsed with pure water.

Afterwards, the copolymer PSBMA-co-PMAEMA was dissolved in pure water and adjusted to a defined pH as the reaction is base-catalyzed. As soon as the copolymer solution was put into the cell, the equivalent amount of cross-linker DTT was added after pre-solving in 500 µL pure water. In order to start the modification, the cell was pressurized and the permeate was collected (J_1). When the modification time was over, the pressure was released, and the membrane was washed first five times with pure water and then five times with 5000 ppm NaCl. After the modification, the pure water permeance (J_2) was measured. The critical parameters for the dead-end modification were:

- Polymer concentration
- Acrylate/cross-linker ratio
- pH value of the solution
- Stirring speed
- Filtration rate
- Filtration time

Depending on the addressed task, different combinations of these parameters were adjusted.

4.3.2 In situ hydrogel coating of flat-sheet membranes in cross-flow

The optimal polymer concentration, pH, acrylate/cross-linker ratio, flux and mass/area were obtained from dead-end modification experiments and were applied to the cross-flow modification experiments. The details regarding transfer will be described thoroughly in the results chapter 5.7.1.

The pre-treatment of the membrane was as described in the previous chapter 4.3.1. The assembly of the flat-channel (active membrane area of 0.0084 m^2) used for the cross-flow modification is shown in Figure 33. A Teflon plate was first placed into the channel followed by a 44 mil (1.12 mm) spacer, the flat-sheet membrane and two porous steel permeate plates.

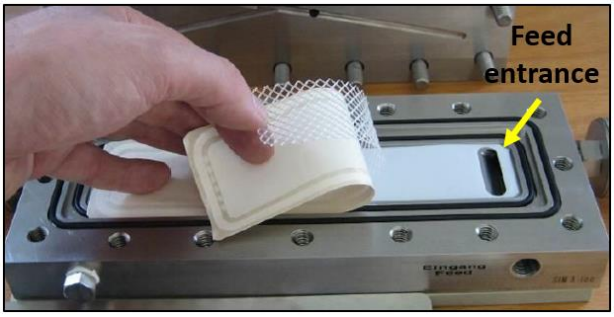

Figure 33: Construction of the spacer-filled channel.

The cell was then screwed tightly, and the tank was filled with 2 L of pure water. The system was operated in a closed loop starting with the compaction of the membrane for 24 h with pure water (30 L/h, 10 bar, 25 °C). The water permeance (J_0) was recorded at 5-min intervals by a measuring box directly linked to the filtration system. After the compaction, the tank was emptied and 550 mL of the linker solution (500 mg/L) was put into the tank. The linker filtration was performed for 1 h at a pressure of 2 bar and a feed flow of 15 L/h in order to allow the adsorption of the linker onto the membrane. In the meantime, the copolymer was dissolved in pure water and the pH was adjusted to 9. After the linker filtration, the solution was released and stored for re-use. The tank was rinsed with pure water and the modification solution was placed inside the tank. The cross-linker DTT (acrylate/cross-linker ratio of 1:1) was added subsequently and the modification was started by adjusting the pressure via pressure control valve to obtain the requested flux (J_1) and by adjusting a certain feed flow. After finishing the modification, the tank was emptied and rinsed with pure water. The system was flushed with 1 L pure water and the water permeance (J_2) was measured for 15 min (30 L/h, 10 bar, 25 °C). The system was then flushed with 5000 ppm NaCl solution followed by

the measurement of pure water permeance (J_3) for 15 min (30 L/h, 10 bar, 25 °C). The critical parameters for the cross-flow modification were:

- Cross-flow velocity
- Filtration time
- Filtration rate

Here again, different combinations of these parameters were applied according to the addressed task.

4.3.3 In situ hydrogel coating of spiral-wound modules

The modification was done first with the module TW30-2521 and then with BW30-4040 from Dow Filmtec. The flow chart of the RO system is depicted in Figure 34.[8] As can be seen, the whole modification procedure was done in a closed loop where the permeate and retentate was back-flowed to the feed tank in order to avoid concentration of the reaction solution.

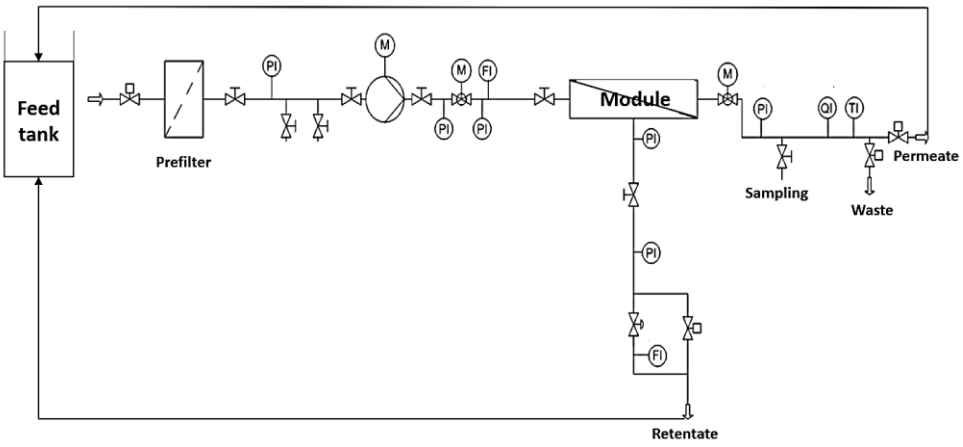

Figure 34: Flow chart of the RO system.

Prior to modification, the module was compacted for 24 h and a performance test was conducted according to the supplier's data sheet. This implies the measurement of the pure water permeate flow at a certain pressure and feed flow to obtain the initial water permeance (J_0) followed by the measurement of salt rejection by a 2000 ppm NaCl solution. During performance test, the linker was dissolved in 2 L pure water (500 mg/L). After the performance test, the linker solution was circulated through the system for 2 h at a low pressure and low feed flow allowing the adsorption to occur. The system was then emptied

[8] Support from Institut für Energie- und Umwelttechnik e.V. (IUTA), Duisburg

and rinsed with pure water in bypass mode. The copolymer was dissolved in pure water, adjusted to pH 8 and blended with the cross-linker (acrylate/cross-linker ratio of 1:1). The modification was started by adjusting the pressure and feed flow and let the solution recirculate for 1 h. Permeate samples were taken several times and weighed to calculate the permeance during the filtration. After modification, the solution was discarded and the performance test was done again to measure the modified permeance (J_2).

4.4 Fouling experiments

4.4.1 Filtration in dead-end mode

Real cooling water from steel industry

The fouling experiments were carried out in the dead-end cell with real cooling water originated from the rolling mill of the Deutsche Edelstahlwerke (CW_DEW) and from a rolling mill in Spain (CW_Sp). The membranes were first mounted into the cell and the pure water permeance (J_0) was measured for 10 min. The weight of the collected permeate was measured on a digital scale connected to the computer to obtain the initial water permeance (J_0). The fouling was characterized in terms of flux decline at a fixed transmembrane pressure of 10 bar, a stirring rate of 300 rpm and a recovery rate of 80 % (J_1). Experiments were also done at higher recovery rates (90 and 95 %) and higher stirring rates (500 rpm). Thereafter, the retentate was discarded and the membrane was rinsed 5 times with pure water. Finally, the pure water permeance (J_2) was measured again. The membrane was taken out of the cell and stored for further characterization.

Synthetic oil/water emulsion

Besides fouling with cooling water, the experiments were also done with a synthetic oil/water emulsion consisting of 3 mL Dodecan and 97 mL water corresponding to a concentration of 22.5 g/L. Both solutions were roughly mixed with a vortex-mixer for 2 min and were then dispersed by ultrasonic treatment for 60 min. A fresh solution was prepared before each experiment.

Crude oil emulsion

Another set of experiments was done with the membranes modified in cross-flow and a crude oil nano-emulsion which was dispersed in advance by a high-pressure homogenizer at 300 bar enabling a stable reproducible emulsion. The droplet size was approximately 0.45 µm, measured with laser diffraction particle size analyzer (*Beckman Coulter Particle sizer)* and was stable for around 5 days.[9] After measuring the initial water permeance (J_0), the fouling was done at 10 bar at a stirring rate of 100 rpm until a recovery of 25 % (J_1). After removing the retentate, the membrane was washed with water 5 times. The pure water permeance (J_2) was measured subsequently. The membrane was further washed with an ethanol/water solution (1:10 vol.%) and the pure water permeance (J_3) was measured again.

4.4.2 Filtration in cross-flow mode

Real cooling water from steel industry

The fouling experiments with cooling water in cross-flow mode were done with the aim to measure the long-term stability of pristine membranes with real cooling water. For that purpose, the membranes were first compacted at 12 bar for 24 h (J_0). Then, 2500 mL of cooling water was placed into the tank and the filtration was done with CW_DEW at 12 bar and a cross-flow velocity of 0.3 m/s to five times of initial concentration. Afterwards, the filtration was pursued by recirculating the solution for 48 h (J_1). After finishing, the system was flushed with pure water and the pure water permeance (J_2) was measured.

Experiments were also done concerning critical flux measurements. These experiments were based on flux-TMP measurements by imposing a pressure, allowing the determination of a steady-state flux. Experiments were done with the Lewabrane membrane and the cooling waters CW_DEW and CW_Sp. The filtration was started at 8 bar and was increased in steps of 4 bar until 32 bar was reached and each pressure step took 30 min. The filtration was first done with pure water and then with cooling water for the same membrane.

[9] Support from mechanische Verfahrenstechnik (MVT), Duisburg

Crude oil

Additionally, experiments were done with the crude oil nano-emulsion which was also dispersed by a high-pressure homogenizer prior to use. Around 600 mL of the emulsion was put into the tank after measuring the pure water permeance (J_0) of the membranes for 10 min (10 bar, 30 L/h, 25 °C). The filtration was done at 10 bar and a feed flow of 33 L/h for 24 h in a closed loop allowing steady-state condition (J_1). The system was washed with 1 L pure water at 15 L/h and 2 bar and then with an ethanol/water solution (1:10 vol.%). The water permeance was measured between the washing steps (J_2) and afterwards (J_3) for 30 min (10 bar, 30 L/h, 25 °C).

4.4.3 Field tests with modules

The two coated BW30-4040 RO modules (RO Mod) were tested in parallel with four conventional RO modules (RO Conv) in on-site trials in the projects´ pilot plant operated by SMS group at Deutsche Edelstahlwerke (cf. Figure 1). The modules were operated with direct cooling water in nine short-term experiments (STE). The STE were carried out, each for 2 h, to investigate the physical properties of the modules. Different influencing parameters (pH, feed flow, recovery and softening using ion exchanger) on the performance of the modules were analyzed in different test series from A1 – A4. A summary of all test series is given in Figure 35. The experiment at a feed flow of 500 L/h and a recovery of 70 % without pH adjustment and softening was done once and represents the experiments A2.2, A3.2 and A4.2 so that nine experiments were done in total. Samples of the feed, permeate and retentate were taken to measure the conductivity, chloride, sulfate, calcium and magnesium amount and thus to calculate the rejection.

RO Conv/Mod			A1 (pH)			A2 (Feed flow)			A3 (Recovery)			A4 (Softening)	
			A1.1	A1.2	A1.3	A2.1	**A2.2**	A2.3	A3.1	**A3.2**	A3.3	A4.1	**A4.2**
Feed flow	[l/h]	400	x	x	x	x					x		
		500					x		x	x		x	x
		570						x					
Recovery	%	60						x	x				
		70	x	x	x	x	x			x		x	x
		80									x		
pH	-	5,5	x										
		6		x									
		6,5			x								
Softening	-	No	x	x	x							x	
		Yes				x	x	x	x	x	x		x

Figure 35: Overview of all test series.

The STE experiments were followed by four long-term experiments (LTE) in which the fouling behaviour was examined over one week each experiment. The influence of various pre-treatments (pH-adjustment, softening by ion exchanger, antiscalant dosage) and the effect of chemical cleaning on the long-term stability and irreversible fouling was investigated. The first LTE B1.1 was carried out without any pre-treatment. In the following LTE B4.1, the pH was set to 6 under otherwise unchanged conditions. B6.1 required 30 ppm antiscalant dosage and the use of ion exchanger for water softening whereas B8.1 involved all three pre-treatments. Before the test began, an activated carbon filter was installed prior to the MF filter. The modules were flushed with RO-permeate during an LTE while they were rinsed with hydrochloric acid (pH 2.5) between each LTE. The active carbon filter was uninstalled and a long-term experiment over three weeks (3W_LTE) was done subsequently by maintaining the maximum recovery at constant concentrate flow. In the last experiment (1W_LTE_IndWa), the modules were operated with indirect cooling water to compare the fouling behaviour of both waters.

4.5 Stability test of hydrogel-coated membranes under cleaning conditions

Coated membranes were washed with three different cleaning solutions for 10 min each time by filling the filtration cell with the cleaning solution and stirring at 300 rpm. Acidic (HCl at pH 2), basic (NaOH at pH 12) and enzymatic (commercial cleaner MembraPas M245, 300 g/L) cleaning methods were tested. After a total washing time of 30 min, the cleaning solution was discarded, the cell was filled with ultrapure water and the flux was measured. All cleaning steps were performed at a temperature of 35 – 40 °C. In addition to the evaluation of flux behaviour, the membranes were also characterized by ATR-FTIR spectroscopy (time-resolved spectra) and SEM images. The removal of hydrogel coating was also evaluated by means of a mass balance using TOC.

4.6 Characterization

4.6.1 Cooling water

4.6.1.1 Photometry

The feed was analyzed quantitatively with the *Nanocolor 500 D* photometer from *Macherey Nagel* for selected ions such as chloride, iron, potassium, sulfate, phosphate, ammonium, magnesium and calcium and for chemical oxygen demand (COD). Photometry is a quantitative method for the determination of dissolved substances based on light absorption of the solution in the visible or ultraviolet spectral range.[136] The measurement was carried out in cuvettes on a small scale already containing the correct amount of reagents in the correct ratio in which a defined amount of feed solution was added starting the reaction. The cuvette reaction tests are based on internationally recognized standards such as DIN, EN, ISO, EPA and APHA enabling reliable and comparable results. The cuvette with reaction solution was placed into the photometer and the concentration determination was conducted.

4.6.1.2 Total organic carbon

The TOC analysis is used to determine the amount of total dissolved organic carbon. Using different methods like UV oxidation or catalytic combustion (used in this work), the carbon compounds are oxidized to carbon dioxide which is detected by a non-dispersive infrared detector (NDIR). By means of a detector signal, the concentration of the total carbon dioxide (TC) is determined. In order to obtain the TOC amount, the inorganic carbon (IC) is subtracted from the total carbon amount (TC).[137] A *TOC-$V_{CPH/CPN}$ Total Organic Carbon Analyzer* from *Shimadzu* was used for the determination.

4.6.1.3 Silt density index

The silt density index (SDI) is an empirical method developed to predict the colloidal fouling potential of feedwaters thus determining feed water quality for RO systems. Silt includes all suspended particles (from organic and inorganic sources) that are deposited on the membrane in the form of particles and can lead to a decrease in water flux. It is calculated by equation (15) and is based on the time required to filter a volume of 500 mL of feedwater through a 0.45 µm filter of a diameter of 47 mm at a constant pressure of 2.07 bar. The filtration is done two times in a row. An SDI of less than 1 %/min means that the reverse osmosis system can run for several years without colloidal fouling. An SDI of less than 3 %/min

means that the system can run several months between cleanings. An SDI of 3 – 5 %/min means that particulate fouling is likely to be a problem and frequent, regular cleaning will be needed. An SDI of more than 5 %/min is unacceptable and indicates that additional feed pre-treatment is required.[29] However, this is highly dependent on the operating conditions and the water to be used, so that waters with an SDI of only 2 %/min may well cause particle fouling.

$$SDI\ [\%/min]\ =\ \frac{1-\left(\frac{T_i}{T_f}\right)}{T_t}\cdot 100 \qquad (15)$$

T_i = Initial time in seconds required to collect the 500 mL sample

T_f = Time in seconds required to collect the second 500 mL sample

T_t = Total elapsed test time (either 5, 10 or 15 min)

In this work, the $SDI_{15\ min}$ was conducted, thus the SDI takes values from 0 – 6.67 %/min.

4.6.1.4 Other tests

Additionally, pH (pH electrode*, Lab 960, Schott Instruments)*, conductivity (conductivity meter*, Lab 960, Schott Instruments),* amount of alkalinity, calcium, magnesium (titration kit, *Macherey Nagel),* silica (colorimetric colour test kit, *Macherey Nagel)*, total solids and total dissolved solids (infrared moisture balance analyzer MA35, *Sartorius*) were determined.

4.6.2 Copolymer

4.6.2.1 Nuclear magnetic resonance spectroscopy (NMR)

Nuclear magnetic resonance spectroscopy (^{1}H-NMR) is a widely used method for elucidating the structure of molecules. During the measurement, the sample is exposed to a strong magnetic field and the interactions between the substance and the magnetic field are examined. An NMR of the type *DMX 300* and *DMX 500* from *Bruker* was used for the analysis of PSBMA-co-PMAEMA and PTMAEMA-co-PMAEMA by dissolving a few milligrams in deuterated water in order to determine the chemical composition and degree of functionalization. The evaluation of spectra was done with the software *MestReNova.*

4.6.2.2 Size exclusion chromatography (SEC)

The size exclusion chromatography is a special form of chromatography where the analytes are separated by differences in the molecular size and hydrodynamic volume V_h. According to equation (16), the hydrodynamic volume V_h is proportional to the molecular mass M and the proportional factor is the intrinsic viscosity η. The column is filled with a porous bead in which small analytes penetrate and diffuse through the pores leading to a delayed elution of the analytes while bigger ones do not penetrate the pores eluting much faster.[138]

$$V_h = [\eta] \cdot M \qquad (16)$$

Molecular weight of individual species is determined by comparison with calibration substances. A distinction can be made between two different calibrations; universal and conventional calibration. Latter one uses polymer standards with known molecular weight and a small polydispersity. From the measured retention times of the standards, a calibration function can be calculated. However, the molecular weight of an unknown polymer sample can only be determined relative to the standard polymer. By using a viscosity and refractive index detector (depending on the concentration), a universal calibration can be carried out. The difference to the conventional calibration is that the product of the intrinsic viscosity and concentration is directly accessible from the measured signal of the viscosity detector. The plot of logarithmic intrinsic viscosity and the logarithmic molecular mass leads to the Mark-Houwink plot and Mark-Houwink equation:

$$\lg([\eta]) = \lg(K) + (a \cdot \lg(M)) \qquad (17)$$

The parameters K and a are assumed to have constant values for a certain polymer solution system. For a large number of polymers these values are already listed in the “Polymer Handbook”.[139]

The SEC was used to determine the molecular weight M_w (mass weight average) and M_n (number weighted average) and the PDI (ratio of M_w and M_n) of the copolymer PDMAEMA-co-PHEMA. For this, both calibration methods were used using a dual detector for refractive index and viscosity (*ETA-2020, WGE Dr. Bures, Germany*). A solution containing 4 g/L of polymer in DMF was prepared. A Gram Column (*PSS, Germany)* with 10 µm particles at a flow rate of 1 mL/min and an injection volume of 200 µL at room temperature was used.

4.6.2.3 Dynamic light scattering (DLS)

Dynamic light scattering is a laser scattering method in which the size of dispersed particles can be determined due to Brownian motion of the dispersed particles which is temperature dependent. If the particles are exposed to monochromatic laser light, scattering occurs in all directions. The interaction of the rays creates interference pattern which depend on the diffusion coefficient D of the particles which in turn can be described by the Stokes-Einstein equation (cf. equation (18)) with k_B as Boltzmann constant, T as temperature, μ as dynamic viscosity of the dispersion medium and r_h as hydrodynamic radius. D is finally measured by the DLS.[140]

$$D = \frac{k_B \cdot T}{6\pi \cdot \mu \cdot r_h} \qquad (18)$$

For the measurement, an aqueous PSBMA-co-PMAEMA solution (1 g/L) was prepared and analyzed with a *Zetasizer Nano ZS ZEN 3600* from *Malvern* to measure the hydrodynamic radius. The refractive index of PMMA (1.49) was chosen as representative index for polymers.

4.6.2.4 Rheology

Rheology studies the deformation and flow behaviour of fluids and the rheological parameters can be described by the two-plates model[141] (cf. Figure 36).

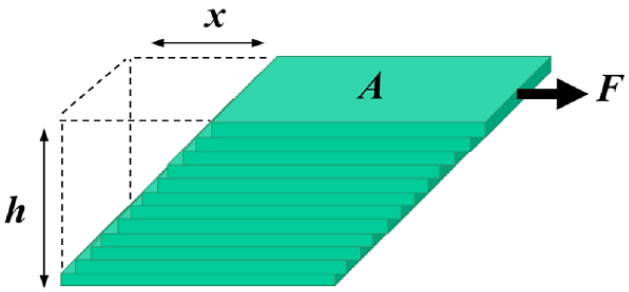

Figure 36: Schematic representation of the two-plates model.[142]

The viscosity of a fluid is defined as the ratio of shear stress and shear rate, as follows:

$$\eta = \frac{\tau}{\gamma} \qquad (19)$$

The shear rate γ is a measure of the mechanical stress applied onto the sample and defined as the ratio of velocity v and a plate with the distance h (cf. equation (20)). The shear stress τ describes the force applied onto the fluid (cf. equation (21)):

$$\gamma = \frac{v}{h} \quad (20)$$

$$\tau = \frac{F}{A} \quad (21)$$

Fluids can be divided into two groups; Newtonian and non-Newtonian fluids. While the viscosity of a Newtonian fluid is independent of the shear rate, non-Newtonian fluids behave inversely:[141]

- Viscosity decreases with increasing shear rate (shear thinning behaviour (pseudoplastic))
- Viscosity increases with increasing shear rate (shear thickening behaviour (dilatant))

Rheological measurements can be conducted with view to analyze the viscosity of a fluid in rotational experiments or to analyze the viscoelastic properties of a fluid in oscillation experiments (cf. chapter 4.6.3.1).

To determine the viscosity of the copolymer PSBMA-co-PMAEMA, tests were carried out at different concentrations (1 – 10 wt%) using the rheometer *Physica MCR 301* from *Anton Paar*. Plotting the shear stress against shear rate allows the determination of fluid type (Newtonian or non-Newtonian fluid). From the viscosity measurement, the overlap concentration (the concentration beyond which the gelation can occur) could also be determined by plotting the viscosity against polymer concentration and performing a linear regression. The concentration at which the slope of viscosity increases, is defined as overlap concentration.

4.6.3 Bulk hydrogel

4.6.3.1 In situ rheology

Using rheology in oscillation mode is a typical technique to define the mechanical properties of in situ formed bulk hydrogels via cross-linking.[143] The most important characteristic determined by rheological measurements is the viscous and elastic behaviour of a sample. Viscous materials include pure liquids (e.g. water) while elastic materials represent solids (e.g. steel). Other materials, such as hydrogels have both, viscous and elastic properties which can be defined as visco-elastic materials characterized by measuring the complex shear modulus G* which is defined as follows:

$$G^* = \frac{\tau\,(t)}{\gamma\,(t)} \qquad (22)$$

The complex modulus G* consists of an imaginary G´´ (loss modulus) and real part G´ (storage modulus). The real part is a measure of the mechanical energy stored by the material during a shear experiment while the imaginary part provides information about the energy loss during the shear experiment. Liquids cannot store mechanical energy in a shear experiment, their storage modulus is therefore zero. For visco-elastic materials such as hydrogels, one part of the energy is stored and another part is dissipated.[141]

The ratio of loss and storage modulus is a measure of the ability of a material to store mechanical energy and is defined as damping factor (DF):

$$tan\,\delta = \frac{G^{''}}{G^{'}} \qquad (23)$$

If the storage modulus equals the loss modulus, then the gel point of the sample is reached. This enables the measurement of the gelation time (G´= G´´), complete gelation time (constant G´) and damping factor (G´´/G´) of a hydrogel.

In this work, the visco-elastic behaviour of the bulk hydrogel (base-catalyzed in situ Michael addition reaction of PSBMA-co-PMAEMA and DTT) was measured in dependence of pH (8, 9, 10), acrylate/cross-linker ratio (1:1, 1:15, 1:10) and polymer concentration (3 – 15 wt%). Immediately before measurement, the prepared copolymer solution was mixed with the cross-linker DTT in an appropriate ratio by a vortex mixer and placed onto the set-up starting the measurement. A conical geometry (CP25-2) with a shear gap height of 0.101 mm was used at an angular frequency of 10 Hz and an amplitude deflection of 0.1 mrad. Total measuring time was considered not to exceed 120 min.

4.6.4 Flat-sheet membranes and spiral-wound modules

4.6.4.1 Chemical structure (ATR-FTIR spectroscopy)

ATR-FTIR is a very useful analytical technique used for analyzing the chemical composition, localization of different compounds and structure of the membrane, enabling both qualitative and quantitative analysis for membrane samples. A unique spectrum for each compound can be detected according to the absorption of energy by the membrane at different characteristic

wavelengths which produce a signal at the IR detector.[144] The limit of penetration depth can be expressed as:

$$d_p = \frac{\lambda}{2\pi n_1 \sqrt{sin^2\theta - (\frac{n_2}{n_1})^2}} \quad (24)$$

The penetration depth depends on the refractive indices of the crystal material n_2 and the sample n_1, the incidence angle θ and the wavelength λ of the incident wave of ATR-FTIR. It is therefore directly related to the wavelength and ranges typically from 1 – 3 µm for an incident angle of 45 °.[145]

An ATR-FTIR of the type *ALPHA Platinum ATR* from *Bruker Optics* was used, equipped with an ATR diamond crystal, to analyze the membranes' top surfaces. Prior to analysis, the measuring arrangement was cleaned with isopropanol and a background measurement was carried out. The membrane samples were dried before, cut to size and placed in the sample holder on the crystal. Finally, the spectra was recorded using the "OPUS" software. Each spectrum was taken using 32 scans at a resolution of 0.7 cm^{-1}. The spectra was normalized to 0 – 1.

4.6.4.2 Membrane surface properties

Zeta potential

The most utilized technique in the characterization of the electrical properties of flat surfaces is the determination of the zeta potential from streaming potential measurements. Zeta potential gives information about the overall membrane surface charge. When the negative charged membrane is brought into contact with an aqueous electrolyte solution a charge separation occurs producing the "electrical double layer" that is formed in the membrane-solution interface. The negative charge is balanced by an excess of counter-ions distributed adjacent to the membrane surface in the Stern layer and the ions distributed farther from the surface in the diffuse layer. The Stern layer thickness is approximated by the hydrated counter-ion radius, r_{hi} (0.22 nm for Na^+), while the diffuse layer thickness is given by the Debye length, λ_D (approximately 3 nm for a 10 mM NaCl solution).[146] The Stern potential, ϕ_S, located at the boundary between the Stern and diffuse layers, cannot be measured, and the zeta potential, ζ, is used instead. Zeta potential is measured at the shear surface between the membrane surface and the surrounding electrolyte solution and is close to the Stern

potential.[147] In the streaming potential process, the salt solution is forced by an external pressure to flow through a channel formed by two membranes (Figure 37).[148]

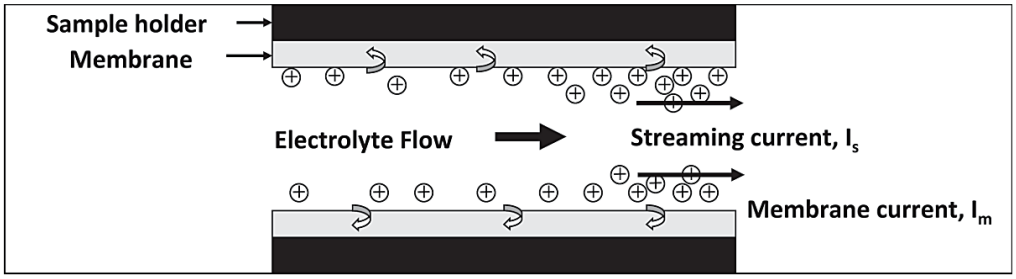

Figure 37: Schematic representation of the streaming current generated by electrolyte flow through the channel and the back flow current through the membrane bulk.[148]

Its flow results in a streaming current, thereby generating a potential difference. This potential resists the transfer of charge, causing back conduction by ion diffusion in the opposite direction. The transfer of charges due to these two processes is called the leak current. In equilibrium conditions, the streaming current balances the leak current, and the measured potential difference is the streaming potential.[147] Zeta potential values were calculated from the streaming potential data using the *Helmholtz-Smoluchowski* equation:[149]

$$\zeta = \frac{\Delta U_S}{\Delta P} \cdot \frac{\eta}{\varepsilon \varepsilon_0} \cdot \frac{L}{A} \cdot \frac{1}{R} \qquad (25)$$

where ζ is the zeta potential [V], $\frac{\Delta U_S}{\Delta P}$ is the slope of streaming current versus pressure [Ampere/Pa], η is the electrolyte viscosity [Pa·s], ε_0 is the vacuum permittivity [F/m], ε is the dielectric constant of the electrolyte, L is the length of the streaming channel [m], A is the cross section of the streaming channel [m^2] and R is the electrical resistance of the channel.

The surface charge property of the membranes was studied with streaming potential measurements using *SurPASS* analyzer (*Anton Paar GmbH, Germany).* Two pieces of the same membrane were fixed in the measuring cell (adjustable gap cell) with double-tape. The height of the cell was always adjusted to a value of 100 µm +/- 5 µm by flow rate. A KCl solution of 0.1 mM was circulated through the measuring cell from both sides, creating a differential pressure and the pH was adjusted to 3 with 0.1 M HCl. The target pressure was 400 mbar and the temperature was 25 ˚C. Solution pH was increased during measurement with 0.1 KOH up to pH 11 by conductometric titration. Streaming potential was measured as a function of pH.

Contact angle

Surface hydrophilicity is commonly determined by the contact angle formed between a membrane surface, a deposited droplet, and the surrounding medium. The contact angle is the angle at which a liquid/vapour interface meets a solid surface. The measured angle can be used to designate the relative hydrophilicity of a membrane or more generally to study the wetting of a solid or liquid interface by another liquid. A smaller angle (< 90 °) indicates a more hydrophilic membrane (high surface tension) while a larger angle (higher than 90°) indicates a more hydrophobic membrane (low surface tension). Contact angle is commonly measured using either the sessile drop or the captive bubble method.

The measurement of the membranes was evaluated using captive bubble mode with the system OCA 15 Plus *(DataPhysics GmbH, Filderstadt)*. Before starting the measurement, the sample holder was cleaned with acetone. Then, the membrane was fixed to the holder using double tape so that measurement could be done properly. The air bubble was released via Hamilton syringe and the dosing volume amounted to be 5 µl. The measurement was performed by employing ellipse fitting while the shape of drop was observed through a camera.

4.6.4.3 Membrane morphology

Scanning electron microscopy

The Scanning Electron Microscope (SEM) is an electron microscope capable of producing high-resolution images of a sample surface and thus, direct information on membrane porous structure and sublayer structure (morphology) is obtained by three-dimensional images of surface or cross-section. In SEM measurements, a fine beam of electrons scans the membrane surface, causing several kinds of interactions which generate signals like secondary electrons (SE) and backscattered electrons (SBE). Preparation of the samples is relatively easy since most SEMs only require the sample to be conductive.[150]

Images of the top surface were taken using high resolution SEM (*FEI Quanta FEG 400).* The sputtering was done by a *K-550* sputter coater (*Emitech, U.K.)*. For the top surface the membrane samples were cut in a suitable size, sputtered and fixed to the platform with silver paint. For cross-section images, membrane samples were obtained by flash-frozen in liquid

nitrogen followed by fracturing the membrane. The fractured edges were grounded to the platform by silver paint after sputtering.

Atomic force microscopy

Surface roughness is typically measured using an atomic force microscope, an instrument that maps surface contours (topology) using a small tip that scans across the surface of a sample. The AFM consists of a cantilever with a sharp tip at its end (radius on the order of nanometers) that is used to scan the surface of the membrane. Two different modes can be executed during measurement. In the tapping mode, short, rapid tapping of the tip on the membrane surface is used to map the surface. In contact mode, the tip is dragged along the surface and the displacement of the tip is used to measure the surface height at a particular position. Thus, every variation of the surface height varies the force acting on the tip and leads to a deflection of the cantilever according to Hooke's law. This deflection/bending is measured and recorded line by line. However, the tapping mode is preferred for soft samples that may be easily deformed by the tip (e.g., polyamide membranes).[151] The AFM measurement was also used to measure the thickness of the hydrogel-coated membranes in a wet state in order to measure the swelling degree from the ratio of wet and dry thickness.

The images were recorded with an *Agilent Technologies 5500* beam deflection AFM using nano-sensors tapping-mode cantilever with silicon tips and the surface roughness was evaluated in terms of the root mean square roughness Rq.

4.7 Calculations

4.7.1 Dead-end and cross-flow filtration parameters

The **permeate flux J_v** describes the volume flowing through the membrane per unit time and area. It is one of the main factors regarding the evaluation of membrane performance. The calculation of permeate flux is given by equation (26):

$$J_v = \frac{Q_P}{A} \qquad (26)$$

J_v = Flux [L/hm^2]

Q_P = Permeate flow [L/h]

A = Membrane surface area [m^2]

The **water permeance P** can be obtained by dividing the permeate flux by the transmembrane pressure TMP, as follows:

$$P = \frac{Q_P}{A \cdot TMP} \quad (27)$$

Also, the **rejection** is a very important indicator, demonstrating the effectiveness of a membrane to remove contaminants. The rejection for specific components can be calculated according to the following equation:

$$R = 1 - \left(\frac{C_P}{C_F}\right) * 100 \quad (28)$$

R = Rejection [%]

C_P = Concentration of solutes in permeate [g/L]

C_F = Concentration of solutes in feed [g/L]

Salt rejection (e.g. NaCl) can be calculated by measuring the conductivity σ of the feed and permeate as it is proportional to the concentration of ions in the solution. Typical salt rejection values for good RO membranes range from 95 – 99 %. Rejection can also be calculated using overall properties, such as TOC concentration, etc.

The **cross-flow velocity v** (CFV) is another important parameter affecting the hydrodynamic conditions during cross-flow filtration and thus the formation of concentration polarization. It is defined as linear velocity of the flow tangential to the membrane surface and calculated by dividing the feed flow Q_F by the cross-sectional area A of the flat channel according to equation (29).

$$v = \frac{Q_F}{A} \quad (29)$$

Since in this work a spacer is used for the cross-flow experiments, the calculation of the **cross-sectional area A** follows the equation (30) for a spacer-filled channel:[90]

$$A = w_{ch} \cdot h_{Sp} \cdot \epsilon_{Sp} \quad (30)$$

in which w_{ch} is the width of the channel, h_{Sp} is the height of the channel which is equal to the spacer height and ϵ_{Sp} is the porosity of the spacer. Details regarding the calculation of porosity can be taken from Siddiqui *et. al.*[90]

In order to evaluate the success of modification by means of filtration data, the **flux recovery ratio (FRR)** is calculated by equation (31):

$$FRR = \left(\frac{J_x}{J_0}\right) \cdot 100 \qquad (31)$$

where J_0 is the water permeance before modification (after compaction) and J_x is the water permeance immediately after modification (x = 1), after washing with pure water (x = 2) and after washing with 5000 ppm NaCl solution (x = 3).

The degree of fouling can also be evaluated on the basis of filtration data and according to the flux recovery ratio from equation (31) where J_0 is the water permeance before fouling (after compaction), J_x is the water permeance immediately after fouling (x = 1), after washing with pure water (x = 2) and after washing with an EtOH/water solution (x = 3).

Additionally, the **maximum mass of reactants per area** during dead-end modification can be quantified by equation (32). If this is divided by the time (equation (33)), then the **maximum mass per area and time** is obtained which controls the reactivity of the system during the modification.

$$Max.\ mass/area\ [g/m^2] = \frac{V_P \cdot C_{Copo}}{A} \qquad (32)$$

$$Max.\ mass/area/time\ [g/m^2h] = \frac{V_P \cdot C_{Copo}}{A \cdot t} \qquad (33)$$

with V_P as permeate volume [L], C_P as polymer concentration (average of feed and retentate concentration) [g/L], A as active membrane area [m^2] and t as filtration time [h].

Dividing the maximum mass per area by the density ρ [g/m^3] of a random polymer, in this case PMMA, the **maximum dry layer thickness** can be calculated:

$$Max.\ dry\ layer\ thickness\ [m] = \frac{V_P \cdot C_{Copo}}{A \cdot \rho_{PMMA}} \qquad (34)$$

4.7.2 Concentration polarization modulus

In order to calculate CPM and c_m (concentration of reactants at the membrane surface) during the modification, the mass transfer coefficient k has to be determined. The methods for calculating k have been described in detail in chapter 2.3.2. As already mentioned, one of the most widely used method is the velocity variation method where the change in observed

rejection R_{obs} with varying stirring rate for the same solution is measured. However, since the copolymer rejection is nearly 100 %, this method cannot be applied in this case. But dimensionless correlations using the Sherwood number can be used instead (cf. equation (12) and (13)). For the dead-end modification experiments, the equation (14) (correlation for a stirred batch cell) by *Colton & Smith*[89] was used.

For the calculation of k, the diffusion coefficient D_i is required, which was calculated using equation (18). For this, the hydrodynamic radius r_h was determined from DLS measurements. For the final estimation of the mass transfer coefficient k, equation (12) was rearranged to k. Apart from k, information about the flux J_v and bulk concentration c_b is also required. As the modification is done under filtration conditions and due to the change in feed concentration in dead-end batch mode, the average flux, and the average bulk concentration (average of feed and retentate concentration) must be considered. Finally, once the mass transfer coefficient k, flux J_v and bulk concentration c_b is known, CPM and c_m can be calculated according to equation (6).

5 Results & Discussion

5.1 Membrane Screening of commercial RO membranes

5.1.1 Membrane performance

A spectrum of different commercial RO TFC membranes was purchased. The focus was on membrane types for industrial applications since the feed solution to be investigated was industrial cooling water from the steel industry. For a comparative characterization, membranes for seawater desalination were also included. A screening was carried out to evaluate the applicability of these membranes. The RO membranes are of the types RO98pHt (Alfa Laval), BW30 (Dow FilmTec), AK, SE and CE (GE Osmonics) and Lewabrane (Lanxess).

The membranes were first compacted at 12 bar until a constant flux value was reached (approx. after 4 h). Afterwards, the pure water fluxes and the NaCl rejections were measured. Due to the measurement setup, it was not feasible to apply the pressure according to the data sheet for all membranes, so a lower but similar pressure was applied.

Table 5 summarizes the average values for the membranes in the compacted state in comparison to the data from the manufacturer's specifications. It was found that membrane samples of the same membrane type had slightly different permeabilities even though samples were punched out of the same sheet. Since only a small part of the membrane area is examined, these deviations are statistically significant and lead to differences in permeance. However, these differences are minor which is reflected in a low standard deviation. It is also noticeable that all polyamide membranes (RO98pHt, BW30, AK, SE, Lewabrane) have different but similar water permeances (WP). AK has the highest WP, followed by RO98pHt, Lewabrane, BW30 and SE. The CE membrane which is a cellulose acetate membrane has the lowest WP of 1.4 LHMbar. This was to be expected since cellulose acetate membranes have much lower fluxes and salt rejections compared to TFC PA membranes. This is because the PA layer is exceedingly thin and also the support is highly porous, thereby resulting in a much higher water flux compared to integrally skinned asymmetric membranes such as cellulose acetate.[152]

Table 5: Membrane performance (water permeance and NaCl rejection) of the investigated commercial membranes compared to the manufacturer's data.

Membrane	WP [LHMbar] Data sheet	WP [LHMbar] Experimental			NaCl rejection [%] Data sheet	NaCl rejection [%] Experimental
		average	n*	Standard deviation		
Alfa Laval RO98pHt	-	3.7	20	0.6	98.5 @ 15.5 bar	98 @ 15.5 bar
FilmTec BW30	2.51	3.1	7	0.4	99.5 @ 17.6 bar	98 @ 16.4 bar
GE Osmonics AK	5.52	4.7	7	0.5	99 @ 8 bar	98 @ 8.9 bar
GE Osmonics SE	1.28	2.5	4	0.4	98.9 @ 30 bar	97 @ 16 bar
GE Osmonics CE	1.38	1.4	4	0.4	97 @ 30 bar	97 @ 16 bar
Lanxess Lewabrane	-	3.7	7	0.5	97 @ 15 bar	97 @ 15 bar

Looking at the salt rejections, it can be observed that all membranes show high salt rejections, as would be expected from RO/NF membranes. It is also apparent that the salt rejections of the RO membranes (e.g. RO98pHt, BW30) according to the data sheet show slightly higher values than those determined experimentally. This can be explained by the fact that the rejection measurements in this work were performed at somewhat lower pressures. Since the water flux but not the solute permeation rate (salt flux) is proportional to the net driving pressure, the water flux and thus the salt rejection are higher at a higher pressure.[153]

As membrane modification is performed in the further progress of the work which results in a permeance reduction, it is unfavourable to use a membrane with an initial low permeance. For this reason, the CE membrane, which also has a comparatively low salt rejection, was excluded from further characterization and subsequent experiments.

5.1.2 Surface characterization

Structure characterization was performed by ATR-FTIR spectroscopy, contact angle and zeta potential measurements. First, the membranes RO98pHt, BW30, AK, SE and Lewabrane were measured in the pristine state by ATR-FTIR to identify if they represent full- or semi-aromatic polyamide membranes (cf. Figure 38).

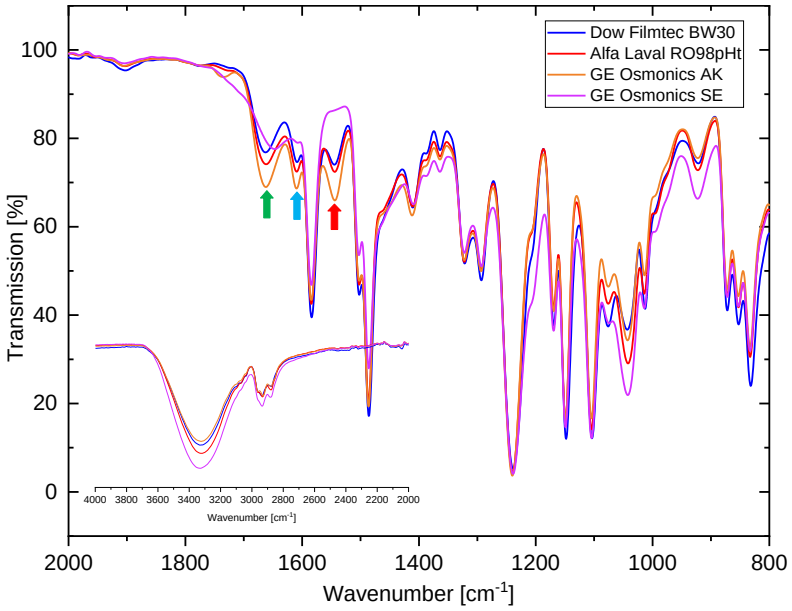

Figure 38: IR spectra of the investigated commercial membranes for structure identification and enlargement of the IR range from 4000 – 2000 cm^{-1}.

As can be seen from the spectrum, the membranes HR98pHt, BW30, AK and Lewabrane exhibit an amide II band at 1544 cm^{-1} (red arrow), aromatic band at 1609 cm^{-1} (blue arrow) and amide I band at 1661 cm^{-1} (green arrow). These bands are characteristic for full-aromatic membranes, which are formed by the synthesis using MPD and TMC.[154] Thus, the membranes HR98pHt, BW30, AK and Lewabrane can be classified as full-aromatic membranes.

Only the spectrum of membrane SE (pink spectrum) is different, since the amide II is absent and the aromatic band is substantially weaker due to weak N-H vibrations. Furthermore, the amide I band is shifted from 1661 to 1646 cm^{-1}. This is characteristic for semi-aromatic polyamide membranes which are synthesized from piperazine (PIP) and TMC.[154] Thus, these findings indicate that a certain amount of MPD may have been blended with piperazine during IP reaction. This observation is indeed surprising because semi-aromatic PA membranes are typically NF membranes whereas SE is an RO membrane according to the manufacture's specifications. However, the same was found in the study of Akin *et al.*[144] Thus, the wavenumbers of the amide peaks underline the presence of both semi-aromatic and fully-aromatic structures for this membrane.

Such commercial membranes are known for being coated with an additional layer (preservative layer) by the manufacturer. After IP, the membranes are usually coated with a protective layer of a water-soluble polymer such as poly(vinyl alcohol) (PVA) to preserve the membrane until it is installed into the module. The PVA layer protects the membrane from

damage during subsequent handling as it is assembled into spiral-wound modules. When the module is used for the first time, the feed water washes off the water-soluble coating to expose the membrane, and the module is ready for use.[29] Such coatings could also represent cross-linked fixed hydrophilic layers, targeting hydrophilic contaminant removal to prevent fouling. These might be for instance cross-linked PVA or PEG-based coatings. Reasons for such coatings could be also the focus on a specific separation application.[144] Unfortunately, manufacturers rarely provide information about such coatings due to proprietary reasons. Furthermore, there are only few studies in which a comparative characterization of commercial membranes has been conducted. For the development and adaptation of an antifouling coating of such membranes, information of this nature is particularly important since the existing protective layer has different properties than the base membrane and can have also an additional influence on fouling.

However, a helpful and useful work is the study of Tang *et al.* from 2007[155] and 2009[156, 157] where different commercial RO and NF membranes of different manufacturers, including Dow Filmtec, Hydranautics, GE Osmonics and Saehan Industries, were investigated to identify the presence of such a coating. FTIR and XPS measurements revealed that coated membranes generally had more hydrophilic, more neutral, and smoother surfaces than uncoated membranes. This coating was rich in oxygen, and the oxygen appeared to be mainly associated with hydroxyl groups. These findings led to the conclusion that the surface coating is likely comprised of poly(vinyl alcohol). Coated membranes included the BW30 membrane. Other membranes such as those from GE Osmonics (e.g. SG membrane) appeared to have a hydrophobic aliphatic surface modification (such as a polyester), but the exact chemical composition of the surface modification was not determined.

Nonetheless, it must be noted that membrane manufacturers are constantly adapting and developing such coatings so that individual testing must be carried out for each membrane type prior to use. For this reason, all membranes were subjected to an extensive cleaning procedure by removing the preservative layer from the membranes in different ways and by comparing the results using ATR-FTIR spectroscopy. It has been tested: pure water; 30:70 EtOH water solution for 1 h at 25 °C; 30:70 EtOH water solution for 24 h at 25 °C; 30:70 EtOH water solution for 1 h at 40 °C; pH 2; pH 11. The spectra of the BW30 membrane is shown in Figure 39, the spectra of the other membranes are in the Appendix, cf. Figure 125.

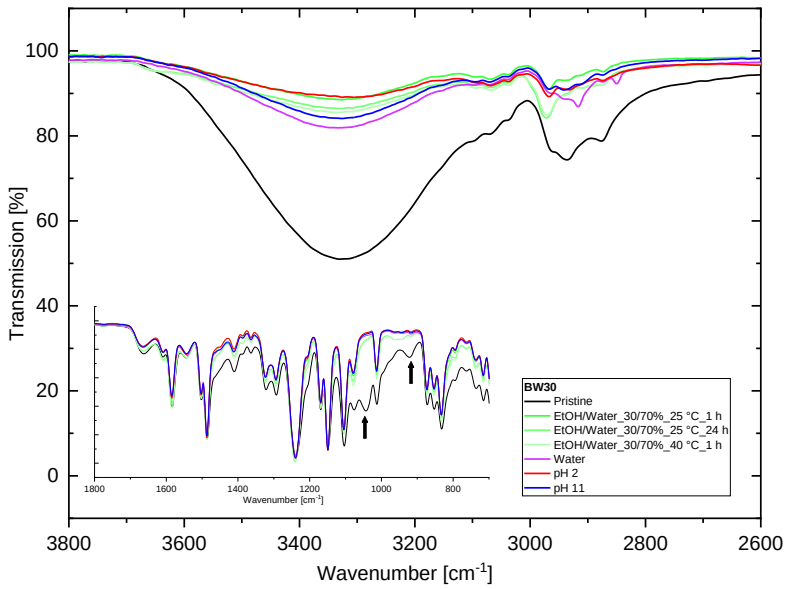

Figure 39: IR spectra of pristine and washed BW30 membrane using different washing solutions and enlargement of the finger print range (1500 – 800 cm^{-1}).

Major differences can be found between the pristine (coated) and washed membrane samples. The pristine membrane exhibits a broad band centered around 3330 cm^{-1} and several smaller peaks around 2900 cm^{-1}. The broad band at 3330 cm^{-1} is a complex band due to the overlapping of stretching vibration of N-H and carboxylic groups of the PA layer and additional groups such as O-H group from the coating, most likely PVA. The high intensity for the pristine membrane is probably due to the over-abundance of O-H groups in the coating. The intensity of these bands has decreased significantly after washing so that most of the coating was probably removed. The peaks around 2920 cm^{-1} can be assigned to stretching of aliphatic C-H bonds. Thus, the coating material is mostly aliphatic with great abundance of OH groups.[155] Also, differences in the fingerprint range (wavenumber 1048 cm^{-1} and 922 cm^{-1}) can be detected between the pristine (coated) membrane and the washed membranes. The absorption band at 1048 cm^{-1} could be attributed to the characteristic absorption band of sulfonic acid group. This additional band might indicate that the coating consists of sulfonated PVA.[158]

However, pure water is sufficient to remove most of this layer. No significant differences in the intensity of these mentioned peaks can be found for the membranes washed with different washing solutions. Thus, it is proven that the pristine membrane is coated with a preservative layer which can be washed away considerably, thus, the coating is not chemically cross-linked.

In addition, the contact angles of all membranes washed with pure water were measured and compared (cf. Figure 40). It is noticeable that the SE membrane has exceptionally high contact angles (approx. 55 °) compared to RO98pHt, BW30, Lewabrane and AK. This contact angle was also determined by Akin *et al*.[144] According to the manufacturer, the SE membrane has an improved chemical stability as it is stable over a wide pH range of 1 – 11 and one of the designated application is chlorine resistant water treatment.[159] Thus, the coating might have been applied to impart chemical resistance to these membranes, at the cost of surface hydrophilicity.

The contact angles for the other full-aromatic membranes BW30, RO98pHt, Lewabrane and AK are lower and even smaller than reported literature values for PA TFC RO membranes (30 ° vs. 43 – 49 °). This is unusual as such low contact angles are actually reported for semi-aromatic NF membranes due to their reduced aromaticity.[156] In fact, these obtained low contact angles are consistent with those reported for coated membranes and can be therefore attributed to a remaining amount of (sulfonated) PVA coating on the surface, resulting in an increased hydrophilicity. However, these low values could be also due to the very rough ridge-and-valley surface structure of the PA layer as rougher surfaces lead to smaller contact angles.[156]

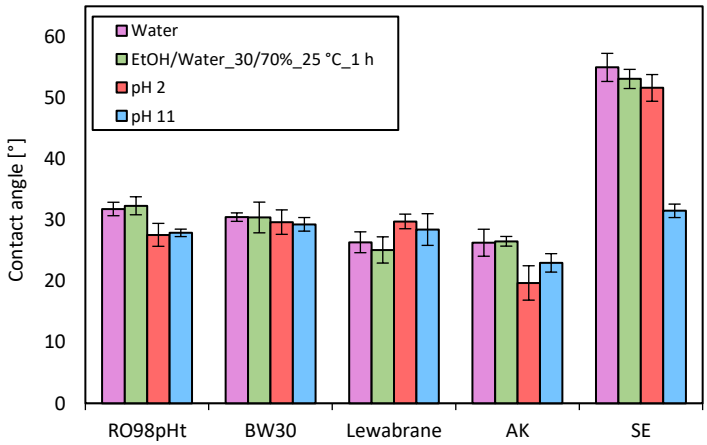

Figure 40: Contact angle of pristine and washed BW30 membrane using different washing solutions.

To complete the surface characterization, the zeta potential of all membranes was investigated after cleaning with pure water (cf. Figure 41). As can be seen from the figure, the isoelectric point of all membranes ranges from 4.1 to 4.9, which corresponds to the value given in the literature for PA TFC RO membranes.[160] That means that these membranes are mildly negatively charged at neutral pH. As some of the acyl chlorides do not react with amines

during IP and are hydrolyzed to form carboxyl groups, the PA layer always possess an anionic charge at neutral pH ranges. It is also visible that the zeta potential is highly pH dependent. The zeta potential is approx. + 30 mV at pH 3 and – 30 mV until – 60 mV at pH 9. Such amphoteric behaviour is due to the presence of both amine and carboxylic acid groups and was already studied and documented in the literature for PA TFC RO membranes.[161] It can be concluded that the Lewabrane membrane is most negatively charged (– 60 mV), indicating the presence of significant amount of free carboxylic groups. This is followed by HR98pHt and BW30 (approx. – 50 mV). The most neutral membranes are AK and SE (approx. – 30 mV).

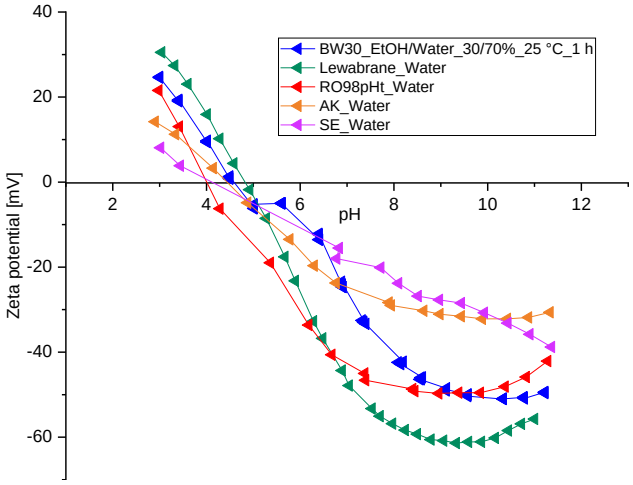

Figure 41: Zeta potential of the commercial membranes BW30, Lewabrane, RO98pHt, AK and SE (after washing).

Unlike the contact angle values, these zeta potentials do not match those values from the literature for coated membranes. For example, the zeta potential for the (coated) BW30 was reported to range from 10 mV at pH 3 to – 10 mV at pH 9 which is not observed here for BW30 (20 mV for pH 3 and – 50 mV for pH 9). In the case of an incomplete coating layer, the surface charge is mainly influenced by the polyamide layer. Thus, the high negative surface charge could point to an incomplete coating layer that has been washed off to a large extent.

It must be also considered that the comparison of zeta potentials is not straightforward as differences can be also ascribed to the different zeta potential measurement systems used. The zeta potential (streaming potential) in the Tang study was measured in an unconventional way and thus, differently to that in this work as a single piece of membrane sample was mounted to a reference PMMA channel plate.[162] In this work however, two identical membrane samples were mounted face to face and separated by a channel spacer. Thus, the

instruments are based on a different measuring principle, probably resulting in different measured zeta potential values.

5.1.3 Interim conclusions

Overall, it can be concluded that the commercial membranes BW30, Lewabrane, RO98pHt and AK investigated in this study are full-aromatic membranes while the SE membrane is a semi-aromatic PA membrane. In addition, all these membranes are provided with a preservative layer, which can be washed off to a considerable extent with only pure water. Therefore, it is most likely a coating that is applied to the membrane for protective purposes prior to use. However, a small proportion of the coating still exists due to the highly hydrophilic membrane surfaces measured via CA. Therefore, the membranes were washed with a 30:70 EtOH/water solution for 1 h at 25 °C for 1 h and then immersed in pure water for 24 h before usage. This ensured an almost complete removal of the protective layer, so that the coating of these membranes is basically uncritical for a further modification of the membrane. In the next chapter, the fouling behaviour of the preselected membranes RO98pHt, BW30, Lewabrane, AK and SE is investigated towards real cooling water from the steel industry.

5.2 Analysis of fouling potential and membrane performance with real cooling water from steel industry

The aim of this chapter was to examine different provided cooling waters regarding their fouling potential. At first, the feed was analyzed in order to predict the fouling potential. Afterwards, different filtration experiments were carried out with the commercial membranes investigated in chapter 5.1 to analyze occurring fouling. Based on this, a suitable antifouling coating for membranes should be selected. It was aimed to choose a membrane with a relatively high fouling resistance, since coated and uncoated membranes are to be tested in a direct comparison in the field tests of the project (cf. chapter 5.9). The effect of the modification may therefore not be clearly noticeable. The aim of a pure modification study, which is to evaluate only the effect of the coating, was therefore not followed.

5.2.1 Fouling prediction by analyzing the feed composition

In practice, membrane fouling is usually caused by a combination of different fouling types.[93] For the design of an RO system, it is therefore desirable to have an analytical procedure available to predict quantitatively how severely a given feedwater will foul a membrane. Unfortunately, no universal technique meets this need adequately, especially if the composition of the feed water varies too much.[5] However, several fouling prediction tools and techniques have been developed to describe membrane fouling.[163-166] For that purpose, two different cooling waters were analyzed for salinity and different ion concentrations via photometry, for organic matter via TOC and DOC and for particles via SDI, total solids and the Hermia model. The waters to be tested are, on the one hand, cooling water from the rolling mill of Deutsche Edelstahlwerke (CW_DEW) and, on the other, from the rolling mill of a plant in Spain (CW_Sp). Both waters were used for direct product cooling. CW_DEW represents the cooling water which will be finally treated in the project's pilot plant.

Table 6: Analysis of the cooling water CW_DEW and CW_Sp for different ion contents.

Analyzed parameters	CW_DEW	CW_Sp
Conductivity [µS/cm]	637	1100
Cl [mg/L]	12	119
Fe [mg/L]	0.11	0.01
Na [mg/L]	61	-
K [mg/L]	7	33
PO_4 [mg/L]	< 0.2	0.7
NH_4 [mg/L]	0.07	0.2
Mg [mg/L]	9	33

When looking at Table 6, it is noticeable that the conductivity and ion concentrations of CW_DEW are significantly lower than those of CW_Sp. The values for CW_DEW are of the same order of magnitude as for potable water.[167] In contrast, the conductivity of CW_Sp is significantly higher and in the range of fresh water.[167] The conductivity is a measure of the ability of water to conduct electrical current and thus, it indicates the amount of dissolved ionic solids in water. If the ionic product of these dissolved solids exceeds the equilibrium solubility product, then scale is formed. In the first place, this indicates that CW_Sp provides a higher potential for scaling compared to CW_DEW. The critical indicators for scaling are discussed in the following.

Scaling caused by $CaSO_4$ is a typical deposit in cooling water processes which leads to an additional resistance and a decrease of the water flux at constant pressure and thus has an huge influence on the functionality and efficiency of an RO plant.[168] Therefore, the critical indicators calcium and sulfate and their solubility product are summarized in Table 7.

Table 7: Analysis of the cooling water CW_DEW and CW_Sp for calcium and sulfate and calculation of ionic (IP) and solubility product (K) of calcium sulfate.

Analyzed parameters	CW_DEW	CW_Sp
SO_4 [mg/L]	62	230
Ca [mg/L]	56	140
IP [$CaSO_4$] [mol^2/L^2]	$9.05 \cdot 10^{-7}$	$1.16 \cdot 10^{-5}$
$K_{[CaSO_4]} \left[\frac{mol^2}{L^2}\right] = 4.93 \cdot 10^{-5}$		

It is apparent that the concentrations of calcium and sulfate in CW_Sp are multiple times higher than in CW_DEW. To predict potential fouling by $CaSO_4$ scaling, the ionic product IP of

Ca and SO_4 is calculated and compared to the solubility product K of $CaSO_4$, which should predict a possible precipitation. The ionic product $IP_{[CaSO4]}$ is calculated as follows:[169]

$$IP_{[CaSO_4]} = [Ca^{2+}] \cdot [SO_4^{2-}] \quad (35)$$

The square brackets represent the concentrations in mol/L and mol^2/L^2, respectively. It must be noted that all cooling waters bear a certain potential for scaling, as salt precipitation and scaling may occur, depending on the operated recovery. However, when comparing the ionic product $IP_{[CaSO4]}$ with the solubility product $K_{[CaSO4]}$ from the literature[169] ($4.93 \cdot 10^{-5}$), it can be concluded that scaling in the form of calcium sulfate represents a minor risk in CW_DEW and could only become critical at high concentrations or recovery rates. When considering the ionic product in CW_Sp, a much higher risk for scaling is revealed, since the value is close to the solubility product of $CaSO_4$ so that, even at low concentrations or recovery rates, calcium sulfate may precipitate. Thus, the DEW cooling water (CW_DEW) shows a generally uncritical behaviour with view to $CaSO_4$ scaling.

The SDI was measured to determine the potential of particle fouling. As described in chapter 4.6.1.3, an SDI of less than 1 %/min means that the reverse osmosis system can run for several years without colloidal fouling whereas an SDI of 3 – 5 %/min means that particulate fouling is likely to be a problem. An SDI of more than 5 %/min is unacceptable and indicates that additional feed pre-treatment is required.[29] For CW_Sp, the maximum SDI is exceeded (cf. Table 8). Also, the silica concentration is remarkable with a value > 30 mg/L. It should be mentioned in this context that silica can occur as crystalline silica and precipitate in the form of silica mineral, promoting scaling but can also exist in colloidal form, causing particle fouling.[170] Due to the high SDI of CW_Sp, it can be presumed that the silica in CW_Sp represents rather particulate silica that has been deposited on the membrane during the determination of the SDI. Hence, CW_Sp must not be applied to the RO membrane without pre-treatment, as this would entail a high risk of particle fouling, resulting in immediate blocking and clogging of the membrane.

Table 8: Analysis of the cooling water CW_DEW and CW_Sp for SDI and silica.

Analyzed parameters	CW_DEW	CW_Sp
SDI [%/min]	2,7	Max.
Silica [mg/L]	6	> 30

Although the SDI for CW_DEW with 2.7 %/min and the silica concentration are below the critical limit, it could result in the deposition of particles on the membrane at high concentrations or recovery rates. In order to accurately predict the degree of particle fouling coming from CW_DEW, the formula (36) was applied which is the ‘‘standard’’ classical blocking model proposed by Hermia in 1982 and is valid for filtration experiments carried out at constant pressure.[171]

$$\frac{d^2t}{dV^2} = K\left(\frac{dt}{dV}\right)^n \qquad (36)$$

Where t is the filtration time, V is total filtered volume, K is a fouling coefficient and n is a dimensionless filtration constant reflecting the mode of fouling. According to Hermia, this equation represents a basic equation for all possible particle fouling models. In this context, cake filtration is of importance, which describes the deposition of particles on the membrane surface and results in a hydraulic resistance. Therefore, formula (36) can be expressed as follows, so that the cake-filtration equation is obtained:[171]

$$K_C V = \frac{2t}{V} - \frac{2}{Q_0} \qquad (37)$$

Where Q_0 is the initial flow rate and K is the constant with the subscript indicating the blocking mechanism. The cooling water was filtered through an RO membrane (Lewabrane) at constant pressure of 10 bar and a recovery rate of 80 %. To illustrate fouling, the reverse cumulative flux was plotted against the permeate volume, which ideally follows a linear relationship if the fouling is governed by the cake filtration mechanism. This can be observed in Figure 42 (a) for CW_DEW as the curves display a steady linear increase in flux. To analyze the fitting range of particle fouling, the cake filtration equation (37) was then applied. Filtration processes that suffer from colloidal fouling show a behaviour that corresponds to that of a cake filtration even at small permeate volumes. A linear relationship must be achieved with a coefficient of determination > 0.95. Figure 42 (b) shows that the linear fit yields a coefficient of determination of 0.99 which is probably due to the formation of an ever-increasing layer of particles. Thus, it can be concluded that there is probably a risk of particle fouling when filtering CW_DEW at a recovery of 80 %.

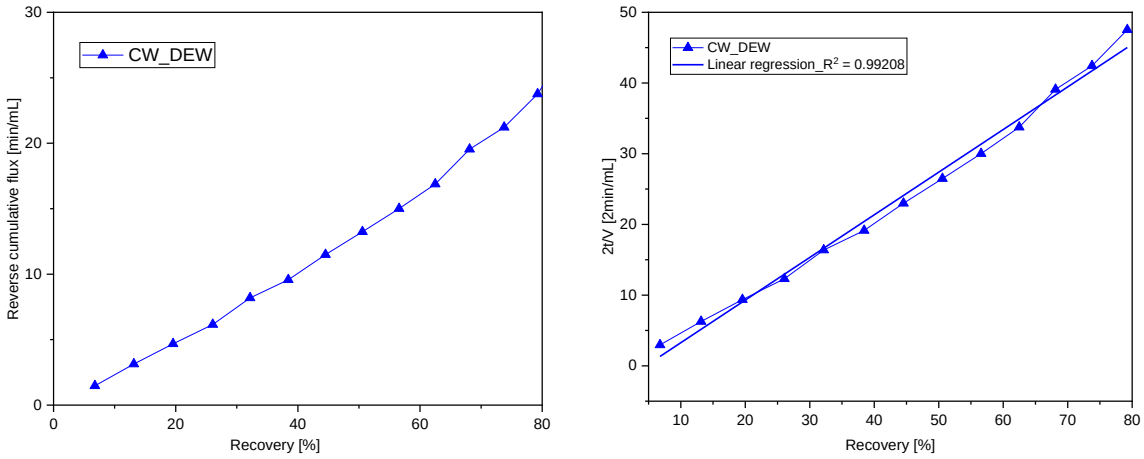

Figure 42: (a) Reverse cumulative flux and **(b)** Plot of 2t/V in dependency of the recovery during constant pressure filtration of CW_DEW at 10 bar and 300 rpm.

TOC and COD measurements were also performed to predict the potential for organic fouling (cf. Table 9). TOC includes all organic carbons that deposit on the membrane and foul the membrane reversibly or irreversibly, resulting in a decrease in water flux. TOC analyses of the cooling water revealed a total organic content of 15 mg/L for CW_DEW and of 3.9 mg/L for CW_Sp. Even if both values exceed the critical value of 3, CW_DEW poses a significantly higher risk for organic fouling due to the fourfold higher concentration of TOC. Also, the COD content in CW_DEW exceeds the critical value of 10.[169] The concentration of organic and lipophilic substances in CW_DEW is mainly attributed to the presence of conditioning chemicals (epichlorohydrin copolymer) and flocculants (distillates (petroleum, crude oil), alcohols, kerosene, etc.) added to the cooling water.

Table 9: Analysis of the cooling water CW_DEW and CW_Sp for TOC and COD.

Analyzed parameters	CW_DEW	CW_Sp
TOC [mg/L]	15	3.9
COD [mg/L]	20	-
Lipophilic substances [mg/L]	0.3	-

Even though, both cooling waters originate from rolling mills, there are significant differences in the degree of contamination, so that different fouling scenarios could be derived. CW_Sp does not represent water that typically causes organic fouling but has a high risk for $CaSO_4$ scaling and fouling by silica particles. In contrast, CW_DEW bears no risk for scaling, but has a slight chance for organic and particle fouling. In the next subchapters, filtration experiments

will be performed to investigate whether and to what extent fouling affects the commercial pre-selected RO membranes examined in chapter 5.1.

5.2.2 Short-term dead-end filtration experiments and surface characterization

In this chapter, dead-end concentration experiments were performed with the pre-selected membranes from 5.1 (RO98pHt, BW30, Lewabrane, AK and SE) and the cooling waters CW_DEW and CW_Sp. The aim was to correlate occurring fouling during filtration with the fouling phenomena predicted in 5.2.1, to further narrow down the choice of membranes to be used. Filtration experiments were carried out at a stirring rate of 300 rpm by concentrating the cooling water volumetrically to five times of its original volume (recovery rate of 80 %). The transmembrane pressures were approx. as given in the respective data sheet of the membrane. As explained in chapter 4.7.1, the FRR value (flux recovery ratio) can be calculated according to equation (31), where J_1/J_0 describes the relative permeance after fouling and J_2/J_0 the relative water permeance after washing with pure water. This allows conclusions to be made about reversible and irreversible fouling with respect to washing with pure water.

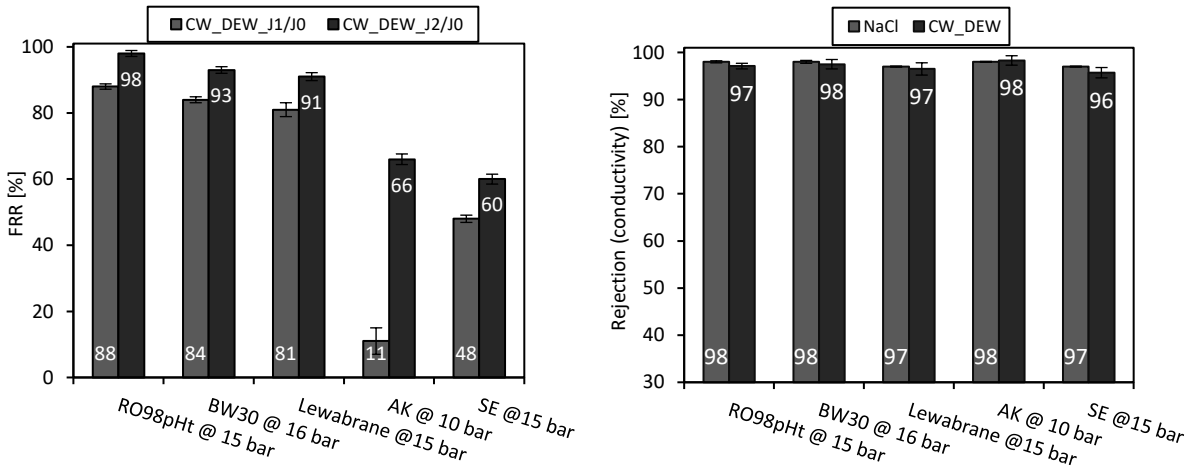

Figure 43: (a) FRR values after a fivefold concentration of CW_DEW at 300 rpm (J_1/J_0) and after washing with pure water (J_2/J_0) during dead-end experiments. **(b)** NaCl rejection and overall salt rejection after filtration of CW_DEW.

By comparing the performance of all membranes after fouling (J_1/J_0), it could be noted from Figure 43 (a) that the membrane AK from GE Osmonics suffers the most from fouling which is reflected in a considerable reduction of permeance. It possesses only 11 % of its initial permeance. This could be the consequence of its relatively high initial water permeance of

4.7 LHMbar without any foulant (cf. Table 5) which causes particles in water getting pulled towards the membrane surface much faster than they are being carried away from the surface. Thus, CP occurs at a larger extent due to the high flux at the beginning of the filtration.[172] This in turn leads to an additional reduction of the flux, which promotes irreversible fouling on the membrane surface. The membrane RO98pHt shows the highest fouling resistance towards the cooling water reflected in a high FRR value (J_1/J_0) of 88 %. The membranes BW30 and Lewabrane show comparable fouling resistances with FRR values of 84 % and 81 %, respectively. In contrast, the SE membrane has a much lower fouling resistance with an FRR value (J_1/J_0) of 48 %.

Looking at the FRR values after washing with water (J_2/J_0), it becomes clear that the permeance of the membranes RO98pHt, BW30 and Lewabrane could be nearly recovered after washing with only pure water. RO98pHt displays the highest value with 98 %, followed by BW30 with 93 % and Lewabrane with 91 %. The water permeance would probably be completely recovered for the three membranes if they were physically and/or chemically cleaned, so that reversible fouling can be expected under the dead-end filtration conditions performed here. In contrast, the water permeance of the AK membrane can only be recovered to an FRR value of 66 %, which would strengthen the argument of a potentially irreversible fouling layer on the membrane. This indicates that the probability of irreversible fouling is higher for AK than for RO98pHt, BW30 and Lewabrane. The SE membrane has the lowest FRR of only 60 %. This is consistent with the fact that the SE membrane is highly hydrophobic (cf. chapter 5.1.2) and thus more prone to fouling. It proves that the focus of this membrane was to impart chemical resistance, at the cost of surface hydrophilicity. Considering the overall salt rejection in Figure 43 (b) (measured via conductivity), it is noticeable that the values barely differ from the values for NaCl. This can be attributed to the low conductivity of CW_DEW as the diffusive salt flux is smaller at lower concentrations or conductivity.

It can therefore be concluded that the tendency for irreversible fouling for the membranes RO98pHt, BW30 and Lewabrane is very low compared to AK and SE, so that the long-term experiments (chapter 5.2.4) are carried out with these three membranes while AK und SE will be excluded.

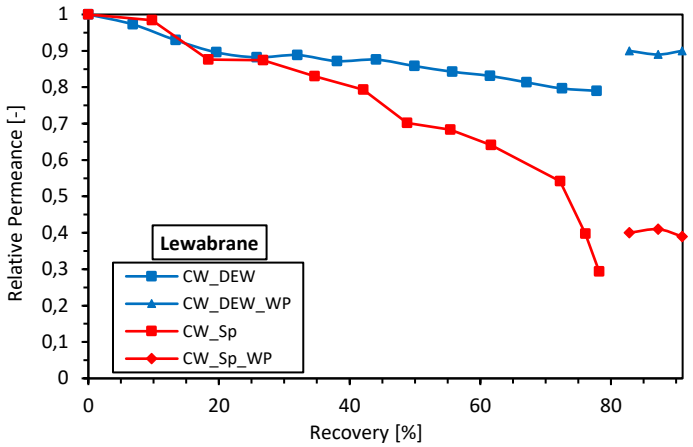

Figure 44: Relative permeance course of Lewabrane during dead-end fouling with CW_DEW (blue) and CW_Sp (red) at 300 rpm as a function of recovery.

Figure 44 also shows the relative permeance course for the Lewabrane membrane exemplary during fouling with CW_DEW as a function of the recovery (blue curve). For comparison, the course of filtration with the higher contaminated water CW_Sp is also depicted (red curve). The relative permeance for CW_DEW is characterized by an almost stable course. The slight decrease is due to the existing osmotic pressure, reducing the driving force for the water transport due to solutes on the feed side so that the flux decreases. However, the water permeance can be recovered almost completely (91 %), as already shown above (J_2/J_0 for Lewabrane). On the contrary, for CW_Sp it is shown that the course of the flux follows a steeper and linear decrease. Since CW_Sp is highly charged with ions and particles (cf. chapter 5.2.1), these solutes become more concentrated on the feed side with increasing recovery which leads to an accumulation of those in a mass transfer boundary layer adjacent to the membrane surface. These dissolved molecules accumulating at the surface, impede the water transport.[173] This results in a decrease of water flux through the membrane. The increased solute concentration at the surface leads to an increase in concentration polarization, which in turn can cause irreversible fouling. In order to estimate whether the formation of scaling is responsible for the strong decrease in permeance, the ionic product for calcium and sulfate in the retentate was calculated and compared with the solubility product of $CaSO_4$. The calculation proved that the solubility product of $CaSO_4$ in the retentate was significantly exceeded, so that scaling is most likely the reason for the strong decline in flux. Scaling in form of $CaSO_4$ can be removed in most cases only by cleaning with an alkaline solution, depending on the viscosity and interactions with the membrane surface.[168] This is probably the reason

why only 40 % of the water permeance is restored after washing the membrane with pure water.

To validate the findings from the dead-end short-term tests, the Lewabrane membrane surface was examined after fouling via SEM, EDX, ATR-FTIR and contact angle measurements. The SEM pictures in Figure 45 a) (fouling with CW_DEW) and b) (fouling with CW_Sp) illustrate the condition immediately after filtration and before washing with pure water. Only a few single gel-like deposits can be observed from a), which could indicate organic material or accumulated particles. By means of EDX measurements it could be found that the fouling layer in a) consists mainly of carbon (83 wt%), oxygen (10 wt%) and sulfur (7 wt%), so that scaling by $CaSO_4$ and fouling by silica particles can be excluded. Even though, a certain risk for organic fouling is existent, it appears to be low. Via ATR-FTIR, no bands different from the base membrane could be detected. This is because ATR-FTIR is not a very surface-specific analysis technique as the ATR-FTIR signal is a combination of both the polyamide layer and the support. The fouling layer has most likely a thickness in the range of several hundred nanometers, compared to the penetration depth of approx. 1 – 3 µm of the ATR-FTIR (cf. equation (24)) so that characteristic peaks of the fouling layer cannot be observed. Contact angle measurements could not provide any additional information neither.

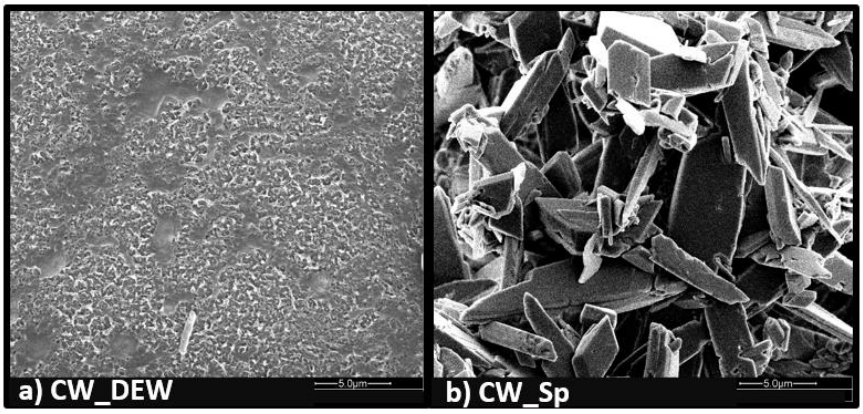

Figure 45: SEM images of Lewabrane immediately after fouling with a) CW_DEW and b) CW_Sp.

The membrane in b) features severe salt precipitation, whose structure can be clearly assigned to $CaSO_4$.[174, 175] According to EDX measurements, the fouling layer is composed of carbon (4 wt%), oxygen (44 wt%), sulfur (21 wt%), calcium (30.5 wt%) and silica (0.5 wt%). This is coherent with the previously made statements that CW_Sp exhibits a very high risk for $CaSO_4$ scaling. However, no silica particles can be observed on the SEM image. This is probably due to the excessive salt precipitation covering the particles, so that particle fouling by silica can

certainly play a significant role. Likewise, further surface characterizations using ATR-FTIR and contact angle measurements did not provide any additional information about the fouling scenarios.

In summary, filtration of RO membranes with CW_Sp involves a great risk for scaling. This was predicted by the feed analysis and confirmed by the filtration experiments. Fouling by silica particles is another source for fouling due to the high SDI level. For this reason, CW_Sp must be pre-treated intensively before applying it to RO membranes, as otherwise strong and eventually irreversible fouling by scaling and particles might occur. For CW_DEW a certain risk of organic and particle fouling was predicted, which turned out to be low during the filtration experiments with BW30, Lewabrane and RO98pHt. Thus, it can be concluded that the risk of fouling by organic and particulate matter caused by CW_DEW is negligible under the dead-end filtration conditions performed here.

5.2.3 Critical flux measurements

In this chapter, critical flux measurements were performed with the waters CW_DEW and CW_Sp using the Lewabrane membrane. Such measurements provide information on whether the reduction in flux during filtration is caused solely by the formation of pure CP or by additional fouling.

The concept of critical flux was originally given by Field *et al*.[176] According to Figure 46 (a), the critical flux can take the strong or weak form. The strong form is defined as the transmembrane pressure at which the flux starts to deviate from the pure linear water line, indicating the occurrence of CP exclusively. The weak form describes the case where fouling starts from the beginning and so the flux-TMP relationship is below that of the pure water line, so that CP and fouling cannot be distinguished. The critical flux is the point at which the curve becomes non-linear.[176] Both types are strongly dependent on the nature of foulant, membrane characteristics and system operating conditions.

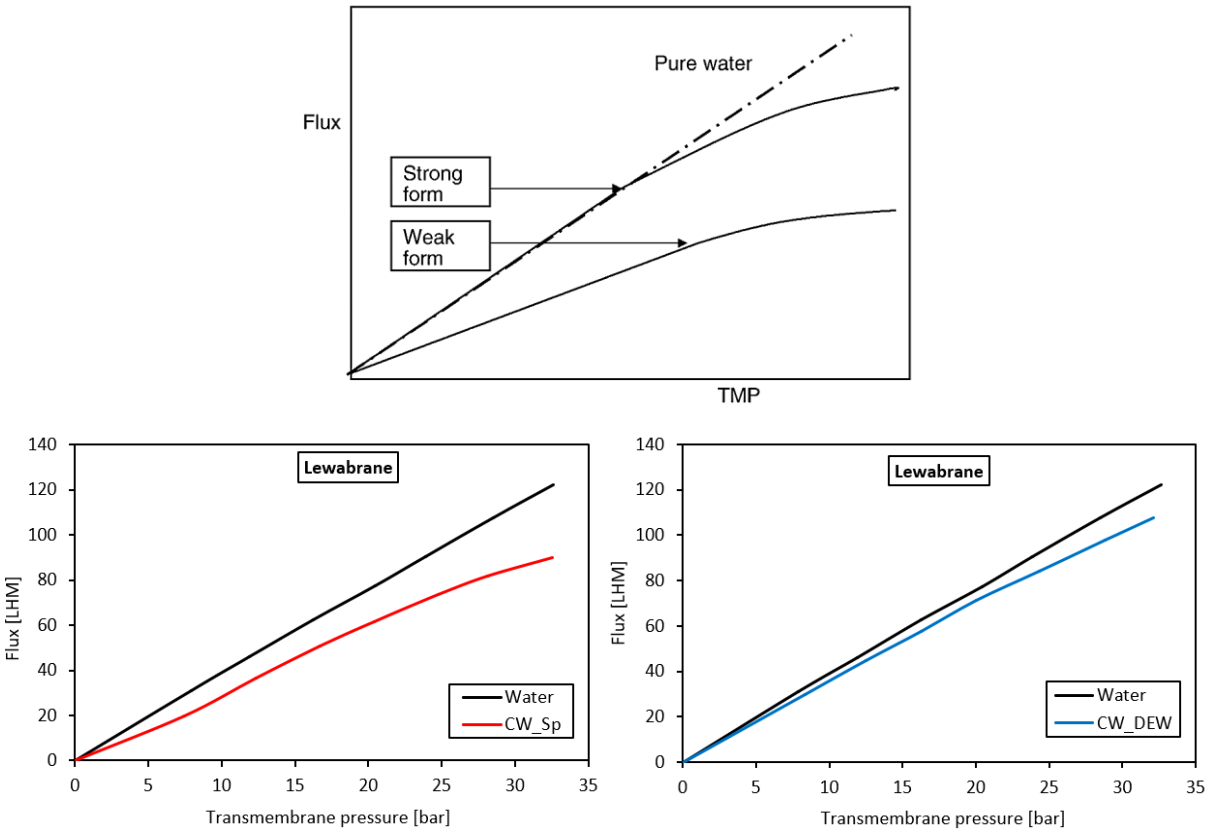

Figure 46: (a) Strong and weak form of critical flux concept.[176] **(b)** Critical flux measurement of CW_Sp during cross-flow, CFV of 0.29 m/s and Reynolds number of 217. **(c)** Critical flux measurement of CW_DEW during cross-flow, CFV of 0.29 m/s and Reynolds number of 216.

Experiments were done with Lewabrane in cross-flow by imposing a pressure, allowing the determination of a steady-state flux. This is reliable with no time dependence since the duration of each pressure step was sufficient (30 min). The results for CW_Sp and CW_DEW are depicted in Figure 46 (b) and (c), respectively. As expected, the weak form of critical flux is obtained for CW_Sp (b). The linear portion is of lower slope than the pure water flux line. That means, that a dynamic transition from CP to fouling starts from the beginning through low intermolecular repulsion and increased membrane-foulant interactions. Therefore, rapid-fouling occurs on start-up so that the flux-TMP relationship is below that of the pure water line. Under consideration of the results of the dead-end short-term experiments, the strong fouling can be attributed to the formation of scale onto the membrane.

For CW_DEW in (c) a less pronounced weak form can be observed since the linear portion is of only slightly lower slope than the pure water flux line. That means that whilst there is little fouling during the period up to the use of the critical flux, some fouling occurs early and changes the apparent membrane resistance. There is only a small part at the beginning of the graph (up to 3 bar) where the feed solution exhibits the same flux as pure water. That means,

there is fouling from the beginning which is very low since convection and back-diffusion of the foulants are such that net transport of foulants to the membrane is marginal.

The flux at which the curves become non-linear indicates the critical flux which is for CW_Sp around 50 LHM and for CW_DEW around 70 LHM. These observations fit with the obtained results from 5.2.1 and 5.2.2 that for both waters, CW_Sp and CW_DEW, fouling can play a role but the probability for fouling to occur is greater for CW_Sp than for CW_DEW. In the next subchapter, long-term filtration experiments are performed under cross-flow conditions with the RO membranes selected from 5.2.2 (RO98pHt, BW30 and Lewabrane) and CW_DEW.

5.2.4 Long-term stability experiments under cross-flow conditions

To investigate the long-term stability of the selected membranes RO98pHt, BW30 and Lewabrane towards CW_DEW, cross-flow filtration experiments were performed over an extended period of time. Based on these data, a final selection of membranes for the further modification experiments of chapter 5.5 is made.

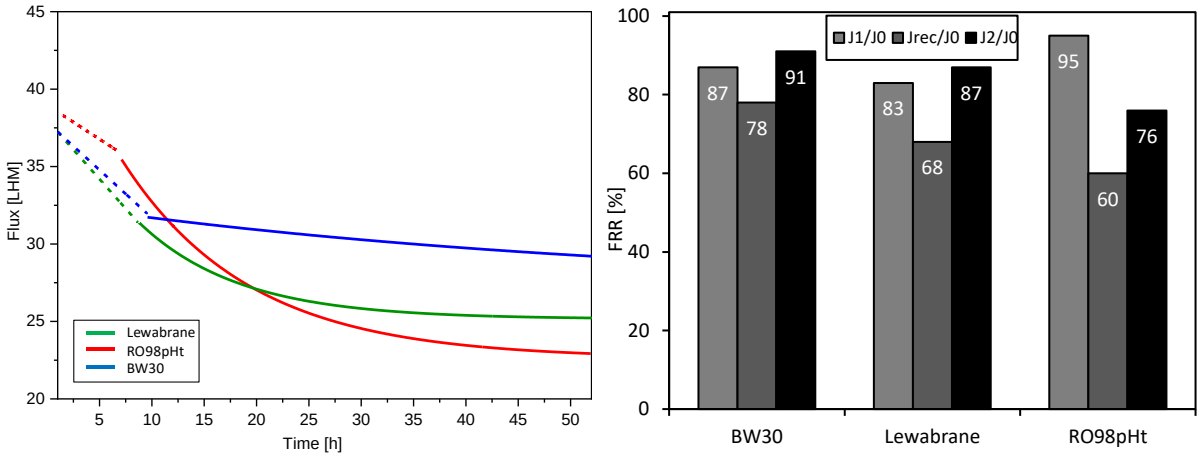

Figure 47: (a) Long-term stability of BW30, Lewabrane and RO98pHt during cross-flow filtration of CW_DEW at a cross-flow velocity of 0.3 m/s (fivefold concentration (dotted line) and recirculation for 48 h (straight line)). **(b)** FRR values after concentration (J_1/J_0), after recirculation (J_{rec}/J_0) and after washing with pure water (J_2/J_0).

In analogy to the dead end tests, the cooling water was first concentrated five times volumetrically (recovery of 80 %) (dotted line) and additionally recirculated for 48 h in cross-flow at 12 bar and a cross-flow velocity of 0.3 m/s (straight line). The course of flux as a function of filtration time is shown in Figure 47 (a), while the corresponding FRR values (J_1/J_0 after concentration, J_{rec}/J_0 after recirculation and J_2/J_0 after washing with pure water) are presented in Figure 47 (b). During concentration, a linear decline is observed for all three

membranes. Interestingly, for Lewabrane and BW30 the flux decreases more rapidly during the fivefold concentration compared to RO98pHt. This is reflected in the different time needed for concentrating the feed water. For RO98pHt the concentration time equals 7 h, while it equals 9 h for Lewabrane and 10 h for BW30. The corresponding FRR values in (b) reveal a reduction in flux for RO98pHt by 5 % after concentration. Lewabrane and BW30, however, lose 17 % and 13 %, respectively. The trend of these values correlates strongly with this after fivefold concentration (J_1/J_0) in the dead-end short-term experiments. A comparison of the FRR values after fivefold concentration (J_1/J_0) for cross-flow and dead-end is given in Figure 48. The slightly lower FRR values for dead-end for each membrane can be attributed to the perpendicular flux towards the membrane and no lateral shear forces, thus leading to a higher foulant propensity.

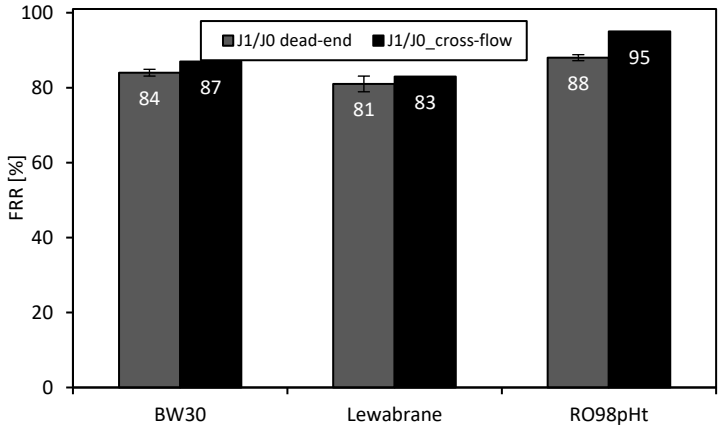

Figure 48: Comparison of FRR values after fivefold concentration (J_1/J_0) obtained from dead-end short-term experiments and cross-flow long-term experiments.

During recirculation (Figure 47 (a) and (b)), however, the flux decreases at a much higher rate for RO98pHt (loss of 40 %) than for Lewabrane (loss of 32 %) and BW30 (loss of 22 %). Furthermore, for RO98pHt no stable state is still reached after 48 h. Even after flushing with pure water, the flux cannot be recovered. At the end, RO98pHt possesses only 76 % of the initial flux, whereas Lewabrane and BW30 achieve 87 % and 91 % of their initial flux.

It can be concluded that the RO98pHt membrane has a higher fouling resistance during concentration compared to Lewabrane and BW30. However, the membranes BW30 and Lewabrane exhibit a higher fouling resistance in the long-term stability test. In addition, the water permeance for these two membranes can be recovered to a higher degree after washing with only pure water. Thus, the cooling water CW_DEW demonstrates a relatively

uncritical fouling behaviour for BW30 and Lewabrane under the cross-flow filtration conditions performed here. As a consequence, the RO98pHt membrane was excluded and the membranes Lewabrane and BW30 were selected for further modification experiments in 5.5.

5.2.5 Interim conclusions

Taking all results of this chapter into account, it must be concluded that the reverse osmosis technology cannot be applied industry-wide for the treatment of cooling water in the steel industry since fouling scenarios of varying severity can occur depending on the cooling water to be treated. As the applications for RO membranes are manifold, different requirements on the membrane properties result, so that not all existing factors for fouling can be considered. For CW_Sp, for example, the filtrate performance of an RO membrane could not be maintained without pre-treatment due to severe scaling, as this is associated with a high technical and economical risk. For the cooling water CW_DEW, which is finally to be treated in the WEISS pilot plant, there is no risk for scaling. Also, the risk for organic and particle fouling is minor under the dead-end and cross-flow filtration conditions performed here. However, depending on the filtration conditions (higher recovery or load (L/m^2), etc.) or fluctuating cooling water composition, an increased risk of fouling by organic and particulate matter might exist. Therefore, for mitigating the fouling potential by CW_DEW, a coating with antifouling properties towards organic fouling by non-migratory and spreadable foulants would provide the solution. By this, the physicochemical and topological structures of the membrane surface will be manipulated so that the interactions between membrane and foulants can be weakened. Thus, the RO membranes Lewabrane and BW30 selected here, will be coated with a novel hydrophilic antifouling coating in the further course of this work.

5.3 Characterization of polymeric building blocks

The general aim of antifouling coatings is to reduce the strength of the interactions between surface and fouling substances. As it was found in the previous fouling analysis in chapter 5.2, the cooling water CW_DEW to be treated in the pilot scale tests bears a certain risk for organic and particle fouling. Zwitterionic materials, which generally have a very low fouling tendency in aqueous media towards a wide range of fouling substances, are thus particularly well suited as antifouling materials (cf. chapter 2.6.3). Therefore, in this work a hydrophilic zwitterionic antifouling hydrogel coating was chosen based on preliminary works for the development of a modular platform for polymer systems.[135, 177]

The zwitterionic copolymer as one component of the hydrogel forming system was synthesized in a three-stage synthesis route, according to Figure 49. First, the educts DMAEMA **1** and HEMA **2** were converted with the radical initiator AIBN into the copolymer PDMAEMA-co-PHEMA **3** in a free radical polymerization (FRP). This was followed by an acrylation with methacryloyl chloride resulting in PDMAEMA-co-PMAEMA **4**. Finally, the zwitterionic side groups were introduced by sulfobetainization with 1,3-propanesultone leading to PSBMA-co-PMAEMA **5**. Since the RO TFC membranes are negatively charged, a cationic surface linker was required, acting as adhesion promoter by adsorbing onto the membrane via electrostatic interactions, enabling later the click reaction with the hydrogel. It was synthesized by quaternization of PDMAEMA-co-PMAEMA **4** with iodomethane, leading PTMA-co-PMAEMA **6**.

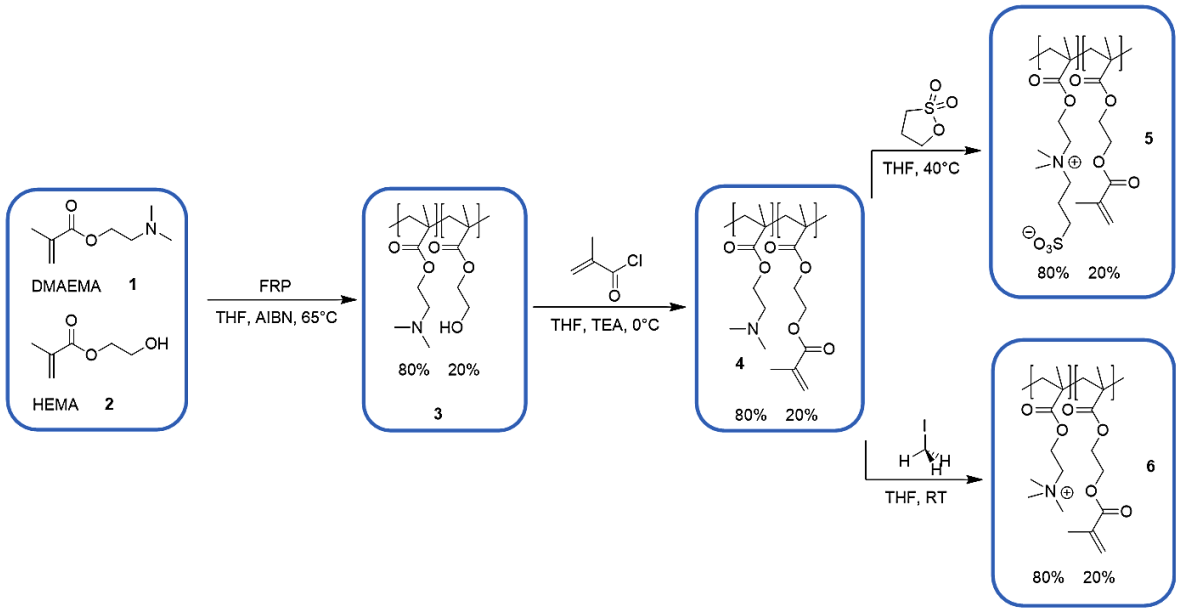

Figure 49: Three-stage synthesis route of the copolymer and surface-linker: Free radical copolymerization of **1** and **2** to **3**; acrylation to **4**; sulfobetainization to **5** and quaternization to **6**.

5.3.1 Degree of functionalization and molecular weight analysis

First, the zwitterionic copolymer PSBMA-co-PMAEMA and the cationic surface linker (CSL) PTMAEMA-co-PMAEMA were investigated by ^{1}H-NMR spectroscopy to determine the chemical composition and the degree of functionalization. Several batches of the copolymer were synthesized, of which the spectrum of the copolymer batch Copo_17 is shown exemplary. Figure 50 shows the assignment of the signals to the corresponding protons in the functionalized copolymer.

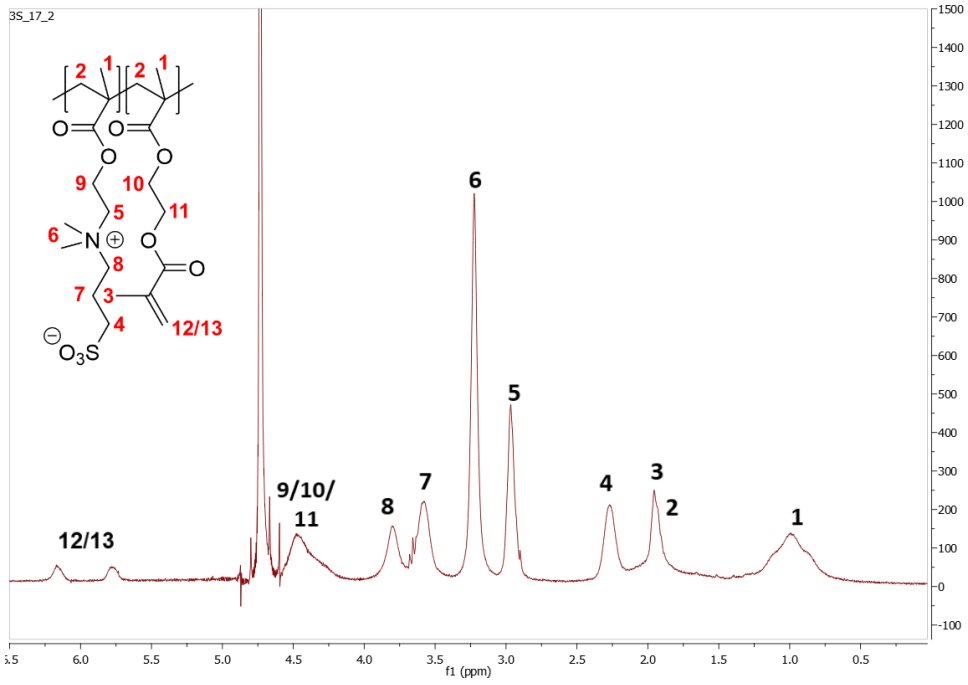

Figure 50: ^{1}H-NMR spectrum and assignment of signals of the copolymer PSBMA-co-PMAEMA.

All signals of the ^{1}H-NMR spectrum could be assigned to the corresponding protons. In addition, unreacted dimethylamino groups cannot be detected (absence of peak at 4.0 ppm),[178] which is an indication for a quantitative conversion. However, small quantities would not be detectable by NMR analysis. Figure 51 also shows an exemplary spectrum of the cationic surface linker CSL_1. Here too, the proton signals can be clearly assigned to the cationic surface linker. In total, successful conversion can be assumed for both copolymers.

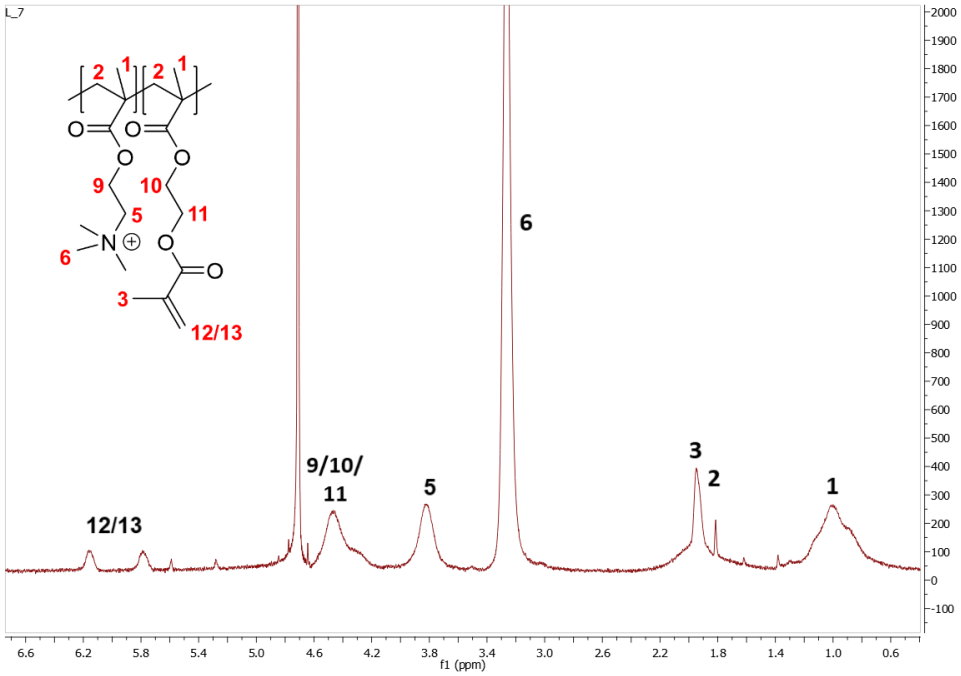

Figure 51: ^{1}H-NMR spectrum and assignment of signals of the cationic surface linker PTMAEMA-co-PMAEMA.

For the zwitterionic copolymer, the degree of functionalization for methacrylate and zwitterionic groups was specified by the synthesis to be 20 % of methacrylate and 80 % of zwitterionic groups. To calculate the experimentally determined fraction of methacrylate groups, the corresponding integrals have to be divided by the number of atoms, according to equation (38). Consequently, the fraction of zwitterionic groups is obtained by equation (39).

$$y_{\mathrm{HEMA/}\mathbf{MAEMA}} = \frac{\frac{\int 13 + \int 12}{2}}{\frac{\int 6}{6}} \qquad (38)$$

$$x_{\mathrm{DMAEMA/}\mathbf{SBMA}} = 100 - y_{HEMA/MAMMA} \qquad (39)$$

For the cationic surface linker, the degree of functionalization for methacrylate and amino units can be calculated analogous. The fraction of methacrylate groups is calculated by equation (40) and the fraction of amino units is obtained by the following equation:

$$x_{\mathrm{DMAEMA/}\mathbf{TMAEMA}} = 100 - y_{HEMA/MAEMA} \qquad (40)$$

GPC analysis was applied to determine the molar mass of the copolymer and cationic surface linker. For the measurement, dimethylacetamide (DMAc) is usually used as eluent. But since the copolymer and the cationic surface linker are only soluble in water, the molar masses could not be accessed directly. However, after copolymerization of HEMA and DMAEMA, the

chain length of the copolymer does not change anymore during acrylation and sulfobetainization. Thus, the fraction of quantity of substances x between the HEMA and DMAEMA units can be used from the NMR spectrum to calculate the theoretical molar masses of the copolymer and linker. For this purpose, a conversion factor $F_{Mw,n}$ is first calculated for the copolymer PSBMA-co-PMAEMA using the formula (41). The molar masses M describe the mass of the repeating unit in the copolymer. By multiplying the factor $F_{Mw,n}$ by the molar mass of the copolymer $M_{PDMAEMA\text{-}co\text{-}PHEMA}$, which is soluble in DMAc, the molar mass $M_{PSBMA\text{-}co\text{-}PMAEMA}$ of the zwitterionic copolymer can be finally calculated:

$$F_{M_{w,n}} = \frac{x_{DMAEMA/SBMA} \cdot M_{SBMA} + y_{HEMA/MAEMA} \cdot M_{MAEMA}}{x_{DMAEMA/SBMA} \cdot M_{DMAEMA} + y_{HEMA/MAEMA} \cdot M_{HEMA}} \quad (41)$$

$$M_{\mathrm{PSBMA-co-PMAEMA}} = F_{M_{w,n}} \cdot M_{\mathrm{PDMAEMA-co-PHEMA}} \quad (42)$$

For the cationic surface linker PTMAEMA-co-PMAEMA the conversion factor $F_{Mw,n}$ is calculated using formula (43), so that the molar mass $M_{PTMAEMA\text{-}co\text{-}PMAEMA}$ of the linker is finally obtained using formula (44):

$$F_{M_{w,n}} = \frac{x_{DMAEMA/TMAEMA} \cdot M_{TMAEMA} + y_{HEMA/MAEMA} \cdot M_{MAEMA}}{x_{DMAEMA/TMAEMA} \cdot M_{DMAEMA} + y_{HEMA/MAEMA} \cdot M_{HEMA}} \quad (43)$$

$$M_{\mathrm{PTMAEMA-co-PMAEMA}} = F_{M_{w,n}} \cdot M_{\mathrm{PDMAEMA-co-PHEMA}} \quad (44)$$

The degree of functionalization, the molar mass M_n and the PDI of the copolymer Copo_17 is shown in Table 10 in comparison to four other copolymers (Copo_18, 19, 20, 21) and the cationic surface linker CSL_1.

Table 10: Degree of functionalization, molecular weight and PDI of specific copolymer batches.

Copolymer/ Cationic surface linker	Degree of functionalization methacrylate:zwitterionic groups [%]	M_n (Universal) [kDa]	PDI (Universal) [-]
Copo_17	22:78	136.0	1.7
Copo_18	22:78	90.1	2.0
Copo_19	22:78	102.6	1.9
Copo_20	24:76	102.3	1.9
Copo_21	23:77	102.5	1.9
CSL_1	23:77	18.0	2.1

As can be seen from the table, the functionalization degrees of different batches show similar values that deviate only slightly from the target value of 20:80 %. For sufficient solubility and

an effective crosslinking, the molar masses of the copolymers should be in the range of 50 to 200 kDa. The obtained molar masses are all in this range and therefore reproducible (90 – 100 kDa). For an ideal free radical polymerization system with termination reaction solely based on recombination, the PDI equals 2. If termination is solely based on disproportionation, then PDI is equal to 1.5.[179] The values of the PDIs obtained here match these values (1.6 – 2.0). Therefore, it can be concluded that, despite free radical polymerization, a sufficiently high molar mass and a low PDI could be obtained for different polymer batches. Also, the cationic surface linker CSL_1 has the same degree of functionalization with a somewhat lower molar mass.

5.3.2 Analysis of copolymer size and solubility behaviour

Dynamic light scattering was used to characterize the size of the copolymer. The hydrodynamic radius is important because it is used to calculate the diffusion coefficient, which in turn is needed to calculate the Sherwood number and the mass transfer coefficient. With this information, the CP during membrane modification can be calculated.

For the measurement, an aqueous solution of the copolymer (0.1 wt%) was prepared and analyzed. Figure 52 (a) shows the intensity versus hydrodynamic diameter for different copolymer batches whose functionalization degree and molar masses have already been discussed in 5.3.1. A broad particle distribution was obtained for all copolymer batches. The particle sizes are in the range of 5 – 20 nm (intensity of 1 %), 100 – 500 nm (intensity of 10 %) and 4000 – 5000 nm (intensity of 6 %). This is an indication of the presence of agglomerates that are larger than the polymer coils. Since the copolymer is a zwitterionic one, self-association exists as a result of the formation of dipole pairs between intra- and inter-zwitterionic groups[129], leading to the formation of agglomerates. Moreover, the copolymer has an amphiphilic character, i.e. in addition to hydrophilic groups, it also has hydrophobic groups (methacrylate), which keep the interaction with the water as low as possible, so that the formation of agglomerates is also favored. The concept of the CP-enhanced crosslinking reaction, however, assumes an ideally dissolved polymer. A gelation and thus formation of the hydrogel should only occur when the critical concentration of the reaction solution (polymer and cross-linker) is exceeded via CP. A large number of existing agglomerates could influence

and complicate the cross-linking reaction by impairing diffusion, so that an irregular and uneven hydrogel network is formed.

However, the scattered intensity is proportional to the hydrodynamic radius to the power of six ($I \sim r^6$). Therefore, care must be taken when interpreting data from samples containing a wide range of size distributions since the scattering signal will be heavily weighted to small numbers of larger particles.[180] Thus, it is likely that the number of agglomerates is small and therefore negligible. For polymers which tend to self-assemble and agglomerate, plotting the number against hydrodynamic radius is more precise and provides more significant results. As can be seen from Figure 52 (b), a monodisperse distribution, thus only a single peak is shown for each copolymer batch. For the different copolymers with comparable molar masses, particle sizes of 4.1 nm (Copo_20), 4.9 nm (Copo_21), 13.5 nm (Copo_19), 28.2 nm (Copo_17) and 68.1 nm (Copo_18) were obtained. There is no straightforward explanation for the different copolymer sizes, as the chemical structure, molecular weight and percentage of size units play important roles in controlling the self-assembly behaviour of the zwitterion and thus macromolecular solubility.[181] Nevertheless, the differences between the different sizes are less attributed to differences in molar mass, as they are highly comparable. It is therefore possible that the difference of 1 – 3 % in the side group fractions (cf. chapter 5.3.1) may have a strong influence on the hydrodynamic diameter and thus complicate the comparison by partially competing intramolecular polymer interactions.

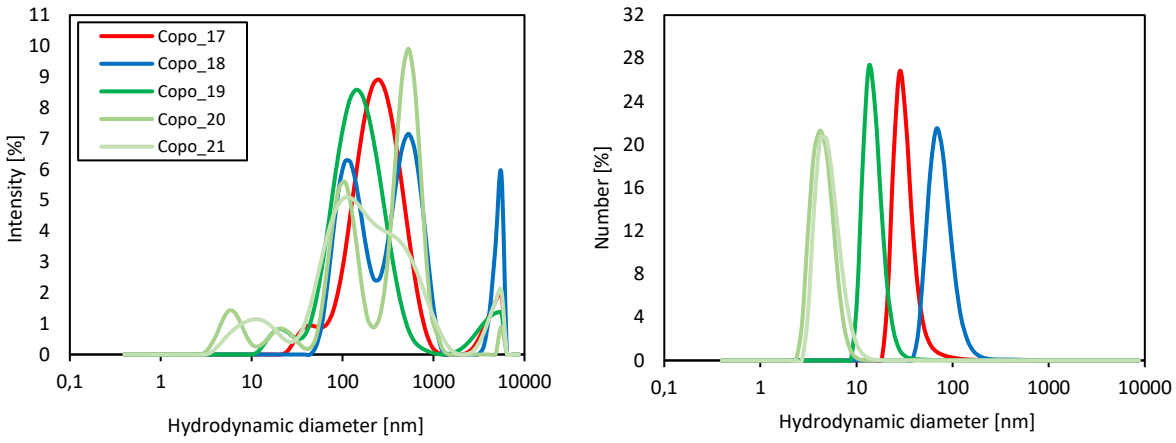

Figure 52: (a) Plot of intensity and **(b)** number vs. hydrodynamic diameter from DLS for specific copolymer batches.

However, for the copolymers Copo_19, 20 and 21, due to the small particle size of up to 13.5 nm, one can assume that the proportion of agglomerates is marginal. For this reason, the

copolymers Copo_20 and 21 with the smallest particle sizes (4.1 and 4.9 nm) were used for the modification experiments in dead-end and cross-flow. Particle sizes > 30 nm indicate that a small proportion of agglomerates may be present. Therefore, Copo_17 (28.2 nm) and Copo_19 (13.5 nm) were investigated for the formation of the bulk hydrogel via in situ rheology.

Since the copolymer Copo_18 has the largest hydrodynamic diameter (68.1 nm), the cloud point of this copolymer was determined after the DLS measurement. The cloud point defines the concentration from which the solubility limit of the polymer solution is exceeded, so that the solution appears turbid. When this occurs, the polymer chain loses its solubility in water and coils upon itself. A two-phase system develops at this point, one phase being polymer rich and the other water rich.[182] Above this concentration, the cohesion forces between the macromolecules are greater than the hydrogen bonding interactions between polymer chains and water. For the measurement, different mass fractions of the copolymer were dissolved in water at room temperature (1 – 10 wt%) and the onset of turbidity was observed. A visual observation of the copolymer solution revealed a turbidity at a concentration of even 1 wt%. This does not seem surprising, since the DLS measurement showed that agglomerates are already present at a lower concentration of 0.1 wt%. According to this, the cloud point is not at 1 wt%, but is rather determined by the fact that the solution consists of differently soluble fractions. So, there is probably an opacity at even much lower concentrations, which is not apparent. A photometric determination would be more accurate here.

To determine the percentage of agglomerates for the copolymer Copo_18, solutions with two different concentrations (0.125 and 0.25 wt%) were prepared and filtered through a MF membrane from Sartorius with a pore size of 100 nm. After filtration, the water was removed by freeze-drying, so that the percentage of the soluble (< 100 nm) and insoluble fraction (> 100 nm) of the copolymer could be obtained. For the polymer concentration of 0.125 wt% a soluble and insoluble fraction of 85 % and 15 % was determined, respectively. For the polymer concentration of 0.25 wt%, the soluble fraction was only 68 % and the insoluble fraction increased to 32 %. Thus, the proportion of agglomerates increases with increasing concentration, but the correlation is not proportional. If the soluble fraction was dissolved in water, turbidity could be observed again. This proves that the agglomerates are constantly reforming due to the nature of the copolymer so that this cannot be prevented.

A size characterization of these solutions was additionally performed using DLS. The intensity plot is shown in Figure 53 (a). The particle distribution for the soluble fractions have become wider but rather monodispersed compared to the unfiltered sample. Particle sizes in the range of 100 – 6000 nm could be identified. The number plot in Figure 53 (b) does also show a broader particle distribution for the soluble fractions. According to this, filtration of the copolymer solution to remove larger particles is not beneficial because the agglomerates are constantly renewing due to the zwitterionic character of the copolymer.

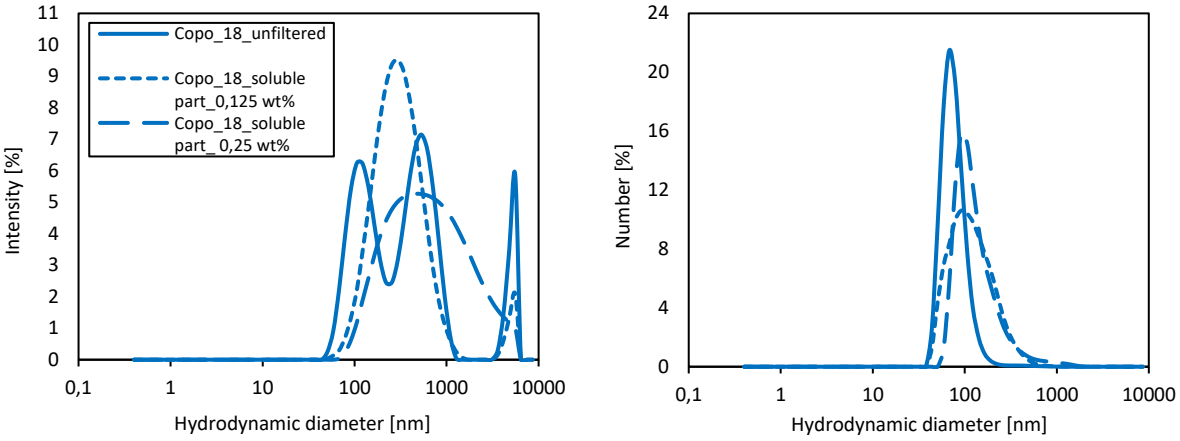

Figure 53: (a) Plot of intensity and **(b)** number vs. hydrodynamic diameter from DLS for the copolymer batch Copo_18 before and after filtration through an MF membrane of 100 nm pore size.

In this section, the particle size distribution of different copolymer batches was analyzed using DLS. From the intensity plot and the cloud point measurement it could be found that the copolymer in water forms more agglomerates with increasing concentration and thus show a more pronounced turbidity. Even after filtration of the copolymer solution through an MF membrane, agglomerates are forming again. However, the copolymers displayed a monodisperse particle distribution when the number was plotted against the hydrodynamic diameter, so that the proportion of agglomerates is negligible. Particle sizes of 4 – 68 nm were obtained for different copolymer batches. As a result, the particle size should not be a limiting factor for the CP-enhanced crosslinking reaction. In addition, for the modification experiments the copolymer is prepared in very low concentrations (up to 0.06 wt%), so that the processing is not affected significantly.

5.3.3 Investigation of viscosity and overlap concentration from rheological measurements

In this chapter the viscosity of the copolymer Copo_19 was investigated. Depending on the characteristic flow curve, the copolymer solution can exhibit Newtonian or non-Newtonian behavior. Therefore, in Figure 54 (b) the shear stress, which is the product of shear rate and viscosity, is plotted against the shear rate. A linear course can be observed in total. Comparing this observation with Figure 54 (a), it can be concluded from the linearity that the polymer solution is a Newtonian fluid. It is also apparent that the shear stress increases with increasing polymer concentration, as the viscosity and thus the probability of polymer chains interacting with each other increases.

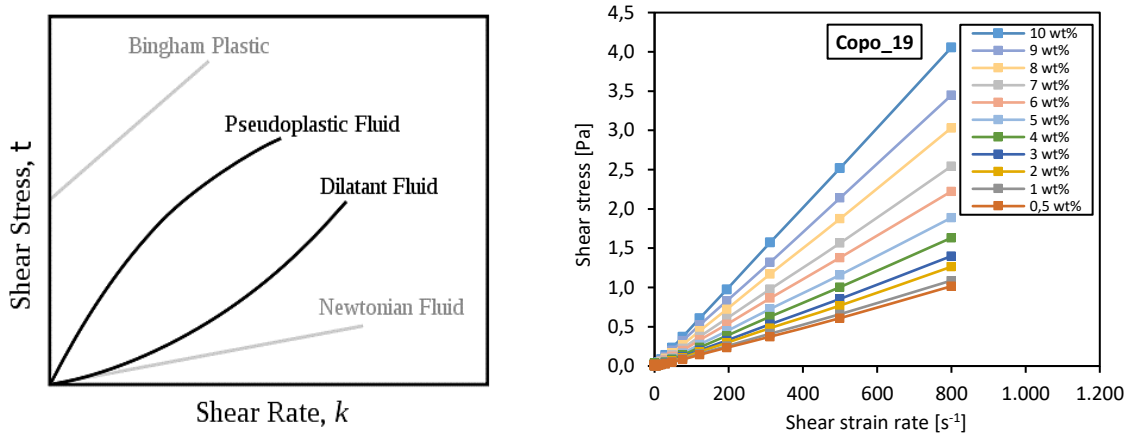

Figure 54: (a) Viscosity behaviour (shear stress vs. shear rate) for Newtonian, pseudoplastic and dilatant fluids.[183] **(b)** Shear stress vs. shear rate for the copolymer batch Copo_19 at different concentrations.

Additionally, in Figure 55 the viscosity is plotted against the mass concentration of the copolymer. It is noticeable that the viscosity increases with increasing polymer concentration, since at higher concentrations the number of coils increases, and thus more frictional forces occur between the polymer chains.

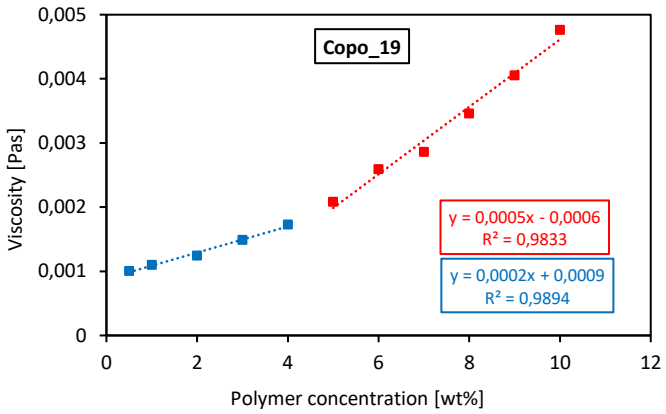

Figure 55: Viscosity vs. polymer concentration for Copo_19 for determination of OLC.

If a linear regression analysis is performed, the increase in viscosity is changing, so that it can be divided into two regimes (blue and red regression). To explain this, the polymer´s behaviour in an aqueous solution must be understood first. For the illustration, the polymer solution is usually pictured as multiple coils. The size of a coil depends on the chain length and interaction between the macromolecule and the solvent. As the polymer chains form, solvent molecules surround all parts of the chains. In solution, the polymer chains (random coils) are expanded and filled with solvent molecules. Hereby, the solvation is dependent on the chemical structure, so that a certain amount of solvent is available per segment. This causes a compact or expended coil to be solvated. With increasing molar mass, the size of the coil increases.[184]

Also, the average distance between the polymer coils in an aqueous solution depends on the polymer concentration. Polymers in aqueous solutions can be generally divided into three concentration regimes, cf. Figure 56:[185] dilute, semi-dilute and concentrated solution. In a dilute solution (c<c*), molecules are well separated on average, thus no interactions between polymer coils exist. At the overlap concentration (c=c*), the coils are getting in contact. Here, the concentration of polymers in solution is equal to the average concentration of segments in an individual coil. In a concentrated solution (c>c*), the polymer coils are strongly entangled and interact with each other.

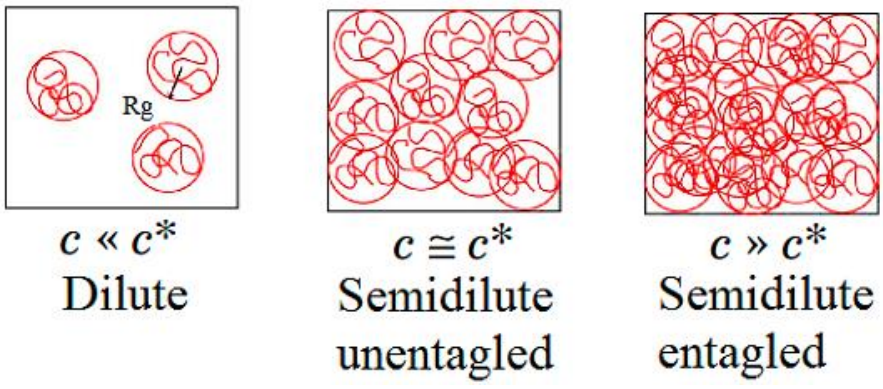

Figure 56: Schematic illustration of a dilute, semi-dilute and concentrated polymer solution according to *De Gennes*.[185]

For the gelation to take place during the crosslinking reaction, the overlap concentration (OLC) must be reached. The concentration at which the viscosity gradient of the polymer solution increases is defined as OLC. From the Figure 55, it is noticeable that the OLC for the copolymer Copo_19 is 4 – 5 wt%. This is illustrated by the different slopes of the regression lines. (An OLC of 4 – 5 wt% was also obtained for Copo_17; the corresponding graph can be found in the

appendix, cf. Figure 126). That means that only at 4 – 5 wt% the polymer chains start to interact, so that gelation is even possible. In the following chapter, bulk hydrogel formation is hence studied via in situ rheology as a function of polymer concentration and in dependency of further parameters.

5.4 Mechanical properties and critical concentration of bulk hydrogel from in situ rheology

The formation of the bulk hydrogel out of the copolymer Copo_19 and cross-linker DTT was first studied via in situ rheology. The complex shear modulus was measured as a function of time for several polymer concentrations in dependency of the pH value and the acrylate/cross-linker ratio. The complex modulus consists of a storage modulus G' and a loss modulus G''. The damping factor is the quotient of loss and storage modulus (cf. chapter 4.6.3.1).

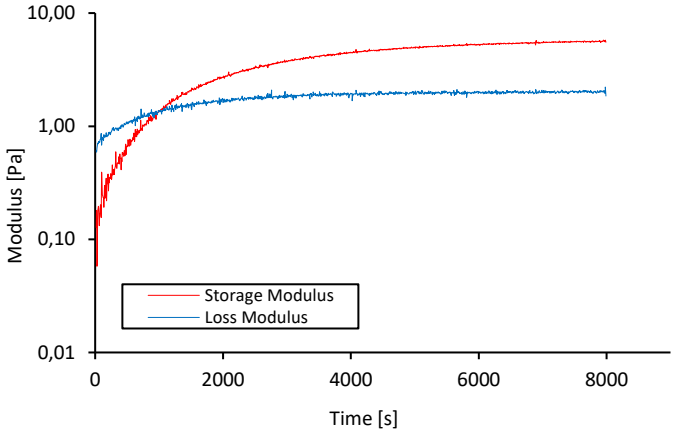

Figure 57: Exemplary representation of complex shear modulus vs. gelation time for a cross-linking reaction.

Figure 57 illustrates the complex modulus as a function of gelation time for a cross-linking reaction, exemplary. At the beginning of the reaction, the storage modulus (red) is below the loss modulus (blue). At this stage, the solution has solely viscous properties. As the gelation progresses, the storage modulus increases and the polymer chains interact with each other, enabling them to store energy. From the point where more energy is stored than is lost through relaxation and inner friction, the moduli will intersect. The gel point is then attained (gelation time) and the visco-elastic properties of the hydrogel dominate. Both moduli increase continuously until the characteristic network strength is reached. The gelation is

completed at the point where a constant storage modulus is measured (complete gelation time).

This allows the dependency of gelation time, complete gelation, storage modulus and damping factor on the polymer concentration at different pH values and acrylate/cross-linker ratios to be investigated. To determine a critical concentration, a gelation time of 10 min was set as target value. Beyond this, the complete gelation time should not exceed 2 hours. Thus, a critical concentration for a certain pH value and a certain acrylate/cross-linker ratio could be identified. The optimal parameters that have been found (pH value and acrylate/cross-linker ratio) serve as a basis for the dead-end modification experiments in chapter 5.6 (investigation of various influencing factors on the modification). Furthermore, the critical concentration can be applied to calculate the flux for the modification experiments using the film model. The aim is to obtain a hydrogel with properties similar to those of the bulk hydrogel.

5.4.1 Variation of pH value

Since the cross-linking reaction is base-initiated, the influence of the pH value was first investigated for a constant acrylate/cross-linker ratio of 1:1. Experiments were carried out with the copolymer Copo_17 at pH values of 8, 9 and 10.

Figure 58 (a) depicts the gelation time as a function of the polymer concentration. As can be seen from (a), the gelation time for the pH values 8 and 9 decreases with increasing polymer concentration. The time decreases for pH 8 from 16 min to 2 min and for pH 9 from 5 min to 2 min. This was to be expected, since a higher polymer concentration leads to more double bonds being available for the reaction. In addition, the segments to be cross-linked by the chemical reaction are coming together more closely so that more collisions occur. This increases the probability for a crosslinking reaction, so that the gelation time becomes shorter. With increasing concentration from 3 wt% to 5 wt%, the gelation time for pH 8 and 9 decreases more severely at first. At a polymer concentration of approx. 5 wt%, however, the polymer proximity appears to be so high that an increase in concentration has no appreciable effect on the gelation time anymore. As already discussed, the OLC must be reached in order to allow gelation to take place. Thus, the higher gelation time at 3 wt% compared to 5 wt% is because the overlap concentration of 4 wt% has not been reached (cf. chapter 5.3.3). This also fits in with the fact that the measurements for pH 8 and 9 at a concentration of 3 wt% had to

be repeated several times to get useful results. So, there is an increased risk that no extensive crosslinking toward a gel takes place at a polymer concentration of 3 wt%.

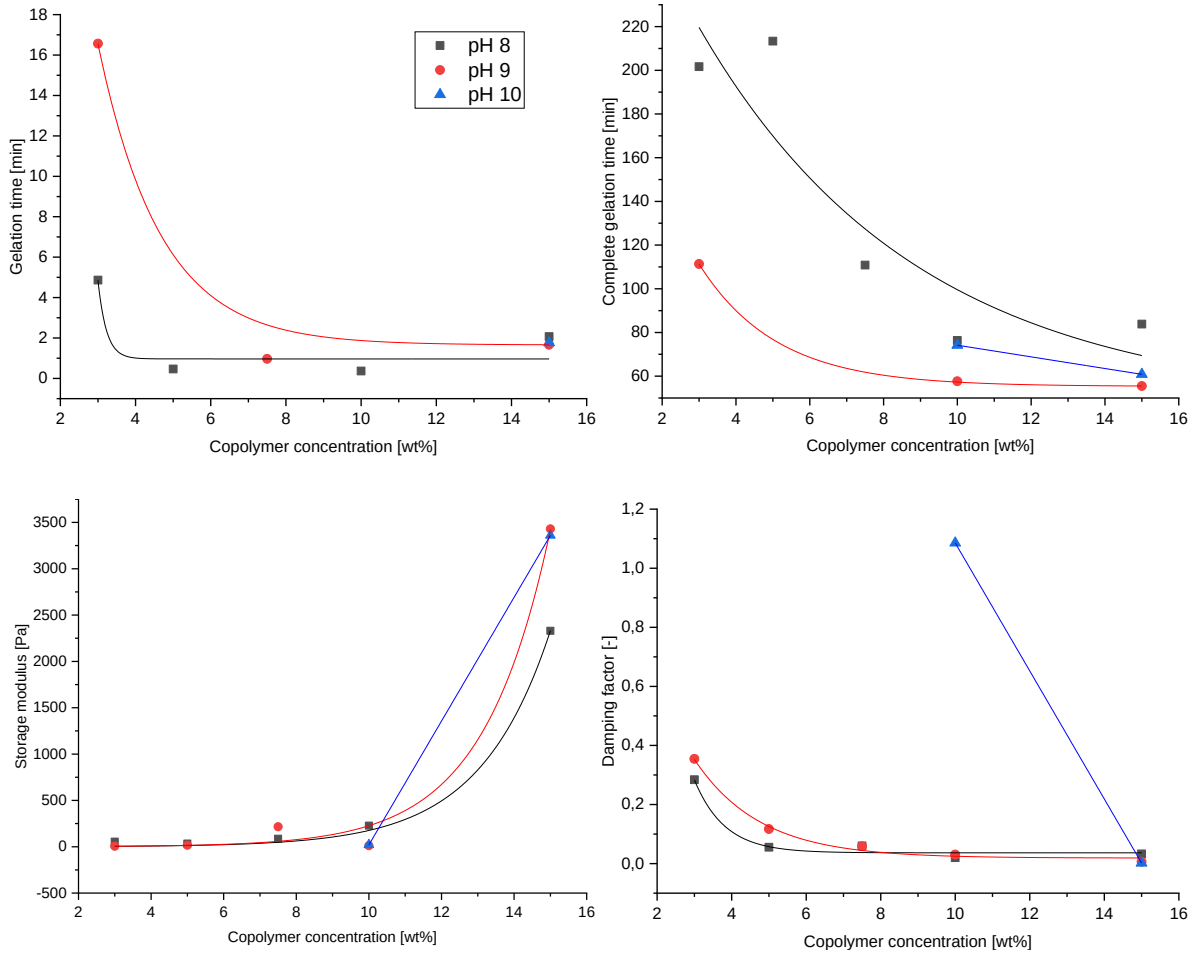

Figure 58: Cross-linking reaction of Copo_17 and DTT at acrylate/cross-linker ratio 1:1 and pH values 8, 9, 10. **(a)** Gelation time vs. copolymer concentration. **(b)** Complete gelation time vs. copolymer concentration. **(c)** Storage modulus vs. copolymer concentration. **(d)** Damping factor vs. copolymer concentration.

A comparison of the pH values 8 and 9 reveals that the gelation time for pH 8 at a concentration of 3 wt% is shorter than for pH 9 (17 min vs. 5 min). This can also be explained by the fact that the OLC of 4 wt% has not been reached, which means that the concentration is too low to measure an effect of the pH value. The influence of the pH value on higher concentrations is complicated by the lack of data points for pH 9 and 10.

In (b) the complete gelation time is plotted against the polymer concentration. Again, the complete gelation time decreases with increasing concentration. A closer look at the pH values reveals that the pH has a much greater influence on the complete gelation time. For pH 9 and pH 10, a shorter gelation time is obtained compared to pH 8. This is plausible since the Michael addition is base-catalyzed. Thus, at a higher pH value, the deprotonation of the

functional thiol group (R-SH) of the crosslinker is energetically favoured, so that a nucleophilic attack of the thiolate anion on the acrylate group can occur more frequently. This accelerates the crosslinking reaction. However, at pH 10, complete gelation is finished later than at pH 9. It seems that an excess of OH^- ions does not necessarily accelerate the reaction. The optimum seems to be pH 9.

In (c) and (d) the storage modulus and the damping factor are plotted against the polymer concentration. The pH values 8 and 9 show almost the same trends for the damping factor. There is a decrease with increasing concentration from 3 wt% to 5 wt%. This signifies that the elasticity of the gels increases. Above 5 wt%, the damping factor is constant. For pH 10 the decrease of the damping factor is much steeper with increasing polymer concentration. Looking at the storage modulus, it becomes clear that the values are extremely low for concentrations up to 10 wt% (20 – 50 Pa). Consequently, the elasticity of the hydrogels increases because of the decreasing damping factor, but the hydrogels are generally inelastic at concentrations up to 10 wt% because of the low storage modulus. Accordingly, the viscous proportion of the samples predominates. Only at a polymer concentration of 15 wt%, a storage modulus of > 3500 Pa is achieved with a low damping factor, which points to an elastic gel. Thus, the pH value in the range up to 10 wt% has no influence, since hydrogels with predominantly viscous properties are obtained.

On the whole, the experiments do not show a clear pH dependence of the gelation time. The gelation takes place within a few minutes from a polymer concentration of 5 wt%, independently of the pH value. However, complete gelation for pH 9 and 10 is achieved faster compared to pH 8. Polymer concentrations up to 10 wt% lead to hydrogels with low storage modulus (up to 50 Pa) and thus mainly viscous proportions. Above 15 wt%, hydrogels with the highest storage modulus (> 3500 Pa) are obtained for pH 9 and 10 compared to pH 8, and thus predominantly elastic components.

Due to the lack of data for polymer concentrations of 11 – 14 wt%, further experiments were carried out to investigate the pH dependence in this range. For these studies, the copolymer Copo_19 was used instead of Copo_17. The gelation and complete gelation time and storage modulus as a function of the polymer concentration are shown in Figure 59 (a) – (c).

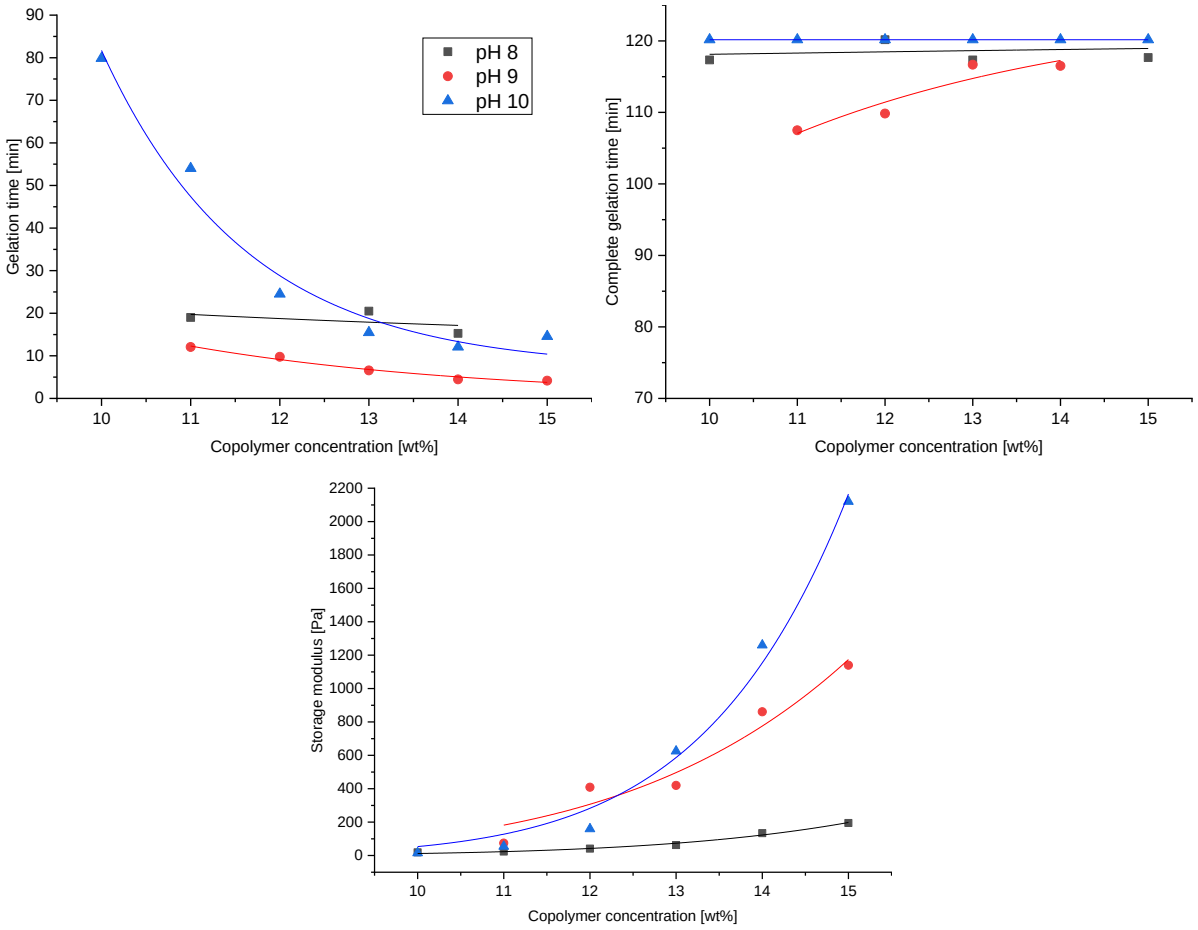

Figure 59: Cross-linking reaction of Copo_19 and DTT at acrylate/cross-linker ratio 1:1 and pH values 8, 9, 10. **(a)** Gelation time vs. copolymer concentration. **(b)** Complete gelation time vs. copolymer concentration. **(c)** Storage modulus vs. copolymer concentration.

Analogous to the experiments with Copo_17, the gelation time for all pH values decreases with increasing polymer concentration (a). When comparing the pH values, it is noticeable that the gelation time is shortest at pH 9. But a conclusive pH dependency cannot be ascertained. For the polymer concentration of 11 wt% and pH of 9, the gelation time is < 15 min. For pH 8, the gelation time increases to 20 min and for pH 10 it is even > 50 min. Thus, the system seems to react faster at pH 9 than at pH 8. This can also be attributed to the deprotonation of the functional thiol group (R-SH) of the crosslinker which is energetically favoured at a higher pH value so that the gelation is speeded up. Yet, a pH value of 10 leads to a more inert system. An excess of OH^- ions thus reverses the effect. This could possibly be the result of a shielding effect of the polymer. In other words, positive charges of the zwitterion are shielded so that the polymer appears to be "negatively charged". As a result, the polymer chains repel each other, decelerating the cross-linking reaction. When looking at

the complete gelation time in (b), the effect is much more pronounced. For both pH values 8 and 10, the gelation is not yet completed within 2 h. For pH 9, this could be observed.

In (c) the storage modulus is also plotted against the polymer concentration. For pH 9 and pH 10, much higher storage modulus are obtained compared to pH 8. The storage modulus for pH 8 increases to a maximum of 200 Pa. Accordingly, at pH 8, hydrogels with mainly inelastic properties are generated for all polymer concentrations where the viscous amount is dominant. Only at pH 9 and pH 10 storage moduli up to 1200 Pa are attained, which points to an elastic gel.

Altogether, no clear pH dependence of the gelation time could be found here either. The pH value of 9 seems to be optimal. A lower pH value of 8 leads to a slower reaction and also to hydrogels with clearly more viscous properties. A higher pH value of 10 effects that the system becomes much more inert, so that the gelation time will increase considerably. Therefore, in the next chapter the dependence of the gelation time on the acrylate/crosslinker ratio for pH 9 and pH 10 will be studied in more detail.

5.4.2 Variation of acrylate/cross-linker ratio

In this section, the cross-linking reaction is analyzed as a function of the acrylate/cross-linker ratios of 1:1, 1:5 and 1:10 for constant pH values of 9 and 10. The copolymer Copo_19 was also used for these tests.

As expected, the gelation time decreases with increasing polymer concentration, cf. Figure 60 (a). However, a steeper decrease can be observed for the ratio 1:1 (black). For the ratio of 1:5 (red) and 1:10 (blue), the curves become much flatter. For the ratio 1:1, the time decreases from 12 min to 4 min, whereas the gelation time for the ratio of 1:5 decreases from 10 min to 4 min and for 1:10 from 7 min to 4 min. Comparing the gelation time for the different acrylate/cross-linker ratios for the polymer concentration of 10 wt%, the gelation time decreases with increasing ratio (12 min vs. 10 min vs. 7 min). Thus, an excess of the cross-linker DTT shortens the gelation time. This is owing to a kinetic effect. With a higher proportion of cross-linker, the rate at which the acrylate groups react with the thiol groups is accelerated due to the increased concentration of one reaction partner. This dependence is much more pronounced for lower concentrations up to 13 wt%. Above 14 wt% this effect is reversed.

Accordingly, the kinetic effect has a smaller influence on higher polymer concentrations. Above 14 wt%, the polymer viscosity and thus density seems to be too high, making the system more immobile. Thus, a high crosslinker concentration and a simultaneously high polymer concentration does not necessarily lead to a faster gelation of the system.

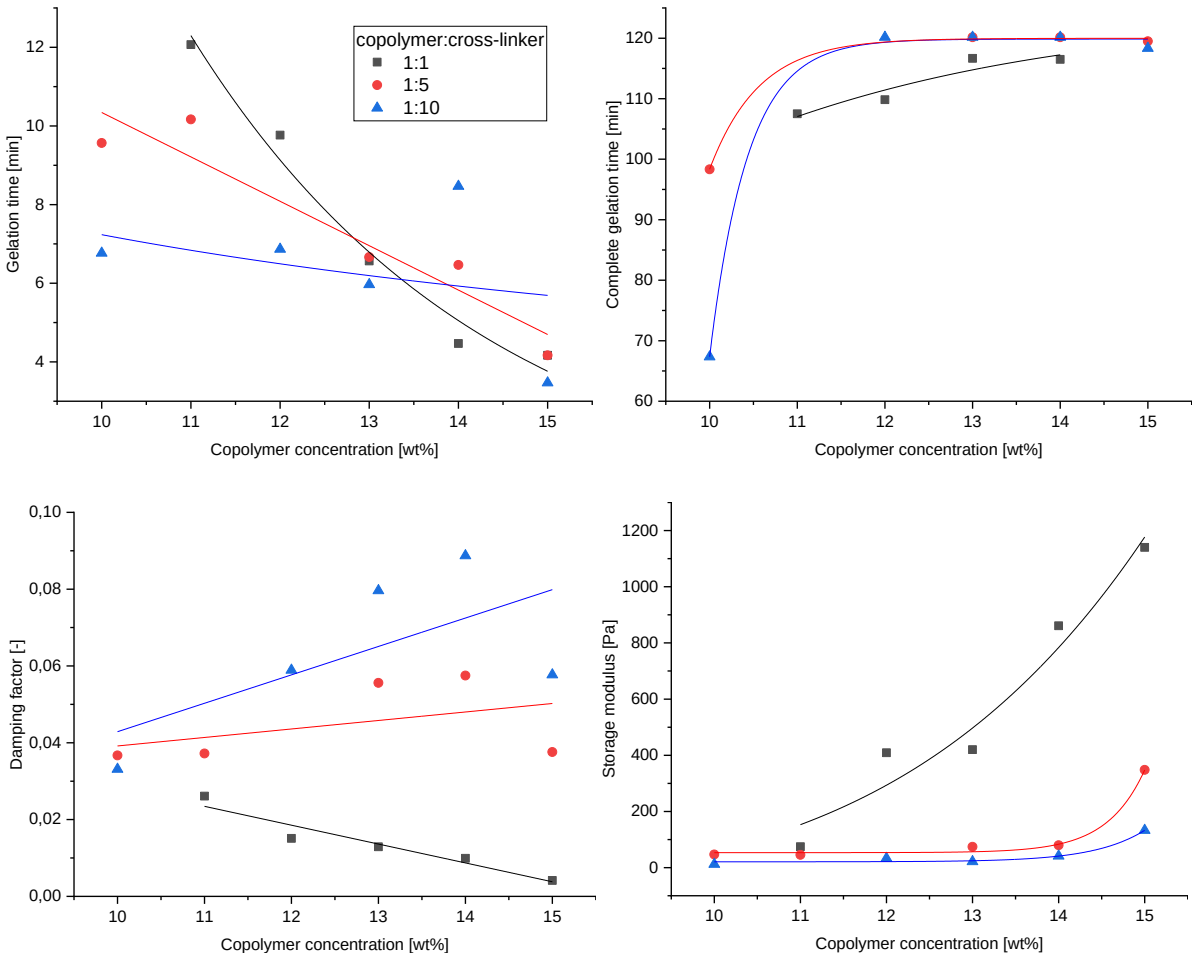

Figure 60: Cross-linking reaction of Copo_19 and DTT at pH 9 and acrylate/cross-linker ratios 1:1, 1:5 and 1:10. **(a)** Gelation time vs. copolymer concentration. **(b)** Complete gelation time vs. copolymer concentration. **(c)** Damping factor vs. copolymer concentration. **(d)** Storage modulus vs. copolymer concentration.

When considering (b), it becomes clear that for all three ratios the complete gelation time increases with increasing polymer concentration. Thus, there is no direct correlation to the gelation time. This is because the measurements for the ratios 1:5 and 1:10 were aborted after 120 min, as the complete gelation time was not yet reached. For the ratio 1:1, gelation was completed after 120 min. A slight upward trend can be observed. Looking at the damping factor in (c), there is a decrease with increasing polymer concentration for the ratio 1:1, contrary to the ratios 1:5 and 1:10. The damping factors for the ratios 1:5 and 1:10 decrease, respectively. This implies that for the ratio 1:1 the elastic proportions and for the ratios 1:5 and 1:10 the viscous proportions of the hydrogel increase. However, this interpretation must

be treated with caution, since the absolute values are very small, so that variations in the damping factor are within the error tolerance.

Much more interesting are the storage moduli for the different ratios, which are shown in (d). For the ratio of 1:1, the storage modulus increases with increasing polymer concentration up to 1200 Pa (15 wt%), so that a hydrogel with predominantly elastic properties is formed. For the ratios 1:5 and 1:10, no change in storage modulus can be observed for polymer concentrations up to 14 wt%. Even for 15 wt%, the storage modulus reaches a value of only 400 Pa. This is relatively low and points to an inelastic hydrogel. Hence, contrary to expectations, an excess of cross-linker leads to a more instable hydrogel while a low concentration leads to the formation of a dense hydrogel network structure. This correlates with the previous statement that gelation occurs faster for higher polymer concentrations and the smallest ratio of 1:1 than for the ratios 1:5 and 1:10. Since the reaction between DTT and side groups of the copolymer is much faster than the reaction between two side groups, an excess of DTT results in an augmented addition of thiols to double bonds. This lowers the probability of the second reaction, so that the proportion of only loose chain linkages is higher.

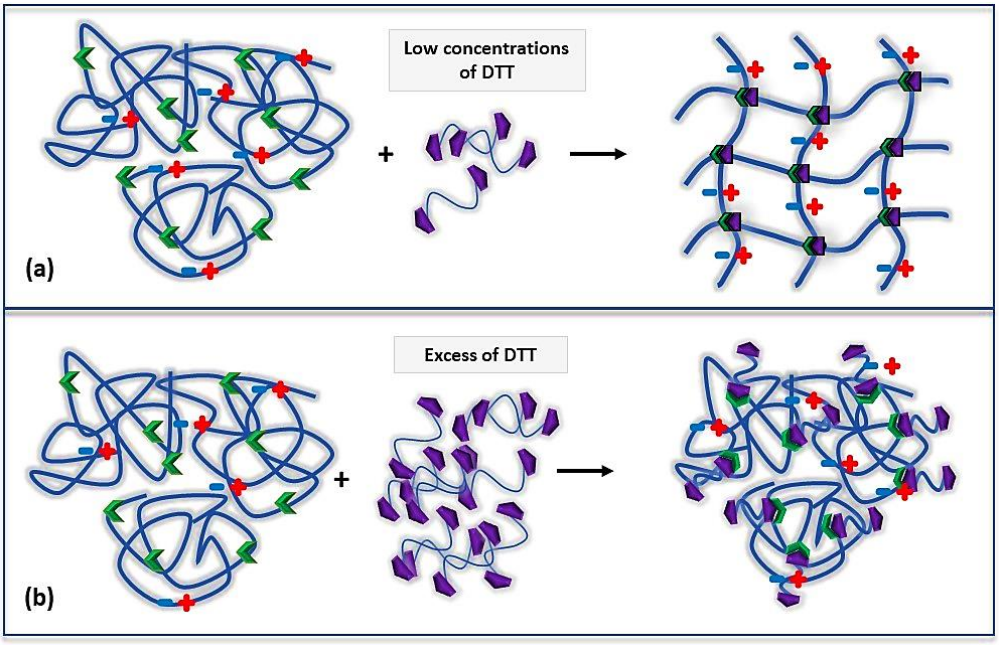

Figure 61: Schematic illustration of **(a)** the formation of a three dimensional network structure at low concentrations of DTT and **(b)** the formation of branched polymer structures with dangling chains at an excess of DTT.

As a result, only branched polymer structures, so-called dangling chains, are formed rather than a cross-linked dense hydrogel network, cf. Figure 61. Furthermore, the probability of DTT

forming disulfide bridges through recombination is enhanced by an excess. Thus, at ratios of 1:5 and 1:10, the system is supersaturated with DTT so that loose hydrogel networks with low storage moduli are obtained.

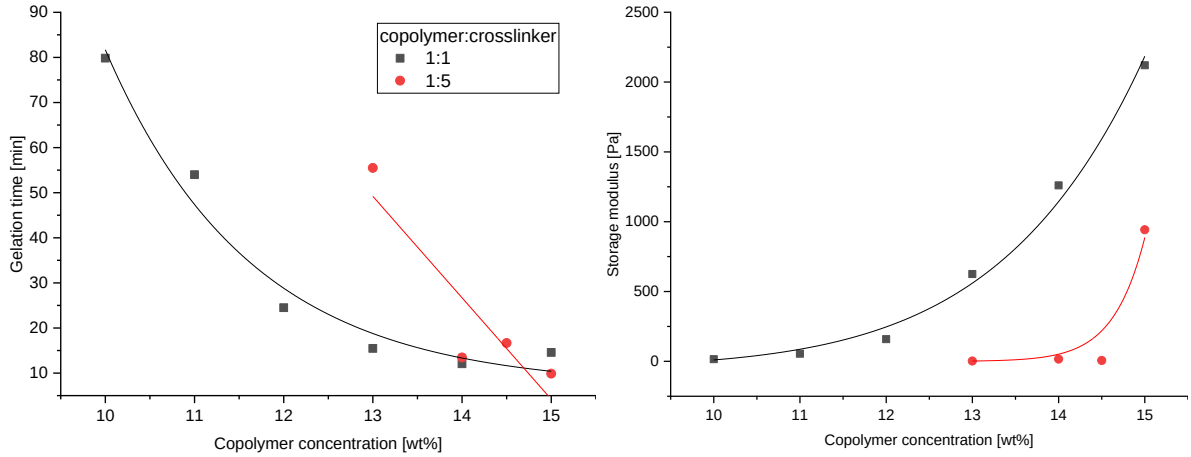

Figure 62: Cross-linking reaction of Copo_19 and DTT at pH 10 and acrylate/cross-linker ratios 1:1 and 1:5. **(a)** Gelation time vs. copolymer concentration. **(b)** Storage modulus vs. copolymer concentration.

The data for pH 10 (Figure 62 (a)) also show a significant decrease of the gelation time with increasing polymer concentration for the ratios 1:1 and 1:5. At a ratio of 1:10, gelation has started immediately after the preparation of the reaction solution, making the measurement of the moduli impossible. From (b) it can also be derived that the storage modulus increases with increasing polymer concentration, meaning that the elastic proportions of the hydrogel increase. For the ratio 1:1, the storage modulus reach values of up to 2100 Pa at 15 wt%, whereas the storage modulus for the ratio 1:5 show values of 1000 Pa. This confirms that an excess of DTT (1:5) leads to branched polymer structures and thus more unstable hydrogels.

Thus, a clear dependence of the storage modulus on the acrylate/crosslinker ratio could be identified. In comparison to 1:5 and 1:10, the acrylate/cross-linker ratio of 1:1 provides hydrogels with high storage moduli and thus a dense cross-linked network structure (for pH 9 up to 1200 Pa and for pH 10 up to 2100 Pa). Also, since gelation occurs significantly faster at pH 9 compared to pH 10, the pH value of 9 and the acrylate/crosslinker ratio of 1:1 were found to be optimal so that these conditions were chosen for the modification experiments in chapter 5.6.

In order to determine a critical concentration for gelation under these conditions, the gelation time, was set as a target value at 10 minutes. Thus, the critical concentration for gelation at pH 9 and an acrylate/cross-linker ratio of 1:1 is 12 wt% (cf. Figure 60 a)). This concentration is

used in chapter 5.6 to calculate the flux for the modification experiments using the film model. In this way, a hydrogel with properties corresponding to those of the bulk hydrogel is intended to be achieved during the modification. Before examining various influencing factors on the modification in chapter 5.6, the next chapter 5.5 first identifies modification conditions under which the hydrogel is successfully formed.

5.4.3 Interim conclusions

The most important conclusions regarding the bulk hydrogel synthesis are summarized below:

1. The gelation time decreases with increasing polymer concentration, as more double bonds are available for the reaction at a higher polymer concentration, which increases the probability of a crosslinking reaction.
2. A straightforward dependence of the gelation time on the pH value could not be demonstrated. If the pH value is increased from 8 to 9, the gelation time initially decreases, since deprotonation of the functional thiol group (R-SH) of the crosslinker is energetically favored. However, a pH value of 10 makes the system substantially slower. The pH value 9 seems to be the optimum.
3. Higher pH values lead to hydrogels with higher storage moduli.
4. The gelation time decreases with increasing acrylate/crosslinker ratio. Above 14 wt% this trend/effect is reversed. A high crosslinker concentration and a simultaneously high polymer concentration will cause the system to gel more slowly.
5. A clear dependence of the storage modulus on the acrylate/crosslinker ratio was identified. The storage modulus decreases with increasing ratio. An excess of cross-linker leads to a more unstable hydrogel. At pH 9 and the ratio 1:1, hydrogels with the following storage moduli are obtained in comparison to 1:5 and 1:10: for 1:1 up to 1200 Pa, for 1:5 up to 300 Pa and for 1:0 up to 200 Pa.
6. A pH value of 9 and an acrylate/crosslinker ratio of 1:1 are therefore optimal conditions for the formation of a hydrogel with elastic properties in a short time. For a gelation time of 10 min a critical concentration of 12 wt% was determined under these conditions, which will be used to calculate the flux for the modification experiments in chapter 5.6.

5.5 Identification of influencing parameters and modification conditions for in situ CP-enhanced hydrogel coating method for flat-sheet membranes in dead-end mode

In this chapter influencing parameters and modification conditions are identified which lead to a successful coating of RO membranes. The influence of CP on the modification is investigated by running experiments without stirring and at different stirring rates and polymer concentrations. Finally, the antifouling properties of modified membranes will be analyzed towards real cooling water from the steel industry and synthetic oil/water emulsions. The conditions under which the membranes exhibit a low flux loss and good antifouling properties are the basis for the modification of membranes in spiral wound modules (cf. chapter 5.9).

5.5.1 Modification without stirring

For the modification experiments in this section, the membranes Lewabrane and BW30 which were selected in chapter 5.2 were applied. The modification is done by in situ crosslinking via Michael addition of the copolymer PSBMA-co-PMAEMA with the crosslinker DTT during filtration in a dead-end batch cell. Thereby, the concentration polarization is exploited, which enables the critical concentration of the reactants at the membrane surface to be exceeded, resulting in the formation of a hydrogel on the surface.

Experiments with Lewabrane membrane

First, modifications were carried out with the Lewabrane membrane at a constant pressure of 10 bar without stirring. The pH of the reaction solution was adjusted to be 8, the acrylate/crosslinker ratio was set to 1:1 and the modification time was 60 min. The aim was to identify the polymer concentration at which a hydrogel is formed on the membrane surface. Figure 63 shows the FRR values (J_3/J_0) after modification (washing with 5000 ppm NaCl solution) against the polymer concentration.

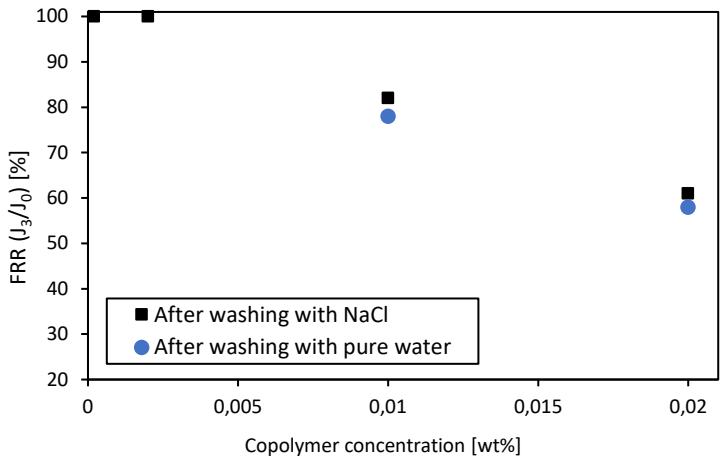

Figure 63: Dead-end modification of Lewabrane (pH 8, acrylate/cross-linker ratio 1:1, 60 min): FRR values after washing with NaCl solution (J_3/J_0) for membranes modified at different copolymer concentrations without stirring at 10 bar.

As shown, at concentrations of 0.0002 wt% and 0.002 wt% the permeance of the membrane could be completely recovered after washing with NaCl solution (FRR of 100 %). During the modification, an average flux of 48.0 LHM (for 0.0002 wt%) and 45.4 LHM (for 0.002 wt%) was recorded. Since the formation of the hydrogel leads to an additional membrane resistance, it can be assumed that no hydrogel is formed at concentrations of up to 0.002 wt% even though the flux was as high as for the concentrations at which a hydrogel was formed (see below). Therefore, these reaction solutions are too diluted in order to exceed the critical concentration of the reactants at the membrane surface to form a hydrogel.

If the concentration is brought up to 0.01 wt%, the membrane loses 22 % of its initial flux after washing with pure water (FRR of 78 %). During the modification, a flux of 40.1 LHM was measured. After washing with a 5000 ppm NaCl solution, it was found that the flux during washing with NaCl was higher than during washing with pure water. This can be attributed to the anti-polyelectrolyte effect which is a reversible effect. The generated hydrogel is zwitterionic and contains a large number of charged groups which attract and neutralize each other under aqueous conditions. As a result, the groups are located very closely together, so that the probability for the formation of internal ion pairs increases. This leads to a collapsing of the polymer structure, making the hydrogel compact and highly viscous.[186] The hydrogel coated membrane therefore has a comparably lower flux while washing with pure water. By adding salt, the ionic strength of the solution is increased, which reduces the electrostatic attractive interaction and weakens the ion pair formation. This leads to a chain expansion, resulting in a reduction of the viscosity and an increase in flux.

It was also found that the water flux increased after washing with NaCl. Therefore, the washing was continued until no increase in flux could be observed. This was achieved by washing the membrane for five times. For the polymer concentration of 0.01 wt%, an increase of FRR from 78 % to 82 % was achieved after washing with NaCl was measured. This is due to an additional irreversible effect that by swelling of the zwitterionic hydrogel on the membrane surface during washing with NaCl, unbound components can be washed out of the hydrogel, so that the flux increases after washing with NaCl.

At a polymer concentration of 0.02 wt%, the membrane has lost even 39 % of its initial flux (FFR of 61 %) after washing with NaCl. This indicates that at polymer concentrations of 0.01 wt% and above, the critical concentration is exceeded at the membrane surface, thus triggering the formation of a hydrogel layer. This is reflected in an additional resistance and thus leads to an irreversible reduction of the flux.

The modified membranes (0.002 and 0.01 wt%) were then analyzed by ATR-FTIR spectroscopy (Figure 64 (a)). The spectrum of the successfully modified membrane (0.01 wt% @ 40.1 LHM) shows the characteristic bands for the hydrogel (sulfonic acid group at 1036 cm^{-1} and carbonyl group at 1722 cm^{-1}) in contrary to the non-modified membrane (0.002 wt% @ 45.4 LHM). Due to the pronounced hydrogel layer on the membrane surface, the bands of the base membrane are also less pronounced. In addition, a decrease in the contact angle of 33 % was measured (cf. Figure 64 (b)), so that the membrane has also become more hydrophilic due to the hydrogel.

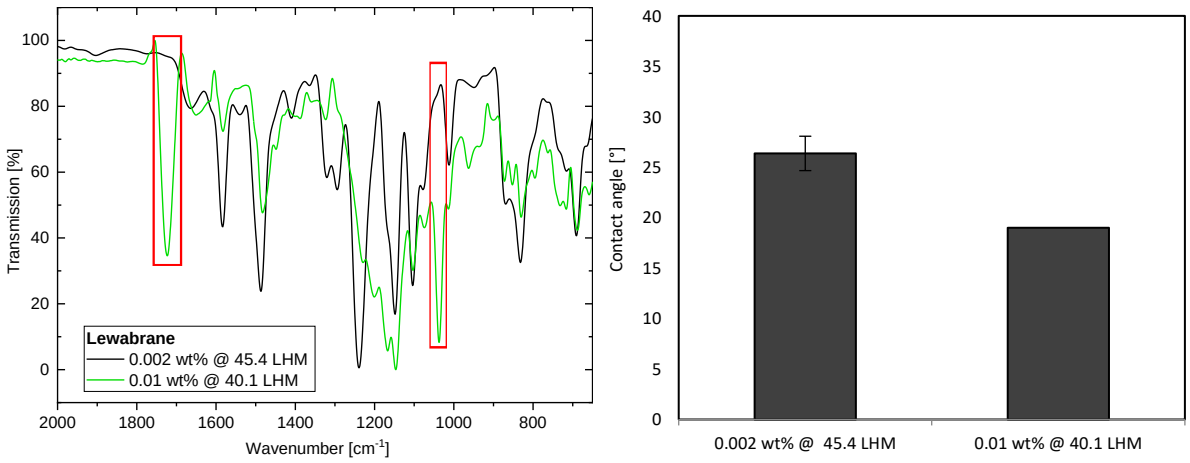

Figure 64: (a) IR spectra and **(b)** contact angle of membranes modified at 0.002 wt% and 0.01 wt%.

The membrane surfaces were also examined by means of SEM (Figure 65). As expected, at a concentration of 0.002 wt% and a flux of 45.4 LHM, the membrane surface exhibits the typical ridge-and-valley structure for PA membranes[31] (a). Thus, no hydrogel has been formed on the surface. The concentration of 0.01 wt% at a flux of 40.1 LHM, however, leads to a smooth and distinct surface where the structure of the base membrane is no longer apparent, meaning that this membrane is coated (b). The SEM images thus confirm the statements made earlier.

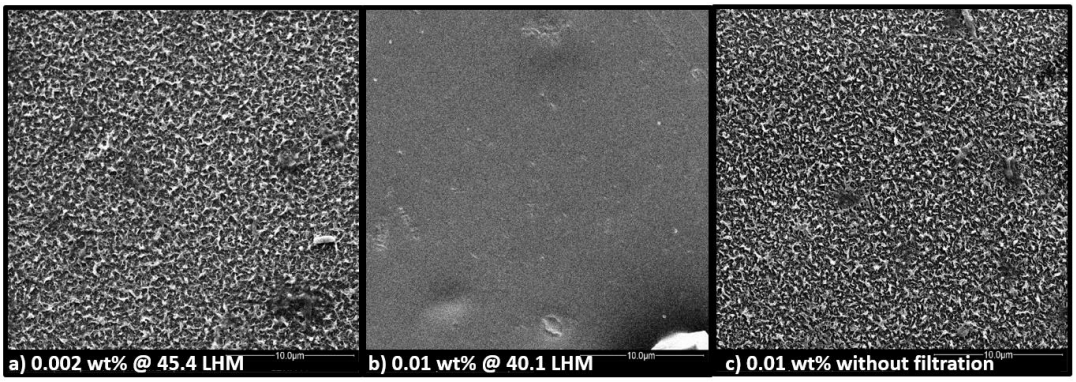

Figure 65: SEM images of membranes modified at a) 0.002 wt%, b) 0.01 wt% and c) 0.01 wt% without filtration.

Tests were also carried out in which the membrane was not filtered but only adsorbed with the reaction solution having a concentration of 0.01 wt%. The surface of this membrane is shown in (c) and displays still the ridge-and-valley structure. Therefore, no hydrogel has built up on the membrane surface. The bulk concentration of 0.01 wt% is accordingly not sufficient to initiate a modification by only adsorption. Only when a flux is applied and the reaction solution is filtered through the membrane, the CP exceeds the required critical concentration, which leads to crosslinking of the copolymer and crosslinker at the membrane surface. This means that the flux induces the critical concentration of the reactants at the membrane surface to be exceeded by the CP. Hence, no hydrogel can be generated on the surface by mere adsorption of the reaction solution with a concentration of 0.01 wt%. The flux is therefore decisive for the CP and the formation of the hydrogel.

Experiments with BW30 membrane

The identified modification conditions leading to a hydrogel coating (acrylate/crosslinker ratio of 1:1, pH of 8 and polymer concentration of 0.01 wt%) were subsequently transferred to the membrane BW30. The tests were also carried out at a constant pressure of 10 bar and without stirring. The average flux during the modification was 37.2 LHM. Also here, the conditions led to a hydrogel on the membrane surface. The relative flux decrease was only 14 % compared

to the Lewabrane membrane with 18 %. Both, the SEM image and ATR-FTIR analysis (Figure 66 (a) a) and (b)) prove the existence of the hydrogel on the membrane surface. The contact angle has also decreased by 28 %, indicating enhanced hydrophilicity.

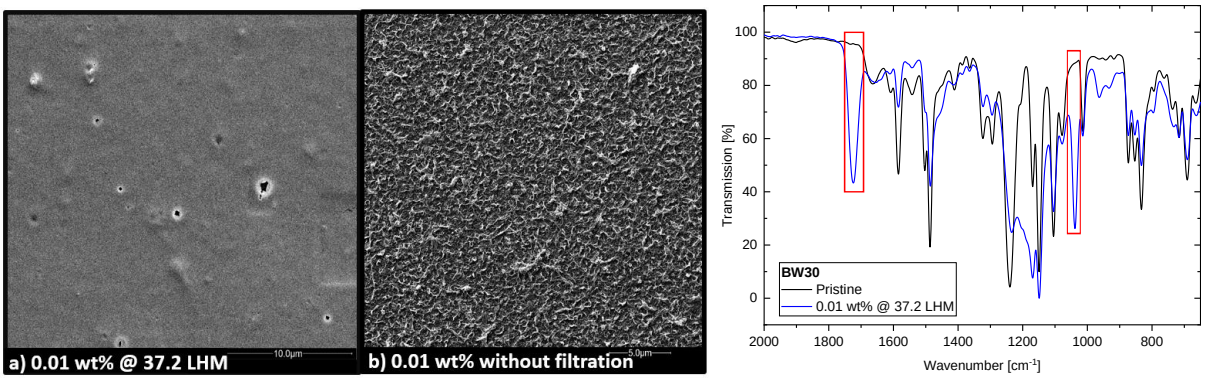

Figure 66: Dead-end modification of BW30 (pH 8, acrylate/cross-linker ratio 1:1, 60 min): **(a)** SEM images of membranes modified at a) 0.01 wt% and b) 0.01 wt% without filtration. **(b)** IR spectra of pristine membrane and membrane modified at 0.01 wt%.

Again, experiments were conducted in which the BW30 membrane was only brought into contact with the reaction solution without filtration. As expected, the topography of the surface clearly shows that no hydrogel has been formed, cf. SEM image b). Since the coated BW30 membrane has a lower flux loss than the coated Lewabrane membrane (14 % vs. 18 %), all further experiments were done with the BW30 membrane.

Overall, it can be deduced that the polymer concentration is not the only factor determining whether a hydrogel is being formed on the membrane surface. The flux through the membrane during the modification is much more crucial for a gelation to occur. Accordingly, the system is influenced by the composition of the reaction solution (minimum concentration) and the filtration conditions (critical flux). Only a suitable combination of polymer concentration and flux will trigger a reaction on the membrane surface.

5.5.2 Modification at different stirring rates

To establish suitable conditions for the transfer of the modification from dead-end to cross-flow, the modification must be done under stirring. In this way, not only the reactive system (composition of the solution and flux) but also the hydrodynamic conditions at the membrane surface (depending on the Reynolds number and cell geometry) are taken into account. This

also allows the concentration of the reactants on the membrane surface during the modification to be calculated for a certain stirring speed using the film model (cf. chapter 5.6).

The influence of the stirring rate on the formation of the hydrogel (acrylate/crosslinker ratio of 1:1, pH value of 8) is examined in more detail hereinafter. Stirring rates of 300 and 400 rpm were tested. To ensure a sufficiently high flux for the modification, the filtrations were performed at a constant pressure of 10 bar. By this, only the influence of the stirring rate on the formation of the hydrogel can be assessed. The FRR values obtained are summarized in Table 11.

Table 11: Dead-end modification (pH 8, acrylate/cross-linker ratio 1:1, 60 min): FRR values after washing with NaCl solution (J_3/J_0) for membranes modified at different stirring rates at 10 bar.

Concentration [wt%]	Stirring rate [rpm]	Stirring speed [m/s]	FRR (J_3/J_0) [%]
0.01	-	-	86
0.01	300	0.24	100
0.02	300	0.24	92
0.03	300	0.24	87
0.03	400	0.31	94

If a stirring rate of 300 rpm is set for the modification with a polymer concentration of 0.01 wt%, the flux is recovered to 100 % compared to the modification carried out without stirring (86 %). This is because stirring counteracts the formation of CP during the modification, impeding the formation of the hydrogel. Accordingly, the concentration of 0.01 wt% is too low for the reactive system to accumulate on the membrane surface under these mixing conditions. Only at a polymer concentration of 0.02 wt% the membrane loses flux, so that a hydrogel is likely formed here again, leading to an irreversible loss of flux (FRR of 92 %). An increase of the concentration to 0.03 wt% leads to a more pronounced hydrogel layer (FRR of 87 %). On the other hand, if the stirring speed is increased to 400 rpm for the same concentration of 0.03 wt%, the CP is reduced again (FRR increases from 87 to 94 %) since the formation of the hydrogel is hampered.

According to this, in addition to the flux and the polymer concentration, the mixing conditions have also a great influence on the CP and thus on the formation of the hydrogel at the membrane surface. For the same polymer concentration, the effect of hydrogel formation can be switched on and off by stirring. Consequently, the formation of hydrogel is controlled by

the combination of stirring rate, polymer concentration and flux. Hence, a stirring rate of 300 rpm was established for all further modification experiments.

To verify that the membrane is coated at a polymer concentration of 0.02 wt%, the surface composition was examined using XPS. A sulfur content of 1.1 at% was determined. This indicates the presence of the zwitterionic coating on the surface, so that the membrane is plainly coated.

5.5.3 Influence of polymer concentration

FRR values and SEM

In this chapter the influence of the polymer concentration on the formation of the hydrogel is examined in more detail. For this purpose, modifications were performed at different polymer concentrations of 0.02 – 0.06 wt%, at a constant pressure of 10 bar and a stirring speed of 300 rpm. In Figure 67, the FRR values are plotted against the polymer concentration.

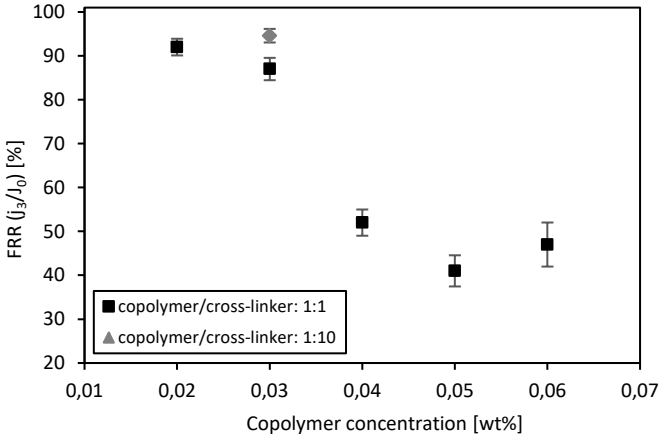

Figure 67: Dead-end modification (pH 8, acrylate/cross-linker ratio 1:1, 60 min): FRR values after washing with NaCl solution (J_3/J_0) for membranes modified at different polymer concentrations at 300 rpm and 10 bar.

For the acrylate/crosslinker ratio of 1:1 two regions can be observed. As already shown in chapter 5.5.2, only a slight irreversible decrease of flux was obtained for the low concentrations of 0.02 and 0.03 wt% (FRR of 92 and 87 %). In addition, the XPS measurement revealed that the membrane surface is clearly coated at a concentration of 0.02 wt% (cf. chapter 5.5.2). However, it is still unclear how the morphology of these layers looks like, how defined these layers are formed, and how thick these layers are. The corresponding SEM images in Figure 68 (b) and (c) show that the ridge-and-valley structure of the polyamide layer

is clearly visible. The hydrogel had preferentially accumulated in the valleys of the rough surface so that only valleys are filled, resulting in valley clogging.[187] In addition, the coating has evolved spot-like in some regions. This is even more pronounced for the concentration of 0.03 wt% (c). Hence, these are generally very thin hydrogel layers. According to this, the low flux loss can be attributed to the very thin and inhomogeneous hydrogel layer on the membrane surface. It must be assumed that these thin layers were already formed under subcritical conditions, since the network structure is not developed completely.

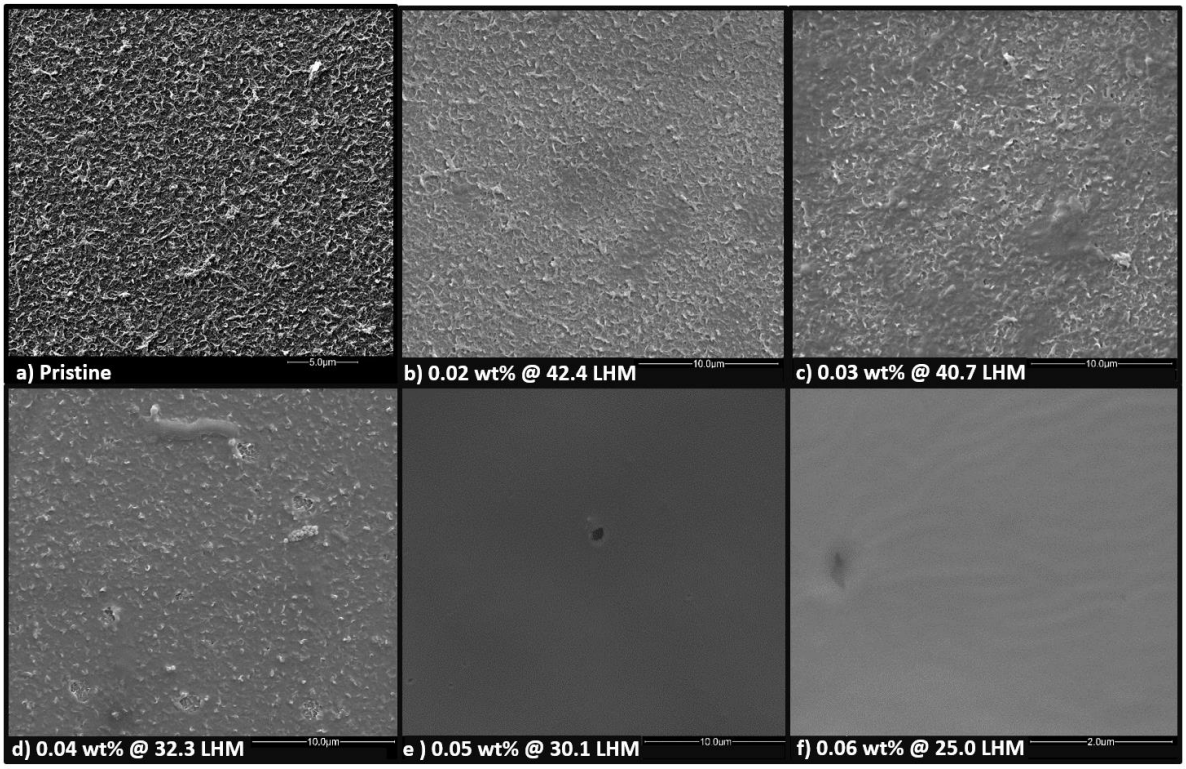

Figure 68: SEM images of a) pristine membrane and membranes modified at b) 0.02 wt%, c) 0.03 wt%, d) 0.04 wt%, e) 0.05 wt% and f) 0.06 wt%.

In contrast, higher concentrations (0.04 – 0.06 wt%) lead to a more significant decrease in flux (FRR of 52 – 47 %). Looking at the respective SEM images (d – f), it becomes clear that the membranes are coated more densely. At a concentration of 0.04 wt% (d), the valleys are filled to such an extent that the ridge-and-valley structure is hardly visible. The substructure shines through only slightly so that the surface is almost completely covered. At concentrations of 0.05 (e) and 0.06 wt% (f) the substructure is no longer apparent. The surface is completely covered with the hydrogel. A difference between 0.05 wt% and 0.06 wt% is no longer visible due to the pronounced and homogeneous layer. Therefore, a concentration of 0.05 wt% leads to a high flux loss of 59 % because of the completely homogeneous and potentially thick

hydrogel layer on the surface. These conditions clearly lead to an exceeding of the critical concentration at the membrane surface. In contrast, the concentration of 0.04 wt% leads to a similarly high flux loss of 48 %, but the hydrogel layer is not completely distinct and homogeneous.

Figure 67 also illustrates the influence of the higher acrylate/crosslinker ratio of 1:10 on the loss of permeance at a polymer concentration of 0.03 wt%. Comparing the FRR values for the two ratios, it is found that the FRR value for the 1:10 ratio is higher than for the 1:1 ratio (95 % vs. 87 %). Thus, the modified membrane has a higher flux loss at a ratio of 1:1. In order to understand this, one has to look again at the rheology results (cf. chapter 5.4.2). These results showed that a ratio of 1:1 compared to 1:5 and 1:10 yields a more elastic hydrogel with higher storage moduli. This could be explained by the fact that an excess of DTT results in branched polymer structures (dangling chains) instead of a cross-linked dense hydrogel. Thus, for the ratio of 1:10, the degree of crosslinking of the hydrogel on the membrane is lower, resulting in a looser network and a lower flux loss.

ATR-FTIR

The ATR-FTIR spectra of the modified membranes (acrylate/crosslinker ratio of 1:1) are presented in Figure 69 (a) compared to the pristine membrane. An increase in the characteristic bands of the hydrogel (sulfonic acid group at 1036 cm^{-1} and carbonyl group at 1722 cm^{-1}) can be observed (circled in red). Since the ATR-FTIR measurement is a measure for the mass of hydrogel deposited, it can be used to calculate the degree of modification, which reflects the mass of coating per area and thus quantifies the extent of the hydrogel layer. This is done by comparing the S-O vibration band of the sulfonate group in the hydrogel (1037 cm^{-1}) with the C-C stretching vibration band of the aromatic benzene ring present in the support layer of the pristine membrane (1485 cm^{-1}). For this purpose, the measured transmission T_i is first converted into absorbance E_i (equation (45)). Consequently, the degree of modification DG can be calculated according to equation (46):

$$E_i = -log(T_i) \quad (45)$$

$$DG = \frac{E_{Sulfonate\ group}}{E_{Benzene\ ring}} \quad (46)$$

The degree of modification was calculated for the hydrogel coated membranes and is shown in Figure 69 (b). Even if the unmodified/pristine membrane does not exhibit a sulfonic acid group band, a blank value for the DG was calculated which is 0.07. In this way, coated membranes with modification degrees smaller than this blank value can be classified as non-modified. For the low concentrations 0.02 wt% and 0.03 wt%, the DG possesses values of 0.15 and 0.24 and is thus different from the blank value. The DG increases further with increasing concentration and reaches a value of 4.8 for the polymer concentration of 0.06 wt%. This strongly correlates with the obtained layer thickness and the corresponding flux loss.

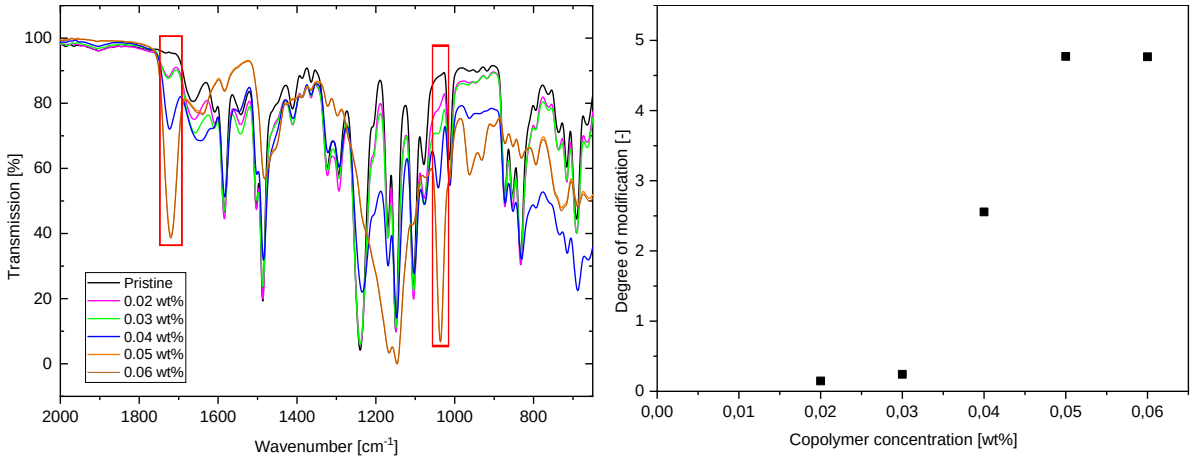

Figure 69: (a) IR spectra of pristine membrane and membranes modified at 0.02 – 0.06 wt% and **(b)** corresponding DGs.

In total, low concentrations of up to 0.03 wt% lead to thin and inhomogeneous hydrogel layers on the membrane surface causing a low flux loss. In contrast, homogeneous and thick layers are obtained at much higher concentrations of 0.05 wt% and 0.06 wt% leading to a much higher flux loss. From this, it can be derived that there are two processes for the hydrogel formation. These can be described as follows: 1) At bulk concentrations of 0.02 wt% and 0.03 wt%, the reactants are filtered through the membrane in a solely branched, gel-particulate state and fixed to the membrane surface below the critical concentration for gelation. This transport-controlled attachment results in a thin and loosely branched polymer on the membrane surface. 2) At a bulk concentration of 0.04 wt% and above there is a significant concentration of the reaction solution at membrane surface above the critical concentration required for gelation. Cross-linking occurs and thus a gel is being formed, which continues to cross-link with the existing thin layer. The branched polymer then becomes a three-dimensionally cross-linked hydrogel layer.

Hence, as soon as the reaction partners come into contact and a bulk concentration ≥ 0.02 wt% is reached, provided that a high flux is maintained, a thin and inhomogeneous layer is formed. This first process is thus preceded to a three-dimensional hydrogel growth. In exceptional cases, thick layers may be formed of two different proportions. However, in practice there is most likely a fluent transition, as the transport-controlled first process passes into a 3D growth. Thus, it can be claimed that concentrations up to 0.03 wt% do not lead to the critical concentration being exceeded in order to form a three-dimensional hydrogel network. However, these concentrations lead subcritically to a thin branched polymer layer. Only at concentrations of 0.05 wt% and higher, the critical concentration is surpassed so that a fully developed and thick hydrogel layer on the membrane surface can be obtained.

Zeta potential

Since the modifications at the concentrations of 0.02 wt% and 0.03 wt% lead to thin and inhomogeneous hydrogel layers with a low flux loss, the zeta potential of these membranes was additionally measured. As discussed in chapter 5.1.2, the isoelectric point is reported to be in the pH range from 4 to 5.[160] The zeta potential of the coated membranes compared to the pristine membrane is shown in Figure 70.

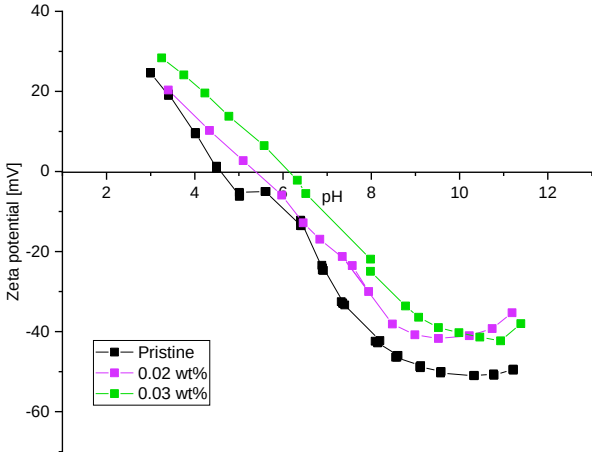

Figure 70: Zeta potential of membranes modified at 0.02 wt% and 0.03 wt%.

A shift of the isoelectric point from 4.5 (pristine membrane) to 5.5 (for 0.02 wt%) and to 6.2 (for 0.03 wt%) was observed. This indicates that the modified membranes became substantially neutral as a result of the coating. Furthermore, the modified membranes possess a lower negative charge compared to the unmodified membrane (– 40 vs. – 50 mV). The lower surface charge for the coated membranes is likely due to the reduced exposure of carboxylic groups upon coating with a neutral hydrogel layer. According to this, thin hydrogel layers

generated under clearly subcritical conditions are sufficient to enhance the charge neutrality of the membranes. The antifouling properties of these membranes (polymer concentration of 0.02 wt% and 0.03 wt%) are therefore examined in more detail in the next chapter.

Salt rejection

The NaCl rejection was also measured with a 2000 ppm NaCl solution. It can be noted that the differences in salt rejection are not very significant. For the coated membranes, 1 – 2 % lower rejection values can be obtained. On the one hand, this can be ascribed to intrinsic differences of the membranes, as variations exist from batch to batch. Furthermore, the chloride rejection is most strongly influenced by inhomogeneities and defects of the PA layer, which can also vary between batches.

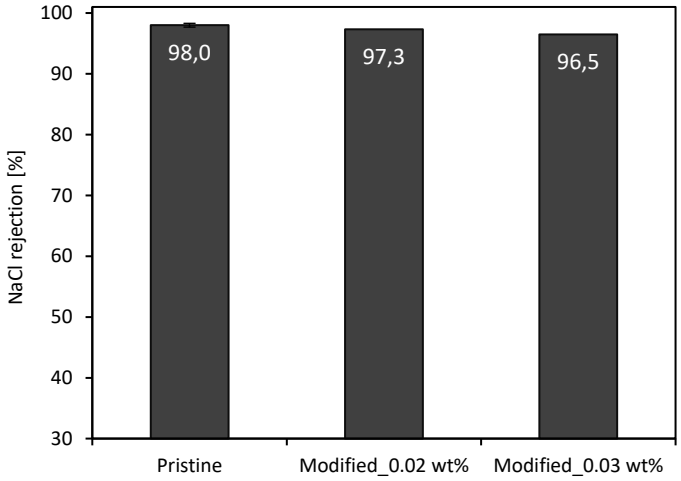

Figure 71: NaCl rejection of pristine and modified membranes at 0.02 wt% and 0.03 wt%.

On the other hand, the slightly lower rejection can be caused by the formation of a salt layer due to a lower mixing effect of the salt solution as a consequence of the hydrogel layer on the membrane surface, which allows substances to accumulate within the hydrogel layer. Thus, the part of the boundary layer where no mixing takes place, becomes thicker. This enables permeable substances, which are not completely rejected by the barrier such as chloride, to penetrate through the membrane more easily at a higher concentration. However, this effect was not studied further, as it was considered as uncritical for the further application.

5.5.4 Investigation of anti-fouling properties of hydrogel-coated membranes

In a simplistic way, the purpose of the modification is based on a cost-benefit assessment. Although the permeance of the membrane is lowered by the coating, this disadvantage can be compensated by a reduction in fouling. This can be illustrated by two straight lines with different gradients, which will intersect the Y-ordinate at different points, cf. Figure 72.

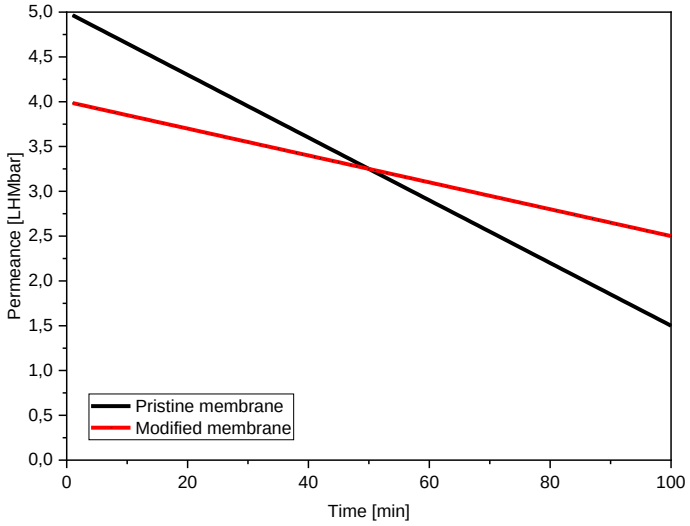

Figure 72: Exemplary, schematic representation of the performance of a modified membrane during fouling.

The unmodified membrane starts with a higher flux, which decreases gradually over time due to fouling. This is reflected in a steeper drop of the straight line. In contrast, the modified membrane has a slightly lower flux at the beginning but does not lose this flux that fast due to the modification. After approximately 50 min the flux of the modified membrane would be higher. Assuming that the previous increased efficiency of the unmodified membrane still has to be compensated, the modified membrane would have filtered the same volume as the unmodified membrane after 100 min and would have shown under unchanged conditions a higher flux until the filtration is stopped. At a certain level of expected fouling it is therefore reasonable to use a coated membrane. In case of reversible fouling, the modified membrane requires additionally less cleaning effort. If the degree of irreversible fouling can be reduced by the coating, its benefit will be further maximized. Thus, the benefit of an antifouling coating can be assessed by the extent to which the permeance loss is reduced by the coating.

Real cooling water from steel industry

Therefore, the antifouling properties of the modified membranes are evaluated in comparison to the unmodified membrane towards industrial cooling water from the steel industry (CW_DEW). First the influence of the acrylate/crosslinker ratio (1:1 and 1:10) on the fouling behaviour was investigated. Other modification conditions were kept constant (polymer concentration of 0.03 wt% and pH value of 8). The influence of the stirring rate on the fouling was also investigated (300 and 500 rpm). The tests were performed in dead-end at a constant pressure of 10 bar until a recovery rate of 80 % was reached. Figure 73 shows the permeance during fouling as a function of the recovery. It is obvious that the course of the permeance is similar for all tested membranes, regardless of the membrane condition. In particular, they have very similar slopes. Thus, the comparison of the FRR values will be complicated, since a small difference in the measured values will not allow meaningful conclusions.

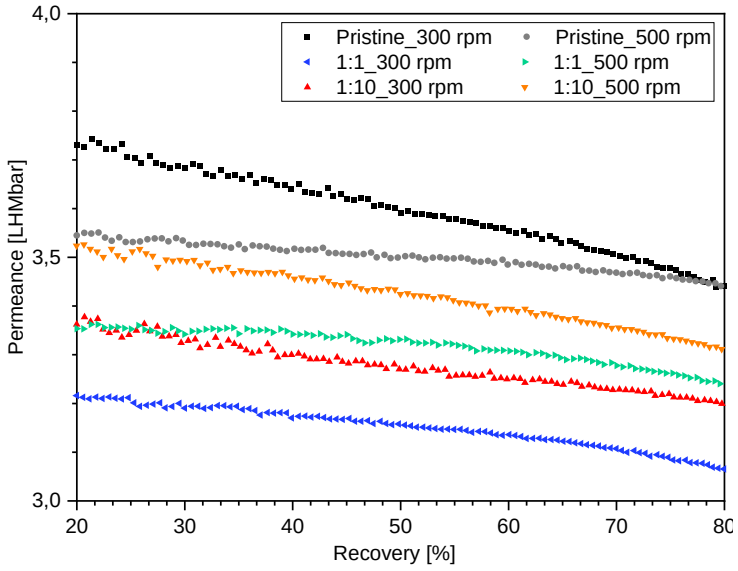

Figure 73: Permeance course of modified BW30 membrane (0.03 wt%, pH 8, acrylate/cross-linker ratio of 1:1 and 1:10) during dead-end fouling with CW_DEW at 300 and 500 rpm and 10 bar as a function of recovery.

The corresponding FRR values are summarized in Table 12 for the experiments at a stirring rate of 300 rpm. It is noticeable that the modified membranes (1:1 and 1:10) have higher FRR values after fouling and after washing with pure water compared to the unmodified membrane. Accordingly, the coated membranes have a higher fouling resistance. However, the differences are very small, which is why these results should only be considered with reservations.

Table 12: FRR values after fouling with CW_DEW and after washing with pure water.

Condition	FRR after fouling [%]	FRR after washing with pure water [%]
Unmod_300 rpm	86.5	93.5
1:1_300 rpm	87.5	99.8
1:10_300 rpm	89.9	95.3

For this reason, analogous comparative measurements were performed to test the reproducibility of these results. However, these measurements showed a low reproducibility, as the FRR values after fouling differed significantly for various membranes under the same filtration conditions. For the ratio 1:1 and 1:10, the standard deviation was 2.3 % and 2.7 %, respectively. In general, an absolute deviation of more than 3 % was found, for some measurements it was even up to 6 %. The differences in the FRR values of the modified and unmodified membranes are based on differences of this order of magnitude, thus no reliable conclusions can be drawn about the antifouling properties of the modified membranes.

Several attempts were undertaken to improve the reproducibility, which was perceived as the main problem in these studies. The primary aim was to increase the degree of fouling. A more severe fouling would be associated with a higher absolute difference in measurement values, which would lead to an improvement in reproducibility if the absolute error remained constant. Therefore, in a first step, the recovery was increased first to 90 %, then to 95 %, which slightly improved the reproducibility. However, it did not lead to significant differences between the modified and unmodified membrane. Even a reduction of the stirring rate from 300 to 100 rpm only led to minor improvements, which were not sufficient.

Overall, it can be concluded that fouling did occur during the filtration tests. However, the effect turned out to be too low so that the difference in the measured values was below the measurement deviations. This is not surprising, since it was already found in chapter 5.2 that the cooling water CW_DEW examined has a low fouling potential. Accordingly, the cooling water is not a suitable test system for the evaluation of the antifouling properties of the coated membranes. For this reason, a different test system was chosen, which was based on an oil/water emulsion.

Synthetic oil/water emulsion

The fouling feed investigated here is a two-component system consisting of dodecane and water. This test system was chosen because oil-in-water emulsions generally cause a higher decline in permeance of RO membranes. In this way, the reproducibility of the results should be ensured. In addition, oil is inevitably encountered during steel processing in the steel industry, so that the test system selected here is certainly a good representative of the cooling water from the steel industry. This time, the influence of the polymer concentration (0.02 wt% and 0.03 wt%) on the fouling behaviour was investigated under otherwise constant modification conditions (acrylate/crosslinker ratio of 1:1 and pH value of 8). The filtration experiments were performed at a stirring rate of 100 rpm. Since the fouling caused a considerable reduction of membrane flux, only a maximum recovery of 25 % was possible. Figure 74 displays the relative permeance against recovery. It can be clearly noticed that the flux curve of the modified membranes (pink and green) is much flatter than that of the unmodified membrane (black). At a recovery of approx. 20 %, the courses become even constant. For the unmodified membrane, on the other hand, a steady linear decline can be observed. Here, emulsified oil droplets are carried towards the membrane surface which is less hydrophilic following the permeate flow and then deposit on the membrane surface. With prolonged filtration time, more and more oil droplets accumulate on the membrane surface, leading to the formation of a cake layer.[188] For the case of modified membranes, a hydration layer is formed on the surface of the zwitterionic hydrogel under water. The water molecules are bound via electrostatic induced hydration and via strong electrostatic interactions due to the strong dipole moments in the zwitterionic units.[189, 190] This hydration layer prevents oil from directly contacting the membrane and thus decreases the fouling tendency.

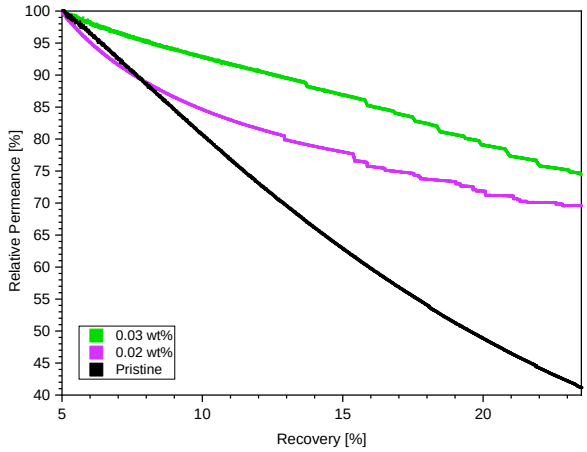

Figure 74: Permeance course of modified BW30 (0.02 and 0.03 wt%, pH 8, acrylate/cross-linker ratio of 1:1) during dead-end fouling with dodecane/water emulsion at 100 rpm and 10 bar as a function of recovery.

The corresponding FRR values are listed in Table 13. Distinct differences between the membranes can be discerned under the selected conditions. Even though the coated membrane loses flux due to the modification itself (8 % for 0.02 wt% and 13 % for 0.03 wt%), the retention of permeance during fouling is considerable. While the unmodified membrane only retains 19.9 % of its original permanence after filtration, the modified membranes still have over 60 % of their previous permeance (FRR of 69.5 % for 0.02 wt% and FRR of 74.6 % for 0.03 wt%). In addition, washing with little water restored the permeance to 83.2 % and 96.6 % for a concentration of 0.02 wt% and 0.03 wt%, respectively, while the unmodified membrane recovered only 78 % of its previous permeance. Thus, the thin hydrogel layer is capable of reducing the fouling significantly.

Table 13: FRR values after fouling with dodecane/water emulsion and after washing with pure water.

Condition	FRR after fouling [%]	FRR after washing with pure water [%]
Unmodified	19.9	78.0
0.02 wt%	69.5	83.2
0.03 wt%	74.6	96.6

By calculating the trade-off (equation (47)), the total remaining permeance after modification and fouling can be estimated for the modified membranes. This can be compared with the remaining permeance after fouling for the unmodified membrane to finally quantify the benefit of the antifouling coating:

$$P_{Remaining}[\%] = FRR_{Modification} \cdot FRR_{Fouling} \qquad (47)$$

Taking the initial flux loss into account, the modified membranes still have a significantly higher flux immediately after fouling than the unmodified membrane (FRR of 63.9 % for 0.02 wt% and 61.4 % for 0.03 wt% vs. 19.9 %). The initial reductions due to the modification could be thus compensated by the achieved fouling resistance.

In summary, differences between modified and unmodified membranes can be distinguished more clearly with the oil/water emulsion. It became clear that a thin hydrogel coating on the membrane surface is enough to significantly increase the antifouling properties of the membrane towards a synthetic oil/water emulsion. Thus, the modified membranes exhibit a higher fouling resistance compared to unmodified ones. Furthermore, it has been demonstrated that the use of such membranes, despite the initial reduction in flux, ultimately leads to an overall improvement in permeance. Based on this, conditions for the modification of membranes in spiral wound modules were derived in chapter 5.9.

5.5.5 Interim conclusions

When investigating the influencing parameters on hydrogel formation, the following conclusions could be drawn:

1. The modification of the Lewabrane and BW30 membranes without stirring only leads to cross-linking on the membrane surface at polymer concentrations higher than 0.01 wt%. The simple adsorption of the polymer solution at this concentration is not sufficient to induce a modification. Accordingly, the flux is the determining factor for the CP and the formation of the hydrogel. Since BW30 has a lower flux loss compared to Lewabrane (14 % vs. 18 %), BW30 was further used for the modification experiments.
2. An increase of the stirring rate leads to a lower flux loss. Thus, the effect of hydrogel formation can be switched on and off by stirring. In order to consider also the hydrodynamic conditions for the transfer of the modification from dead-end to cross-flow, further experiments were carried out at a stirring rate of 300 rpm. At this stirring rate, crosslinking occurs at polymer concentrations above 0.02 wt% (8 % flux loss, DG of 0.15 and ΔIEP of 1).
3. The variation of the polymer concentration showed that hydrogel formation consists of two processes: At a polymer concentration of up to 0.03 wt%, the reactants are filtered below the critical concentration in a gel-particulate state towards the membrane in a transport-controlled process, so that thin hydrogel layers are formed. From a bulk concentration of 0.04 wt%, the reaction solution is concentrated above the required critical concentration, resulting in crosslinking and the formation of a three-dimensional hydrogel.
4. Industrial cooling water from the steel industry is not a suitable test system for investigating the antifouling properties due to the low level of contaminants. Oil/water emulsions are far better for the evaluation of the antifouling properties. Despite the thin hydrogel layer, the membranes modified at concentrations of 0.02 wt% and 0.03 wt% have superior antifouling properties compared to the unmodified membrane.

5.6 Investigation of filtration parameters on the hydrogel formation during in situ modification of flat-sheet membranes in dead-end mode

In this chapter, various influencing factors on the modification are specifically examined. Since the extent of the CP is determined by the flux, experiments were carried out at different filtration rates. In addition, tests were performed at a constant filtration rate at different filtration times. The extent of the CP and the concentration at the membrane surface c_m is estimated using the film model. The results of this chapter are the basis for the modification of flat membranes in cross-flow in chapter 5.7.

5.6.1 Influence of filtration rate

Flux prediction with the aid of critical concentration from bulk hydrogel analysis

From the bulk hydrogel studies using the in situ rheology in chapter 5.4, it was determined that a pH value of 9 and an acrylate/crosslinker ratio of 1:1 results in a cross-linked hydrogel with a high storage module. In addition, in chapter 5.5.3 it was found that polymer concentrations beyond 0.05 wt% and 0.06 wt% lead to a homogeneous and dense three-dimensional hydrogel layer on the membrane surface. This identified optimal composition of the solution (polymer concentration of 0.05 and 0.06 wt% in combination with filtration through the membrane, acrylate/crosslinker ratio of 1:1 and pH value of 9) was adopted in order to investigate the influence of the filtration rate in more detail in this section.

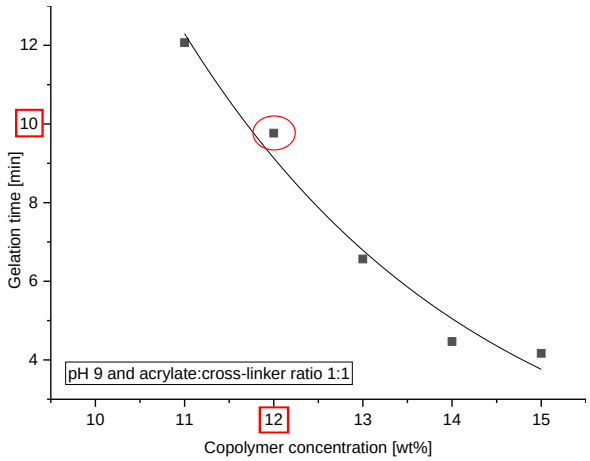

Figure 75: Gelation time vs. copolymer concentration for the bulk hydrogel formation via in situ rheology (pH 9, acrylate/cross-linker ratio 1:1).

For the gelation, which was completed within 10 min at a pH of 9 and an acrylate/crosslinker ratio of 1:1, a critical concentration c_{crit} of 12 wt% was detected (cf. Figure 75). With the aid

of c_{crit} the flux can be calculated via film model, which is used for the modification experiments. In this way, a hydrogel with properties comparable to those of the bulk hydrogel should be obtained during the modification. The concentration of the reactants at the membrane surface c_m should represent the critical concentration c_{crit}. The mass transfer coefficient k_i is also required, which can be calculated using formula (12) by rearranging to k_i. For the copolymer Copo_20 which was used for these experiments, a hydrodynamic radius r_h of 4.1 nm was determined via DLS measurement. For the calculation of the diffusion coefficient D_i, the determined hydrodynamic radius and the viscosity of water was applied to equation (18) which yielded a value of $1.1 \cdot 10^{-10}$ m^2/s. The Sherwood number was calculated to be 1050 using the correlation from equation (14). With a stirring rate of 0.24 m/s and a radius of stirred batch cell of $1.75 \cdot 10^{-2}$ m, the mass transfer coefficient k_i is calculated to be $6.5 \cdot 10^{-6}$ m/s. Using formula (6), the required flux can be finally calculated by inserting the mass transfer coefficient k_i, the bulk concentration c_b and the critical concentration c_{crit} with $c_m = c_{crit}$ by rearrangement as follows:

$$J_v = \ln\left(\frac{c_{crit}}{c_b}\right) \cdot k_i \qquad (48)$$

For a bulk concentration of 0.05 wt% and 0.06 wt%, a flux of 128 LHM and 124 LHM is calculated, respectively. However, this flux could not be realized with the BW30 RO TFC PA membrane used, so that lower fluxes had to be chosen. Tests were carried out at different filtration rates to determine the rate at which the cross-linked layer could be controlled under the selected conditions. Due to set-up and dead-end conditions it was not possible to adjust a constant flux, so that filtration was done at constant pressures of 3 – 10 bar to investigate the change in flux during modification.

Flux behaviour and FRR values

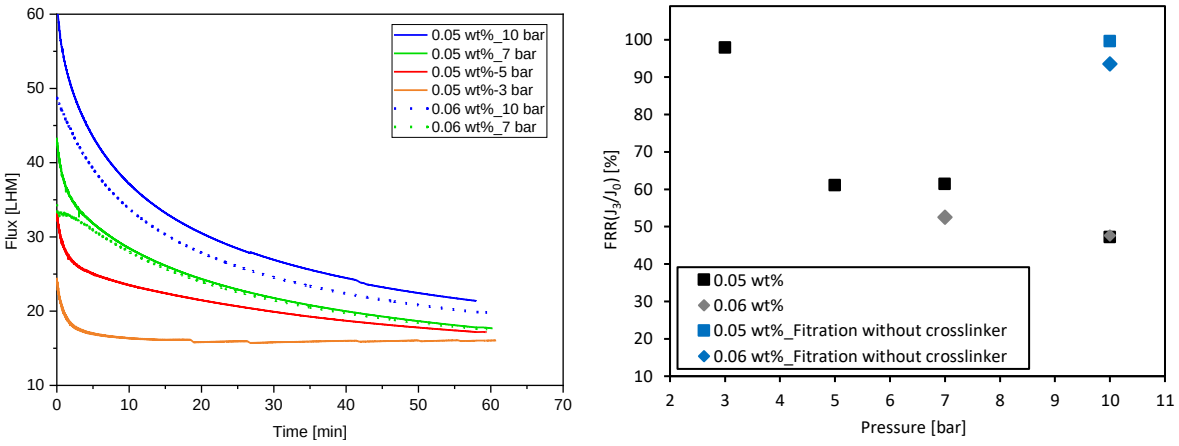

Figure 76: Dead-end modification (0.05 and 0.06 wt%, pH 9, acrylate/cross-linker ratio 1:1, 60 min): **(a)** Flux course during modification for membranes modified at different pressures (3, 5, 7 and 10 bar). **(b)** Corresponding FRR values after washing with NaCl solution (J_3/J_0).

Figure 76 (a) displays the flux as a function of the filtration time, which was 60 min. For all measurements, a decrease in flux over the entire measurement period can be observed, independent of the bulk concentration. This can be ascribed to various effects. First, concentration polarization is formed during the modification as this is a natural consequence of the selectivity of a membrane (cf. chapter 2.3). Since the experiments are carried out in dead-end mode, the reaction solution is additionally concentrated with increasing filtration time. These two effects lead to a reduction of flux. As a result, no steady state can be achieved. If the CP is sufficient to initiate a cross-linking reaction, gelation can occur as well, which causes the flux to decrease additionally. A higher initial flux amplifies these effects. For this reason, a stronger decrease of flux with increasing pressure is observed (steeper course of the curves). The modifications at 10, 7 and 5 bar show an exponential decrease of flux, whereas the flux for the 3 bar measurement is nearly constant except for the short initial phase. As a result, the fluxes exhibit very similar values at the end of the modification (flux last minute) regardless of the pressure, in contrast to the beginning of the modification (flux initial 10 min), where they differ significantly. This can be illustrated by means of Table 14.

Table 14: Comparison of the flux over the initial 10 min, over the last minute and over the whole modification time for the membranes modified at different pressures.

Pressure [bar]	500 mg/L			600 mg/L		
	Average Flux[LHM] initial 10 min	Average Flux[LHM] last minute	Average Flux[LHM] 60 min	Average Flux[LHM] initial 10 min	Average Flux[LHM] last minute	Average Flux[LHM] 60 min
10	45.7	21.4	29.9	40.5	19.8	26.08
7	33.0	17.7	23.4	31.2	17.4	22.66
5	25.9	17.2	20.7	-	-	-
3	17.7	16.1	16.3	-	-	-

This table also depicts the average flux over the entire modification period. Due to the increasing slope with increasing pressure, the difference between average and initial flux increases accordingly. Hence, the average flux for the modification at 3 bar does not deviate from the initial flux due to the almost constant course. However, for all other modifications the difference between average and initial flux is considerable.

Due to these different effects on the modification, the reduction of flux over time is not an exclusive indicator for the formation of the hydrogel. For an independent assessment, the FRR values shown in Figure 76 (b) are taken into account. To classify the obtained FRR values, modifications were also done at 10 bar without adding the cross-linker. The resulting FRR value was 99.6 %. For the modifications at 5, 7 and 10 bar (0.05 wt%), FRR values in the range of 61 – 48 % are achieved. For the polymer concentration of 0.06 wt% the same trend can be observed (53 – 47 %). Only for the 3 bar measurement an FRR value of 98 % was obtained. Therefore, a pressure of 3 bar (average flux of 16.3 LHM) is not high enough to initiate a crosslinking reaction through the CP. This indicates that the decrease in flux for the 5, 7 and 10 bar measurement is mainly induced by the gelation so that the contribution of the concentration must be low. For the measurements, which were done at significantly lower polymer concentrations (0.02 wt% and 0.03 wt%) at a pressure of 10 bar (chapter 5.5.3 Figure 67), lower FRR values were obtained (92 % and 87 %). This demonstrates that the flux has a significantly higher influence on the gelation compared to the polymer concentration. If the flux does not reach a minimum value, no crosslinking takes place.

Due to the significantly lower FRR values at 5, 7 and 10 bar, it can be concluded that beyond a pressure of 5 bar (average flux of 20.7 LHM), not only is the critical concentration exceeded, but also hydrogel layers are formed which must be clearly pronounced. Thus, the required flux

was exceeded significantly. It is striking here that the average fluxes of the 3 and 5 bar measurement barely differ from each other (16.3 LHM vs. 20.7 LHM). This implies that the hydrogel formation must take place in the initial phase in which the flux has a higher value than the average flux.

Mass per area and dry layer thickness

In addition to the flux, which determines the degree of CP, the maximum filtered mass per area and the maximum thickness of the coating were calculated using the equations (32) and (34), respectively. The calculations are based on the simplified assumption that the total mass of polymer from the permeate volume taken off, contributes to the formation of the hydrogel layer. Due to the concentration of reaction solution during modification, an average concentration over the entire filtration time is assumed. The maximum filtered mass per area and the maximum thickness of the coating are shown in Figure 77 (a) and (b).

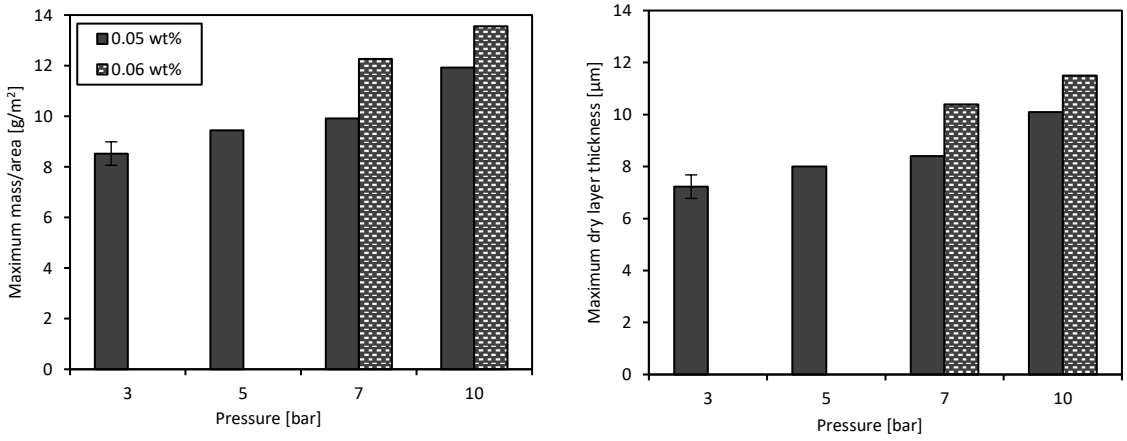

Figure 77: (a) Max. mass/area and **(b)** max. dry layer thickness of modified membranes in dependency of the applied pressure.

As expected, for both polymer concentrations the maximum mass per area increases with increasing pressure, since at a higher pressure more volume permeates through the membrane and thus more polymer mass is transported and filtrated to the surface. The values for the polymer concentration of 0.06 wt% are higher than for 0.05 wt%, which appears logical. In the same way, the maximum thickness of coating increases with pressure. It is shown that at 3 bar a coating of approx. 7 µm is obtained. However, it is known from the FRR values that the required flux for the crosslinking reaction was not reached. According to this, not the entire transported mass could have been involved in the build-up of the coating layer,

so that the thickness of 7 µm does not represent a realistic value. This leads to the conclusion that the transported mass is not decisive for the formation of a hydrogel on the membrane surface. Thus, the flux through the membrane is the crucial factor. Maximum coating thicknesses of 8 – 11 µm are estimated for the 5, 7 and 10 bar measurements. Based on the low FRR values, the required flux was clearly exceeded at a pressure of 5 bar. Therefore, it is most likely that the calculated thicknesses are in line with the real hydrogel thicknesses. Also, the calculated thicknesses are very similar and correlate strongly with the low FRR values, which also show comparable values.

Although an average concentration over the entire modification period was assumed for the calculation of the maximum thickness, realistic hydrogel thicknesses could be still calculated for the 5, 7 and 10 bar measurements, which correlate strongly with the high flux losses of the membranes. In addition, it could be proven again that it is not the quantity (filtered mass), but rather the quality (filtration conditions), especially the flux, that is responsible for the initiation of the crosslinking reaction via the CP, which leads to the formation of the hydrogel on the membrane surface.

ATR-FTIR and zeta potential

The modified membranes were also examined by ATR-FTIR to obtain information on the degree of modification, which is shown in Figure 78 (a).

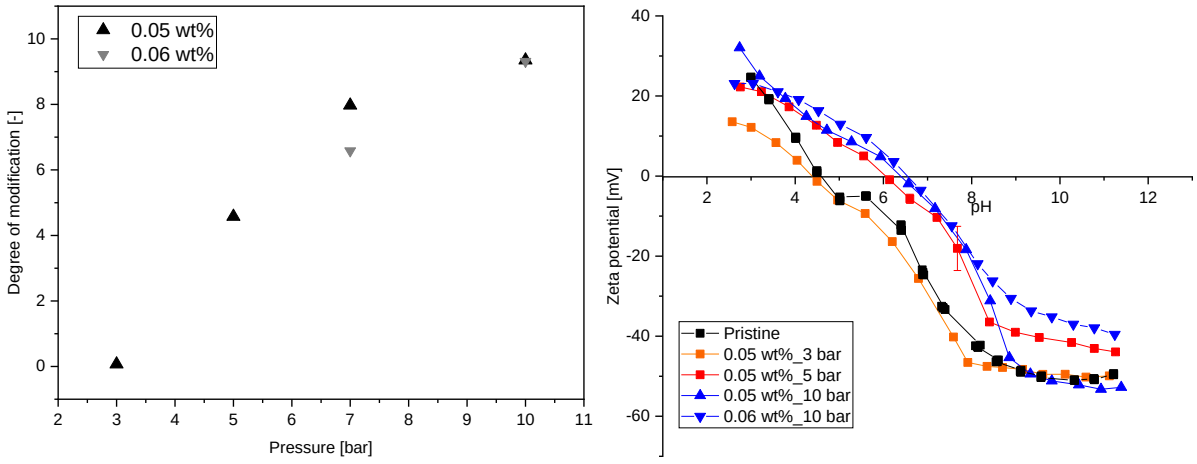

Figure 78: (a) IR spectra and **(b)** zeta potential of modified membranes in dependency of the applied pressure.

As expected, for the 5, 7 and 10 bar experiment, degrees of modification from 4 to 9.4 are achieved. For the 3 bar measurement, a value of only 0.07 is obtained and thus corresponds to the blank value of the unmodified membrane. These results support the previously shown

findings that the hydrogel layer is already clearly pronounced at a pressure of 5 bar and becomes thicker with increasing pressure, whereas no hydrogel layer has been formed on the membrane surface during the 3 bar experiment.

The zeta potential of the coated membranes was also measured and is shown in Figure 78 (b). The potential curve and the isoelectric point of the 3 bar measurement agree well with that of the unmodified membrane. Thus, the surface charge of the membrane has not changed. For the 5 and 10 bar measurement, a clear shift to a more neutral pH can be recognized. Furthermore, these membranes have a lower negative charge compared to the unmodified membrane (approx. – 40 vs. – 50 mV). Both factors indicate that the modified membranes have become more neutral due to the hydrogel coating. However, only a slight gradation between the zeta potentials of the modified membranes can be seen (from 4.5 (unmodified) to 6.2 (5 bar) and 6.5 (10 bar)). If the membrane is sufficiently coated, a thicker hydrogel layer will not cause any further meaningful shift of the IEP. It can also be assumed that the zeta potential measurement is less sensitive towards an increase in layer thickness compared to the ATR-FTIR measurement.

Interestingly, for the experiments carried out at far lower polymer concentrations (0.02 wt% and 0.03 wt%) at a pressure of 10 bar (chapter 5.5.3 Figure 69 (b)) higher modification degrees (0.15 and 0.24) could be observed compared to the 3 bar measurement (0.07). In addition, a shift of the IEP was obtained, which was not obtained for the 3 bar measurement (ΔIEP of 1 and 1.7 vs. 0). This again shows that a modification effect can be achieved at low polymer concentrations if the flux is sufficiently high. In contrast, no coating is obtained at extremely high polymer concentrations but a very low flux. Accordingly, the modification can be controlled much more effectively via flux.

SEM

To obtain detailed information about the morphology and topography of the membrane surface, SEM images were taken (cf. Figure 79). It can be observed that the membrane surface of the 3 bar experiment (b) is almost identical to the unmodified membrane surface (a). The ridge-and-valley structure is clearly visible and seems to be covered only at very few areas with hydrogel particles. This is not sufficient to refer to a successful crosslinking reaction. This observation is consistent with the results already shown above (no flux loss, modification degree identical to blank value and zeta potential comparable to unmodified membrane).

In contrast, membranes modified at 5, 7 and 10 bar show smooth and homogeneous surfaces (c – e). Considering the high flux losses, modification degrees and calculated dry layer thicknesses, it can be assumed that these layers are also very thick. Thus, the hydrogel formation consists of two consecutive processes here, too. During the modifications, loose, branched polymer particles have initially formed below the critical concentration. Only at 5, 7 and 10 bar the critical concentration for the gelation could be exceeded through the CP at significantly higher fluxes so that a three-dimensional distinct hydrogel network could be formed beyond that. This finding was already discussed in the previous chapter 5.5.3, in which the concentration dependence of hydrogel formation was investigated.

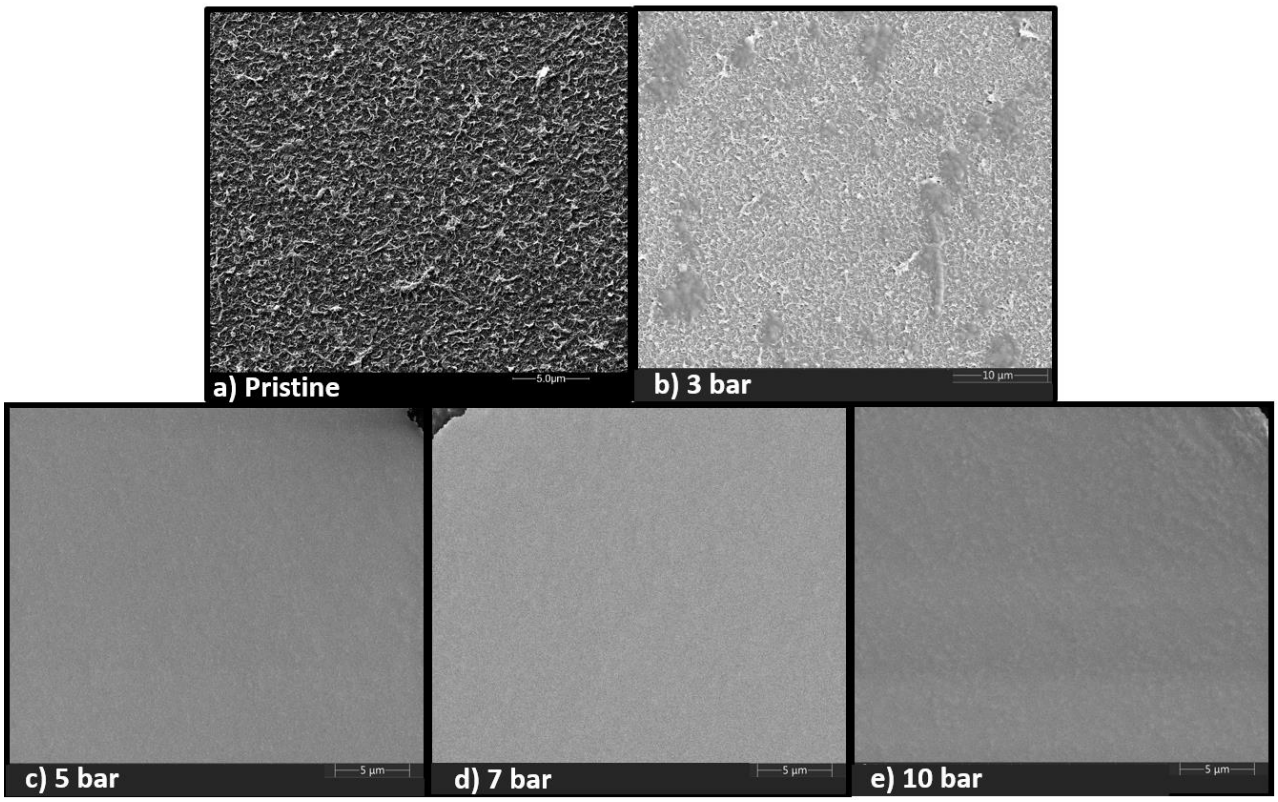

Figure 79: SEM images of a) pristine membrane and membranes modified at 0.05 wt% at b) 3 bar, c) 5 bar, d) 7 bar and e) 10 bar.

In summary, it can be stated that under subcritical conditions a transport controlled deposition of loose branched polymer particles on the membrane surface takes place. The thin and loose polymer layer turns into a coherent three-dimensional hydrogel network of thick dimensions only when the flux is high enough and thus the critical concentration is reached.

Contact angle

The hydrophilicity of coated membranes was investigated by contact angle measurements with the captive bubble method. The results are shown in Figure 80 and demonstrate that all contact angles are in a comparable range of approx. 25 – 35° if the standard deviation is included. Thus, the surfaces are altogether very hydrophilic. This is not surprising, since it has already been revealed in chapter 5.1.2 that the base membrane BW30 used here is a relatively hydrophilic membrane. As a result, no significant differences between the modified membranes can be detected.

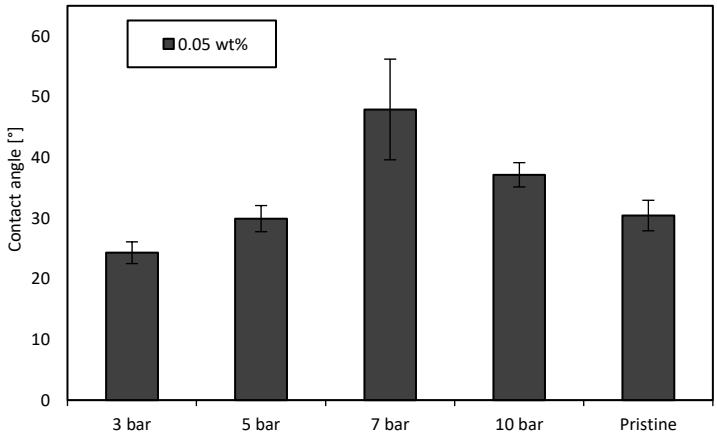

Figure 80: Contact angle of pristine membrane and modified membranes in dependency of the applied pressure.

Alternatively, experiments with the sessile drop method could be carried out with three different liquids, such as distilled water, glycerol and diiodomethane. The different polar and disperse fractions of the surface tension of the liquids allow the surface free energy to be calculated, which reveals more subtle differences in the membrane surface characteristics.[191]

For heterogeneous surfaces, which possess both hydrophilic and hydrophobic moieties, the measurement of the dynamic contact angle is much more promising. In this method, the advancing and receding CA is measured. These contact angles are measured from dynamic experiments where droplets or liquid bridges are in movement. A perfectly homogeneous surface has a theoretical contact angle hysteresis of 0 °. A larger hysteresis is measured for larger amounts of surface heterogeneity, and vice versa.[192] In this way, differences between the thick coated membranes at 5, 7 and 10 bar and the barely coated membrane at 3 bar could be measured more precisely. However, the coated membranes are altogether very

hydrophilic, so that these subtle differences would not provide any added value. Therefore, contact angle measurement will be omitted in the further course of this work.

5.6.2 Influence of filtration time

FRR values

When investigating the influence of different fluxes on hydrogel formation, it has been assumed that at high pressure, hydrogel formation already occurs in the initial phase of filtration. For this reason, the time dependence of the modification at a polymer concentration of 0.06 wt% (pH 9 and acrylate/crosslinker ratio of 1:1) at a pressure of 10 bar was analyzed in more detail. The filtration time ranged from 10 – 60 min. The corresponding FRR values are shown in Figure 81.

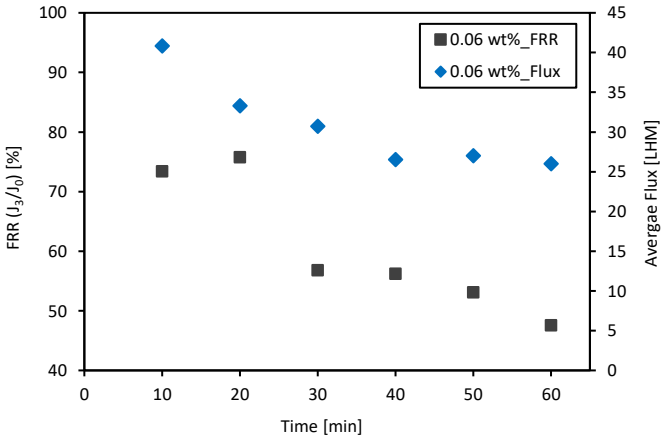

Figure 81: Dead-end modification (0.06 wt%, pH 9, acrylate/cross-linker ratio 1:1): Flux course and corresponding FRR values (J_3/J_0) for membranes modified for different modification times (10 – 60 min) at 10 bar.

Interestingly, after a filtration time of only 10 min, a significantly low FRR value is obtained. The membrane has irreversibly lost more than 20 % of its initial flux. After 20 min a comparable flux loss is obtained (FRR of 74 %). A filtration time of 30 min or longer causes the FRR value to drop significantly and falls to a value of 57 %. Only a slight decrease in the FRR values is obtained thereafter. The figure also depicts the average fluxes during the modification. Here again, it is clearly visible that the average flux gradually shifts away from the initial flux as the filtration time progresses. Analogous to the FRR values, only a slight decrease of the flux can be observed after 30 min. Both observations underline the assumption that hydrogel formation must be completed in the initial phase (20 – 30 min). Any

additional filtered mass would only contribute to the hydrogel thickness. Since this supplementary filtered mass is relatively small, this has only a minor impact on the flux, so that the decrease in flux is becoming continuously smaller.

Dry layer thickness and mass per area and time

The maximum dry layer thickness and the maximum filtered mass per area and time were also calculated and are shown in Figure 82 (a) and (b). As expected, the dry layer thickness increases with increasing filtration time. After 10 and 30 min hydrogel thicknesses of 3 and 11.5 µm are obtained, respectively. From (b), it can be seen that the mass per area and time (rate) decreases with increasing time until steady state is reached after 30 min. According to this, the change in the rate at which the reactive mass is transported, becomes continuously smaller. This is because the flux is relatively high within the first 10 – 20 min, so that the change in the rate is greatest at the beginning. Since the hydrogel formation is expected to be completed after 30 minutes and thus the flux changes only slightly, less mass is transported beyond that time, so that the change in rate becomes smaller and will become finally constant.

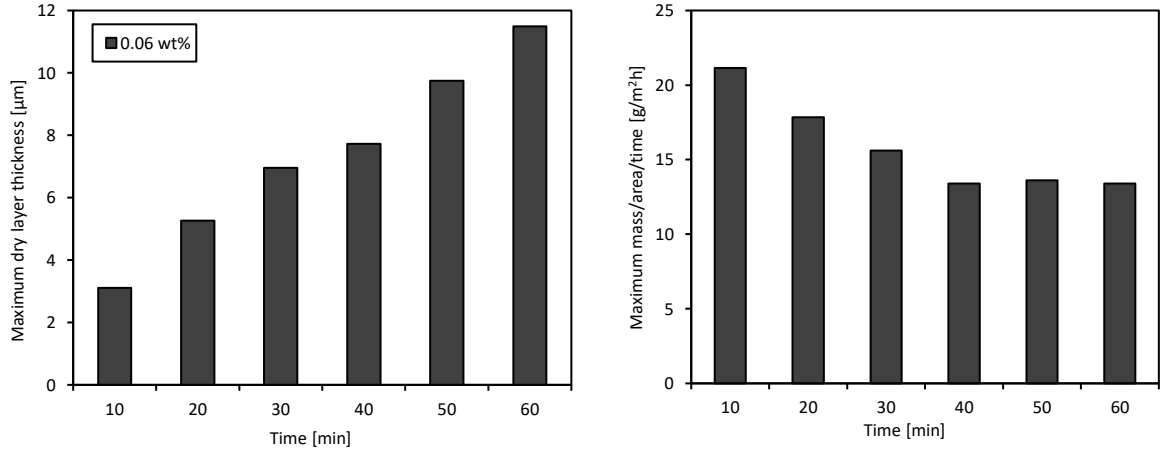

Figure 82: (a) Max. dry layer thickness and **(b)** max. mass/area/time of modified membranes in dependency of the modification time.

ATR-FTIR and zeta potential

The modification degrees and zeta potentials of the modified membranes are shown in Figure 83 (a) and (b) below. Based on the data in (a), it is shown that a high DG can be measured after only 10 minutes (DG of 7). This correlates strongly with the FRR values and supports the theory that the crosslinking reaction leads to a relatively thick hydrogel layer on the membrane surface within a short time. The experiments carried out for longer modification times, do not show significantly higher values (DG of up to 9.4), so that the

thickness of the coating does not increase essentially with longer filtration time. The measured value at 30 min must be considered as an outlier when considering the FRR values. It is most likely that the hydrogel layer has detached from the membrane during sample preparation due to the pronounced thickness of the hydrogel.

The isoelectric point has also shifted clearly into the neutral pH range (from 4.5 (unmodified) to 6 (10 min)), cf Figure 83 (b). However, as it was also found during the flux variation experiments (chapter 5.6.1), the gradation of the isoelectric points is rather small. Only a slight shift from 6 (10 min) to 6.1 (30 min) and 6.5 (60 min) is observed. This strengthens the supposition that after only 10 min a thick hydrogel layer is formed, which is adequate to increase the neutrality of the membrane in such a way that any further increase in the layer thickness will no longer affect the membrane charge noticeable. Thus, an increase of the filtration time beyond 10 min only contributes to minor changes of the charge.

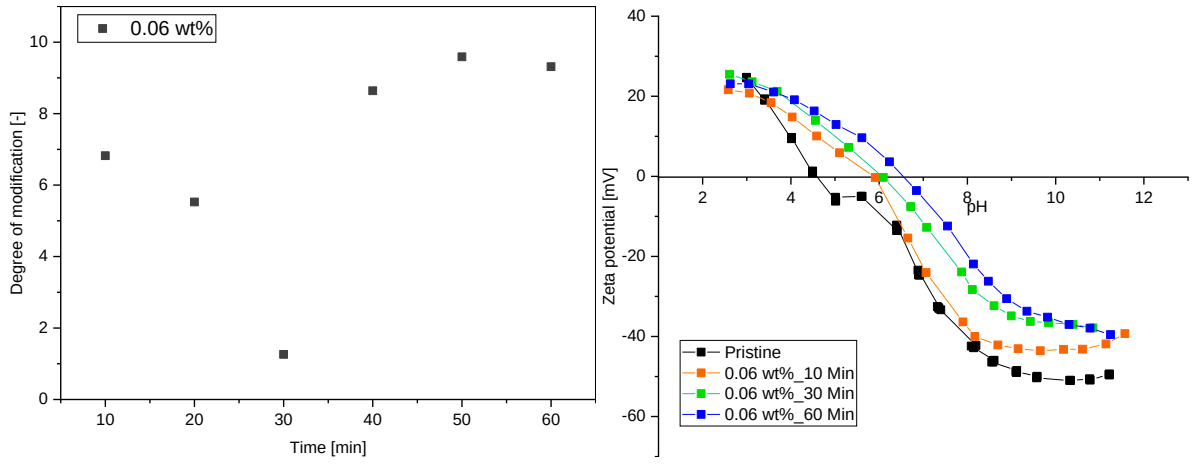

Figure 83: (a) IR spectra and **(b)** zeta potential of modified membranes in dependency of the modification time.

SEM and AFM

SEM images were also taken to examine the topography of the coated membranes and to estimate the thickness of the hydrogel layer. The surface and cross-section of the membranes are presented in Figure 84. The images of all surfaces show a homogeneous coating. No sub-structure is longer visible. Differences between the membrane surface of the 10 min and 60 min measurement cannot be found. From the cross-sectional images almost for all membranes, the coating thickness can be recognized very clearly. Only the 60 min measurement does not show any coating in the cross section. Similar to the IR analysis, the hydrogel probably detached from the surface during sample preparation. Therefore, no

coating thickness could be determined. This assumption is confirmed by the fact that with AFM of such a membrane, the hydrogel was present, see below.

However, the coating thickness is increasing with prolonged filtration time. It is striking here that the change in coating thickness is greatest from 20 to 30 minutes. This coincides exactly with the period where mass per area and time became constant (cf. Figure 82 (b)). With advancing filtration time above 30 min, the hydrogel thickness increases only moderately. This proves that the hydrogel formation is already completed after 30 minutes. This is strongly in line with the FRR values and fluxes already shown. The obtained thicknesses additionally support the hypothesis that a modification time of 10 min is sufficient for the formation of a hydrogel of considerable thickness.

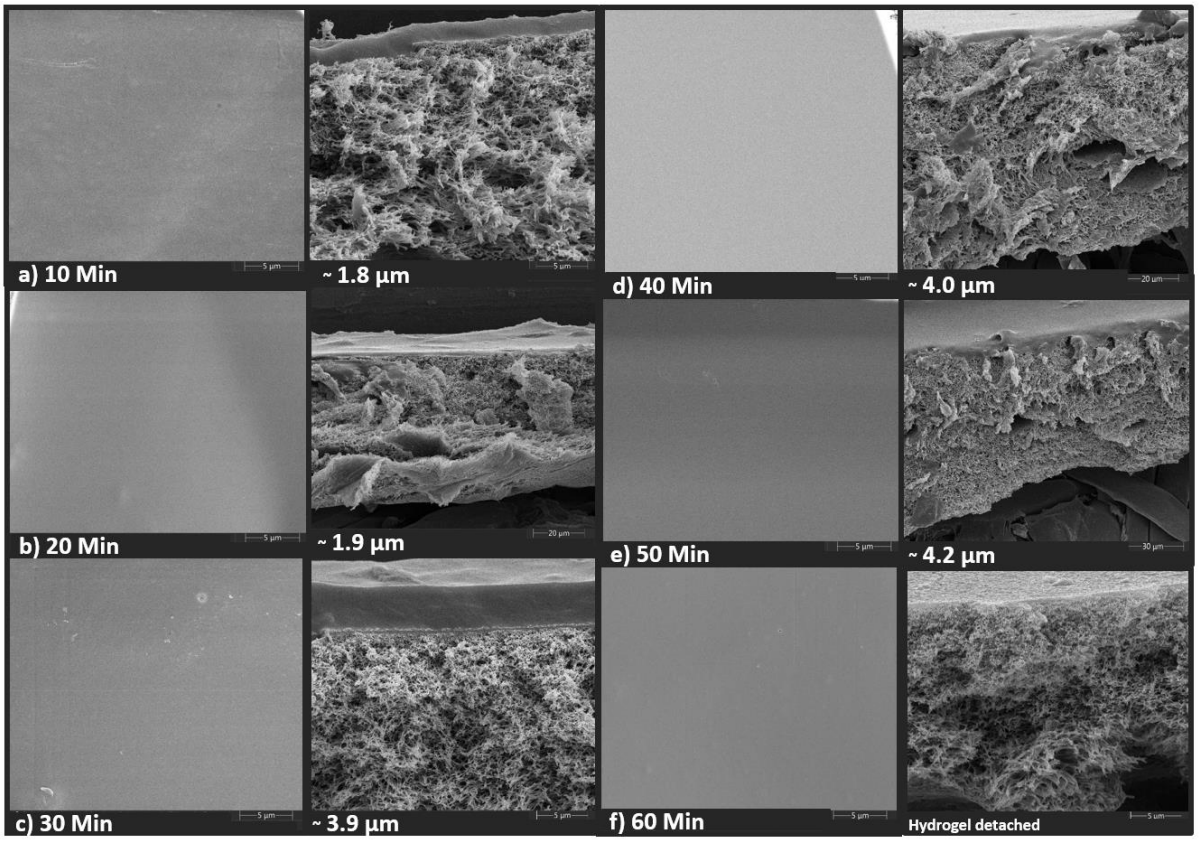

Figure 84: SEM images of membranes modified for a) 10 min, b) 20 min, c) 30 min, d) 40 min and e) 50 min and f) 60 min.

AFM measurements were carried out to obtain further information about the topography and roughness. The membrane modified for 60 min was examined in a dry and wet state. Figure 85 gives a direct comparison of the polyamide layer (PA layer), the hydrogel layer (HG layer) and both layers. All images represent an area of 50 µm x 50 µm; the bar at the right side of each image indicates the vertical deviations in the sample with the yellowish region being the

highest and the black regions the lowest. By means of the punctual brightness gradations, the roughness of the PA surface is clearly visible which can be assigned to the ridge-and-valley structure. The hydrogel layer, on the other hand, has a much lower surface roughness, which is evident from the large colour ranges. However, the underlying, rough polyamide layer can be perceived, as small bright spots are visible. The topographical differences are particularly noticeable in the two central images in Figure 85, which were measured at the boundary between the unmodified and modified part.

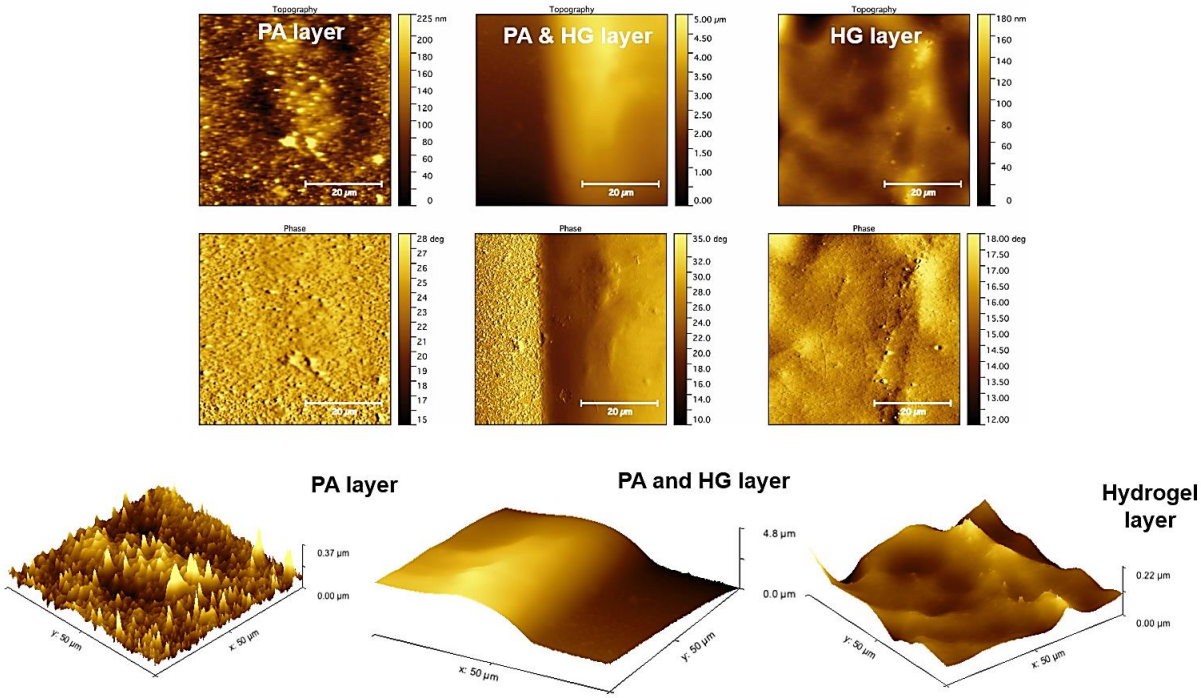

Figure 85: AFM images (topography and phase) of the PA layer, PA & HG layer and HG layer (top) and two-dimensional images (bottom) for the modified membrane at 0.06 wt% for 60 min at 10 bar.

In Figure 85 at the bottom, computer-generated two-dimensional images of specific areas are shown. The images clearly show the different topography of the unmodified rough polyamide layer and the rather smooth hydrogel layer. In addition, the height profile of both surfaces shows that the coating leads to a thicker layer. One of the most important contributors to fouling in RO membranes is the surface roughness. Therefore, it is favourable to have membranes with a smooth surface that mitigate the fouling propensity. The measured roughness of the hydrogel is 16 +/- 6 nm, whereas that of the polyamide layer is 34 +/- 8 nm. Accordingly, the roughness of the membrane surface could be reduced by more than half due to the hydrogel layer. The layer thickness of the hydrogel in a swollen state amounts to 15.7 +/- 3.8 µm.

Furthermore, the degree of swelling was calculated according to formula (49):

$$Swelling\ degree = \frac{h_{wet}}{h_{dry}} \quad (49)$$

The degree of swelling is a measure of the absorption capacity of water or solvent by the hydrogel. Here, h_{wet} corresponds to the layer thickness in the wet state and h_{dry} to the thickness in the dry state. A degree of swelling of 9.2 ± 2.2 was calculated. Both, the layer thickness and the degree of swelling indicate that the layers are very thick, which correlates with the high flux losses and modification degrees.

5.6.3 Dependency of all measurables on filtration time and rate

During the investigation of the filtration parameters time and flux it was found that at high polymer concentrations (0.05 and 0.06 wt%) short modification times are sufficient to allow a thick hydrogel to form on the membrane surface. However, if the flux does not reach a critical value, no crosslinking takes place despite sufficiently high polymer concentration. Therefore, a certain minimum flux during filtration/modification is required. To illustrate the obtained results more clearly, the measurables that describe the modification effect and are proportional to it, are shown as a function of flux and time. The measured variables include the shift of the isoelectric point (ΔIEP), the flux loss (1-FRR), the degree of modification (DG) and the dry layer thickness determined by SEM (LT). As the measured values of different experiments are summarized in a single graph for a given filtration parameter, the trends can be demonstrated more clearly. The dependencies on time and flux are shown in Figure 86 (a) and (b).

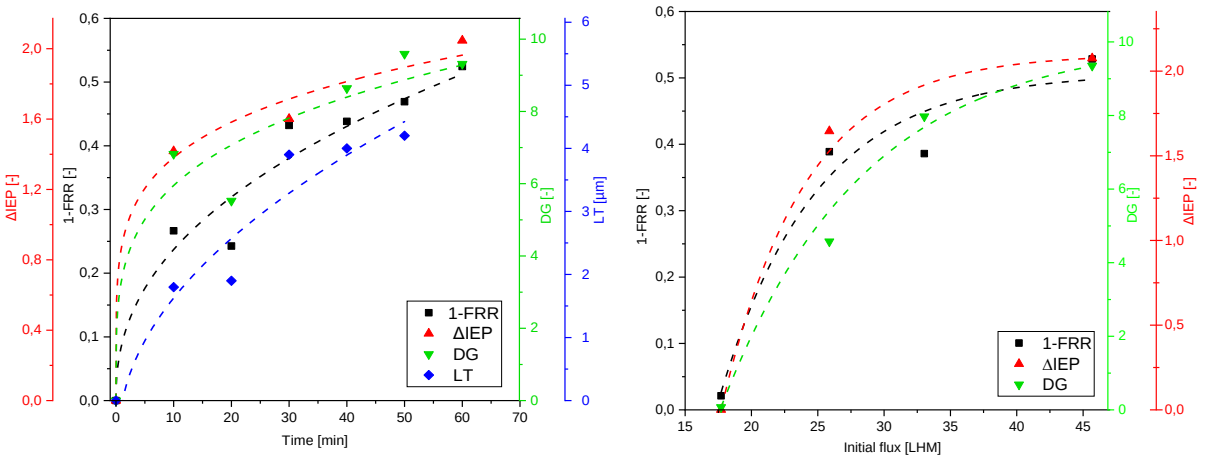

Figure 86: (a) Plot of measurables (ΔIEP, 1-FRR, DG and LT) obtained from filtration time variation experiments in dependency of modification time. **(b)** Plot of measurables (1-FRR, DG and ΔIEP) obtained from flux variation experiments in dependency of flux (average of first 10 min).

For the filtration time, an exponential increase of the measurables can be observed. However, the similarities/correlations between the measurables are less pronounced. With the zeta potential measurement, which is a pure surface measurement method, the effect of the modification is either measured or not. If the surface is (sufficiently) covered with hydrogel, there is a large and instantaneous change of the IEP. This is why the slope is steepest for ΔIEP. The change then becomes flatter with increasing time. In the later course, almost no effect can be measured anymore. This is due to the reason that an increase of the layer thickness has hardly any influence on the shift of the IEP. In the case of the layer thickness, however, the slope is less steep, and the extreme increase is much weaker as the time has a greater influence on the hydrogel thickness. According to this, the course of ΔIEP (red) does not correlate with that of the layer thickness (blue) while the course of the flux reduction (black) is similar to that of the layer thickness. In fact, it can be stated that the different measurables reflect different aspects of the modification so that the curves follow indeed different courses.

However, for all measurables, the greatest effect can be measured in the very first minutes. The largest change of IEP, 1-FRR, DG and LT is the greatest for the modification time from 0 to 10 min. With increasing time, the change of these measurables becomes gradually smaller. It becomes clear that even one minute would be sufficient to achieve a significantly high modification effect. Thus, the hydrogel formation occurs in less than 10 min. An increase of the modification time beyond that primarily contributes to the hydrogel thickness, whereas this effect is minor.

When investigating the filtration rate on the hydrogel formation, it was found that the flux decreases with increasing filtration time for all pressure values and that a stronger reduction of flux is obtained as pressure increases. In order to determine a minimum flux required to trigger a crosslinking reaction under the selected conditions (polymer concentration of 0.05 wt% and 0.06 wt%, pH 9 and acrylate/crosslinker ratio of 1:1), the various measurements need to be narrowed to a single flux first. As the decline in flux becomes greater with increasing pressure, it is therefore not reasonable to establish an average flux. Figure 86 (a) revealed already that the cross-linking reaction takes place within the first few minutes. Therefore, the measurements at the different pressure steps can be reduced to the flux of the first 10 min, which is mainly responsible for the hydrogel formation.

In Figure 86 (b) the measured values are thus plotted against the initial flux (average value of the first 10 min). Here also, the curve follows an exponential and thus limited increase which is much more pronounced and distinct as for the filtration time in (a). Thus, one can conclude that the flux and especially the absolute values are extremely important for the cross-linking reaction to take place. From the plot, it can be deduced that for a flux of 18 LHM all measured variables show a value of nearly zero. Accordingly, this flux is not sufficient to induce a crosslinking reaction at the membrane surface. However, at a flux of 26 LHM, the measurables exhibit considerably high values. Coated membranes are obtained which have a flux loss of 39 %, a degree of modification of about five and a clearly changed surface charge. From this critical flux of 26 LHM upwards, the modification effect is that distinct so that its influence is no longer appreciable. Hence, a flux of 18 LHM does not cause a crosslinking reaction to occur while a flux of 26 LHM results in a significantly high modification effect. Thus, the following conditions were selected for the transfer of the modification from dead-end to cross-flow: Polymer concentration of 0.06 wt%, pH value of 9, acrylate/crosslinker ratio of 1:1 and average flux of 26 LHM.

5.6.4 Calculation of membrane surface concentration and correlation with critical concentration from rheology data

It could be demonstrated that at 5, 7 and 10 bar, fluxes are generated which result in a sufficiently high CP so that the critical concentration of the reactants at the membrane surface was clearly exceeded. This allowed to obtain distinct, thick and homogeneous hydrogel layers. The concentration of the reactants at the membrane surface c_m during the cross-linking reaction can be calculated with the aid of the film model using formula (6) by rearrangement as follows:

$$c_m = \exp\left(\frac{J_v}{k_i}\right) \cdot c_b \qquad (50)$$

Analogous to the calculation of flux in chapter 5.6.1, the mass transfer coefficient k_i is calculated to be $6.5 \cdot 10^{-6}$ m/s using equation (12) with a diffusion coefficient D_i of $1.1 \cdot 10^{-10}$ m^2/s, a Sherwood number of 1050 and a radius of the stirred batch cell of $1.75 \cdot 10^{-2}$ m. Using formula (50), the required concentration c_m can be finally calculated by inserting the mass transfer coefficient k_i, the bulk concentration c_b and the applied flux during modification experiment.

As already mentioned, under dead-end conditions no stationary state can be reached, so that a continuous decline in flux occurs. Moreover, the additional reaction (gel formation) leads to a further decrease in flux. This results in a reduction of driving force for the CP, which is crucial for the hydrogel formation. For this reason, the CP and the concentration of reactants c_m at the membrane surface is variable under dead-end conditions. However, the film model assumes a stationary state, so that the calculation of the surface concentration is only an average value and thus an approximation. As the results so far have shown that hydrogel formation takes place within the initial phase, the average flux of the first 10 min was chosen for the calculation and inserted into the equation. This enables a surface concentration c_m to be calculated, which corresponds to the concentration in the initial phase, in which the hydrogel formation takes place predominantly. The calculated concentrations as a function of pressure are shown in Figure 87.

At this point, it should be reiterated that using the critical concentration of 12 wt%, fluxes of 128 and 124 LHM (0.05 wt% and 0.06 wt%) were predicted for the modification in dead-end. However, these fluxes could not be adjusted, so that pressures were chosen that generated

lower fluxes. Consequently, none of the surface concentrations calculated here match the critical concentration of 12 wt% determined from rheology. For the polymer concentration of 0.05 wt% and 0.06 wt%, values are obtained which are two orders of magnitude smaller (0.15 – 0.3 wt%). According to this, even at clearly subcritical concentrations, local cross-linking occurs on the membrane surface. In other words, the reaction under dead-end conditions starts before the gelation point. This is an interesting finding and is discussed in more detail below.

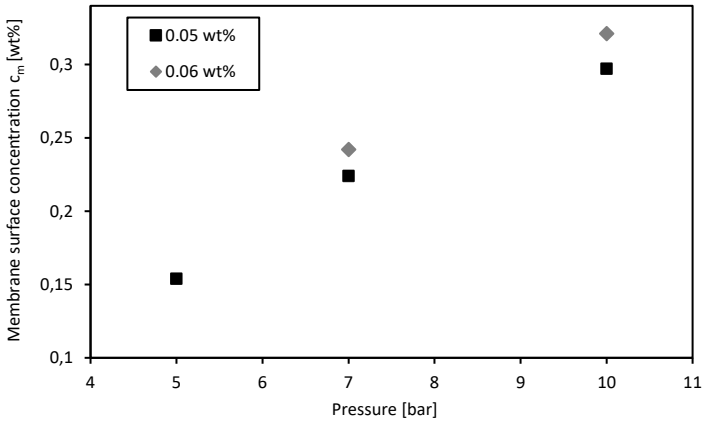

Figure 87: Calculated membrane surface concentration c_m for modified membranes in dependency of the applied pressure.

First, it must be stressed that a gelation time of 10 min has been defined as the target value for the determination of critical concentration. For the modification in dead-end, a modification time of 60 min was chosen. If the gelation time for the rheology experiments, for which the critical concentration is determined, was set to 60 min instead of 10 min, a significantly lower concentration would be obtained. This can be explained by the fact that at 60 min, the reactive system would have more time for the reaction and therefore lower concentrations than 12 wt% would be sufficient to initiate the gelation. This can be illustrated by the curve in Figure 75. By extrapolating the curve to longer gelation times, lower polymer concentrations would be obtained. Thus, the discrepancy between c_{crit} and c_m is reinforced by the fact that the gelation time to which the critical concentration is referred, is significantly shorter than the modification time in the dead-end experiments.

Furthermore, the gelation time is measured at the gel point (cross-over of storage and loss modulus). This point defines the time at which the viscoelastic state is achieved. That means that the gel point only indicates the transition from the liquid to the gel state. However, prior

to the gel point, cross-linking takes place at subcritical concentrations, which is not detected. This is the very fact that was found in the preceding dead-end experiments (variation of polymer concentration (chapter 5.5.3) and flux dependency (chapter 5.6.1)). It was shown that hydrogel formation undergoes two processes. Cross-linking starts below the critical concentration (first process) and (complete) gelation takes place above the critical concentration (second process). Therefore, significantly lower surface concentrations c_m are obtained using the film model compared to the critical concentration c_{crit} measured by rheology.

Assuming that the cationic surface linker adsorbs optimally, a series of bimolecular reactions between the surface linker and crosslinker would also trigger a crosslinking reaction and finally cause a gelation. This reaction always takes place simultaneously. This is yet another reason why the surface concentration may not match the critical concentration. Thus, setting the gelation time as a target value inevitably leads to a discrepancy between c_{crit} and c_m.

Moreover, c_m was calculated using the film model. This model presumes a convective mass transport towards the membrane surface and a diffusive back transport of solutes away from the surface.[82] According to this model, the reactants are transported back continuously with a certain probability. A stationary state is then achieved between the convective transport and the back diffusion. As already explained in the beginning of the chapter, no steady state can be attained here due to the dead-end conditions. This is further intensified by the cross-linking reaction at the membrane surface. The cross-linking reaction leads to a reduction of the driving force for the back transport in the boundary layer, since the reactants, which would be transported back traditionally, accumulate at the surface and are finally converted into other components. Thus, less reactive mass is transported back than is transported towards the surface. However, this additional reaction is not considered in the classical film model for characterization of CP. In other words, in the film model, the accumulation in the boundary layer caused by the reaction is diminished by the term describing the back transport. As a consequence of the back transport, the concentration at the membrane cannot increase significantly. This also contributes to the big gap between c_{crit} and c_m. Thus, an average surface concentration can be calculated using the film model, however, due to the non-existing reaction term and the previously mentioned other limitations (no steady-state, concentration in dead-end, etc.) this is only an approximation.

Overall, it can be concluded that the rheology can be applied to investigate the influence of different parameters (pH, acrylate/crosslinker ratio) on gel formation. From this, data on crosslinking time and storage module as a function of concentration can be obtained. This allows the determination of optimal parameters for the composition of the solution for the dead-end modification experiments. However, the reactivity of the system cannot be reduced to a critical concentration since the gel point as an assessment criterion is not representative for the reaction taking place at the membrane surface. Even though, the calculation of c_m using the film model is only an approximation, the greater challenge is to use the rheological information and apply these to the same system under dead-end conditions. Hence, rheology cannot be used to predict a priori conditions that lead to a certain coating effect. However, it can be used to support the understanding of hydrogel formation and to determine optimal parameters for the composition of the solution.

5.6.5 Remaining challenges during dead-end modification

One problem that has not yet been addressed is the reproducibility of modifications that successfully lead to a coating on membrane surface. In experiments with filtration conditions that clearly lead to membrane modification (0.05/0.06 wt%, 10 bar, 60 min), only more than every third experiment showed a decrease in flux over the entire measurement period. Figure 88 (a) shows the constant flux course of several modifications in which in fact a clear decrease should be apparent. Although a slight decrease of the initial flux occurs in some measurements, the flux remains constant over the entire modification time. This indicates that the modification has failed or has not started at all. The corresponding FRR values are shown in (b).

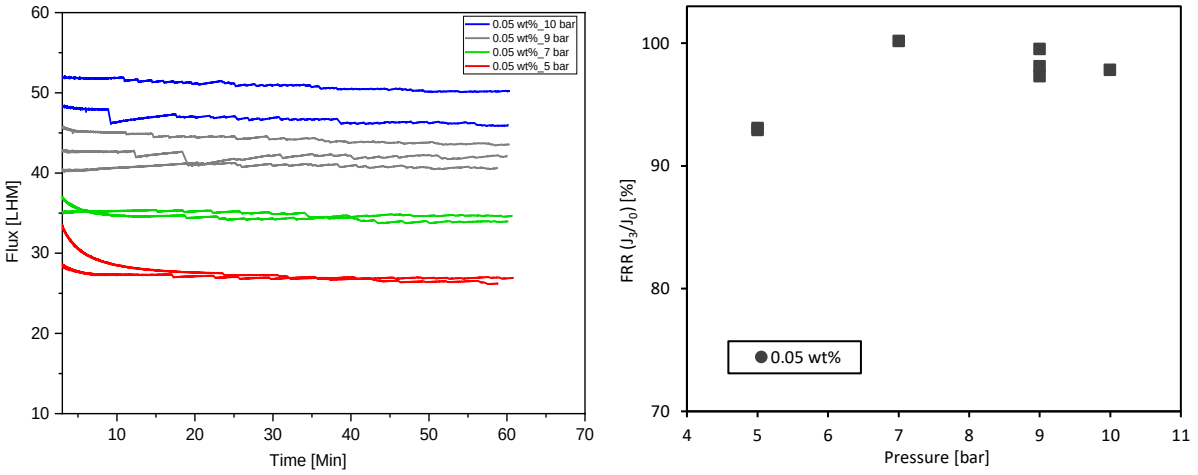

Figure 88: Unsuccessful dead-end modifications (0.05 wt%, pH 9, acrylate/cross-linker ratio 1:1, 60 min): **(a)** Flux course during modification at different pressures (5, 7, 9 and 10 bar). **(b)** Corresponding FRR values after washing with NaCl solution (J_3/J_0).

The FRR values also tend to be very high (FRR values > 90 %) regardless of the applied pressure. This confirms the argument that a comparatively poor or no hydrogel layer has been formed on the membrane surface. However, it has been proven that under these selected filtration conditions the critical concentration is exceeded and thus a three-dimensional defined hydrogel network should be formed. The modification degrees below 0.07 shown in Figure 89 (a) are also very low and do not comply with the expected DG of 5 – 10 of successfully modified membranes. Furthermore, the zeta potential curves of both membranes (5 and 10 bar measurement) in (b) are identical to those of the unmodified membrane. All results shown point to a problem of reproducibility of the modification under dead-end conditions. Therefore, some sources of error and possible weak points were investigated.

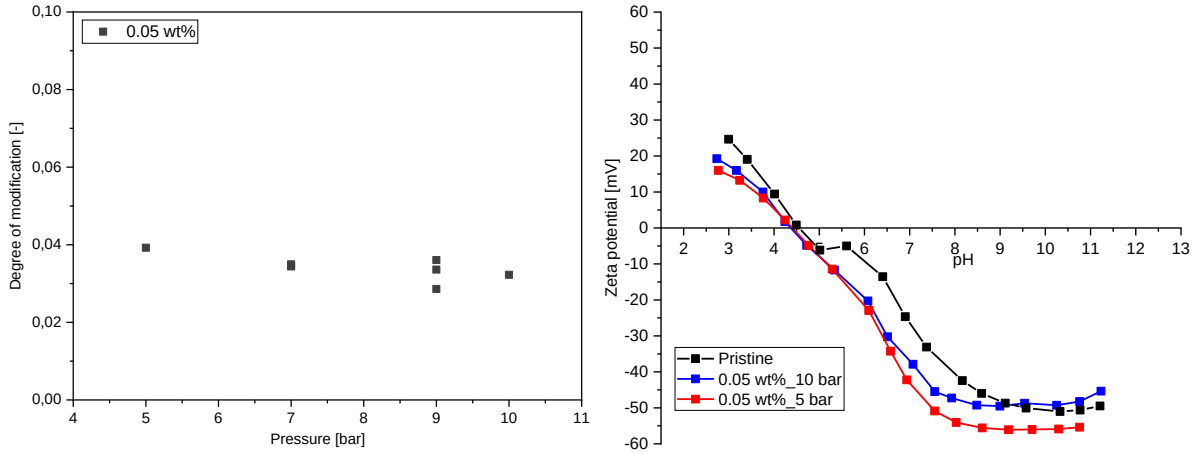

Figure 89: Unsuccessful dead-end modifications: **(a)** IR spectra and **(b)** zeta potential of modified membranes in dependency of the applied pressure.

Since the coating is intrinsically stable, it is possible that the adsorption of the cationic surface linker on the BW30 membrane is per se insufficient. Therefore, the adsorption/adhesion of the cationic surface linker was investigated as a weak point. Membranes were adsorbed only with the cationic surface linker and analyzed by zeta potential and ATR-FTIR measurements. Unfortunately, these measurement methods were not sensitive enough to prove the existence of the linker on the surface (cf. Figure 127 in the Appendix). However, it is known from previous works that the adsorption of the cationic surface linker on a NF270 membrane performs very well and leads to a more neutral to positive surface until pH 7.[177] Still, there is a certain risk that the adsorption on the BW30 membrane works less effective if the charge density differs significantly from that of the NF270 membrane since the charge density is crucial for a successful adsorption. During the crosslinking of the aromatic polyamide, negatively charged carboxylic acid groups are formed since not all carboxylic acid chlorides of the TMC react with the amines of the MPD. A direct relationship exists between the proportion of free carboxylic acid groups (charge density) and the degree of crosslinking of the PA layer. In order to discover differences in the charge density of the NF270 and BW30 membranes, the degree of crosslinking was measured using XPS. The calculation was carried out using formula (51):[193]

$$Crosslinked\ [\%] = 1 - \frac{(O/N)_{observed} - (O/N)_{fully\ cross-linked}}{(O/N)_{fully\ linear} - (O/N)_{fully\ cross-linked}} \cdot 100\ \% \qquad (51)$$

in which $(O/N)_{observed}$ indicates the O/N molar ratio measured by XPS. A fully cross-linked polyamide has an O/N molar ratio of 1 and a theoretically fully linear polyamide has an O/N molar ratio of 2.

Using formula (51), a degree of cross-linking of 95 % and 53 % could be calculated for the NF270 and BW30 membrane, respectively. Since a lower degree of crosslinking implies a higher charge density, it follows that the charge density of BW30 is higher than for the NF270 so that the adsorption should be more efficient for BW30. However, these values are highly erroneous, since oxygen impurities on the membrane surface falsify the values strongly. Therefore, no reliable conclusions can be drawn regarding the degree of cross-linking and thus the charge density. As successful modifications are also achieved, it can be generally presumed that the cationic surface linker is not the main reason for the poor reproducibility.

Next, the influence of the base membrane itself on the modification was investigated. Although the permeance of the base membrane is relatively constant on average over a large area, smaller areas can exhibit varying permeabilities after compaction. Therefore, the influence of the fluctuating permeance of the base membrane could be a possible source of error. To identify a possible correlation, some FRR values after modification (J_3/J_0) were plotted against the permeance of the base membrane after compaction, cf. Figure 90. This was done to figure out whether the high FRR values (low flux loss) were attributable to an undersized flux of the membrane at compacted state. A clear linear relationship cannot be identified (R^2 = 0.31). According to this, the success of the modification is not necessarily dependent on the flux of the membrane in the compacted state. Also, further investigations could not clarify the reason for the lack of reproducibility.

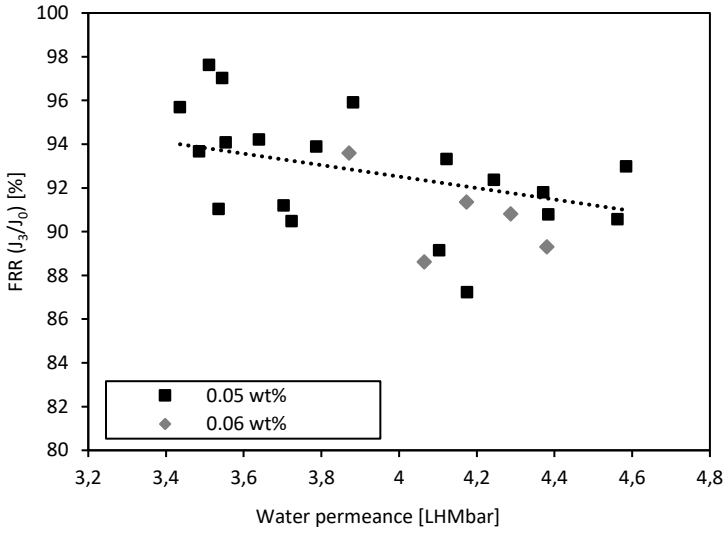

Figure 90: FRR values after washing with NaCl solution (J_3/J_0) for various modified membranes in dependency of the water permeance at compacted state.

Nevertheless, it could be shown that a bulk concentration of 0.06 wt%, a pH of 9 and an acrylate/crosslinker ratio of 1:1 leads to a pronounced hydrogel layer on the membrane surface when the minimum flux during filtration/modification is reached, even within a short modification time. From the results of the dead-end experiments, conditions for the modification in cross-flow could be derived (chapter 5.7), which have a significantly higher relevance.

5.6.6 Interim conclusions

The main conclusions regarding the adjustability of the modification via filtration rate and filtration time are as follows:

1. The parameters for hydrogel formation determined by rheology (pH value of 9 and acrylate/crosslinker ratio of 1:1) were applied for these experiments. The flux calculated via the critical concentration could not be realized with the BW30 RO membrane used. Therefore, experiments were carried out at constant pressures of 3 – 10 bar and the change in flux was investigated. During the modification, the flux decreased with increasing filtration time. A stronger decrease occurred at higher pressures.
2. A pressure of 3 bar and a polymer concentration of 0.05 wt% and 0.06 wt% are not sufficient to initiate a crosslinking reaction via the CP only (2 % flux loss, DG of 0.07, ΔIEP equals 0). At 5, 7 and 10 bar a homogeneous and distinct hydrogel layer is formed on the membrane surface (flux loss > 39 %, DG > 4 and ΔIEP > 1.7).
3. The cross-linking reaction takes place within the first few minutes and is completed after approx. 30 min. Increasing the modification time beyond that mainly contributes to the hydrogel thickness, although this effect is very small.
4. With this understanding, it was possible to reduce the variables during experiments at different pressures to the flux of the first 10 minutes to identify the minimum flux required for the crosslinking reaction. Since no modification effect was obtained at a flux of 18 LHM but a significantly high modification effect was achieved at 26 LHM, it can be concluded that the minimum flux at the selected conditions must be higher than 18 LHM. Thus, if the flux does not reach a minimum value, no crosslinking takes place despite a sufficiently high polymer concentration and reactivity of the system (cf. first point).
5. For the transfer of the modification from dead-end to cross-flow, the following conditions were consequently chosen: Polymer concentration of 0.06 wt%, pH value of 9, acrylate/crosslinker ratio of 1:1, flux of 26 LHM.
6. The surface concentration c_m calculated via film model is significantly lower than the critical concentration c_{crit} estimated from rheology. This is primarily caused by the fact that the gel point as an evaluation criterion is not representative for the reaction taking place at the membrane surface. Hence, the reactivity of the system cannot be reduced to a critical concentration only.

5.7 Transfer of in situ modification in dead-end to flat-sheet membranes in cross-flow

In this chapter, the conditions leading to a successful modification in dead-end (chapter 5.6) were transferred to the case of a narrow spacer-filled channel, operated in cross-flow mode. Such flat channels are representative for SWMs since conditions in an SWM can be approximated. This is done, for instance, by using a spacer, which is a key component of a SWM, so that the channel height and thus similar hydrodynamic conditions can be achieved.[194] However, the flow conditions over the membrane length in a flat channel do not reflect those of a SWM due to the significantly shorter membrane dimensions. Nevertheless, conditions can be simulated that represent a section of a SWM. Thus, a comprehensive understanding of hydrogel formation in cross-flow can be gained in this chapter, which can be used to transfer the modification to SWM.

5.7.1 Derived parameters from dead-end as basis for modification of flat-sheet membranes in cross-flow

The data gained from the dead-end experiments can be used now to derive optimal parameters for the modification in cross-flow. For a successful transfer, the reactive system, consisting of the composition of solution (polymer concentration, pH value and acrylate/crosslinker ratio), the flux and the filtered mass per area must be applied. In addition, the hydrodynamic conditions must be considered.

The basis for the cross-flow experiments was the modification experiment, in which the minimum flux during filtration/modification was reached and polymer content exceeded the critical concentration, resulting in a distinct hydrogel layer on the membrane surface. These conditions could be achieved at a pressure of 10 bar, an applied polymer concentration of 0.06 wt%, a pH value of 9 and an acrylate/crosslinker ratio of 1:1. The average flux was 26 LHM and thus surpassed the required minimum flux of > 18 LHM. Since the polymer concentration increased during the test due to concentration of the reaction solution, an average polymer concentration of 0.0681 wt% was obtained. The maximum filtered mass of polymer and crosslinker was 13.56 g/m^2. These parameters are summarized again in Table 15.

Table 15: Derived parameters from dead-end for the transfer to cross-flow modification.

Parameters from dead-end modification		
Average copolymer concentration C_{copo}	wt%	0.0681
pH value	-	9
Acrylate/cross-linker ratio	-	1:1
Average Flux J	LHM	26
Mass/area	g/m^2	13.56

The composition of solution (average polymer concentration, pH value and acrylate/ crosslinker ratio) can be adopted directly from the dead-end experiments. To set the same flux of 26 LHM, the corresponding permeate volume flow must be adjusted. This is calculated using formula (26) and equals 0.22 L/h. The minimum volume of modification solution required to bring the local concentration in the boundary layer above the critical concentration, can be calculated by using the filtered mass per area of 13.56 g/m^2. This volume is calculated from formula (32) and is 167 mL.

In addition to the composition of the solution and the flux, the hydrodynamic conditions in dead-end and cross-flow must also match. The comparison of the rotational Reynolds number in the dead-end stirred cell and the Reynolds number for a cross-flow module is insufficient and not applicable due to the different cell geometries and constructions and the use of a 44 mil spacer which induce turbulences and an associated different flow profile. Another approach is to apply the cross-flow velocity corresponding to the stirring rate in dead-end which was 0.24 m/s. To obtain a cross-flow velocity of 0.24 m/s, a feed volume flow of 32 L/h must be set which can be calculated using the formula (29) and applies to a spacer-filled channel. In order to investigate the influence of the cross-flow velocity on the formation of the CP, modifications were also done at lower CFVs of 0.1 m/s and 0.19 m/s. A modification time of 50 min was chosen.

5.7.2 Influence of cross-flow velocity on the modification degree

Modification at different cross-flow velocities

The evaluation of this chapter focuses at the beginning on the modification experiments, which were carried out at cross-flow velocities of 0.1, 0.19 and 0.25 m/s corresponding to recovery rates of 20.3, 10 and 7 %. Two experiments per modification condition were carried

out. Different from dead-end, a constant flux of 25.6 LHM could be maintained during the modification by readjustment (increase) of pressure. The following Figure 91 shows the resistance which is the reciprocal of the permeance during the modification against the modification time for the different experiments. As can be seen, the resistance at a CFV of 0.1 m/s and 0.19 m/s increases with increasing filtration time. This could be a first indication for the formation of a hydrogel layer, which results in an additional membrane resistance. In contrast, the increase/change in resistance for the CFV of 0.25 m/s is very low. Also, the resistances for the CFV 0.1 m/s and 0.19 m/s are in total higher than for 0.25 m/s. According to this, hydrogel formation is promoted by a lower CFV.

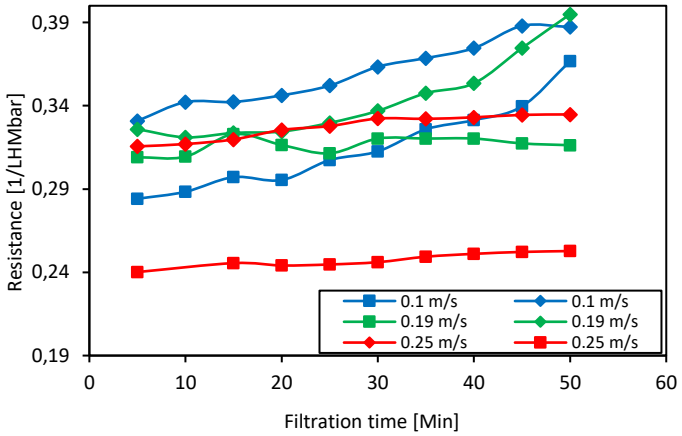

Figure 91: Cross-flow modification (0.06 wt%, pH 9, acrylate/cross-linker ratio 1:1, 50 min, 26 LHM): Resistance during modification for membranes modified at different CFVs (0.1, 0.19 and 0.25 m/s).

Figure 92 also shows the FRR values against the cross-flow velocity. The recovery which is the ratio of the permeate flow to the feed flow is also plotted against the CFV. J_1/J_0, J_2/J_0 and J_3/J_0 represent the FRR value immediately after modification, after washing with pure water and after washing with a 5000 ppm NaCl solution, respectively. If the FRR values J_1/J_0, J_2/J_0 and J_3/J_0 are first compared with each other, the highest flux loss can be recorded immediately after modification and the lowest after washing with NaCl, regardless of the selected CFV. This can be attributed to an irreversible washing effect and was already discussed in chapter 5.5.1. Briefly, by washing the hydrogel-coated membranes with NaCl, swelling of the zwitterionic hydrogel on the membrane surface occurs so that unbound components can be washed out of the hydrogel, leading to a lower flux loss afterwards.

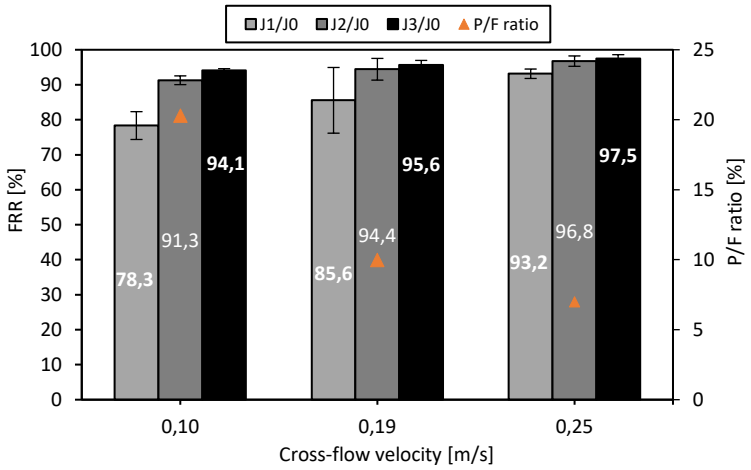

Figure 92: FRR values after modification (J_1/J_0), after washing with pure water (J_2/J_0) and after washing with NaCl solution (J_3/J_0) of modified membranes in dependency of the CFV.

When comparing the FRR values after washing with NaCl, it is evident that the FRR values increase with increasing CFV (94.1 vs. 95.6 vs. 97.5 %). Hence, the modified membranes have a lower flux loss at a higher CFV and at a correspondingly lower recovery, and vice versa. A higher CFV which corresponds to a lower recovery at constant flux, results in a larger mass transfer from boundary layer to the bulk solution by virtue of its sweeping action on the surface. Thus, the back transport of solutes away from the membrane increases by increasing the shear rate, reducing the effectiveness of the crosslinking reaction and preventing hydrogel formation on the membrane. At lower CFV, the mass transfer coefficient is considerably lower, and more solutes are convected towards the membrane surface so that the sweeping action of the cross-flow becomes less, leading to an increase of CP layer. Thus, the critical concentration of the reactive system required for a successful crosslinking reaction is much more likely to be exceeded.

However, it is striking that the FRR values obtained are not comparable to the FRR values obtained in the dead-end tests (FRR of 50 – 70 %), where the same parameters were applied (composition of the solution, filtered mass, flux and velocity). This discrepancy is discussed in more detail at the end of the chapter.

The modified membranes were also examined by ATR-FTIR spectroscopy. Since the flat-sheet membranes are cross-flowed lengthwise, four location-dependent samples (0, A, B, C) were analyzed, see Figure 93. The aim was to examine whether a uniform and homogeneous hydrogel layer has been formed over the entire membrane length during the modification experiments.

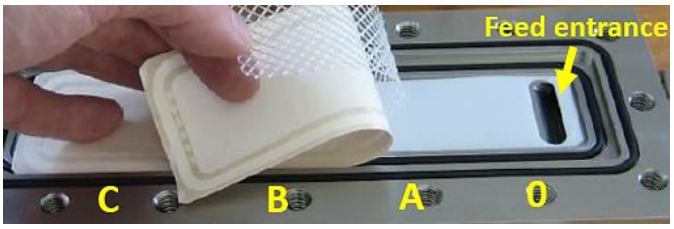

Figure 93: Positions (0, A, B and C) from which the membrane samples were cut and analyzed.

From the ATR-FTIR spectra the modification degree was calculated as described in chapter 5.5.3 using formula (46). The calculated modification degrees are shown in Figure 94.

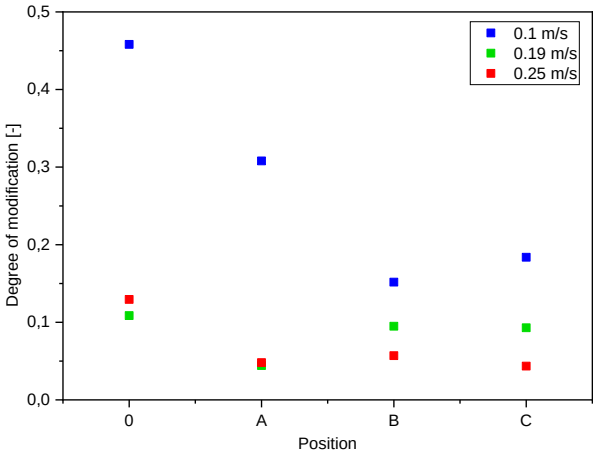

Figure 94: Modification degree of modified membranes in dependency of the applied CFV and the location (0, A, B and C).

First, it is noticeable that the membrane modified at a CFV of 0.1 m/s shows the highest modification degrees. This appears logical and correlates with the obtained FRR values. Interestingly, the DG for this membrane is highest at position 0 and decreases over the length of the membrane. Due to the geometry of the flow channel, at position 0, the feed solution flows in a highly concentrated form directly towards the membrane at an oblique angle, thus creating unique boundary layer conditions. The transport of the reaction solution becomes much more effective so that the laminar boundary layer in which the CP is formed tends to become thicker. As a result, the conditions for the formation of the hydrogel layer are most favorable at position 0 and the DG is thus the largest.

Also, a decrease in DG from A to C is observed for the CFV of 0.1 m/s. This could be the consequence of a slight pressure difference measured between the inlet and outlet area caused by the tangential flow along the channel. This reduces the driving force for the permeation along the membrane. With other words, the distribution of hydrogel formation would follow the TMP distribution, with a more pronounced build-up near the entrance in the

flow channel at position A. This could be the reason for the obtained decrease in DG from A to C. If the difference in TMP is considered quantitatively, the pressure drop of 0.1 bar is not high enough to have an influence, so that this discussion cannot fully explain the decrease of the DG from A to C. However, the effect of TMP is counteracted by the effect of decreasing CFV along the channel/membrane length due to the loss of solvent through the membrane. As a consequence, the CP would be highest at position C, resulting in a higher DG at position C. But the tangential decrease in cross-flow is most likely negligible because of the spacer used which has an additional influence on the mixing conditions. Furthermore, it can be assumed that the change in CFV on the retentate side is minor due to the adjusted high ratio of retentate to permeate. To sum up, both effects (pressure drop and decreasing CFV) are not very conclusive to explain the decrease of the DG from A to C. This is further complicated by the fact that the decreasing trend of DG is absent for the CFV of 0.19 m/s and less pronounced for the CFV of 0.25 m/s. For the CVFs of 0.19 m/s and 0.25 m/s the greatest effect can be also observed at position 0 due to the mentioned modified boundary layer conditions. However, there is a decrease afterwards and then a relative even distribution of DG. In total, there is the same effect at the beginning and at the end of the membrane.

The zeta potential was also examined in dependency of the positions A and C. From the zeta potential measurements in Figure 95 (a) – (c), it can be observed that all membranes show a more or less large shift of the IEP into the neutral pH range. Against expectations, the largest shift of the IEP is observed for the membrane at 0.25 m/s, followed by the membrane at 0.1 m/s and 0.19 m/s ($\triangle$IEP of 1.2 vs. 1.0 vs. 0.4). Thus, a dependence of $\triangle$IEP on the CFV cannot be determined. It can be assumed that the zeta potential measurement is less sensitive to minor changes in coating thickness compared to the ATR-FTIR measurement. This was also observed in the dead-end experiments. Thus, the membranes seem to be sufficiently coated at all CFVs in order to enhance the overall charge neutrality. In addition, unlike the modification degrees, for all CFVs the IEPs at position A and C barely differ from each other. Since the sample area for the zeta potential measurement is larger than the sample area measured by the ATR-FTIR crystal, it is very likely that the location dependency is no longer captured during the zeta potential measurement. This could also indicate that the local inhomogeneity of the coating is greater so that the differences between the different positions are no longer detected.

Similar to the FRR values, it is striking that the membranes as a whole exhibit much lower modification degrees and that the shift of the IEP is significantly lower than for the dead-end experiments (DG of 4 – 10 and ΔIEP of 1.7 – 2). This is also taken up and discussed again at the end of the chapter.

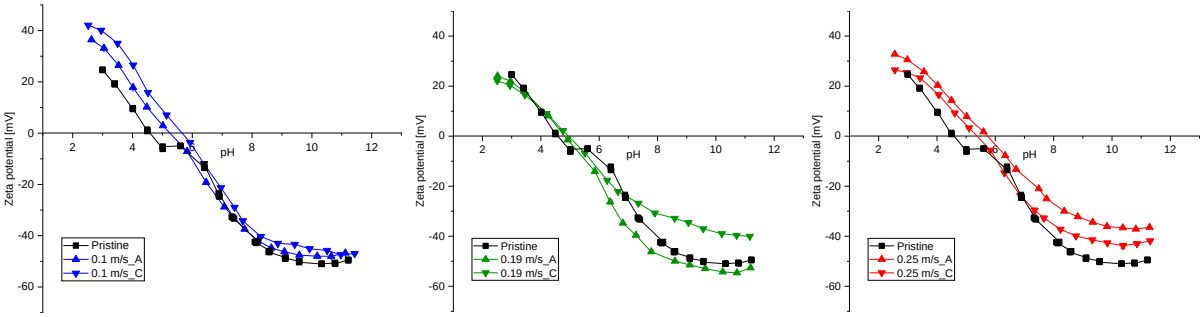

Figure 95: Zeta potential of modified membranes at CFVs of **(a)** 0.1 m/s, **(b)** 0.19 m/s and **(c)** 0.25 m/s.

Figure 96 presents the SEM images of the modified membranes compared to the unmodified membrane. Independently of the CFV, the ridge-and valley structure of the polyamide layer is apparent in all images. The modified membranes (b), (c) and (d)) exhibit a slightly more homogeneous surface structure compared to the unmodified membrane in (a), indicating a thin hydrogel coating. However, as expected, the membranes in (b) and (c) (CFV of 0.1 m/s and 0.19 m/s) are coated a bit denser than the membrane in (d) (CFV of 0.25 m/s). By comparing position A and C, a slightly thicker hydrogel layer can be observed on position A for the membrane in (b) (CFV of 0.1 m/s). This coincides with the results of the modification degrees. This is also shown for the membrane in (c) (CFV of 0.19 m/s), though it is more difficult to assess due to an artefact at position A caused by the spacer. No thicker coating can be observed on position A for the membrane in (d) (CFV of 0.25 m/s). Unevenly coated spot-like areas are rather visible. The CFV of 0.25 m/s thus leads to a greater shear force resulting in a thinner hydrogel layer and an additional irregular and inhomogeneous distribution of hydrogel fragments on the membrane which is probably due to uneven flow conditions caused by the spacer.

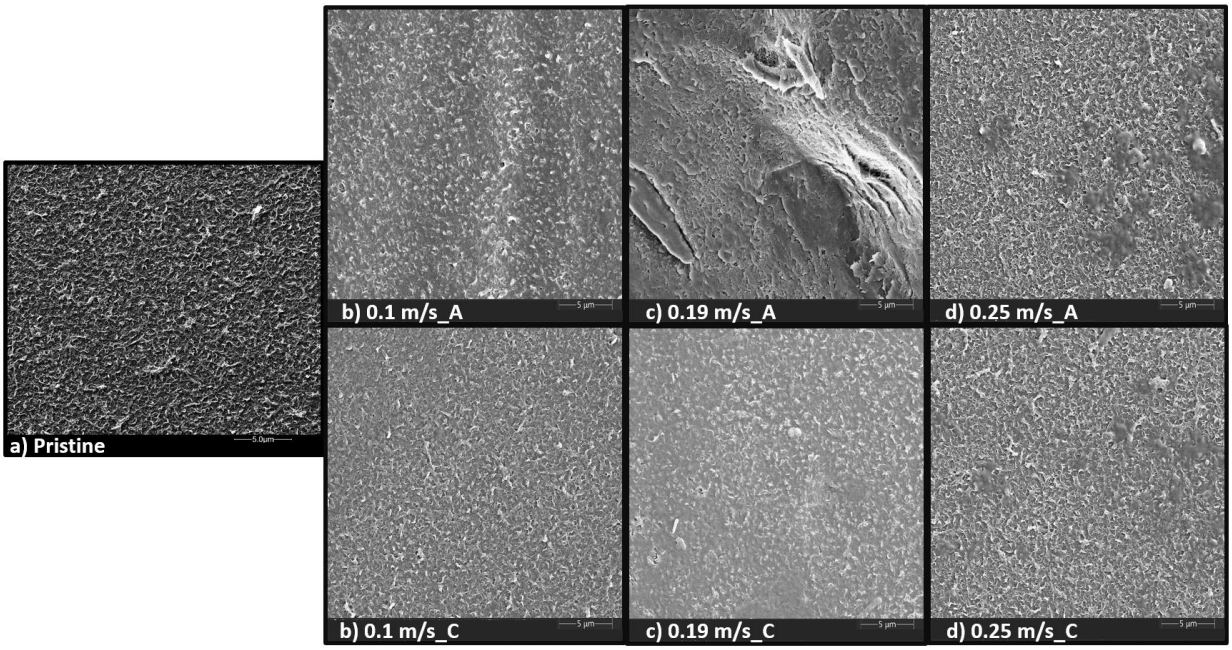

Figure 96: SEM images of a) pristine membrane and membranes modified at b) 0.1 m/s at position A and C, c) 0.19 m/s at position A and C and d) 0.25 m/s at position A and C.

Due to the overall very thin hydrogel layers, the influence of the different CFVs is small. Analogous to the results shown so far, the hydrogel layers are all significantly thinner than those obtained during the dead end experiments.

Accordingly, two conclusions can be made. First, the different results (FRR values, ATR-FTIR, zeta potential and SEM images) show that larger modification effects can be achieved at a CFV of 0.1 m/s compared to the CFVs of 0.19 and 0.25 m/s. This is consistent with the assumption that the laminar boundary layer in which the CP is formed is thicker at a lower CFV. Thus, the critical concentration of the reactive system necessary for a successful crosslinking reaction and the formation of the hydrogel can be exceeded much more likely. Hence, it could be demonstrated that the CFV has a clear influence on the CP and thus on the hydrogel formation.

Unfortunately, it was also shown that the obtained modification effects are significantly smaller than those measured in dead-end under the same filtration conditions, independent of the CFV. The FRR values, modification degrees and $\triangle$IEPs obtained here are comparable to the values obtained in dead-end at significantly subcritical conditions, where only thin and inhomogeneous hydrogel layers were formed. Finally, it can be assumed that the critical concentration was not exceeded under the cross-flow conditions performed here. Thus, only a transport-controlled deposition of a thin cross-linked hydrogel layer occurred. Also interesting is that the modification solutions became turbid after each modification, cf.

Figure 97. The turbidity is probably caused by partially cross-linked polymer chains which are present in the solution as a disperse phase. Thus, hydrogel segments have formed as a result of the concentration but were not completely cross-linked on the membrane surface and were therefore transported away with the cross-flow. According to this, the conditions were not sufficient to exceed the critical concentration in order that macroscopically cross-linked polymer continues to cross-link with the thin layer already present on the surface, thus forming a three-dimensional hydrogel layer.

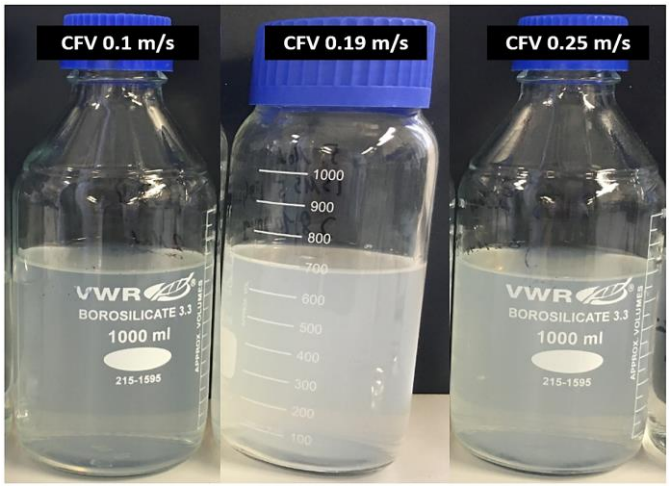

Figure 97: Turbidity of the modification solution after modification at CFVs of 0.1 m/s, 0.19 m/s and 0.25 m/s.

It can be concluded that conditions that led to a pronounced thick hydrogel layer on the membrane surface in the dead-end experiments could not be translated to the cross-flow experiments. This is unexpected as the reactive system (composition of the solution, flux and filtered mass), which is required for a successful transfer of the modification conditions, was considered. Also, the cross-flow velocity matched the stirring rate set in the dead-end experiments.

In fact, the main difference between both modification systems is the use of a spacer with a thickness of 44 mil (1.12 mm) in the cross-flow experiments. Therefore, it is most probable that the unsuccessful transfer with respect to the quantity is due to the spacer, which creates turbulences and eddies near the membrane surface, thus decreasing the CP by increasing friction factor and bulk velocity. The flow through a spacer-filled channel cannot be described straightforward as the flow characteristics of a spacer-filled channel are too complicated.[195] There are indeed studies in which the velocity profiles in spacer-filled channels are predicted with numerical models[196-198] but such models are adapted to a particular type of feed water

and cannot be transferred to other system as interactions between the solutes in the feed have to be studied individually. This leads to unique boundary layer conditions near the membrane surface, especially if an additional reaction occurs at the surface.

However, in order to identify the boundaries of the flow regimes (laminar, transitional, turbulent) during the cross-flow modification experiments, the Reynolds number can be used. The precise transition from laminar to turbulent flow regime in spacer-filled channels is a complex function of size and shape of the spacers and packing characteristics. Numerical simulations of flow through spacer-filled channels with commercial spacers have shown that the transition from laminar to turbulence occurs at Reynolds numbers in the range of 300 – 400 as reported for packed beds.[195, 199] The Reynolds numbers obtained for the different modifications at CFVs of 0.1, 0.19 and 0.25 m/s were 88, 167 and 232, respectively. According to this, laminar flow conditions prevailed during the modification in cross-flow. However, it was found that at Reynold numbers of 180 – 280, most geometries start to exhibit oscillations so that instabilities in the flow appear as a result. At Re = 250 – 300, the flow becomes unsteady and wavy, and at Re > 300, the flow shows a very unsteady behaviour.[195, 200] This leads to the conclusion that the applied conditions were sufficient to affect the flow being unsteady, thus to increase eddies which results in a reduction of CP so that the critical concentration could not be exceeded within the boundary layer. Hence, the use of the spacer has a considerable influence on hydrogel formation and cannot be neglected.

In order to optimally meet the conditions for a potential upscaling of the modification conditions to SWM, the spacer was maintained, and an attempt was made to overcome and compensate the turbulence with a significantly higher flux. Therefore, the next step was to increase the flux from 26 LHM to 40 LHM. The CFV of 0.1 m/s was chosen as this velocity led to the highest modification effect.

Modification at higher filtration rates

In this section two modification experiments (membrane I and II) were performed at a flux of 40 LHM and a CFV of 0.1 m/s. Due to the higher flux, the recovery (ratio of permeate flow to feed flow) increased to 31 % since the CFV remained constant. The FRR values, resistances, zeta potentials and modification degrees of membrane I are shown in Figure 98 (a) – (d)

compared to the membrane modified at a flux of 26 LHM and a CFV of 0.1 m/s. Membrane II was used for the subsequent fouling tests.

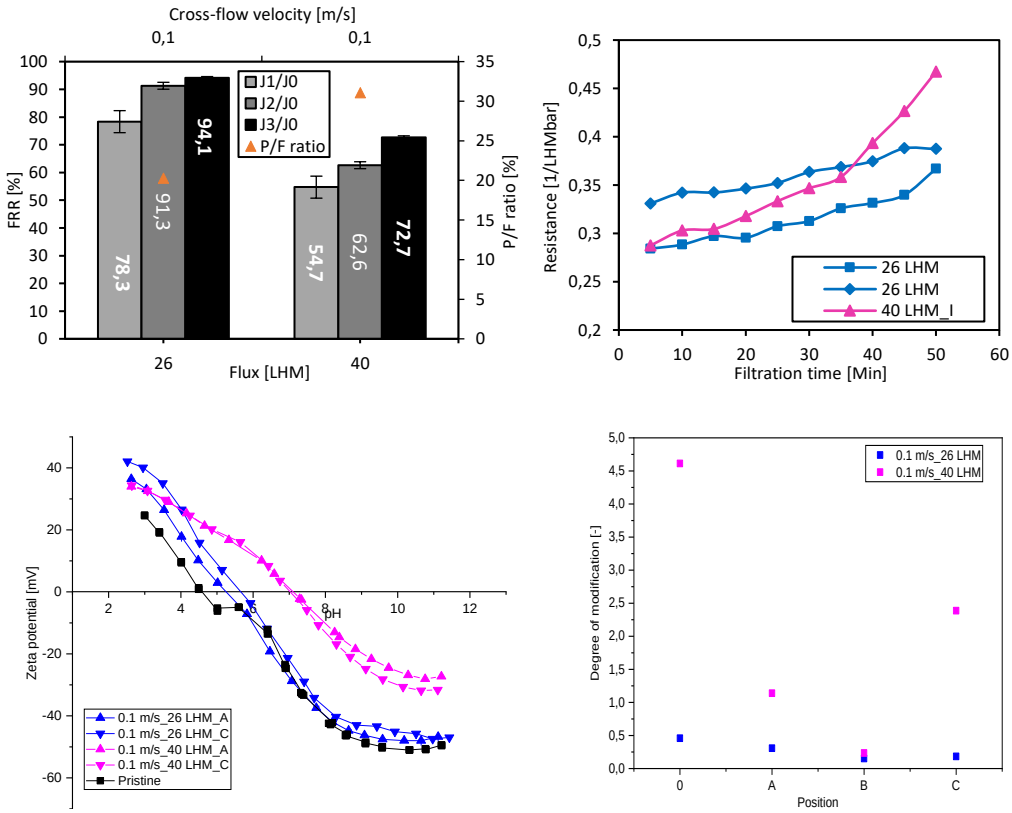

Figure 98: Cross-flow modification (0.06 wt%, pH 9, acrylate/cross-linker ratio 1:1, 50 min, 40 LHM, 0.1 m/s): **(a)** FRR values, **(b)** resistance during modification, **(c)** zeta potential and **(d)** modification degree in comparison to the membrane modified at 26 LHM.

From the FRR values in (a), it is quite obvious that increasing the flux to 40 LHM leads to a significantly higher flux loss. In contrast to the modification at 26 LHM, which has lost only about 6 % of its initial flux after washing with NaCl (FRR of 94.1 %), the flux loss for the modification at 40 LHM is a remarkably high and equals 27 % (FRR of 72.7 %). The resistance during the modification also increases more steeply from 30 min (cf. Figure 98 (b)). Furthermore, the zeta potential measurements in (c) show a distinct shift of the isoelectric point from the acidic to the neutral or slightly basic pH range, independent of the position, compared to the unmodified and modified membrane at 26 LHM. It is the largest shift obtained so far (from 4.5 to 7.1). This strong shift points to a very pronounced hydrogel coating on the membrane surface.

Also, the modification degrees in (d) are altogether higher than the DG obtained for the 26 LHM measurement. However, the DG does not seem to follow a clear location dependency. At position 0 the highest DG of 4.5 is measured. The DG decreases then to the positions A and

B and increases again to position C, so that a DG of 2.5 is measured at C. The fact that the DG is extraordinarily high at position 0 is due to the already mentioned different boundary layer conditions at this position, caused by the geometry of the flow channel (cf. Figure 93). However, the trend from A to C contradicts the trend of the modification degrees obtained for the 26 LHM modification. Since the flux of 40 LHM is much higher, the loss of solvent through the membrane is much greater. That means that the feed solution concentrates more strongly and progressively along the membrane channel (from A to C), so that the accumulation is greatest at position C and the hydrogel formation is much more pronounced. Thus, in this case, the concentration effect is predominant. The effect of decreasing CFV can be applied here as the CFV decreases more strongly along the membrane length because of the higher flux (40 vs. 26 LHM) and the associated smaller ratio of retentate to permeate. Consequently, the CP is highest at position C, resulting in a higher DG.

The obtained SEM images (cf. Figure 99) correlate strongly with the DG. The image of position A shows an inhomogeneous spot-like hydrogel layer and that of position C a comparably distinct and homogeneous hydrogel layer. This supports the hypothesis that the hydrogel layer has formed most densely at position C due to the increasing concentration of reaction solution along the membrane length.

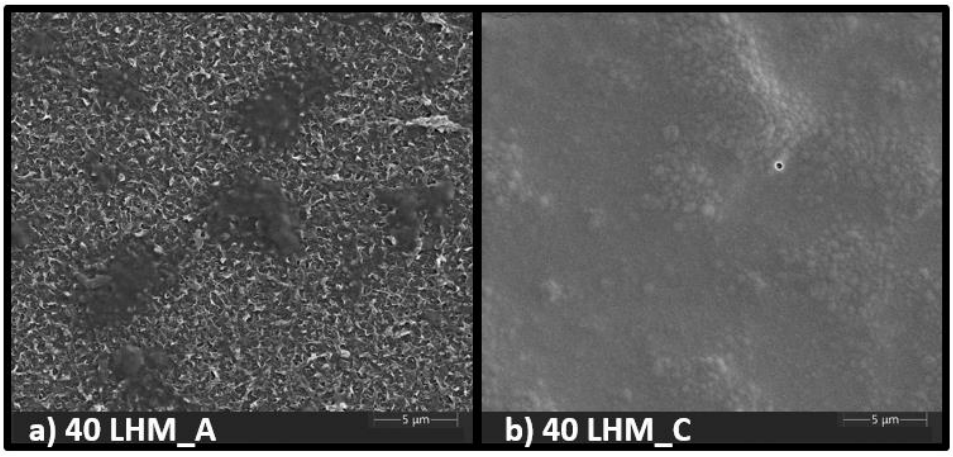

Figure 99: SEM images of membrane I modified at 40 LHM a) position A and b) position C.

Since membrane I and II were modified under the same conditions, it can be expected that the same modification effects (degree of modification, zeta potential and topography) were achieved for membrane II. The flux loss for membrane II is slightly higher in contrast to membrane I (32 % vs. 27 %). Also, the resistance during the modification increased much stronger and almost exponentially compared to membrane I, cf. Figure 100.

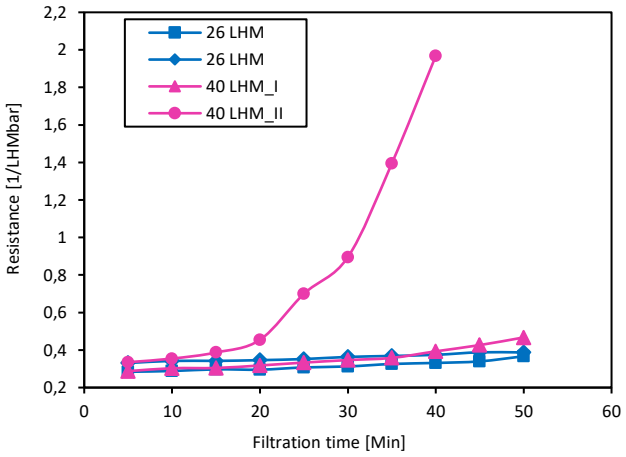

Figure 100: Resistance during modification for membrane II modified at 40 LHM and 0.1 m/s in comparison to membrane I modified at 40 LHM and 0.1 m/s and the membrane modified at 26 LHM and 0.1 m/s.

As shown, the resistance of membrane II increases exponentially during the modification. After 30 min it was not possible to keep the flux constant by increasing the transmembrane pressure. To ensure that the operating parameters of the plant were not exceeded, the modification was stopped after only 40 minutes. The resistance after washing with NaCl was approx. 0.38 $LHMbar^{-1}$, while the resistance of membrane I was approx. 0.35 $LHMbar^{-1}$. Since a thicker hydrogel coating correlates with a higher membrane resistance, it can thus be concluded that a substantially thicker hydrogel layer has been formed on membrane II, covering the PA more homogeneously.

In total, it was possible to form a distinct hydrogel layer on the membrane surface by increasing the flux, even though a spacer was used. Similar to the dead-end experiments, it could be demonstrated that the crosslinking reaction is mainly controlled by the flux, since the flux is the determining factor for whether a sufficiently high CP is formed to exceed the critical concentration required for gelation. While the formation of the hydrogel layer was not yet homogeneous over the entire membrane surface, the charge neutrality, which is crucial for the antifouling properties of the membrane, could be significantly enhanced. Therefore, in the next chapter the antifouling properties of both, thin and thick coated membranes are investigated.

5.7.3 Anti-fouling properties of hydrogel-coated membranes

In this chapter the antifouling properties of the previously modified membranes (26 and 40 LHM) are shown. As the results of the antifouling tests with the dodecane/water emulsion (chapter 5.5.4) could not be reproduced at higher oil concentrations, a new test system consisting of a crude oil emulsion was chosen for these tests. This emulsion was dispersed at 1500 bar using a high-pressure homogenizer. The average oil droplet size was 0.45 µm and was controlled by laser diffraction particle size analysis. As the diameter of the droplets remained stable over 5 days, the feed could be used within this period. By this, stable and reproducible emulsions could be generated in large quantities, so that several tests could be carried out with the same batch.

Membranes modified at 26 LHM

The antifouling properties of the membranes, which were modified at a flux of 26 LHM and the CFVs of 0.1, 0.19 and 0.25 m/s, were first investigated in dead-end. Two samples were cut out of the flat-sheet membranes for the dead-end batch cell. The assignment 0–A and B–C refers to the area from which the samples were cut (cf. Figure 93). The carbon concentration of the crude oil emulsion was 321 mg/L (unmodified, 0.1 m/s_A–B and 0.19 m/s_A–B) and 846 mg/L (remaining experiments). The filtrations were operated at a constant pressure of 10 bar up to a recovery of 30 % and the stirring speed was 0.24 m/s. The course of permeance and FRR values are shown in Figure 101 (a) and (b), respectively.

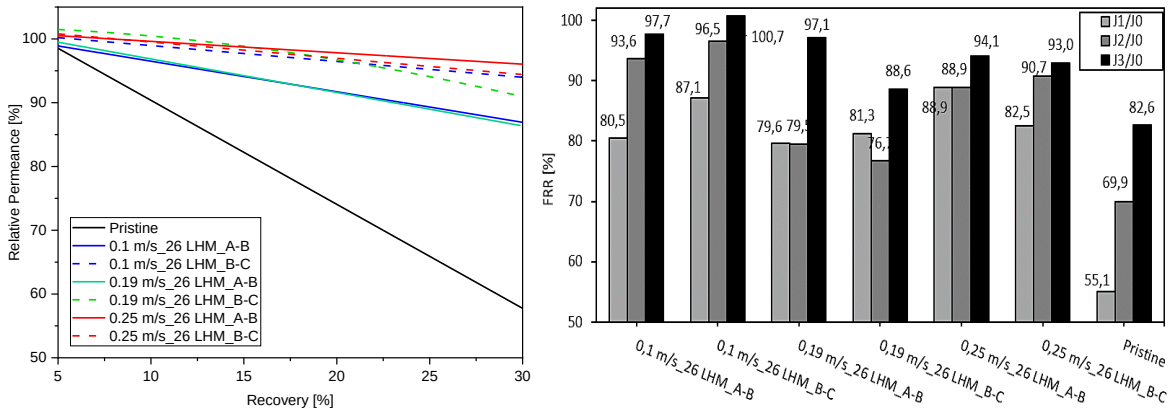

Figure 101: (a) Relative permeance and **(b)** FRR values of modified membranes (0.06 wt%, pH 9, acrylate/cross-linker ratio 1:1, 50 min, 26 LHM (CFVs of 0.1, 0.19 and 0.25 m/s)) during dead-end fouling with crude oil at 300 rpm (0.24 m/s) and 10 bar as a function of recovery.

The course of the permeance of the unmodified membrane (black) differs considerably from the one of the modified membranes (blue, green, red) by a much stronger and linear decrease.

In contrast, all modified membranes show a significantly lower decline, thus an almost constant course of permeance with increasing recovery. No distinct difference can be observed between the position at which the sample was cut out (A–B and B–C) and the selected CFV (0.1, 0.19 and 0.25 m/s), as no clear relationship can be discerned. Despite the lower crude oil concentration used (321 mg/L), the membranes at 0.1 m/s_A–B and 0.19 m/s_A–B show a slightly stronger decrease in permeance compared to the membranes operated at higher crude oil concentrations (846 mg/L). However, all modified membranes show almost constant courses that are very comparable.

In (b), the FRR values directly after oil fouling (J_1/J_0), after washing with water (J_2/J_0) and after subsequent cleaning with a 10 vol.% ethanol solution (J_3/J_0) are plotted for the different membranes. The FRR values (J_1/J_0) are in good agreement with the courses of the permeance decrease. The experiments at 0.1 m/s_A–B and 0.19 m/s_A–B show the lowest FRR values and simultaneously the highest drop in permeance. In addition, the membranes with the smallest decrease in permeance (0.25 m/s_A–B and B–C as well as 0.1 m/s_B–C) show the highest FRR values directly after oil fouling.

It is also interesting that the membranes at 0.1 m/s show the highest increase in FRR values after washing with water. Similarly, the flux of these two membranes recovers most strongly after washing with 10 vol.% ethanol solution. Thus, the major part of the crude oil emulsion could be successfully removed. One reason is that the adsorption of the oil film on the modified membrane is entropically unfavorable. Furthermore, there are no adhesion forces since the hydration shell of the zwitterionic polymer prevents virtually any interaction with the hydrophobic oil layer. As a result, this layer can be largely washed off with water only. As the FRR values of the membranes at 0.19 m/s_A–B and B–C and 0.25 m/s_A–B deteriorate to some extent after washing with water, it indicates that an oil film might have been deposited directly onto the membrane surface. Therefore, the coated membranes at 0.1 m/s provide the best antifouling behaviour compared to the coated membranes at 0.19 and 0.25 m/s.

However, the FRR values of all coated membranes recover far better after cleaning with 10 vol.% ethanol solution than the FRR value of the unmodified membrane. This points to a superior antifouling behaviour of all modified membranes compared to the unmodified membrane. Thus, it is remarkable that these membranes modified in cross-flow show an

improved antifouling behaviour towards crude oil emulsion despite the very thin hydrogel layer.

For all modified membranes, a trade-off > 75 % can be calculated immediately after fouling. According to this, the total loss of flux is < 25 % and that of the unmodified membrane > 44 %. Thus, the former flux reduction induced by the coating can be unequivocally compensated through the improved fouling resistance. Cleaning cycles can thus be shortened, and the cleaning effort becomes smaller. Even after washing with the ethanol solution the trade-off is >> 83 % compared to the unmodified membrane with 82.6 %. Thus, the coating leads overall to a total profit of permeance.

The antifouling properties of the membranes, which were modified under the conditions mentioned above (flux of 26 LHM and CFV of 0.1, 0.19 and 0.25 m/s), were also investigated in cross-flow. The carbon concentration of the emulsion was 265 mg/L (membrane at 0.1 m/s), 305 mg/L (membranes at 0.19 and 0.25 m/s) and 33 mg/L (unmodified membrane). The tests were performed at a constant pressure of 10 bar and a CFV of 0.28 m/s. The filtration time took 24 h in order to meet real conditions of a continuously operated plant. The permeance course and the FRR values are shown in Figure 102 (a) and (b).

Analogous to the dead-end experiments, an almost constant course can be observed for the modified membranes, cf. Figure 102 (a). In contrast, the permeance for the unmodified membrane decreases linearly. The modified membranes have FRR values of around 97.8 % immediately after fouling, whereas the unmodified membrane has an FRR value of only 91.9 %. In addition, only pure water is sufficient to recover the permeance of the modified membranes almost completely (FRR > 99 %). For the unmodified membrane, the permeance is recovered only up to 96.3 %. It is also striking that in dead-end the decrease in permeance during fouling and the overall flux loss after fouling is greater than in cross-flow. This is due to the greater concentration of feed solution and the associated more severe filtration conditions in dead-end as the feed flows perpendicular to the membrane surface while the oil emulsion accumulates on the membrane surface. In cross-flow, the feedwater flows tangentially to the membrane surface and carries the oil away so that the permeate flux does not drop as fast as in dead-end. By calculating the trade-off for the modified membranes at 0.1, 0.19 and 0.25 m/s after washing with the ethanol solution, values of 93.3, 94.7 and 96.5 % are obtained, respectively. The initial flux reduction could thus be compensated here, as well.

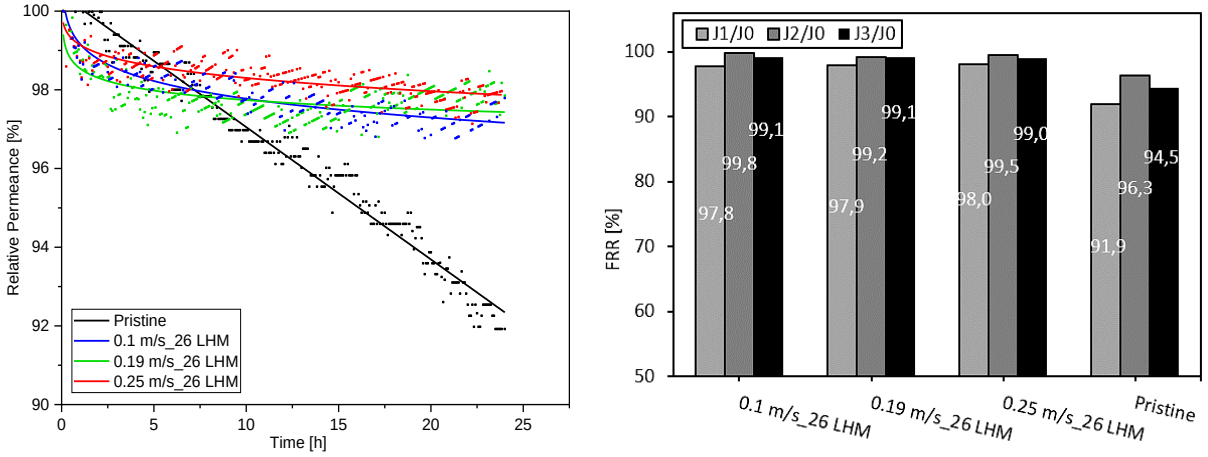

Figure 102: (a) Relative permeance and **(b)** FRR values of modified membranes (0.06 wt%, pH 9, acrylate/cross-linker ratio 1:1, 50 min, 26 LHM (CFVs of 0.1, 0.19 and 0.25 m/s)) during cross-flow fouling with crude oil at 0.28 m/s and 10 bar for 24 h as a function of filtration time.

According to these results, the modified membranes exhibit excellent antifouling properties despite the very thin hydrogel coating. Thus, it could be demonstrated that thin-coated membranes can achieve a significant improvement over oil fouling.

Membranes modified at 40 LHM

The antifouling properties of the membrane, which was modified at a flux of 40 LHM and a CFV of 0.1 m/s, were also investigated in cross-flow. The carbon concentration for the modified membrane was 33 mg/L. The experiments were performed at a constant pressure of 10 bar and a CFV of 0.27 m/s. The permeance curve and the FRR values are shown in Figure 103 (a) and (b).

For the unmodified membrane in black, a steady linear decrease over time can be observed, as described above. For the modified membrane at 40 LHM (magenta), a stronger decrease in permeance is initially obtained. Also here, emulsified oil droplets deposit on the membrane surface. With prolonged filtration time, more and more oil droplets accumulate on the membrane surface, leading to the formation of a cake layer. Since oil droplets are deformable, the resultant cake layer is densely packed and shows high resistance to water permeation. The oil droplets in the cake layer are thermodynamically unstable and tend to coalesce which leads to formation of larger oil droplets and a contiguous oil film. This film may experience a wetting transition on the membrane.[188] The additional resistance compacts and thus compresses the existing hydrogel layer, which acts as a hydrogel “pad”. Due to the very thick layer (cf. results in 5.7.2), the compression of the hydrogel is particularly pronounced.

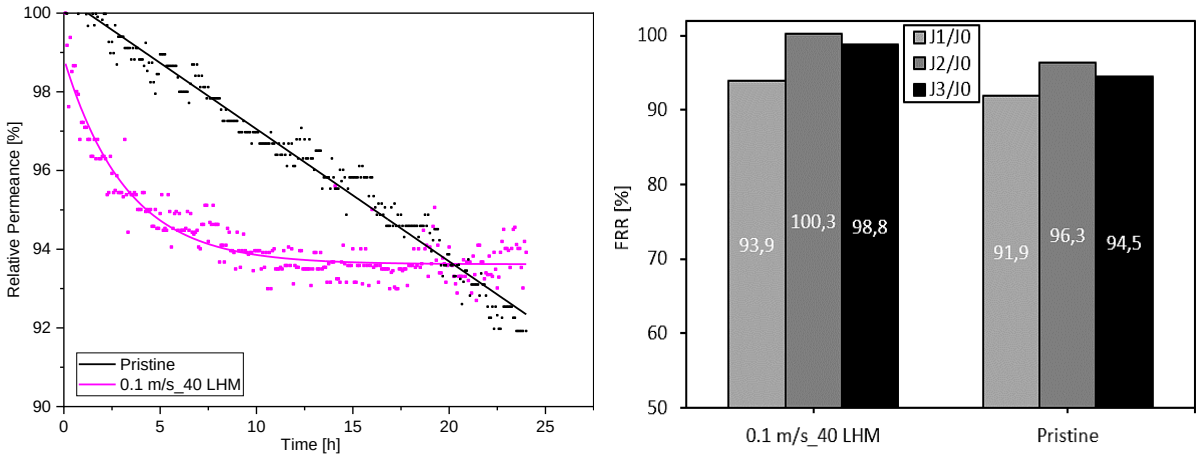

Figure 103: (a) Relative permeance and **(b)** FRR values of modified membranes (0.06 wt%, pH 9, acrylate/cross-linker ratio 1:1, 50 min, 40 LHM, 0.1 m/s) during cross-flow fouling with crude oil at 0.27 m/s and 10 bar for 24 h as a function of filtration time.

This compression is also apparent in the initial stage for the other membranes modified at 26 LHM (cf. Figure 102 (a)). However, due to the very thin layer, this compression, which is a kind of conditioning, is very low and thus minor. As a consequence, for the modified membrane at 40 LHM no further decrease but rather a constant course can be recorded from a filtration time of approx. 10 h, and after approx. 20 h the curves of the modified and unmodified membrane intersect. It can be assumed that the antifouling behaviour of the modified membrane will become even more apparent at longer test periods.

The FRR values after fouling of the unmodified and modified membrane at 40 LHM shown in Figure 103 (b) do not reveal significant differences (93.9 vs. 91.9 %). This is not surprising, since the values for the relative permeance after 24 h in (a) are in a comparable range for both membranes. However, the oil layer formed on the modified membrane surface could be completely removed by washing with pure water (FRR of 100 %), which was only partially successful for the unmodified membrane (FRR of 96 %). Again, this can be explained by the entropically unfavourable compression of the hydrogel layer, as well as the weak interaction between oil and hydration shell so that the oil film can be removed more easily.

Nevertheless, the trade-off for this modified membrane is only 72 % after washing with the ethanol solution. The FRR value for the modified membrane is 94.5 %. Consequently, the coating could not compensate its permeance reduction of 30 % by an enhanced antifouling behaviour. At this point, it should be emphasized that the exact benefit of the coating depends primarily on the time the membrane has to remain in operation and how much fouling should be prevented. The higher the load, the greater the added value of the coating. Thus, a process

can adapt to a membrane that has a lower initial permeance due to the coating but a more stable flux during the operation because of enhanced antifouling.

5.7.4 Stability test of modification solution

It was also of interest to investigate the long-term stability of the modification solution. For this purpose, a solution was prepared (polymer concentration 0.06 wt%, pH 9, acrylate/crosslinker ratio 1:1), agitated thoroughly and then left in a glass bottle for 25 days at room temperature without stirring. This solution was then used for modification after adding new DTT, as the half-life of DTT is only 1.4 h at a pH of 8.5 and a temperature of 20 °C. This was to determine whether the reactive system is also stable after a longer period of time and whether membranes could still be modified with the solution successfully.

After 25 days, no turbidity could be detected, which was actually typical for the modification solutions being used. However, a few apparent flakes were formed in the reaction solution during this time. These flakes could be related to a base-catalyzed cross-linking during this time, but the polymer concentration might not be high enough for larger particles to form a network of larger particles, which would have led to cloudiness of the solution. Also, the DTT was likely oxidized and intramolecular disulfide bridges were formed, so that further crosslinking could not take place at all.

The FRR values and modification degrees of the membranes modified with a "fresh" and "old" solution (membrane 1 and 2) are shown in Figure 104 (a) and (b). Both modifications were performed at a CFV of 0.1 m/s and a flux of 26 LHM. These conditions were chosen intentionally, as they result in a thin hydrogel layer on the surface and thus differences can be detected more differentiated.

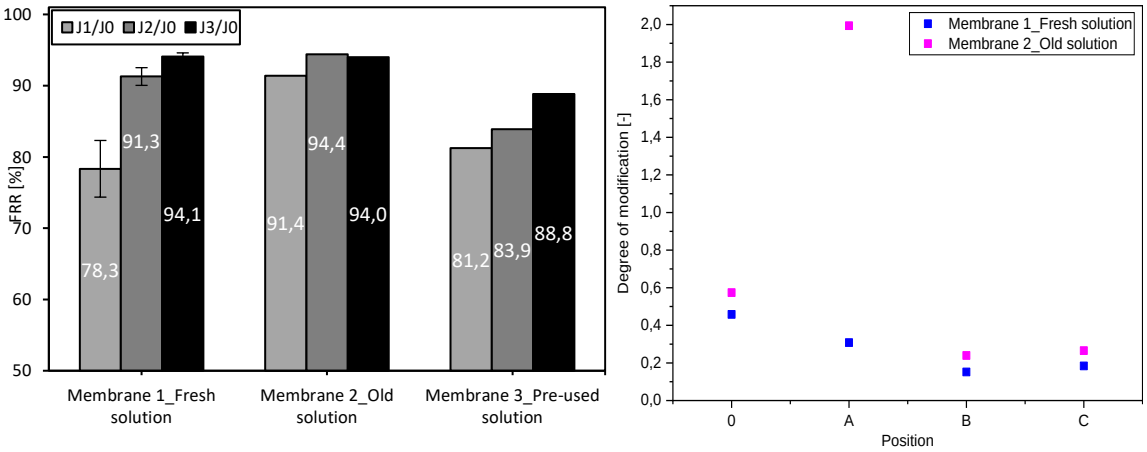

Figure 104: (a) FRR values of membranes modified with a fresh, old and pre-used modification solution (26 LHM, 0.1 m/s) and **(b)** corresponding modification degree in dependence of the location.

From (a), it is clear that the FRR values after washing with NaCl are equal for both membranes (membrane 1 and 2) modified with a fresh and old solution, respectively (94 %). From (b) it can be concluded that the modification degrees for membrane 2 are only slightly higher compared to membrane 1. Only position A is outstanding with a DG of 2. The SEM pictures in Figure 105 also show a relatively dense and homogeneous hydrogel layer at position A, which becomes thinner and more heterogeneous over the membrane length (position C). This therefore is in accordance with the measured modification degrees. Thus, in contrast to membrane 1, an even more pronounced hydrogel layer could be obtained at the same low flux loss. The few particles pre-formed in the modification solution could be the reason why the coating is much more pronounced at position A. During the modification, the particles have cross-linked most likely with the new DTT to form a denser hydrogel network on the membrane surface due to the concentration of reaction solution that occurred, so that a thicker and homogeneous layer could be formed at position A.

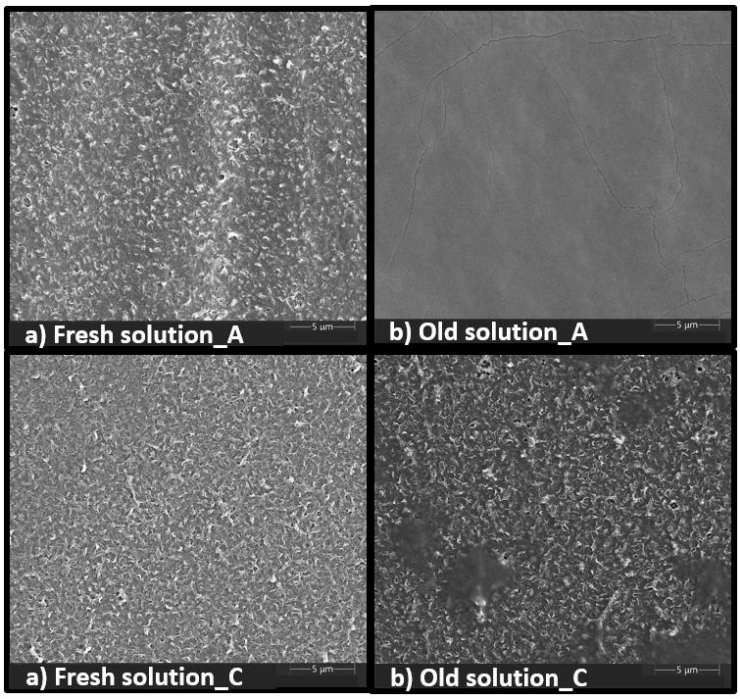

Figure 105: SEM images of membranes modified at 26 LHM and 0.1 m/s with a) a fresh modification solution at position A and C and b) old modification solution at position A and C.

Overall, this experiment shows that the reaction solution is stable for at least several weeks and that a comparable result can be achieved with re-added DTT as with a freshly prepared solution that is used immediately. This becomes clear from the FRR values, modification degrees and SEM images of the membrane, which demonstrate even stronger coated areas.

A modification was also done with an already used modification solution, after it was filtered through several blue band filters of a pore size of 2 µm due to the turbidity caused by the first modification (cf. Figure 104, membrane 3). However, the turbidity could not be removed by simple filtration through blue band filter. The solution was readjusted to pH 9 and new DTT was added. In this experiment a slightly lower FRR value of 88 % was obtained (Figure 104 (a)). During the second modification, the partially crosslinked polymer chains remaining in the solution, which are responsible for the turbidity, further cross-linked with the new DTT, forming an even denser network, similar to the modification with the "old" solution, so that the flux loss was even higher. Modification degrees of 0.3 – 0.8 were achieved (cf. Figure 104 (b)). These somewhat higher but still low DG indicate that the existing layer may have been merely filled with polymer mass. Thus, the hydrogel layer was most likely densified, whereby the membrane resistance increased (higher flux loss), without further cross-linking. On the whole, it was demonstrated that during the modification only a small fraction of the polymer

reacts to form the hydrogel and that the polymer concentration is subsequently high enough to reuse the modification solution multiple times.

5.7.5 Interim conclusions

From the modification of flat-sheet membranes in cross-flow the following conclusions can be made:

1. Dead-end conditions were chosen for the transfer of the modification to cross-flow, which led to a distinct hydrogel layer on the membrane surface (average polymer concentration of 0.0681 wt%, pH value of 9, acrylate/crosslinker ratio of 1:1, average flux of 26 LHM, maximum filtered mass of 13.56 g/m^2).
2. The CFV has a clear influence on the CP and thus on the hydrogel formation. At a lower CFV, hydrogel formation is much more likely to occur since the laminar boundary layer in which the CP is formed is thicker and the critical concentration of the reactive system is more likely to be exceeded.
3. The conditions that led to a distinct and thick hydrogel layer on the surface in the dead-end tests could not be transferred to the cross-flow experiments. The critical concentration was not exceeded so that only thin and heterogeneous hydrogel layers were formed (3 – 6 % flux loss, average DG of 0.14 and average ΔIEP of 0.86). The failed transfer of the modification conditions can be attributed to the substantially changed boundary layer conditions near the membrane surface caused by the spacer.
4. By increasing the flux from 26 to 40 LHM and maintaining the spacer, the critical concentration of the reaction solution could be exceeded by increasing the CP, so that a clearly pronounced hydrogel layer could be formed on the membrane surface (27 % flux loss, average DG of 2.1 and average ΔIEP of 2.6). Even if the formation of the hydrogel layer was not homogeneously formed over the entire membrane area, the charge neutrality could be improved significantly.
5. The membranes modified at 26 LHM have both, in dead-end and in cross-flow despite the thin hydrogel layer compared to the unmodified membrane, a superior antifouling behaviour towards an oil/water emulsion. In case of the membrane modified at 40 LHM, compression/compaction effects initially occur due to the thick hydrogel layer, which caused the flux to decrease significantly in the initial phase and show therefore a constant and stable flux from 10 h onwards.

6. With a modification solution that has been in storage for several weeks, a comparable modification effect can be achieved as with a freshly prepared solution that is used immediately. This demonstrates the stability of the reaction solution over several weeks. Furthermore, the reusability of the modification solution could be demonstrated after it had been previously used for a modification.

5.8 Stability test of hydrogel-coated membranes under cleaning conditions

In membrane processes, frequent chemical cleaning is needed due to occurring (irreversible) fouling.[100] Therefore, it is important to investigate the stability of hydrogel-coated membranes against common cleaning agents because correct performance of coated membranes requires their appropriate stability under the pertinent conditions. In this way, cleaning conditions can be adapted to the coating properties. Based on this, a method for regeneration of the hydrogel coating by a more harsh cleaning and reapplication can be developed and established after losing its antifouling effect.

Le *et al.* already investigated the stability of polysulfobetaine hydrogels synthesized by the formation of a C-C bond under acidic (pH 2) and basic (pH 12) cleaning conditions which was evaluated through membrane water flux changes and evaluation of antifouling performances.[201] It was found that the flux changes of the pristine and polyzwitterion grafted membranes are identical which may suggest that the polyzwitterion layer is stable under the investigated acidic and basic conditions. However, the polyzwitterionic hydrogel investigated in this work was prepared by the reaction of a zwitterionic copolymer and a thiol crosslinker (linkage of a C–S bond). This difference can affect the stability of the hydrogel significantly. For this reason, the stability of the hydrogel coated membranes developed here was investigated against basic, acidic and enzymatic cleaning solutions. For this, thin and thick coated membranes with modification degrees < 1 and > 2, respectively, were exposed to the cleaning procedure of DOW Filmtec for BW30 membranes and evaluated by flux changes, chemical structure via ATR-FTIR and TOC measurements to analyze removed organic matter.

5.8.1 Basic and acid cleaning

In case, the coating is not stable against the cleaning agent used, it can be assumed that the coating will be removed gradually. This would also cause the permeance to increase steadily until it reaches its initial value again once the coating has been removed completely. Since the permeance of individual membranes differs from each other, a relative value was calculated from the absolute values, which is referred to as recovery of permeance and primarily estimates the removal of the coating. This is calculated as follows:

$$Recovery\ of\ permeance\ [\%] = \left(\frac{P_{cleaning} - P_{modification}}{P_{compaction} - P_{modification}}\right) \cdot 100 \qquad (52)$$

Figure 106 (a) shows the time-resolved recovery of permeance for the basic (blue) and acidic (red) cleaning for membranes with a low modification degree (< 1). In (b), the overall course (state after compaction, modification and cleaning) of permeance is shown.

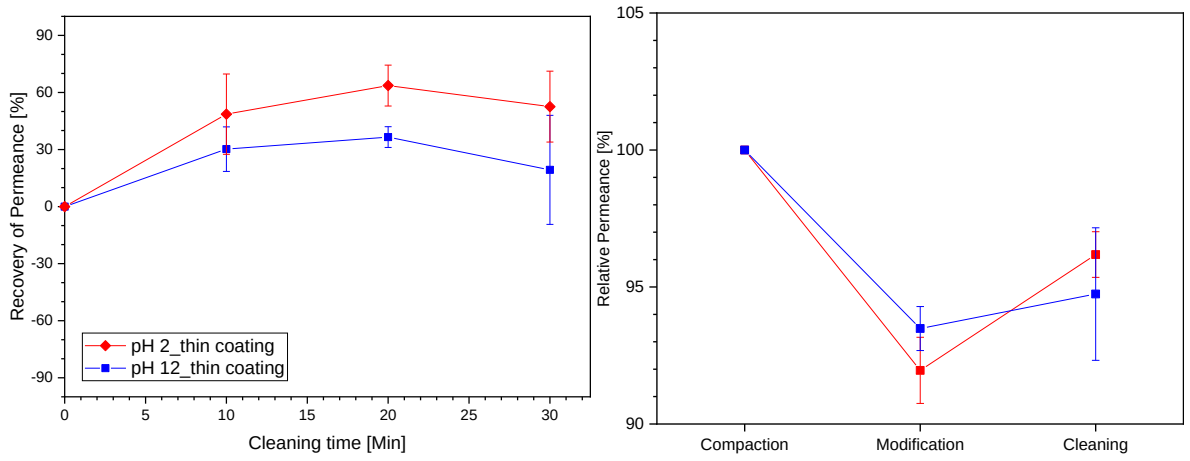

Figure 106: (a) Recovery of permeance of thin-coated membrane after basic cleaning at pH 12 (blue) and acidic cleaning at pH 2 (red). **(b)** Relative permeance of membrane after compaction, modification and cleaning.

Basic cleaning leads to a non-linear increase in permeance (cf. (a)), which is an evidence of the detachment of the hydrogel layer from the surface. However, the initial permeance is not yet recovered after 30 min (cf. (b), so that parts of the coating have certainly remained on the membrane. Looking at the results of the acidic cleaning in (a), a recovery of the permeance can also be observed after the cleaning. Analogous to the basic cleaning, it can be found that the permeance increases most in the first cleaning interval after 10 min, while the increase is significantly lower in the second cleaning interval after 20 min and the permeance in the third is only slightly higher than the value after the first cleaning after 10 min. The overall course of

permeance in (b) is also comparable to that of the basic cleaning. The original permeance is not recovered here either.

It is also noticeable that in (a), the standard deviation after the third cleaning interval is in both cases (basic and acidic cleaning) such that the second measurement is almost completely lost in it. As a reduction in permeance is not supposed to occur in the third cleaning interval, it is most probable that the real curves follow a saturation curve. Thus, it is expected that the removal of the hydrogel is completed after 30 min. The recovery of permeance relative to the state of the modification amounts 94.7 ± 2.4 % for the basic cleaning and equals 96.2 ± 0.8 % for the acidic cleaning. Therefore, it can be concluded that only one part of the hydrogel layer has been removed and thus a presumably large proportion is still present on the membrane. Accordingly, the hydrogel is not completely removed.

ATR-FTIR spectra were also measured after each cleaning interval. Again, the bands of the carbonyl and sulfonic acid groups were used as indicator for the presence of the hydrogel. The modification degree of the membrane was derived from the IR data, as explained in chapter 5.5.3. The calculated degrees are shown in Figure 107.

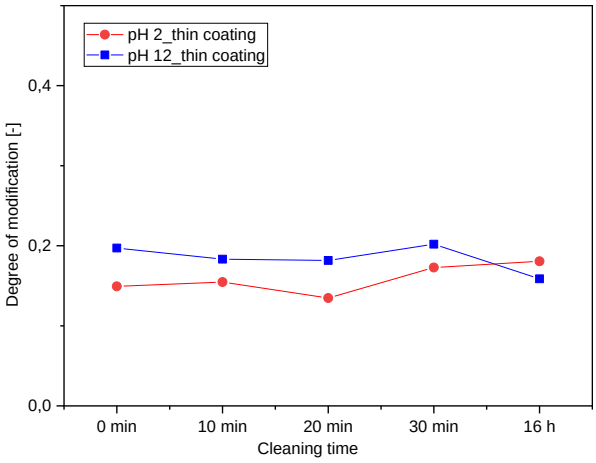

Figure 107: Modification degree of thin-coated membrane after basic cleaning at pH 12 (blue) and acidic cleaning at pH 2 (red) for the different time intervals.

At first, it can be observed that the modification degrees for the basic and acidic cleaning fluctuate over the entire cleaning time and do not show a linear decrease. However, for the basic cleaning (blue), an overall decreasing trend can be observed. After 16 h, the DG has dropped to its minimum, but not to zero. This observation would be consistent with the permeance behaviour already discussed, that basic cleaning leads to the removal of the hydrogel. Therefore, it must be critically emphasized that, due to the uneven removal of the

hydrogel, the modification degree varies significantly within a small surface area. A reproducibility test revealed that a deviation of more than 45 % occurred when the measuring points on the membrane were only 2 cm apart. Even if this deviation is an extreme value, it should become clear that a comparison of the modification degrees calculated in this way is only reasonable in case of large differences. These variations in the DG are more apparent for the acidic cleaning (red). Here, the modification degree initially decreases after 20 min and increases again after 16 h, which seems to be illogical and inconsistent when considering the flux data.

In addition, the carbon concentration of the cleaning solutions after cleaning the coated membranes was measured by means of TOC analysis. In this way, the removal of the coating by the respective cleaning process can be quantified via a mass balance according to formula (53).

$$m_{Polymer\ loss} = c_{cleaning\ solution} \cdot V_{cleaning\ solution} \qquad (53)$$

Moreover, the maximum filtered mass of the polymer during modification was determined. This was calculated from the average value of the feed and retentate concentration obtained from TOC measurement and from the filtered permeate volume according to formula (54):

$$m_{Maximum\ filtered\ mass} = (c_{Feed} + c_{Retentate}) \cdot 0.5 \cdot V_{Permeate} \qquad (54)$$

In both cases, it must be considered that the TOC analysis only measures the carbon concentration. However, the concentration of the removed hydrogel is proportional to it. From the known prepared feed concentration (copolymer and crosslinker) and the carbon concentration in the feed measured via TOC, a proportionality factor could be calculated, which was multiplied with the specific carbon concentration. Thus, the mass of the removed hydrogel and the maximum filtered mass of polymer could be calculated approximately.

Table 16: Filtered polymer mass of thin-coated membrane and polymer mass washed off after basic cleaning and acidic cleaning for the different time intervals.

Condition	Filtered polymer mass [g/m²]	Polymer mass washed off [g/m²] after 10 min	Polymer mass washed off [g/m²] after 20 min	Polymer mass washed off [g/m²] after 30 min
Basic cleaning	**19.14**	0.659	0.451	0.266
Acid cleaning	**22.68**	0.304	0.143	0.094

The calculated values for the basic and acidic cleaning are listed in Table 16. The removed masses of hydrogel are only a fraction of the filtered polymer mass, indicating that the coating removal seems to be minor. Also, it can be noted that the amount of mass removed decreases over time. These results are in accordance with the previous results of flux and IR data. Nevertheless, due to the insufficient accuracy and thus reliability of the TOC analysis at very low concentrations (such as those presented here), no reliable conclusions can be drawn regarding the absolute values.

Overall, it was found that both basic and acidic cleaning leads to an increase in permeance and thus to a partial removal of the hydrogel layer from the membrane. However, the differences measured via ATR-FTIR and TOC were relatively small, so that the exact degree of damage could not be determined exactly.

Therefore, the influence of acidic cleaning on coated membranes with a higher modification degree (> 2) was investigated in the further course. By a higher DG, the relation of the unavoidable fluctuation of the measured values to the size of them should be reduced, so that the differences would be more pronounced if the hydrogel is partially detached. Figure 108 (a) shows the course of the permeance of a thick coated membrane over six ten-minute cleaning intervals.

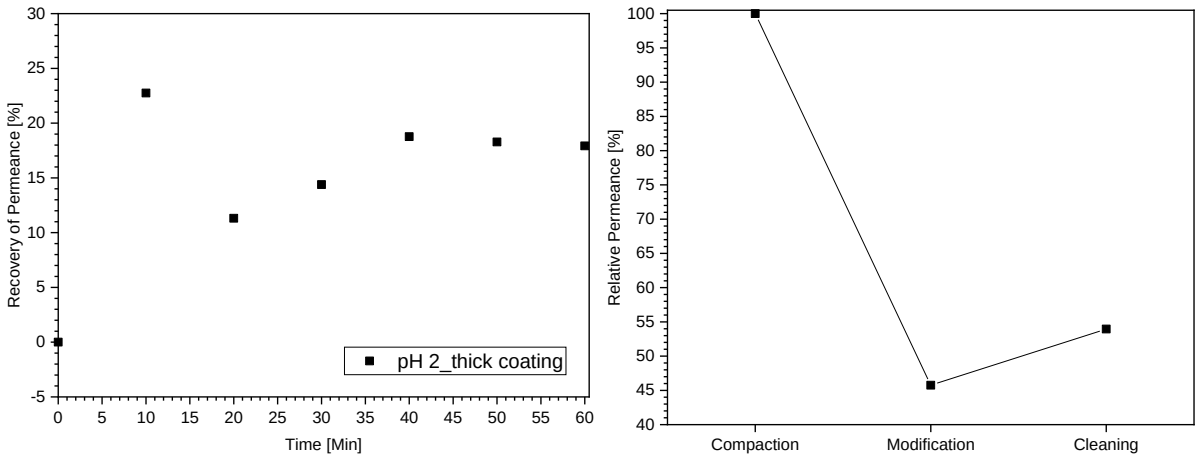

Figure 108: (a) Recovery of permeance of thick-coated membrane after acidic cleaning at pH 2. **(b)** Relative permeance of membrane after compaction, modification and acidic cleaning.

The first measured value after 10 min differs considerably from the others, which is probably due to a measurement error caused by the short measuring time for the permeance assessment. At the following measuring points, the threefold measurement duration was applied, which ensures a previous stabilization of the system. For the further course, it is

obvious that the increase in permeance is rapidly reduced after the first cleaning intervals (~ 30 min). This confirms the previous hypothesis that the removal of the hydrogel has no linear relationship to the cleaning time. Based on (b), it can be seen from the very high difference between the last cleaning interval and the state of compaction that at high modification degrees, the cleaning only damages and thus removes a relatively small portion of the hydrogel.

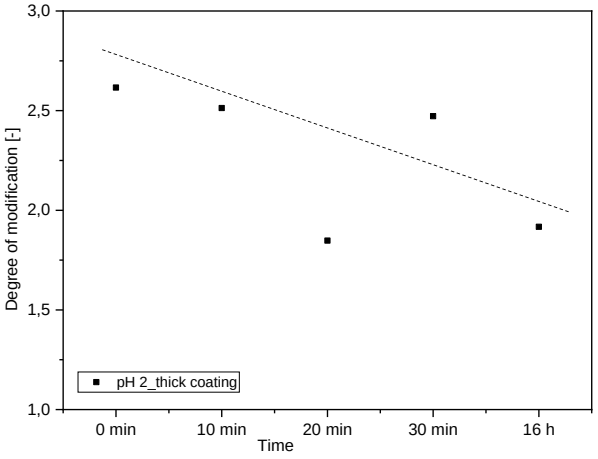

Figure 109: Modification degree of thick-coated membrane after acidic cleaning at pH 2 for the different time intervals.

It is also evident from the calculated modification degrees from Figure 109 that the damage caused by acid cleaning is not too heavy. The modification degree has decreased by less than 30 % after 16 h of cleaning time. However, a non-linear decrease can also be observed here, which can be likewise attributed to the fluctuating modification degrees depending on the examined membrane surface area. Regardless of the exact values, it can be clearly ascertained from the modification degrees that the coating is stable against acidic cleaning even over extended periods of time.

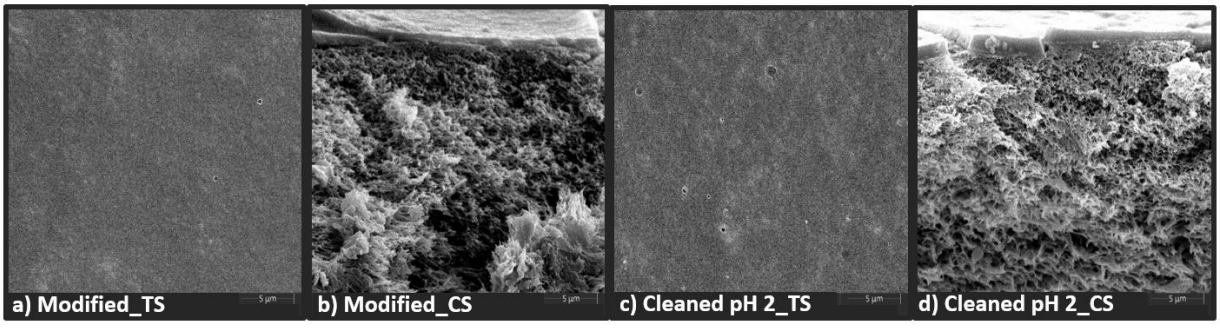

Figure 110: SEM images of thick-coated membrane a) before (top surface and cross-section) and b) after 16 h of acidic cleaning at pH 2 (top surface and cross-section).

Figure 110 also shows SEM images of the top surface (TS) and cross-section (CS) of the coated membrane before (a & b) and after 16 hours of acidic cleaning (c & d). From the smooth and homogeneous surface of the membrane in (c), it can be clearly seen that even after 16 h only minor damages to the coating has been caused. Unfortunately, the cross section of the coated membrane in (b) is only to limited extent suited for an exact comparison due to the unfavorable position, where the thickness of the coating does not seem to be homogeneous. But even from the cross-section in (d), a clearly defined layer can still be seen after cleaning.

In total, the investigation of the stability under acid and basic conditions showed that partial removal of the hydrogel occurs during both basic and acidic cleaning. However, from the investigation of membranes with a higher modification degree (DG > 2), it was found that the hydrogel was virtually stable so that acidic cleaning is generally feasible, which was confirmed by the flux behaviour, IR data and SEM images. The coating proved to be stable over several hours, so that an average cleaning time of 30 min would allow more than 30 cleaning cycles.

These findings are consistent with those found by Le *et al.*[201] Also, Schönemann *et al.*[202] demonstrated a particularly high hydrolysis stability of zwitterionic polymethacrylates upon extended storage (over one year) in aqueous acidic and basic solution. In general, this hydrolysis resistance was ascribed to steric effects. When attached to the polymer backbone, the carboxyl ester functions are effectively shielded against attack by water molecules due to the neighboring methyl groups in the backbone which create a highly crowded local environment. Also, the low polarity of this environment restrains protonation of the carboxyl ester groups, thus limiting acid catalysis and enhancing the stability.[202] Also, the backbone of the polymer is all-carbon so that the risk for backbone hydrolysis is additionally non-existent. The slight amount of removed hydrogel is therefore much more likely due to mechanically or physically bound components that are only loosely bound in the hydrogel network and can therefore be removed under acidic and basic cleaning conditions.

5.8.2 Enzymatic cleaning

In contrast to acidic and basic cleaning solutions, commercial enzymatic cleaners often consist of a variety of components that interact with the membrane as a complex system. However, the exact composition of the cleaning mixture is often not specified. It was therefore deemed reasonable to test the stability of the coating against such a complex mixture using a detergent

used in industry. For this purpose, the enzymatic cleaner MembraPas M 245 was purchased from Schlüsselburg Wasseraufbereitung. The known ingredients include the components subtilisin, benzene sulfonic acid and ethoxylated cocoamine. The manufacturer's recommendations envisaged a cleaning solution concentration of 400 g/L, but this proved to be impractically high in a first test run due to the poor solubility of the cleaning mixture. Various concentrations were therefore tested, of which the highest tested concentration was 300 g/L, which was relatively close to the manufacturer's recommendations.

Figure 111 (a) and (b) displays the time-resolved recovery of permeance including the standard deviation and the overall course of permeance. Interestingly, in contrast to the basic and acidic cleaning, a decrease in permeance is observed with the cleaning time. The decline in permeance resembles a limited reduction but cannot be clearly identified as such. Since the loss of permeance can only be attributed to the cleaning solution, a modification of the hydrogel must have been induced by it. A chemical reaction of components of the detergent would be possible, leading to a decomposition of the hydrogel. Subtilisin, as a component in the cleaner, is a serine protease which serves to decompose proteins on the membrane surface. As an enzyme, Subtilisin reacts very specifically, so that a reaction with the polymer can be virtually excluded. No such reaction can be expected from benzene sulfonic acid neither. Furthermore, an increase in permeance would have been measured if the hydrogel had been decomposed. According to this, an inclusion of certain components in the interstitial spaces of the swollen gel under displacement of the water present there is much more likely.

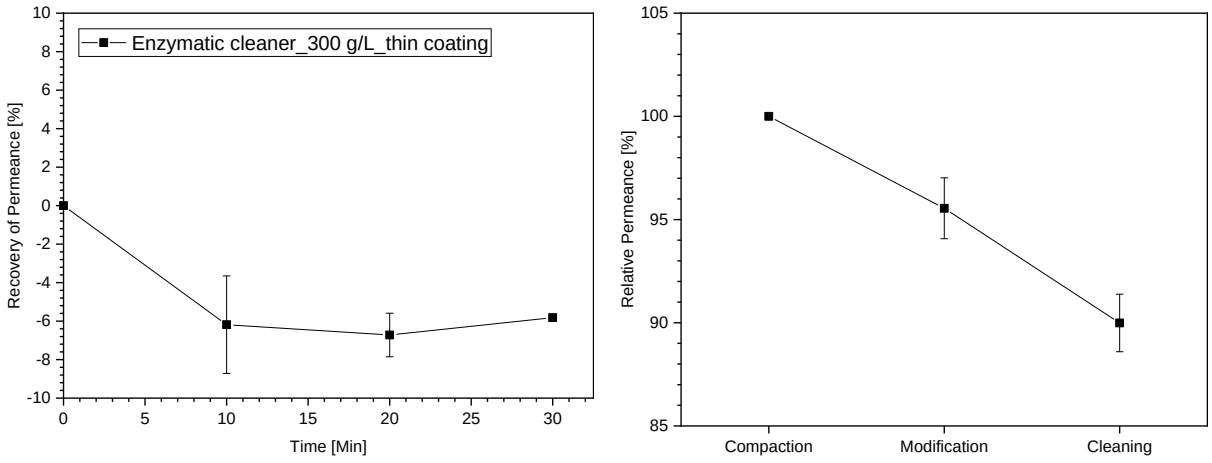

Figure 111: Recovery of permeance of thin-coated membrane after enzymatic cleaning (300 g/L). **(b)** Relative permeance of membrane after compaction, modification and cleaning.

For a more detailed examination, IR spectra were recorded and the modification degrees were calculated again, which are shown in Figure 112. It can be seen that the DG increases with increasing cleaning time. However, the increase in the modification degree cannot be interpreted as a real increase in the hydrogel content at the membrane surface. Since the intensity of the sulfonic acid band specific for the coating has increased significantly, an increase in the modification degree can also be detected. Consequently, the benzenesulfonic acid included in the detergent has most likely been incorporated into the hydrogel and caused an increase in the intensity of the sulfonic acid band.

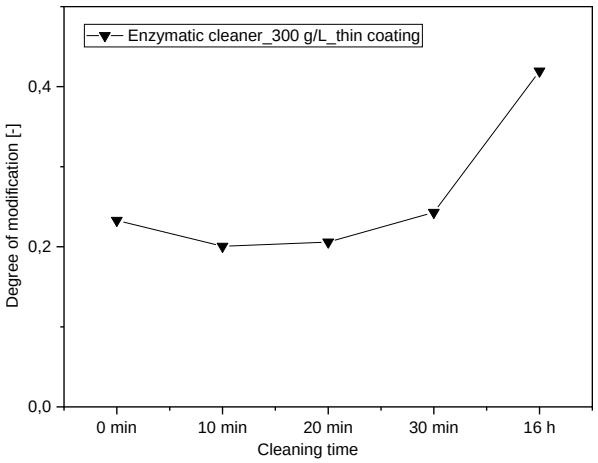

Figure 112: Modification degree of thin-coated membrane after enzymatic cleaning (300 g/L) for the different time intervals.

The results of the TOC measurements of the cleaning solutions used (cf. Table 17) are also relatively conform with this interpretation. Accordingly, a part of the mixture has indeed remained in the hydrogel structure, which is then absent in the cleaning solution and expressed in the negative difference. The value after 30 min can be regarded as an outlier, since the apparent modification degree in Figure 112 increased continuously indicating that the incorporation was not yet complete after 30 min. However, as with the basic and acidic cleaning, the TOC measurements must be considered as supporting data due to their insufficient accuracy at very low concentrations. In addition, in contrast to the other cleaning solutions, the mixture contains a carbon fraction that leads to an additional measurement inaccuracy, which is also included in the calculation.

Table 17: Polymer mass washed off after enzymatic cleaning (300 g/L) for the different time intervals.

Cleaning time [min]	Polymer mass washed off [g/m²]
10	- 0.204
20	- 0.256
30	- 0.053

Accordingly, the membrane must be subjected to extensive washing (e.g. pure water) after using the enzymatic cleaner in order to completely remove the embedded components. In this study, the membranes were only rinsed with pure water, which is not sufficient when considering the results. However, a removal or damage of the hydrogel by the detergent could not be determined.

5.8.3 Interim conclusions

In this chapter it could be found out that the coated membranes are virtually stable under the cleaning conditions of Dow Filmtec (pH 2 and 12, 40 °C, 30 min). For modified membranes with a modification degree > 2, an average cleaning time of 30 min would allow 30 cleaning cycles under acidic cleaning conditions. Apparently, enzymatic cleaning does not cause damages to the hydrogel at all.

5.9 Up-Scaling of in situ modification to commercial spiral-wound modules and pilot scale tests

The aim of this chapter is to modify spiral-wound modules in order to operate them in parallel to conventional modules in on-site trials in the project's pilot plant at DEW using real cooling water. The up-scaling was done in two steps. First a small TW30 2521 module was modified and then cut open and analyzed to evaluate the success of the coating. Subsequently, two large BW30 4040 modules were modified and then implemented in the project's pilot plant for on-site testing. After the field tests, the modules were autopsied by performing a coating and membrane analysis.

5.9.1 Modification parameters

It should be noted that the modification of the SWM was carried out prior to the modification of flat-sheet membranes in cross-flow from chapter 5.7. For this reason, the obtained filtration conditions from the cross-flow experiments, which led to pronounced and thick coatings, could not be applied. Instead, the parameters from the dead-end modification tests from chapter 5.5, which led to a thin coating with a low flux loss and good antifouling properties, served as basis for the transfer of the modification to these SWM.

As already described in chapter 5.7, for a successful transfer of the modification from dead-end to cross-flow, the reactive system, consisting of the composition of the solution (average polymer concentration, pH value and acrylate/crosslinker ratio), the flux and the filtered mass per area must be applied. The parameters from dead-end determined for the transfer are summarized in Table 18. Here too, the composition of solution can be transferred directly. The required permeate flow for the cross-flow experiments was calculated from the flux and active membrane area (equation (26)) while the minimum volume of modification solution was calculated from mass per area, polymer concentration and active membrane area (equation (32)).

Table 18: Derived parameters from dead-end for the transfer of the modification to SWMs in cross-flow.

Parameters from dead-end modification		
Average copolymer concentration C_{copo}	wt%	0.023
pH value	-	8
Acrylate/cross linker ratio	-	1:1
Average Flux J	LHM	21
Mass/area	g/m^2	4.8

Since the driving force for the filtration in the module depends on the cross-flow velocity and the ratio permeate flow to feed flow (P/F), to be explained further ahead, the flow dynamics are variable, changing differentially depending on time and location,[58] cf. Figure 113. The consequence is a pressure drop along the element length and inhomogeneous flow ratios leading to intensified irregular boundary conditions for the filtration.

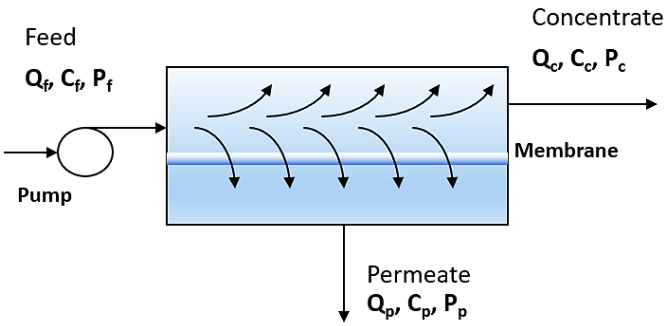

Figure 113: Schematic illustration of the flow dynamics in a SWM.

For the modification of SWM, it is therefore important to adjust appropriate hydrodynamic conditions to allow homogeneous coating along the whole membrane area. There are two options how to perform the modification of a SWM. One option is to do the modification at low cross-flow velocities (high P/F ratio) which lead to a rather uniform pressure along the module but the homogeneous mixing of the reactive solution at the feed side cannot be realized by convection. The modification can also be done at high cross-flow velocities (low P/F ratio) leading to a homogeneous mixing at the feed side but at the same time to a higher pressure drop along the membrane. This is why the velocity (stirring rate) of the dead-end experiments cannot be selected, as it is too high (0.24 m/s) and would result in an enormous pressure drop. For this reason, the modification was performed at the lowest possible P/F ratio (highest possible cross-flow velocity at constant permeate flow), while keeping the pressure drop < 1 bar. By this, a good compromise, i.e. a homogeneous mixing at the feed side and approximately constant boundary conditions during the filtration could be realized.

5.9.2 TW30 2521 module

Modification

Before the modification of the small TW30 2521 module containing a 28 mil spacer was done, a performance test was first carried out according to the manufacturer's data sheet (feed flow of 638 L/h and pressure of 15.5 bar) to determine the initial permeance and salt rejection. A temperature corrected permeance of 2.79 LHMbar and a salt rejection of 99.2 % were measured. The permeance and salt rejection deviate only slightly from the specified values (2.79 vs. 2.74 LHMbar and 99.2 % vs. 99.5 %).

The cationic surface linker was then circulated through the system at a feed flow of 140 L/h and a pressure of 5 bar for 2 h to allow the adsorption on the membrane surface. For the modification, the composition of the solution from Table 18 was used. The calculated minimum volume of modification solution was 25 L. The overall construction of the set-up is shown in Figure 114.

Figure 114: Overall construction of the modification set-up of TW30 2521.

For the modification itself, a permeate flow of 25 L/h was set and the modification was carried out for 60 min. The measured parameters are summarized in Table 19. All values are average values over the entire modification time. As can be seen from the table, the flux of 21 LHM from the dead-end tests could be adjusted approximately. Furthermore, a P/F ratio of 26 % (feed flow of 106 L/h) could be established which corresponds to an average cross-flow velocity of 0.04 m/s, while measuring a pressure drop of only 0.2 bar.

Table 19: Obtained filtration parameters during modification of TW30 2521.

Parameters obtained during modification of TW30 2521		
Permeate flow Q_P	L/h	28
Flux J	LHM	24
Ratio P/F	%	26
Cross-flow velocity v	m/s	0.04
Pressure drop ΔP	bar	0.2

After modification, a performance test was carried out again to determine the relative flux decrease. A decrease of 5 % was identified, which is comparable to the relative flux decrease of the membrane, which was modified in dead-end under analogous modification conditions (5 % vs. 8 %). This is a first indicator of the module being modified. To verify the success of the modification in more detail, the module was cut open subsequently and analyzed using ATR-FTIR, XPS and SEM. The results are presented in the next chapter.

Characterization of element after destructive opening

After opening the module, two membrane envelopes could be identified. One envelope consists of two membrane sheets with the active side facing outwards and an internal permeate spacer. The membrane envelopes were separated by two feed spacers. An XPS measurement was first carried out to identify the surface composition and thus to verify whether the membrane is coated. A sulfur content of 0.8 at% was obtained for the module. Even though this value is lower than the value of the dead-end reference membrane (1.1 at%), it is still significant so that it can be concluded that the module is indeed coated.

Subsequently, ATR-FTIR measurements were performed, from which the modification degree was calculated. Since the module was cross-flowed lengthwise during the modification, two location-dependent samples (A = feed side and C = opposite side) were investigated. This was to prove whether a uniform and homogeneous hydrogel layer was formed over the entire length of the membrane during the modification tests. Furthermore, several positions along the width of the module were investigated (positions 1, 2 and 3). As the module consists of two envelopes with two membrane sheets each, the different membrane sheets were also analyzed (envelope 1, sheet 1 & 2 and envelope 2, sheet 1 & 2). The DG for the different envelopes and membrane sheets is shown in Figure 115 in dependence of the location A and C. The blank value for the unmodified membrane and the reference value for the dead-end

membrane modified under the same conditions are also presented. It is also obvious here that all modification degrees are clearly larger than the blank value for the unmodified membrane. However, the DG at the different positions deviate from each other noticeably. A clear location dependency was not found. But this is because the DG, including the reference value, are very small in total.

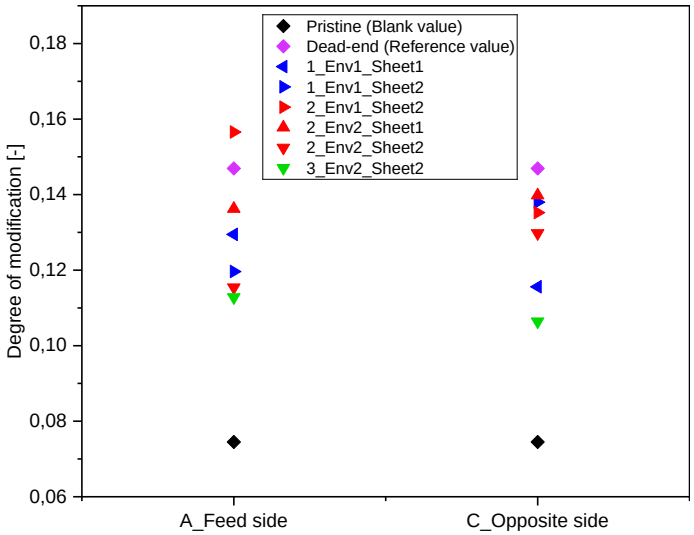

Figure 115: DGs of the module TW30 2521 after destructive opening depending on the location.

Some of the corresponding SEM images are shown in the following Figure 116 (the remaining pictures are in the Appendix, cf. Figure 128 – Figure 130). As can be seen, the roughness of the polyamide layer is obviously influenced by the hydrogel coating. Although the ridge-and-valley structure is still visible, the valleys seem to be filled and the ridges are covered. Overall, it is a very thin hydrogel layer. According to this, the topography of the membrane in the module has changed in the same way as the dead-end reference membrane had changed. Thus, the modification conditions could be successfully transferred from dead-end to the module in cross-flow.

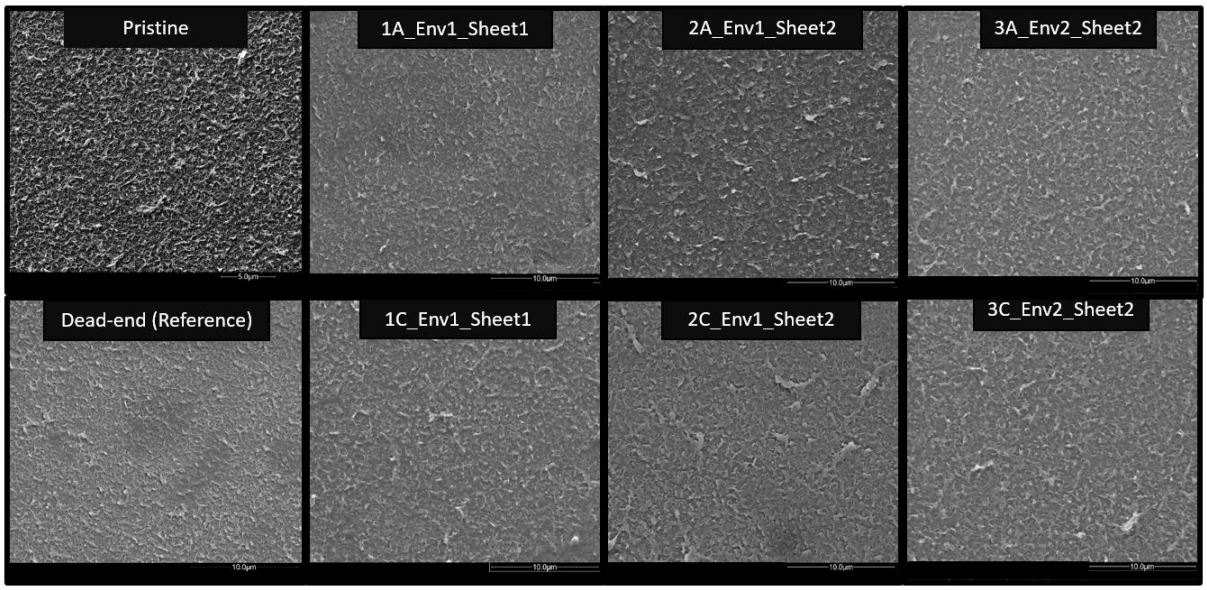

Figure 116: SEM images of the module TW30 2521 after destructive opening depending on the position along the width of the module (position 1, 2 and 3) and on the location (A and C) in comparison to the pristine membrane and reference membrane modified in dead-end.

Even if the selected modification conditions lead to thin hydrogel layers under dead-end conditions as well as here in cross-flow, it could be shown in chapters 5.5.4 and 5.7.3 that such membranes have a significantly higher fouling resistance towards a synthetic oil/water emulsion compared to unmodified membranes. The parameters were therefore applied to transfer the modification to the larger BW30 4040 modules.

5.9.3 BW30 4040 module

Modification

For the modification of the two BW30-4040 modules (34 mil spacer) the procedure was the same as for the small module. But during the performance test, the feed flow of 2527 L/h according to the data sheet could not be adjusted due to the limitation of pump capacity. Instead, the maximum possible feed flow of 2000 L/h and a pressure of 15.5 bar were set. However, the pressure drop was 4.9 bar, so that the performance test was finally carried out at a feed flow of 1330 L/h and a pressure of 15.5 bar. A temperature corrected permeance of 2.51 LHMbar was measured. Due to the still prevailing high pressure drop of 2.2 bar, the permeance deviated significantly from the value given in the data sheet (2.51 vs. 3.39 LHMbar).

After the performance test, the cationic surface linker was adsorbed at a feed flow of 371 L/h and a pressure of 4.5 bar for 2 h. The composition of the solution from Table 18 was also used for this modification. Only the polymer concentration was increased from 0.23 wt% to 0.3 wt% to achieve a greater modification effect. The calculated minimum volume of modification solution was 158 L. The plant set-up is shown in Figure 117.

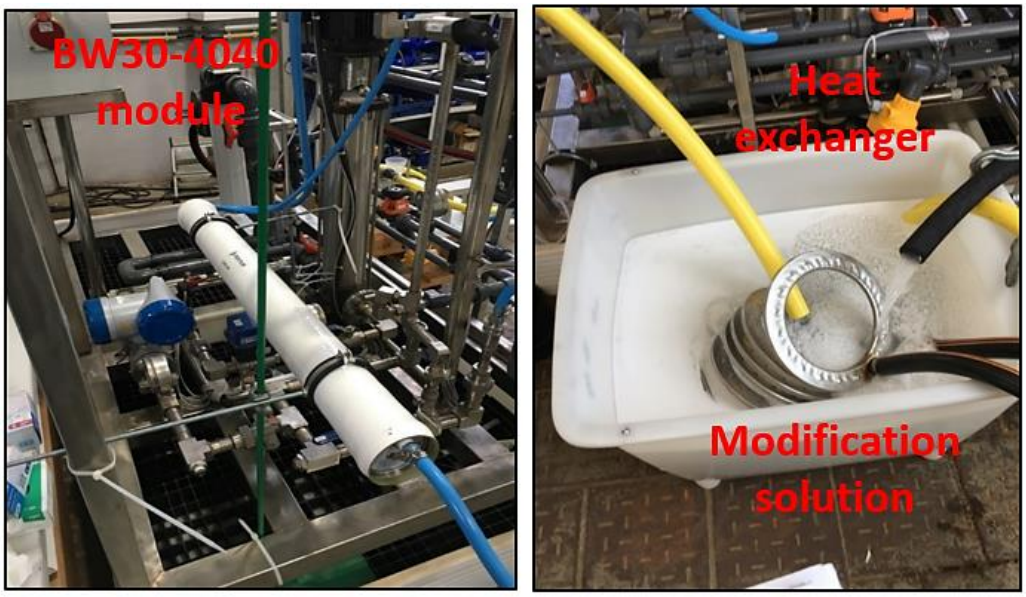

Figure 117: Overall construction of the modification set-up of BW30 4040.

For the modification, a permeate flow of 158 L/h was set and the modification was carried out for 60 min. The measured parameters are summarized in Table 20. Again, all listed values are average values. As can be seen from the table, the flux of 21 LHM from the dead-end experiment could be adjusted here as well. Based on the modification of the small module, a P/F ratio of 25 % (feed flow of 644 L/h) was adjusted, corresponding to an average CFV of 0.09 m/s. Due to the twofold length of the module compared to TW30 2521, a larger pressure drop of 0.6 bar was measured here.

Table 20: Obtained filtration parameters during modification of BW30 4040.

Parameters obtained during modification of BW30 4040		
Permeate flow Q_P	L/h	158
Flux J	LHM	23
Ratio P/F	%	25
Cross-flow velocity v	m/s	0.09
Pressure drop ΔP	bar	0.6

After modification, the performance test was done again. As in the beginning, very high pressure drops were measured for both feed flows of 2000 L/h and 1330 L/h (4.9 and 2.2 bar). Consequently, no precise permeance could be determined. Hence, no reliable conclusions could be made about the relative decrease in permeance and thus about the existence of the coating. However, in the next chapter, these two modules will be tested in field trials in comparison to conventional modules. Short-term and long-term tests were carried out to investigate the physical properties and the fouling behaviour over a longer period of time.

Field tests with real cooling water from steel industry

The two coated BW30-4040 modules (RO mod) were tested parallel to two conventional BW30-4040 modules (RO conv) in on-site trials in the project's pilot plant at DEW. The modules were operated with direct and indirect cooling water. As described in chapter 4.4.3, nine short-term tests (STE1) were first performed with direct cooling water to investigate the physical properties of the modules. Different test series (A1 – A4) were carried out (cf. Figure 35) to test the influence of the feed flow (400, 500, 570 L/h), the recovery (60, 70, 80 %) and softening by ion exchanger (with and without). In Figure 118 (a) and (b) the permeance and the overall salt rejection of RO mod (red) and RO conv (blue) is depicted as a function of the time sequence of the STE1.

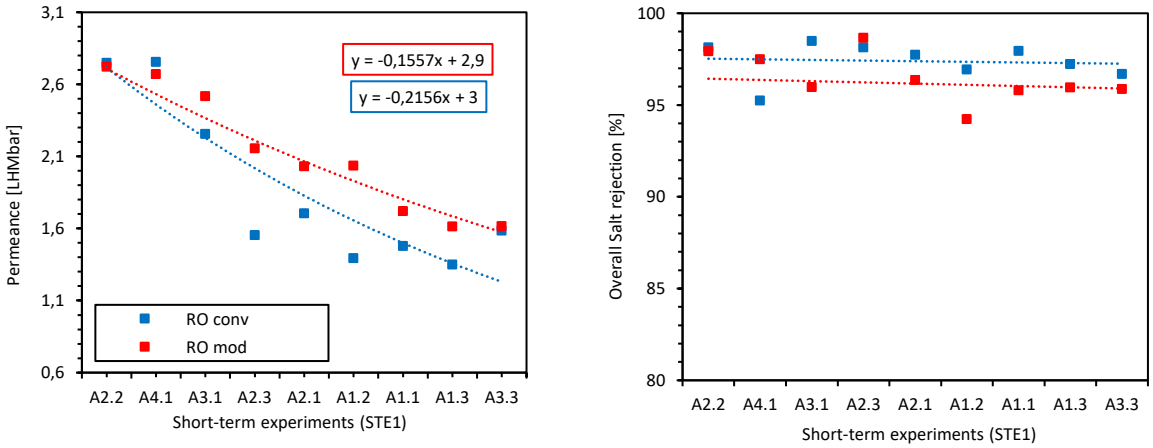

Figure 118: (a) Membrane performance and **(b)** overall salt rejection of RO mod (red) and RO conv (blue) for different experiments during STE1.

For both modules, a steady approximately linear decrease in permeance can be observed with progressive testing. However, the slope and thus the decrease in permeance for RO mod is slightly smaller (– 0.15 vs. – 0.21). This appears positive at first, as this is an indication of the presence of the hydrogel coating, which led to an improved fouling resistance. When

considering (b), it becomes apparent that the overall salt rejection of RO mod is slightly lower compared to RO conv. The differences in the overall salt rejection can be attributed to the differences in chloride rejection. Since the chloride rejection for the modified membrane is slightly lower than for the unmodified membrane, the differences seem to be reasonable, which was already observed and discussed in chapter 5.5.3. Furthermore, it can be ascribed to intrinsic differences in the module, as variations exist from module to module. Also, the chloride rejection is most strongly influenced by inhomogeneities and defects of the PA layer, which can also vary between modules. This depends additionally on the assembly and the gluing of the module. Overall, the rejections of both modules are very high (> 95 %), so that such effects are minor.

In order to evaluate the influence of the different factors (recovery, feed flow and softening), the rejection of some ions (sulphate, magnesium, calcium and chloride) are plotted against these factors in Figure 119 (a) – (c). Only the results of RO mod are shown below.

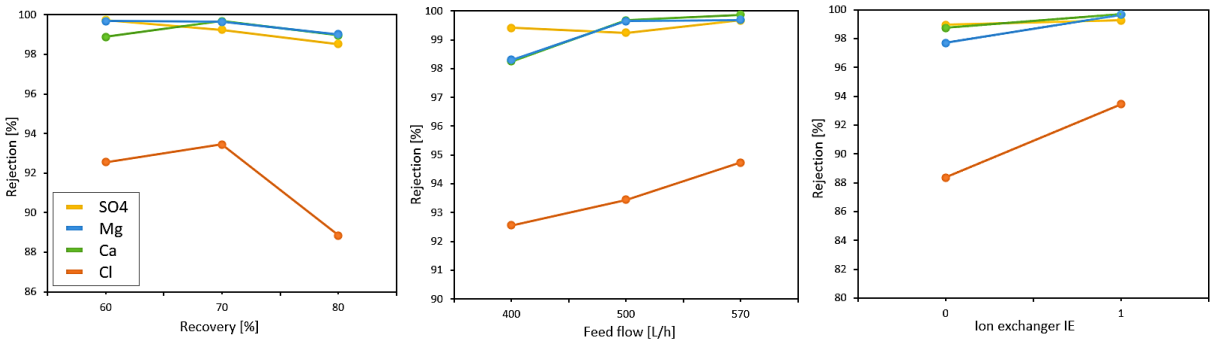

Figure 119: Results for RO mod: Sulfate, magnesium, calcium and chloride rejection in dependency of **(a)** recovery, **(b)** feed flow and **(c)** use of ion exchanger (0 = off, 1 = on).

The analysis showed that larger ions, such as SO_4 (yellow) and Mg (blue) are rejected much better than smaller ions, such as Cl (orange). This was to be expected as divalent ions have greater electrostatic repulsion in accordance with their higher charge and molecular size (sieving effect).[203] Considering (a), one can also notice that the rejection of all ions decreases with increasing recovery. Higher recovery rate leads to larger flow stream to permeate side perpendicular to the membrane surface and less cross-flow to retentate side parallel with membrane, resulting in the accumulation of rejected components on the membrane surface. This accumulation causes an increase in the surface concentration on the membrane surface and mass transfer through the membrane as the driving force for salt flow increases. As a result, the CP increases with recovery rate and deteriorates the permeate quality.[204] For SO_4,

Mg and Ca, however, the percentage reductions are less than 1 %. Only for Cl a slight increase of 1 % can be observed at first and then a stronger decrease of about 5 %. In contrast but expected, the rejection increases with increasing feed flow, cf. (b). The increase in feed flow rate reduces CP values due to increase in turbulence near the membrane surface and consequently, the salt rejection increases. Here again, the percentage reductions for SO_4, Mg and Ca are below 1 % and for Cl around 5 %.

The use of ion exchanger (cf. (c)), which is a cation exchanger that replaces Mg and Ca ions with Na ions, increased the rejection of Mg and Ca ions, which appears logical. Also, the rejection of Cl and SO_4 ions increased by ion exchanger. The higher rejection was likely to be achieved as the ion exchange experiment was the first experiment to be performed (A2.2), which is why the modules have the highest rejection for almost all ions.

Even though the percentage in- and decreases are small due to the overall high rejections (> 90%), trends and dependencies on the recovery, the feed flow and the ion exchanger could be identified. However, because the tests were carried out in different sequences, the influence of these parameters cannot be considered completely independently.

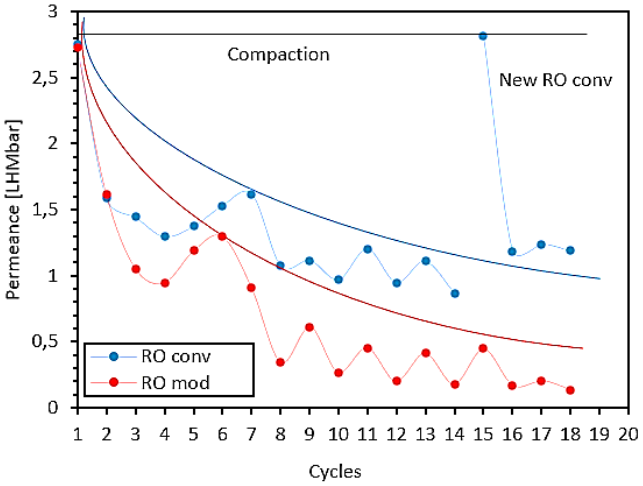

Figure 120: Overall course of permeance for RO mod (red) and RO conv (blue) over the entire five month of field tests. **1->2:** STE1, **2->3:** cleaning of RO conv with acid at pH 2 and RO mod with RO permeate, followed by 2 days of shutdown, **3->4:** STE2, **4->5:** cleaning with RO permeate, **5->6:** enzymatic cleaning, **6->7:** acid cleaning, **7->8:** B1.1, **8->9:** acid cleaning, **9->10:** B4.1, **10->11:** acid cleaning, **11->12:** B6.1, **12->13:** acid cleaning, **13->14:** B8.1, **14->15:** acid cleaning, **15->16:** 3W_LTE, **16->17:** acid cleaning, **17->18:** 1W_LTE_IndWa.

As already shown in Figure 118, both modules RO mod and RO conv experienced a strong decrease in permeance by approx. 43 % during STE1 **(1->2)**. After STE1, the permeance of both module types deteriorated progressively. Figure 120 shows the total course of permeance of

both modules RO mod and conv over the entire five months of the operational tests. As can be seen, the shutdown of two days after the STE1 **(2->3)** led to a further decrease in permeance. Since RO conv was rinsed with HCl at pH 2.5 and RO mod with only RO permeate before the shutdown, the decrease in permeance for RO conv is significantly smaller in comparison to RO mod (– 9 vs. – 32 %). The subsequent STE2 **(3->4)** led to a continued reduction in permeance. After rinsing with RO permeate **(4->5)** and enzymatic cleaning **(5->6)**, the performance of both modules improved again. A following acidic cleaning **(6->7)** led to a further deterioration of the permeance for RO mod by – 31 %, whereas the permeance for RO conv increased by 6 %. Therefore, it can be assumed that the coating had already lost its function at this stage.

The influence of different pretreatments (B4.1: pH 6, B6.1: 30 ppm antiscalant dosage and B8.1: use of ion exchanger) and the influence of acidic cleaning on long-term stability and irreversible fouling should be investigated in the following LTE's. It was found that the performance during the first LTE B1.1 without pretreatment **(7->8)** decreased further, for RO conv by – 34 % and for RO mod by – 66 %. After acid cleaning **(8->9)** the flux could be increased, but no complete recovery could be achieved. Due to the lack of pre-treatment in B1.1, fouling became more severe so that permeance dropped gradually in the further experiments B4.1 **(9->10)**, B6.1 **(11->12)** and B8.1 **(13 >14)** in spite of pre-treatment. Each following acidic cleaning between the LTE's **(10 >11, 12->13, 14->15)** raised the permeance, but the change became continuously smaller. After completion of the LTE **(13->14)** the permeance for RO conv was only 0.9 LHMbar and that of the RO mod was just 0.2 LHMbar.

The two RO conv modules were then replaced by four new conventional modules. From this point, no further comparison can be made between the two module types (RO mod and RO conv). Most striking is that the new RO conv modules also had to suffer a considerable loss of flux during the three-week long-term test 3W_LTE **(15->16)**. The decrease in permeance was 60 %. The acid cleaning afterwards **(16->17**) could hardly enhance the permeance. The one-week long-term test with indirect cooling water (1W_LTE_IndWa) **(17->18)** resulted only in a further decline of the permeance. In total, the permeance of RO mod decreased by approx. 94 %, whereas the permeance of RO conv decreased by approx. 70 %.

Both module types, whether coated or not, thus experienced severe irreversible fouling. This is somewhat surprising at first, since little or no irreversible fouling was detected during dead-

end and cross-flow laboratory tests with this cooling water and the same membrane type BW30 (cf. chapter 5.2.2 and 5.5.4). In order to understand this, a further in-depth analysis of the direct cooling water was carried out. A comparison of the cooling water composition of 2017 and 2019 showed a production-related increase in the organic content from 15 to 38 mg/L. Furthermore, a defect in an operational oil and solids separator was detected, which led to a further increase in solid particles. As a result, the SDI increased from 2.7 %/min to its maximum. Accordingly, the composition of the water during the field tests did not correspond to the composition of the water samples used for the laboratory tests. Due to the fluctuating cooling water composition, the randomly taken water samples used for the laboratory tests are therefore not representative of the real process conditions.

Thereupon, the 5 µm MF filter 1F0 positioned upstream of the feed was examined. Figure 121 illustrates the new condition of the filter and the condition after one and after four weeks of operation. It can be clearly seen that the filter was already discolored brown after one week. A complete brown coloration occurred after four weeks. The filter was then incinerated and the solid matter was regained which had magnetic properties. The load of the filter was 25 %. Based on the brown colour and the magnetic properties, it could be concluded that the particles are most likely iron oxide.

Figure 121: Appearance of the 1F0 MF-filter after 4 weeks of operation, 1 week of operation and new state (from left to right).

In addition to that, the membranes were operated continuously over five months during the field tests, which could not be reproduced adequately on a laboratory scale owing to the low capacity during the dead-end filtration experiments. For a comparison, the load can be referred to, which represents the total amount of filtered volume per area. In the field tests, the load during STE1 and LTE was 380 L/m^2 and 1600 L/m^2, respectively, while the total load during one single dead-end laboratory test was only 33 L/m^2.

Furthermore, the overflow pump used, was able to achieve an average CFV of only 0.01 m/s. Moreover, the tests during the LTE were carried out in such a way that the maximum possible recovery should be achieved at a constant retentate flow. To maximize the recovery, the feed flow was reduced when the flux dropped. This led to a reduction of the CFV, which caused the laminar boundary layer, in which the concentration polarization is formed, to become increasingly thicker, thus promoting fouling. This resulted in an additional reduction of flux. Also, the Reynolds number dropped from 14 to 8. These are obviously laminar flow conditions which strongly favoured irreversible fouling. Thus, the type of operational management also contributed to an increase in fouling.

Overall, the antifouling effect of the coated modules could be detected at the very beginning of the field tests. The transfer of the modification conditions from dead-end to membranes in the SWM and the general feasibility of coating such modules could thus be demonstrated. However, due to the fluctuating cooling water composition caused by production conversion and defects at the plant and the type of operation management (insufficient overflow), strong irreversible fouling of both module types (conventional and coated) was experienced during the tests. Because of the severe fouling, the modification effect of the coated modules could therefore no longer be proven. Occurring fouling is therefore not only dependent on the membrane properties, but also strongly on the feed composition and process conditions. A membrane module autopsy was subsequently performed to identify the fouling type.

Autopsy of the elements

A membrane module autopsy was conducted to investigate the composition and morphology of the fouling layer on the membrane surface that emerged under the conditions of the field tests which enables the identification of fouling type. The autopsy is a destructive technique in which the membrane modules to be investigated are cut open and both the deposits on the surface and the membrane sheets themselves are examined using analytical measurement methods.[205] The autopsy was done of both RO mod modules, which were operated with the cooling water for five months continuously. The two RO conv modules, which were operated parallel to the RO mod modules from the very beginning, could not be examined due to strong biofouling caused by prolonged storage. Instead, the 1st and 4th module of the four new RO conv modules were autopsied, which were operated for only one month.

After the membrane elements were cut open, six membrane envelopes could be identified. One envelope consists of two membrane sheets with the active side facing outwards and an internal permeate spacer. The membrane pockets are separated by six feed spacers. A red-brownish deposit was observed for all membrane sheets (RO mod and RO conv), which also possessed magnetic properties, cf. Figure 122 (a). These observations are consistent with the observations already made for the MF filter, that this deposit is most likely iron oxide. The feed spacers also revealed a distinct brown colouration. However, it is much more pronounced for RO mod which is due to the much longer operation time (five vs. one month, cf. Figure 122 (b)). On the permeate side, neither a deposit nor a brown coloration could be detected which implies no damage to the membranes.

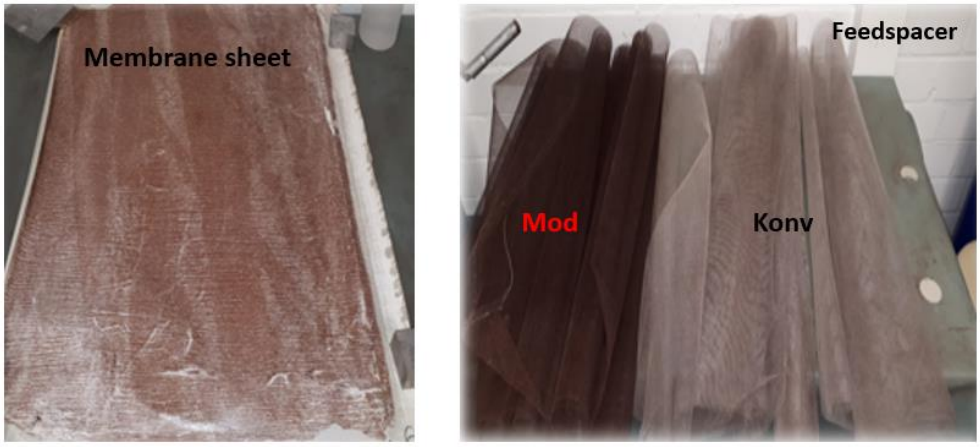

Figure 122: (a) Exemplary representation of a membrane sheet of RO mod after field tests and autopsy. **(b)** Representation of RO mod feed spacer and RO conv feed spacer.

The coating was wetted, mechanically removed and suspended in water. The suspension was centrifuged for 45 min at 4500 rpm. Besides the brown solid, an oily residue could also be identified. Different methods were used to analyze the deposit and the membranes. The following analyses were performed:

Analysis of deposit:

- Gravimetric determination of load per m^2
- Analysis of chemical structure of deposit via ATR-FTIR
- Determination of ignition loss via pyrolysis and TGA
- Elemental analysis for determination of C, N, S, H
- EDX for determination of other elements
- X-ray diffraction for determination of iron oxide modification

- Particle size analysis of iron oxide particles via laser granulometry and SEM

Analysis of membrane sheets:

- Examination of membrane performance
- Analysis of physical and chemical damage via ATR-FTIR, zeta potential and methylene blue test

Due to the different operation time (five months for RO mod vs. one month for RO conv), the module types (conventional and modified) could not be compared directly. By gravimetric determination of the loading, it could be confirmed that the loading was significantly higher for RO mod than for RO conv. For RO mod it was about 2x higher than for RO conv (8.6 g/m^2 vs. 4 g/m^2). Therefore, the results of the deposit and membrane analysis are only briefly summarized below and evaluated with regard to the fouling that has occurred. The differences between the module types are not evaluated.

In addition to the gravimetric determination of the load, ATR-FTIR measurements were also carried out, which provide information about the composition of the deposit. For each module, the positions A and E (feed side and end side) were investigated. The IR measurements (Figure 123) identified the band for iron oxide at 526 cm^{-1} and further bands at 3273 cm^{-1} (O-H stretching), 2852 cm^{-1} (C-H stretching/NH_2 stretching) and 1692 cm^{-1} (C=O stretching), independent of the module type and position. This is a clear evidence of the presence of aliphatic hydrocarbons such as alcohol, amines, alkanes and carbonyl compounds. Thus, the fouling consists not only of iron oxide particles, but also of organic material and potentially oil.

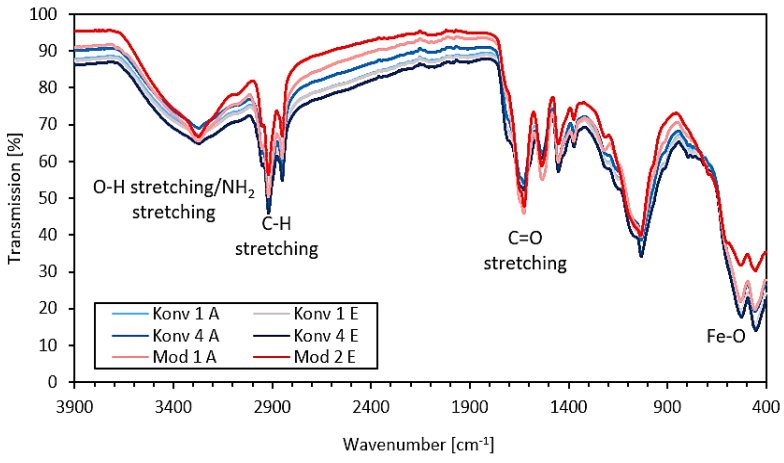

Figure 123: IR spectra of the deposit.

Further, the ignition loss was determined, which is a common method to measure the organic content of a material. First, the moisture of the samples was removed in a high vacuum. The coating was then calcined at 1000 °C. For the final determination, the remaining solid was pyrolyzed using TGA. The average inorganic content for all modules was 20 % and the organic content equaled 80 %. Using elemental analysis (EA), it was also possible to reveal that the organic matter was composed of 50 – 60 % carbon, 10 % hydrogen, 5 % nitrogen and 1 – 2 % sulfur. Using EDX, further elements, such as chromium, silicon, phosphorus, aluminum and manganese could be identified, although their percentage share was < 1 %. The average percentage of iron was 9 %. When determining the oxygen to iron ratio, no clear information about the valence of the iron oxide could be gained. The ratio of 4/3 could only be calculated for a few samples. In some cases, higher ratios were obtained. This is because the oxygen is also organically bound, which makes it difficult to determine the exact ratio.

In order to gain information about the iron oxide modification (maghemite, hematite or magnetite), the particles were also examined by X-ray diffraction (XRD). The obtained diffractogram revealed a mixture of hematite and maghemite (Fe_2O_3) in all samples. This is in line with the red-brown colour and the magnetism. Magnetite on the other hand has a black colour. To ascertain the particle size, a particle size analysis was first carried out using laser granulometry. This revealed that 90 % of the particles had a size of 7.52 µm, 50 % a size of 1.37 µm and 10 % a size of 0.21 µm. According to this, the particles have a size in the sub-micrometer range and in the range exceeding the exclusion limit of the 5 µm MF filter. Thus, the MF pre-filtration was not sufficient to remove the iron oxide particles that lead to the blocking and thus fouling of the membrane modules.

Furthermore, SEM images were recorded to identify the primary particle size (cf. Figure 124). First, the SEM images show that the membrane surface is completely covered with a fouling layer consisting of at least two different materials. Considering the previous results, it is most likely iron oxide particles embedded in organic material. The particle size was measured to be approx. 0.5 µm and corresponds to the particle size determined by laser granulometry. Thus, the inadequate pre-treatment by means of MF pre-filter also contributed to the strong fouling.

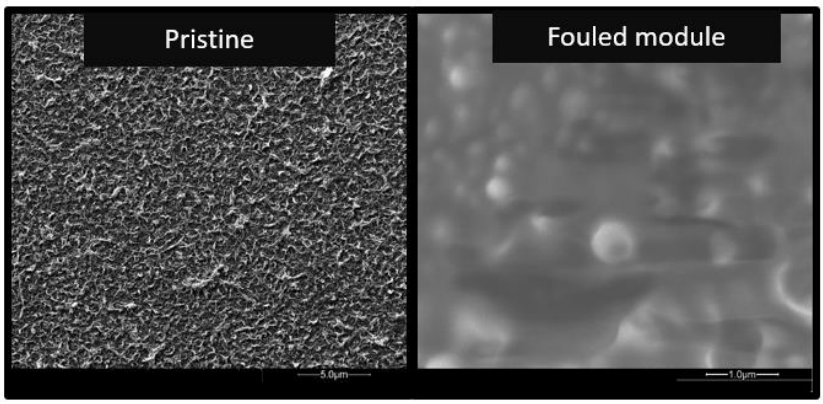

Figure 124: SEM images of the deposit.

In the second part, the membrane sheets were examined. The aim was to determine whether the formation of the deposit had physically or chemically damaged the membrane. For this, the membrane was cleaned with an acidic HCl solution of pH 2 for 30 min to remove the remaining deposit. The water permeance and the salt rejection were measured with a 2000 ppm NaCl solution. For RO conv and RO mod, the permeance has increased twofold and tenfold, respectively. The salt rejection decreased by approx. 10 %. The increase in WP can be attributed to the cleaning effect and the decrease in rejection is most likely the result of physical damage to the membrane sheets during sample preparation. Likewise, spacer imprints during field tests may have led to a change in the integrity of the separation layer.

By means of the methylene blue dye test, the physical damage could be visualized, cf. Figure 131 in the Appendix). This dye test is based on the passage of a high molecular weight component through the PA layer which is supposed to be retained by the PA layer unless it is damaged.[205] The test was carried out by filtrating the dye solution under dead-end conditions through the membrane samples. During the tests, the membrane samples and the permeates turned blue. A correlation between higher coloration in blue and lower salt rejection was found. However, the ATR-FTIR measurement did not reveal any chemical changes in the polyamide structure. No change in the surface charge could be detected by the zeta potential measurement neither. Thus, no chemical damage to the membranes occurred during the field tests.

Thus, the complex fouling could be characterized by means of different analytical methods. The deposit analysis showed that the fouling is composed of a mixture of particle fouling in the form of iron oxide particles, organic and oil fouling. From the membrane analysis it could be demonstrated that no chemical damage to the membranes occurred during field tests. In

addition to the fluctuating cooling water composition and the type of operation management, the inadequate pre-treatment of the water by means of 5 µm MF pre-filter also contributed to the massive fouling. These mentioned problems led to the fact that the antifouling properties of the coated modules could not be demonstrated comprehensively. In addition, the two module types (conventional and modified) were operated for different periods of time and under different conditions, so that a comparison between both types during autopsy was not possible and, in any case, obsolete. However, the general feasibility of coating SWM and the application of such modules for the treatment of cooling water of the steel industry could be demonstrated.

5.9.4 Interim conclusions

The most important conclusions regarding module modification are summarized below:

1. Dead-end conditions resulting in a thin hydrogel layer with good antifouling properties were chosen for the transfer of the modification (average polymer concentration of 0.023 wt%, pH value of 8, acrylate/crosslinker ratio of 1:1, average flux of 21 LHM, maximum filtered mass of 4.8 g/m^2).
2. After modification of the small module TW30 2521, a relative flux decrease of 5 % was measured which is comparable to the flux decrease of the reference membrane in dead-end. The characterization showed that the module is coated homogeneously over the module length, even though the coating is thin. The transfer of the modification was thus successful.
3. When modifying the larger BW30 4040 modules, no conclusions could be drawn about the relative flux decrease due to the pressure drop at the performance tests. During field tests, a higher permeance/fouling resistance was found for the modified modules compared to the conventional modules for a number of different experiments in the initial phase.
4. In the later stages, the performance of both module types deteriorated significantly. In contrast to the dead-end laboratory tests, massive irreversible fouling arose. The fluctuating cooling water composition, the type of operation management and the inadequate pre-filtration by an MF filter, led to this extreme fouling. By means of a module autopsy, it was ascertained that the fouling includes particle fouling (iron oxide particles), organic and oil fouling.

6 Overall conclusions and outlook

The main target of this work was the development of a novel in situ anti-fouling coating for RO membranes. By this, the barrier properties of the membrane and the arising CP were exploited allowing the selective modification of the surface of the membrane with a hydrogel coating, which made it feasible to apply the coating to membrane modules.

The screening study of commercial RO membranes (BW30, RO98pHt, Lewabrane, AK and SE) showed that BW30, RO98pHt, Lewabrane and AK are full-aromatic membranes. Contrary to expectations, only the SE membrane from GE Osmonics turned out to be a blend of full- and semi-aromatic membrane. Furthermore, it was found that all membranes are coated with a preservative layer, most likely PVA, that protects the membranes before application but can be washed off easily to a considerable extent. To guarantee the removal of this coating, the membranes were washed with a 30:70 EtOH/water solution, followed by the immersion in pure water prior to usage.

The fouling analysis of both cooling waters CW_DEW and CW_Sp revealed that the filtration of RO membranes with CW_Sp entails a great risk for scaling. This was predicted by the feed analysis and clearly confirmed by the dead-end short-term experiments. For CW_DEW a moderate potential for organic and particle fouling was predicted. However, the membranes BW30 and Lewabrane showed a very high fouling resistance and no irreversible fouling during the dead-end short-term and cross-flow long-term tests. For this reason, the Lewabrane and BW30 membranes were pre-selected for further modification.

After synthesis of the zwitterionic copolymer, all signals of the ^{1}H-NMR spectrum could be assigned to the corresponding protons, pointing to a successful conversion. The acrylate/crosslinker ratio of the copolymer was on average 20:80 %. In addition, reproducible molar masses in the range of 90 – 100 kDa could be attained. With the aid of DLS and cloud point measurements, it was possible to determine that aqueous solutions of the copolymer form agglomerates and thus exhibit turbidity. Even after filtration of the copolymer solution through a 100 nm filter, agglomerates were formed again. This is due to self-association of zwitterionic polymers as a consequence of the formation of dipole pairs between intra- and inter-zwitterionic groups. However, it could be shown that the proportion of agglomerates is relatively small and therefore negligible at low polymer concentration. When plotting the number against the hydrodynamic diameter, it was shown that a monodisperse particle

distribution and particle sizes in the range of 4 – 30 nm could be achieved. The cross-linking of the zwitterionic copolymer with the cross-linker 1,4 dithiothreitol (DTT) via thiol-ene Michael addition click reaction was first studied in the bulk via in situ rheology. A straightforward dependency of the gelation time on the pH values 8, 9 and 10 could not be ascertained. The pH value of 9 seems to be the optimum. The dependency of the storage modulus on the acrylate/crosslinker ratio revealed a decrease with increasing ratio. For the ratio 1:1 and the pH of 9, storage modules up to 1200 Pa were obtained. These conditions (pH value of 9, acrylate/crosslinker ratio of 1:1) are thus optimal for the formation of a hydrogel with elastic properties in a short time, which is why these conditions were chosen for the modification experiments. For a gelation time of 10 min a critical concentration of 12 wt% was established under these conditions, which was to be used to calculate the flux for the modification experiments via film model.

To gain a fundamental understanding of the hydrogel formation, the crosslinking reaction of the zwitterionic copolymer with DTT was first carried out under dead-end filtration conditions. When the Lewabrane and BW30 membranes were modified without stirring, a crosslinking reaction on the membrane surface only occurred at a polymer concentration of 0.01 wt% and above. It was also found that the mere adsorption of the polymer solution is not sufficient to trigger a modification. Consequently, the flux is decisive for the CP and the formation of the hydrogel. Furthermore, it could be demonstrated that the effect of hydrogel formation can be switched on and off by stirring. Thus, the formation of the hydrogel can be controlled by the combination of polymer concentration, flux and stirring rate. In order to consider the hydrodynamic conditions for the transfer of the modification from dead-end to cross-flow, for further experiments the stirring rate was set to 300 rpm. At this stirring rate, crosslinking occurs at a polymer concentration of 0.02 wt% and above. By varying the polymer concentration, it was detected that only thin hydrogel layers are formed at polymer concentrations of up to 0.03 wt% under subcritical conditions. Only at a bulk concentration of 0.04 wt% a three-dimensional hydrogel network was formed above the required critical concentration. It was also found that the NaCl rejection for the modified membrane was 1 – 2 % lower compared to the unmodified membrane. This observation was not followed up, so that in future work this measured effect should be thoroughly investigated in detail. It is expected that the intrinsic properties of the hydrogel-coated membrane should not have any influence on the rejection. However, the rejection could be influenced by the real

concentration at the membrane surface. Further fouling tests with an oil/water emulsion showed that the membranes modified at 0.02 and 0.03 wt% exhibit better antifouling properties compared to the unmodified membrane, despite the thin hydrogel layer. The industrial cooling water from the steel industry was not suitable for testing the antifouling properties due to the low degree of contamination.

The parameters determined via rheology were applied for the further modification experiments. However, the flux which was calculated from the critical concentration via film model was too high to be realized with the BW30 RO TFC membrane. The experiments were therefore carried out at constant pressures from 3 – 10 bar and the change in flux during the modification was evaluated. It could be shown that a pressure of 3 bar and polymer concentrations of 0.05 wt% and 0.06 wt% are not sufficient to initiate a crosslinking reaction via the CP. At 5, 7 and 10 bar a homogeneous and distinct hydrogel layer was formed on the membrane surface. From the time variation analysis, it could be determined that the crosslinking reaction starts within the first few minutes (LT of 1.8 µm) and is completely finished after about 30 min (LT of 3.9 µm). An increase of the modification time beyond that mainly contributed to the hydrogel thickness, even though this effect was very small (LT up to 4.2 µm). With this understanding, the minimum flux for the crosslinking reaction could be calculated. It was ascertained that no modification effect occurs at a flux of 18 LHM. In contrast, at 26 LHM a clearly high modification effect was obtained. Thus, for successful crosslinking, the minimum flux must be greater than 18 LHM. Accordingly, it is not the transported filtered mass per area, but rather the filtration conditions, particularly the flux, that is crucial for triggering a crosslinking reaction via the CP and thus for the adjustability of the hydrogel formation on the membrane surface. For overall optimization, it would be interesting to perform parameter variations (variation of flux and time), in which substantially thinner hydrogel layers are obtained and the membranes accordingly only show a maximum flux loss of 20 %.

When calculating the surface concentration during the modification, significantly lower values (two orders of magnitude) were obtained than the critical concentration determined by rheology. This is mainly due to the reason that the gelation point as an evaluation criterion is not representative for the reaction taking place at the membrane surface. Rheology can therefore be used to support the understanding of hydrogel formation and to determine

optimal parameters for the composition of the solution. However, it cannot be used to select a priori conditions that lead to a specific coating effect. Thus, in future works the interface between the dead-end modification experiments (calculation of c_m) and the rheology experiments (estimation of critical concentration c_{crit}) must be studied in more detail.

During the investigation of the stability of hydrogel coated membranes, it could be shown that the coated membranes are virtually stable under the cleaning conditions of Dow Filmtec. For modified membranes with a modification degree > 2, it would be possible to run 30 cleaning cycles with an average cleaning time of 30 min under acidic cleaning conditions. In future works, emphasis should be given on developing and establishing a method for regeneration of the hydrogel coating after it had lost its antifouling effect. Based on the cleaning results, a method for the regeneration (removal and reapplication) of the hydrogel coating can be adapted to the hydrogel characteristics. For the removal, the coated membranes would need to be cleaned for more than 16 h at a pH value of 2, or for shorter time, at lower pH values and higher temperature that are tolerable for the PA layer. Furthermore, higher shear rates could contribute to a more efficient removal of the coating.

For the transfer of the modification to cross-flow, the conditions from dead-end were chosen, which led to a distinct hydrogel layer on the membrane surface. It was shown that the CFV has a clear influence on the CP and thus on modification degree. With a lower CFV, hydrogel formation is much more likely to occur because the laminar boundary layer in which the CP is formed is thicker and the critical concentration of the reactive system is more likely to be exceeded. Unfortunately, the conditions that led to a pronounced thick hydrogel layer on the membrane surface in the dead-end experiments could not be transferred to the cross-flow experiments. The critical concentration was not exceeded so that only thin inhomogeneous hydrogel layers were formed. The failed transfer could be attributed to the changed boundary layer conditions caused by the spacer. By increasing the flux from 26 to 40 LHM, the critical concentration of the reaction solution could be exceeded by increasing the CP despite the application of the spacer, so that a distinct hydrogel layer could be generated on the membrane surface. Even if the formation of the hydrogel layer was not homogeneously formed over the entire membrane surface area, the charge neutrality could be significantly increased. Hence, analogous to the dead-end tests, it was proven that the crosslinking reaction is mainly controlled via flux even if a spacer is used. Despite the thin hydrogel layer,

the membranes modified at 26 LHM displayed in dead-end and cross-flow experiments an extraordinarily good antifouling behaviour towards crude oil emulsions compared to the unmodified membrane. The membrane modified at 40 LHM initially showed compression effects due to the thick hydrogel layer, which led to a significant decrease in flux in the initial phase and a constant and stable course after only 10 h. At last, the stability and reusability of the modification solution could be demonstrated.

For the transfer of the modification to the SWM, dead-end conditions were chosen, resulting in a thin hydrogel layer with good antifouling properties. After the modification of the small module TW30 2521, a relative flux decrease of 5 % was measured, which is comparable to the flux decrease of 8 % of the membrane modified in dead-end. The characterization showed that the module is evenly coated over the entire module length. The transfer of the modification can thus be regarded as successful. When modifying the larger BW30 4040 modules, no information could be gathered on the relative flux decrease after the modification due to the high pressure drop during the performance test. However, a higher fouling resistance could be measured for the modified modules compared to the conventional modules during the initial phase of field tests for a number of different experiments. In the further course of the field tests, the performance of both module types deteriorated significantly. In contrast to the dead-end laboratory tests, massive irreversible fouling occurred. The fluctuating cooling water composition, the type of operation (laminar flow conditions), defects at the plant and the inadequate pre-filtration using a 5 µm MF filter led to this extreme fouling. By means of a module autopsy it was determined that the fouling includes particle fouling (iron oxide particles), organic and oil fouling. Thus, fouling is not only dependent on the membrane characteristics, but also strongly on process conditions and feed pre-treatment. The anti-fouling effect of the coated modules measured at the beginning of the field tests could therefore not be detected in the further course of the process due to the serious fouling. In order to reduce the fouling in future works, there is an increased need for adaptation of the field tests. The separation of the magnetic particles by means of magnetic separation as a pre-treatment would be one possible solution. Similarly, a pre-filter with a lower exclusion limit of 5 µm could provide considerable improvements with regard to particle fouling. Overall, turbulent flow conditions during the tests could reduce fouling by increasing shear forces.

However, the general feasibility of coating SWM by means of a gradual transfer from dead-end to cross-flow and the application of such modules for the purification of cooling water of the steel industry could be demonstrated. In the future, work should be devoted to the investigation of the in situ coating modification under cross-flow conditions in lab-scale to get a deeper understanding of all influences which are relevant for the transfer to the modules.

7 Literature

1. https://www.planet-wissen.de/natur/umwelt/wassernot/index.html; last checked on 29.07.2020.
2. Wang, Z.; Fan, Z.; Xie, L.; Wang, S., Study of integrated membrane systems for the treatment of wastewater from cooling towers. *Desalination* **2006,** *191*, 117-124.
3. http://www.bfi.de/de/projekte/weiss-effiziente-kreislauffuehrung-von-kuehlwasser-durch-integrierte-entsalzung-am-beispiel-der-stahlindustrie/.
4. https://www.umweltbundesamt.de/indikator-nutzung-der-wasserressourcen#welche-bedeutung-hat-der-indikator; last checked on 29.07.2020.
5. Potts, D. E.; Ahlert, R. C.; Wang, S. S., A critical review of fouling of reverse osmosis membranes. *Desalination* **1981,** *36*, 235-264.
6. Colla, V.; Branca, T. A.; Rosito, F.; Lucca, C.; Vivas, B. P.; Delmiro, V. M., Sustainable Reverse Osmosis application for wastewater treatment in the steel industry. *Journal of Cleaner Production* **2016,** *130*, 103-115.
7. https://en.wikipedia.org/wiki/Membrane_fouling; last checked on 29.07.2020.
8. She, Q.; Wang, R.; Fane, A. G.; Tang, C. Y., Membrane fouling in osmotically driven membrane processes: A review. *Journal of Membrane Science* **2016,** *499*, 201-233.
9. Ismail, A. F.; Khulbe, K. C.; Matsuura, T., RO Applications. In *Reverse Osmosis*, **2019**.
10. Zhao, D.; Yu, S., A review of recent advance in fouling mitigation of NF/RO membranes in water treatment: pretreatment, membrane modification, and chemical cleaning. *Desalination and Water Treatment* **2014,** *55*, 1-22.
11. Bernstein, R.; Belfer, S.; Freger, V., Improving performance of spiral wound RO elements by in situ concentration polarization-enhanced radical graft polymerization. *Journal of Membrane Science* **2012,** *405-406*, 79-84.
12. Shultz, S.; Freger, V., In situ modification of membrane elements for improved boron rejection in RO desalination. *Desalination* **2018,** *431*, 66-72.
13. Baransi-Karkaby, K.; Bass, M.; Freger, V., In Situ Modification of Reverse Osmosis Membrane Elements for Enhanced Removal of Multiple Micropollutants. *Membranes (Basel)* **2019,** *9*, 28.
14. Provided by SMS group GmbH.
15. Oren, Y., Capacitive deionization (CDI) for desalination and water treatment — past, present and future (a review). *Desalination* **2008,** *228*, 10-29.
16. https://www.google.de/url?sa=t&rct=j&q=&esrc=s&source=web&cd=&cad=rja&uact=8&ved=2ahUKEwiwntuUzfPqAhWI-6QKHTrBDfAQFjAKegQIBBAB&url=https%3A%2F%2Fpubs.usgs.gov%2Fwsp%2F1330h%2Freport.pdf&usg=AOvVaw2oljhtsqJEQdiej2E_Gj8u; last checked on 29.07.2020.
17. http://www.ionxchng.com/kms/techpaper%5Csteel_twms_nr.pdf; last checked on 29.07.2020.
18. Sinha, S.; Sinha, V.; Pandey, S.; Tiwari, A., A study on the wastewater treatment technology for steel industry—recycle & reuse. *American Journal of Engineering Research* **2014,** *3*, 309-315.
19. https://www.academia.edu/35056416/NALCO_COMPANY_OPERATIONS; last checked on 29.07.2020.
20. https://www.spire2030.eu/sites/default/files/users/user500/04_Water%20Management%20Steel%20Industry_Thoerner.pdf; last checked on 29.07.2020.

21. https://www.academia.edu/36363758/Cooling_Water_Problems_and_Solutions_Course_No_M05-009_Credit_5_PDH; last checked on 29.07.2020.
22. Lee, J.-W.; Kwon, T.-O.; Moon, I.-S., Performance of polyamide reverse osmosis membranes for steel wastewater reuse. *Desalination* **2005,** *177*, 69-82.
23. Fritzmann, C.; Löwenberg, J.; Wintgens, T.; Melin, T., State-of-the-art of reverse osmosis desalination. *Desalination* **2007,** *216*, 1-76.
24. Madsen, H. T., Chapter 6 - Membrane Filtration in Water Treatment – Removal of Micropollutants. In *Chemistry of Advanced Environmental Purification Processes of Water*, Søgaard, E. G., Ed. Elsevier: Amsterdam, **2014**.
25. Greenlee, L. F.; Lawler, D. F.; Freeman, B. D.; Marrot, B.; Moulin, P., Reverse osmosis desalination: Water sources, technology, and today's challenges. *Water Research* **2009,** *43*, 2317-2348.
26. https://puretecwater.com/reverse-osmosis/what-is-reverse-osmosis; last checked on 29.07.2020.
27. Glater, J., The early history of reverse osmosis membrane development. *Desalination* **1998,** *117*, 297-309.
28. Cadotte, J. E.; Petersen, R. J.; Larson, R. E.; Erickson, E. E., A new thin-film composite seawater reverse osmosis membrane. *Desalination* **1980,** *32*, 25-31.
29. Baker, R. W., Membrane Technology and Applications, third ed., John Wiley & Sons, New York, **2012**.
30. Mulder, M., Basic Principles of Membrane Technology, Kluwer Academic Publishers, Boston, **1996**.
31. Lee, K. P.; Arnot, T. C.; Mattia, D., A review of reverse osmosis membrane materials for desalination—Development to date and future potential. *Journal of Membrane Science* **2011,** *370*, 1-22.
32. https://www.google.de/url?sa=t&rct=j&q=&esrc=s&source=web&cd=&ved=2ahUKEwjHvp_X1vPqAhUcwQIHHabKAhMQFjABegQIARAB&url=https%3A%2F%2Fwww.eolss.net%2FSample-Chapters%2FC07%2FE6-144-46-00.pdf&usg=AOvVaw1SBDx3nvn8HddS-XM1aCvU; last checked on 29.07.2020.
33. https://www.google.de/url?sa=t&rct=j&q=&esrc=s&source=web&cd=&ved=2ahUKEwiW3bTG0vPqAhXP_qQKHcy7CBAQFjAJegQIAhAB&url=http%3A%2F%2Fimgs.khuyenmai.zing.vn%2Ffiles%2Ftailieu%2Fky-thuat-cong-nghe%2Fhoa-dau%2Fro_reviewe_427.pdf&usg=AOvVaw240O-rdYW8boFCk-YgDzGe; last checked on 29.07.2020.
34. Khorshidi, B.; Thundat, T.; Fleck, B. A.; Sadrzadeh, M., A Novel Approach Toward Fabrication of High Performance Thin Film Composite Polyamide Membranes. *Scientific Reports* **2016,** *6*, 22069.
35. Rana, D.; Matsuura, T.; Kassim, M. A.; Ismail, A. F., Reverse Osmosis Membrane from: Handbook of Membrane Separations, Chemical, Pharmaceutical, Food, and Biotechnological Applications, CRC Press, **2015**.
36. Freger, V., Nanoscale Heterogeneity of Polyamide Membranes Formed by Interfacial Polymerization. *Langmuir* **2003,** *19*, 4791-4797.
37. Freger, V., Kinetics of Film Formation by Interfacial Polycondensation. *Langmuir* **2005,** *21*, 1884-1894.

38. Ehrenstein, G. W.; Pongratz, S., Resistance and Stability of Polymers, Hanser Publishers, Munich, **2013**.
39. Kesting, R. E., The four tiers of structure in integrally skinned phase inversion membranes and their relevance to the various separation regimes. *Journal of Applied Polymer Science* **1990,** *41*, 2739-2752.
40. Zhao, C.; Zhou, X.; Yue, Y., Determination of pore size and pore size distribution on the surface of hollow-fiber filtration membranes: a review of methods. *Desalination* **2000,** *129*, 107-123.
41. Nakao, S.-i., Determination of pore size and pore size distribution: 3. Filtration membranes. *Journal of Membrane Science* **1994,** *96*, 131-165.
42. Lekang, O. I., Aquaculture Engineering. Blackwell Publishing Ltd., Oxford, UK, **2007**.
43. Lonsdale, H. K.; Merten, U.; Riley, R. L. Journal of Applied Polymer Science **1965**, *9*, 1341–1362.
44. Paul, D. R., Reformulation of the solution-diffusion theory of reverse osmosis. *Journal of Membrane Science* **2004,** *241*, 371-386.
45. Sagle A. C. PEG hydrogels as anti-fouling coatings for reverse osmosis membranes. PhD thesis. Austin,TX: The University of Texas, **2009**.
46. Kucera, J., Reverse Osmosis: Design, Processes, and Applications for Engineers, John Wiley & Sons, **2010**.
47. Malaeb, L.; Ayoub, G. M., Reverse osmosis technology for water treatment: State of the art review. *Desalination* **2011,** *267*, 1-8.
48. Bartels, C.; Franks, R.; Rybar, S.; Schierach, M.; Wilf, M., The effect of feed ionic strength on salt passage through reverse osmosis membranes. *Desalination* **2005,** *184*, 185-195.
49. Peeters, J. M. M.; Boom, J. P.; Mulder, M. H. V.; Strathmann, H., Retention measurements of nanofiltration membranes with electrolyte solutions. *Journal of Membrane Science* **1998,** *145*, 199-209.
50. Yaroshchuk, A. E., Non-steric mechanisms of nanofiltration: superposition of Donnan and dielectric exclusion. *Separation and Purification Technology* **2001,** *22-23*, 143-158.
51. Szymczyk, A.; Fievet, P., Ion transport through nanofiltration membranes: the steric, electric and dielectric exclusion model. *Desalination* **2006,** *200*, 122-124.
52. Nicolaisen, B., Developments in membrane technology for water treatment. *Desalination* **2003,** *153*, 355-360.
53. Wagner, J., Membrane Filtration Handbook, Practical Tips and Hints, 2nd Edition, Osmonics, Inc, NewYork, **2001**.
54. Aptel, P.; Buckley, C. A., Categories of membrane operations in: Water Treatment Processes, Mac Graw Hill, AWWARF, Lyonnaise des Eaux, Water Research Commission of South Africa, **1996**.
55. https://synderfiltration.com/learning-center/articles/module-configurations-process/spiral-wound-membranes/; last checked on 29.07.2020.
56. http://www.pe.tamu.edu/gprinew/home/BrineDesal/MembraneWkshpAug06/Hallsby8-06.pdf; last checked on 29.07.2020.
57. Cath, T. Y.; Childress, A. E.; Elimelech, M., Forward osmosis: Principles, applications, and recent developments. *Journal of Membrane Science* **2006,** *281*, 70-87.
58. Schwinge, J.; Neal, P. R.; Wiley, D. E.; Fletcher, D. F.; Fane, A. G., Spiral wound modules and spacers: Review and analysis. *Journal of Membrane Science* **2004,** *242*, 129-153.

59. Avlonitis, S.; Hanbury, W. T.; Boudinar, M. B., Spiral wound modules performance. An analytical solution, part I. *Desalination* **1991,** *81*, 191-208.
60. Gupta, S. K., Design and analysis of reverse osmosis systems using three parameter models for transport across the membrane. *Desalination* **1992,** *85*, 283-296.
61. Vrouwenvelder, J. S.; Graf von der Schulenburg, D. A.; Kruithof, J. C.; Johns, M. L.; van Loosdrecht, M. C. M., Biofouling of spiral-wound nanofiltration and reverse osmosis membranes: A feed spacer problem. *Water Research* **2009,** *43*, 583-594.
62. Peinemann, K. V.; Nunes, S. P.; Schrotter, J.C., Membranes for water treatment: Current and Emerging Membrane Processes for Water Treatment, Weinheim: Wiley–VCH Verlag GmbH & Co. KGaA; **2010**.
63. Mezher, T.; Fath, H.; Abbas, Z.; Khaled, A., Techno-economic assessment and environmental impacts of desalination technologies. *Desalination* **2011,** *266*, 263-273.
64. Alghoul, M. A.; Poovanaesvaran, P.; Sopian, K.; Sulaiman, M. Y., Review of brackish water reverse osmosis (BWRO) system designs. *Renewable and Sustainable Energy Reviews* **2009,** *13*, 2661-2667.
65. Galiana-Aleixandre, M. V.; Iborra-Clar, A.; Bes-Piá, B.; Mendoza-Roca, J. A.; Cuartas-Uribe, B.; Iborra-Clar, M. I., Nanofiltration for sulfate removal and water reuse of the pickling and tanning processes in a tannery. *Desalination* **2005,** *179*, 307-313.
66. Ranganathan, K.; Kabadgi, S., Studies on Feasibility of Reverse Osmosis (Membrane) Technology for Treatment of Tannery Wastewater. *Journal of Environmental Protection* **2011,** *2*, 37-46.
67. Suksaroj, C.; Héran, M.; Allègre, C.; Persin, F., Treatment of textile plant effluent by nanofiltration and/or reverse osmosis for water reuse. *Desalination* **2005,** *178*, 333-341.
68. Gozálvez-Zafrilla, J. M.; Sanz-Escribano, D.; Lora-García, J.; León Hidalgo, M. C., Nanofiltration of secondary effluent for wastewater reuse in the textile industry. *Desalination* **2008,** *222*, 272-279.
69. Yu, L.; Han, M.; He, F., A review of treating oily wastewater. *Arabian Journal of Chemistry* **2017,** *10*, S1913-S1922.
70. https://www.google.de/url?sa=t&rct=j&q=&esrc=s&source=web&cd=&ved=2ahUKEwiktOGf3_PqAhWP5KQKHfubDW8QFjAAegQIAhAB&url=https%3A%2F%2Flfu.rlp.de%2Ffileadmin%2Flfu%2FDownloads%2FAbfallwirtschaft%2FMerkblattOEl_monitor_12072012.pdf&usg=AOvVaw2-G_bSjQG62aLQwyyoAsO7; last checked on 29.07.2020.
71. Miller, D. J.; Huang, X.; Li, H.; Kasemset, S.; Lee, A.; Agnihotri, D.; Hayes, T.; Paul, D. R.; Freeman, B. D., Fouling-resistant membranes for the treatment of flowback water from hydraulic shale fracturing: A pilot study. *Journal of Membrane Science* **2013,** *437*, 265-275.
72. Mallevialle, J.; Odendaal, P. E.; Wiesner, M. R., Water Treatment Membrane Processes, Mc Graw-Hill, USA, **1996**.
73. Goosen, M. F. A.; Sablani, S. S.; Al-Hinai, H.; Al-Obeidani, S.; Al-Belushi, R.; Jackson, D., Fouling of Reverse Osmosis and Ultrafiltration Membranes: A Critical Review. *Separation Science and Technology* **2005,** *39*, 2261-2297.
74. Bacchin, P.; Si-Hassen, D.; Starov, V.; Clifton, M. J.; Aimar, P., A unifying model for concentration polarization, gel-layer formation and particle deposition in cross-flow membrane filtration of colloidal suspensions. *Chemical Engineering Science* **2002,** *57*, 77-91.
75. Shirazi, S.; Lin, C.-J.; Chen, D., Inorganic fouling of pressure-driven membrane processes — A critical review. *Desalination* **2010,** *250*, 236-248.

76. Asadollahi, M.; Bastani, D.; Musavi, S. A., Enhancement of surface properties and performance of reverse osmosis membranes after surface modification: A review. *Desalination* **2017,** *420*, 330-383.
77. Paul, D.; Abanmy, A. R. M., Membrane fouling - The final frontier. *Ultra Pure Water* **1990,** *7*, 25-36.
78. Strathmann, H.; Keilin, B., Control of concentration polarization in reverse osmosis desalination of water. *Desalination* **1969,** *6*, 179-201.
79. Sherwood, T. K.; Brian, P. L. T.; Fisher, R. E.; Dresner, L., Salt Concentration at Phase Boundaries in Desalination by Reverse Osmosis. *Industrial & Engineering Chemistry Fundamentals* **1965,** *4*, 113-118.
80. Ahmad, A. L.; Lau, K. K.; Abu Bakar, M. Z., Impact of different spacer filament geometries on concentration polarization control in narrow membrane channel. *Journal of Membrane Science* **2005,** *262*, 138-152.
81. Geraldes, V. t.; Semião, V.; de Pinho, M. N., Flow and mass transfer modelling of nanofiltration. *Journal of Membrane Science* **2001,** *191*, 109-128.
82. Sutzkover, I.; Hasson, D.; Semiat, R., Simple technique for measuring the concentration polarization level in a reverse osmosis system. *Desalination* **2000,** *131*, 117-127.
83. Michaels, A.S., New separation technique for the CPI. Chemical Engineering Progress **1968**, *64*, 31-42.
84. Ghosh, A., Ray, H.S., Principles of Extractive Metallurgy, 2nd Edition, Wiley Eastern Ltd., New Delhi, **1991**.
85. Opong, W. S.; Zydney, A. L., Diffusive and convective protein transport through asymmetric membranes. *AIChE Journal* **1991,** *37*, 1497-1510.
86. Schock, G.; Miquel, A., Mass transfer and pressure loss in spiral wound modules. *Desalination* **1987,** *64*, 339-352.
87. Koutsou, C. P.; Karabelas, A. J., Shear stresses and mass transfer at the base of a stirred filtration cell and corresponding conditions in narrow channels with spacers. *Journal of Membrane Science* **2012,** *399-400*, 60-72.
88. Koutsou, C. P.; Yiantsios, S. G.; Karabelas, A. J., A numerical and experimental study of mass transfer in spacer-filled channels: Effects of spacer geometrical characteristics and Schmidt number. *Journal of Membrane Science* **2009,** *326*, 234-251.
89. Colton, C. K.; Smith, K. A., Mass transfer to a rotating fluid. Part II. Transport from the base of an agitated cylindrical tank. *AIChE Journal* **1972,** *18*, 958-967.
90. Siddiqui, A.; Lehmann, S.; Haaksman, V.; Ogier, J.; Schellenberg, C.; van Loosdrecht, M. C. M.; Kruithof, J. C.; Vrouwenvelder, J. S., Porosity of spacer-filled channels in spiral-wound membrane systems: Quantification methods and impact on hydraulic characterization. *Water Research* **2017,** *119*, 304-311.
91. Zhang, R.; Liu, Y.; He, M.; Su, Y.; Zhao, X.; Elimelech, M.; Jiang, Z., Antifouling membranes for sustainable water purification: strategies and mechanisms. *Chemical Society Reviews* **2016,** *45*, 5888-5924.
92. Shi, X.; Field, R.; Hankins, N., Review of fouling by mixed feeds in membrane filtration applied to water purification. *Desalination and Water Treatment* **2011,** *35*, 68-81.
93. Jiang, S.; Li, Y.; Ladewig, B. P., A review of reverse osmosis membrane fouling and control strategies. *Science of The Total Environment* **2017,** *595*, 567-583.
94. Tang, C. Y.; Chong, T. H.; Fane, A. G., Colloidal interactions and fouling of NF and RO membranes: A review. *Advances in Colloid and Interface Science* **2011,** *164*, 126-143.
95. Tijing, L. D.; Woo, Y. C.; Choi, J.-S.; Lee, S.; Kim, S.-H.; Shon, H. K., Fouling and its control in membrane distillation—A review. *Journal of Membrane Science* **2015,** *475*, 215-244.

96. He, M.; Gao, K.; Zhou, L.; Jiao, Z.; Wu, M.; Cao, J.; You, X.; Cai, Z.; Su, Y.; Jiang, Z., Zwitterionic materials for antifouling membrane surface construction. *Acta Biomaterialia* **2016,** *40*, 142-152.
97. Guo, W.; Ngo, H.-H.; Li, J., A mini-review on membrane fouling. *Bioresource Technology* **2012,** *122*, 27-34.
98. Miller, D.; Dreyer, D.; Bielawski, C.; Paul, D.; Freeman, B., Surface Modification of Water Purification Membranes: a Review. *Angewandte Chemie* **2017,** *56*, 46-62.
99. Song, L., Flux decline in crossflow microfiltration and ultrafiltration: mechanisms and modeling of membrane fouling. *Journal of Membrane Science* **1998,** *139*, 183-200.
100. Saqib, J.; Aljundi, I. H., Membrane fouling and modification using surface treatment and layer-by-layer assembly of polyelectrolytes: State-of-the-art review. *Journal of Water Process Engineering* **2016,** *11*, 68-87.
101. Kang, G.-d.; Cao, Y.-m., Development of antifouling reverse osmosis membranes for water treatment: A review. *Water Research* **2012,** *46*, 584-600.
102. Bae, H.; Kim, H.; Jeong, S.; Lee, S., Changes in the relative abundance of biofilm-forming bacteria by conventional sand-filtration and microfiltration as pretreatments for seawater reverse osmosis desalination. *Desalination* **2011,** *273*, 258-266.
103. Yiantsios, S. G.; Karabelas, A. J., The effect of colloid stability on membrane fouling. *Desalination* **1998,** *118*, 143-152.
104. Choudhury, R. R.; Gohil, J. M.; Mohanty, S.; Nayak, S. K., Antifouling, fouling release and antimicrobial materials for surface modification of reverse osmosis and nanofiltration membranes. *Journal of Materials Chemistry A* **2018,** *6*, 313-333.
105. Rudolfs, W.; Balmat, J. L., Colloids in Sewage: I. Separation of Sewage Colloids with the Aid of the Electron Microscope. *Sewage and Industrial Wastes* **1952,** *24*, 247-256.
106. Buffle, J.; Wilkinson, K. J.; Stoll, S.; Filella, M.; Zhang, J., A Generalized Description of Aquatic Colloidal Interactions: The Three-colloidal Component Approach. *Environmental Science & Technology* **1998,** *32*, 2887-2899.
107. Lee, S.; Kim, J.; Lee, C.-H., Analysis of CaSO4 scale formation mechanism in various nanofiltration modules. *Journal of Membrane Science* **1999,** *163*, 63-74.
108. Chen, W.; Su, Y.; Peng, J.; Dong, Y.; Zhao, X.; Jiang, Z., Engineering a Robust, Versatile Amphiphilic Membrane Surface Through Forced Surface Segregation for Ultralow Flux-Decline. *Advanced Functional Materials* **2011**, 191-198.
109. Drewes, J. E.; Fox, P., Fate of natural organic matter (NOM) during groundwater recharge using reclaimed water. *Water Science and Technology* **1999,** *40*, 241-248.
110. Yu, W.; Yang, Y.; Graham, N., Evaluation of ferrate as a coagulant aid/oxidant pretreatment for mitigating submerged ultrafiltration membrane fouling in drinking water treatment. *Chemical Engineering Journal* **2016,** *298*, 234-242.
111. Henthorne, L.; Boysen, B., State-of-the-art of reverse osmosis desalination pretreatment. *Desalination* **2015,** *356*, 129-139.
112. Li, Q.; Elimelech, M., Organic Fouling and Chemical Cleaning of Nanofiltration Membranes: Measurements and Mechanisms. *Environmental Science & Technology* **2004,** *38*, 4683-4693.
113. Ochando-Pulido, J. M.; Victor-Ortega, M. D.; Martínez-Ferez, A., On the cleaning procedure of a hydrophilic reverse osmosis membrane fouled by secondary-treated olive mill wastewater. *Chemical Engineering Journal* **2015,** *260*, 142-151.
114. Chen, J. P.; Kim, S. L.; Ting, Y. P., Optimization of membrane physical and chemical cleaning by a statistically designed approach. *Journal of Membrane Science* **2003,** *219*, 27-45.

115. Ramon, G. Z.; Nguyen, T.-V.; Hoek, E. M. V., Osmosis-assisted cleaning of organic-fouled seawater RO membranes. *Chemical Engineering Journal* **2013,** *218*, 173-182.
116. Goosen, M.; Sablani, S.; Jackson, D., Fouling of Reverse Osmosis and Ultrafiltration Membranes: A Critical Review. *Separation Science and Technology* **2005,** *39*, 2261-2297.
117. Kochkodan, V.; Sharma, V., Graft Polymerization and Plasma Treatment of Polymer Membranes for Fouling Reduction: A Review. *Journal of environmental science and health. Part A, Toxic/hazardous substances & environmental engineering* **2012,** *47*, 1713-27.
118. Cheng, Q.; Zheng, Y.; Yu, S.; Zhu, H.; Peng, X.; Liu, J.; Liu, J.; Liu, M.; Gao, C., Surface modification of a commercial thin-film composite polyamide reverse osmosis membrane through graft polymerization of N-isopropylacrylamide followed by acrylic acid. *Journal of Membrane Science* **2013,** *447*, 236-245.
119. Jee, K. Y.; Shin, D. H.; Lee, Y. T., Surface modification of polyamide RO membrane for improved fouling resistance. *Desalination* **2016,** *394*, 131-137.
120. Gudipati, C. S.; Greenlief, C. M.; Johnson, J. A.; Prayongpan, P.; Wooley, K. L., Hyperbranched fluoropolymer and linear poly(ethylene glycol) based amphiphilic crosslinked networks as efficient antifouling coatings: An insight into the surface compositions, topographies, and morphologies. *Journal of Polymer Science Part A: Polymer Chemistry* **2004,** *42*, 6193-6208.
121. Gudipati, C. S.; Finlay, J. A.; Callow, J. A.; Callow, M. E.; Wooley, K. L., The Antifouling and Fouling-Release Perfomance of Hyperbranched Fluoropolymer (HBFP)−Poly(ethylene glycol) (PEG) Composite Coatings Evaluated by Adsorption of Biomacromolecules and the Green Fouling Alga Ulva. *Langmuir* **2005,** *21*, 3044-3053.
122. Goh, P. S.; Zulhairun, A. K.; Ismail, A. F.; Hilal, N., Contemporary antibiofouling modifications of reverse osmosis desalination membrane: A review. *Desalination* **2019,** *468*, 114072.
123. Ulbricht, M., Advanced functional polymer membranes. *Polymer* **2006,** *47*, 2217-2262.
124. Quilitzsch, M.; Osmond, R.; Krug, M.; Heijnen, M.; Ulbricht, M., Macro-initiator mediated surface selective functionalization of ultrafiltration membranes with anti-fouling hydrogel layers applicable to ready-to-use capillary membrane modules. *Journal of Membrane Science* **2016,** *518*, 328-337.
125. Bernstein, R.; Belfer, S.; Freger, V., Surface Modification of Dense Membranes Using Radical Graft Polymerization Enhanced by Monomer Filtration. *Langmuir* **2010,** *26*, 12358-12365.
126. Zhao, X.; Zhang, R.; Liu, Y.; He, M.; Su, Y.; Gao, C.; Jiang, Z., Antifouling membrane surface construction: Chemistry plays a critical role. *Journal of Membrane Science* **2018,** *551*, 145-171.
127. Kolb, H. C.; Finn, M. G.; Sharpless, K. B. Angewandte Chemie International Edition **2001**, *40*, 2005 – 2021.
128. Cai, T.; Neoh, K. G.; Kang, E. T.; Teo, S. L. M., Surface-Functionalized and Surface-Functionalizable Poly(vinylidene fluoride) Graft Copolymer Membranes via Click Chemistry and Atom Transfer Radical Polymerization. *Langmuir* **2011,** *27*, 2936-2945.
129. Zhang, Y.; Ren, B.; Zhang, D.; Xie, S.; Chang, Y.; Yang, J.; Wu, J.; Xu, L.; Zheng, J., Fundamentals and applications of Zwitterionic antifouling polymers. *Journal of Physics D: Applied Physics* **2019,** *52*.
130. Peppas, N.A., R.M. Ottenbrite, K. Park,T. Okano, Biomedical Applications of Hydrogels Handbook, Springer New York, **2010**.
131. Shibayama M,; Tanaka T., Volume phase transition and related phenomena of polymer gels, Advances in Polymer Science **1993**, *109*, 1–62.

132. https://www.semanticscholar.org/paper/Hydrogel-based-pH-sensors-%3A-Development-and-of-and-Hammarling/3892d6705d76d2fed78320016d21f1d86aae430a; last checked on 29.07.2020.
133. Eshet, I.; Freger, V.; Kasher, R.; Herzberg, M.; Lei, J.; Ulbricht, M., Chemical and Physical Factors in Design of Antibiofouling Polymer Coatings. *Biomacromolecules* **2011,** *12*, 2681-2685.
134. Nair, D. P.; Podgórski, M.; Chatani, S.; Gong, T.; Xi, W.; Fenoli, C. R.; Bowman, C. N., The Thiol-Michael Addition Click Reaction: A Powerful and Widely Used Tool in Materials Chemistry. *Chemistry of Materials* **2014,** *26*, 724-744.
135. Daumann, K.; May, P.; Brückerhoff, J.; Ulbricht, M., Synthesis of well-defined cross-linkable zwitterionic macromolecular building blocks for hydrogels. *Reactive and Functional Polymers* **2018,** *131*, 251-257.
136. M. Hesse, H. Meier, B. Zeeh, Spektroskopische Methoden in der organischen Chemie, 8. Auflage Thieme Verlag, Stuttgart, **2012**.
137. https://www.google.de/url?sa=t&rct=j&q=&esrc=s&source=web&cd=&ved=2ahUKEwjV-c7f5vPqAhXKCewKHTxuAAQQFjAAegQIBRAB&url=http%3A%2F%2Fwww.ecs.umass.edu%2Feve%2Ffacilities%2Fequipment%2FTOC%2FTOCV%2FTOC-V_CP_Users_Manual_E.pdf&usg=AOvVaw0NMpWXMvYIdPLJhUuumC4b; last checked on 29.07.2020.
138. http://www.chemgapedia.de/vsengine/vlu/vsc/de/ch/9/mac/charakterisierung/d3/gpc/gpc.vlu.html; last checked on 29.07.2020.
139. Brandrup J, Immergut EH. Polymer Handbook. 3. New York: Wiley,**1989**.
140. Chu, B.; Wang, Z.; Yu, J., Dynamic light scattering study of internal motions of polymer coils in dilute solution. *Macromolecules* **1991,** *24*, 6832-6838.
141. Mezger, T. G., The Rheology Handbook. Vincentz Network, **2012**.
142. https://cdn.technologynetworks.com/TN/Resources/PDF/WP160620BasicIntroRheology.pdf; last checked on 29.07.2020.
143. Chiou, B.-S.; Khan, S. A., Real-Time FTIR and in Situ Rheological Studies on the UV Curing Kinetics of Thiol-ene Polymers. *Macromolecules* **1997,** *30*, 7322-7328.
144. Akin, O.; Temelli, F., Probing the hydrophobicity of commercial reverse osmosis membranes produced by interfacial polymerization using contact angle, XPS, FTIR, FE-SEM and AFM. *Desalination* **2011,** *278*, 387-396.
145. https://sundoc.bibliothek.uni-halle.de/diss-online/01/02H012/t4.pdf; last checked on 29.07.2020.
146. Probstein, R. F., Physicochemical Hydrodynamics: An Introduction 2nd Edition, John Wiley & Sons, Inc., New York, **1994**.
147. Salgin, S.; Salgin, U.; Soyer, N., Streaming Potential Measurements of Polyethersulfone Ultrafiltration Membranes to Determine Salt Effects on Membrane Zeta Potential. *International journal of electrochemical science* **2013,** *8*, 4073-4084.
148. Xie, H.; Saito, T.; Hickner, M. A., Zeta Potential of Ion-Conductive Membranes by Streaming Current Measurements. *Langmuir* **2011,** *27*, 4721-4727.
149. https://wiki.anton-paar.com/de-de/zetapotenzial/; last checked on 29.07.2020.

150. Wagner, E.; Freeman, B.; Hickner, M.; Altman, S., Polyamide Desalination Membrane Characterization and Surface Modification to Enhance Fouling Resistance. *Sandia National Laboratories, Albuquerque, New Mexico* **2010**.
151. Haugstad G. Atomic force microscopy: understanding basic modes andadvanced applications. New York: John Wiley&Sons; **2012**.
152. Cath, T. Y.; Elimelech, M.; McCutcheon, J. R.; McGinnis, R. L.; Achilli, A.; Anastasio, D.; Brady, A. R.; Childress, A. E.; Farr, I. V.; Hancock, N. T.; Lampi, J.; Nghiem, L. D.; Xie, M.; Yip, N. Y., Standard Methodology for Evaluating Membrane Performance in Osmotically Driven Membrane Processes. *Desalination* **2013,** *312*, 31-38.
153. https://www.sciencedirect.com/topics/engineering/permeate-flow-rate; last checked on 29.07.2020.
154. Hilal, N.; Ismail, A. F.; Wright, C., Membrane Fabrication, CRC Press **2015**.
155. Tang, C. Y.; Kwon, Y.-N.; Leckie, J. O., Probing the nano- and micro-scales of reverse osmosis membranes—A comprehensive characterization of physiochemical properties of uncoated and coated membranes by XPS, TEM, ATR-FTIR, and streaming potential measurements. *Journal of Membrane Science* **2007,** *287*, 146-156.
156. Tang, C. Y.; Kwon, Y.-N.; Leckie, J. O., Effect of membrane chemistry and coating layer on physiochemical properties of thin film composite polyamide RO and NF membranes: II. Membrane physiochemical properties and their dependence on polyamide and coating layers. *Desalination* **2009,** *242*, 168-182.
157. Tang, C. Y.; Kwon, Y.-N.; Leckie, J. O., Effect of membrane chemistry and coating layer on physiochemical properties of thin film composite polyamide RO and NF membranes: I. FTIR and XPS characterization of polyamide and coating layer chemistry. *Desalination* **2009,** *242*, 149-167.
158. Zhang, Y.; Wan, Y.; Pan, G.; Shi, H.; Yan, H.; Xu, J.; Guo, M.; Wang, Z.; Liu, Y., Surface modification of polyamide reverse osmosis membrane with sulfonated polyvinyl alcohol for antifouling. *Applied Surface Science* **2017,** *419*, 177-187.
159. https://www.sterlitech.com/ge-osmonics-flat-sheet-membrane-se-tfc-ro-cf016-5-pk.html; last checked on 29.07.2020.
160. Ismail, A. F.; Rahman, M. A.; Dzarfan-Othman, M. H.; Matsuura, T., Membrane Separation Principles and Applications, Elsevier Science, **2019**.
161. Childress, A. E.; Elimelech, M., Effect of solution chemistry on the surface charge of polymeric reverse osmosis and nanofiltration membranes. *Journal of Membrane Science* **1996,** *119*, 253-268.
162. Tang, C. Y.; Fu, Q. S.; Robertson, A. P.; Criddle, C. S.; Leckie, J. O., Use of Reverse Osmosis Membranes to Remove Perfluorooctane Sulfonate (PFOS) from Semiconductor Wastewater. *Environmental Science & Technology* **2006,** *40*, 7343-7349.
163. Taheri, A. H.; Sim, L. N.; Chong, T. H.; Krantz, W. B.; Fane, A. G., Prediction of reverse osmosis fouling using the feed fouling monitor and salt tracer response technique. *Journal of Membrane Science* **2015,** *475*, 433-444.
164. Taheri, A. H.; Sim, S. T. V.; Sim, L. N.; Chong, T. H.; Krantz, W. B.; Fane, A. G., Development of a new technique to predict reverse osmosis fouling. *Journal of Membrane Science* **2013,** *448*, 12-22.
165. Ho, J. S.; Sim, L. N.; Webster, R. D.; Viswanath, B.; Coster, H. G. L.; Fane, A. G., Monitoring fouling behavior of reverse osmosis membranes using electrical impedance spectroscopy: A field trial study. *Desalination* **2017,** *407*, 75-84.

166. Janghorban Esfahani, I.; Kim, M. J.; Yun, C. H.; Yoo, C. K., Proposed new fouling monitoring indices for seawater reverse osmosis to determine the membrane cleaning interval. *Journal of Membrane Science* **2013,** *442*, 83-96.
167. https://sensorex.com/blog/2017/11/09/electrical-conductivity-of-water/; last checked on 29.07.2020.
168. Boerlage, S. F. E., Scaling and particulate fouling in membrane filtration systems, Dissertation, Delft, **2001**.
169. https://www.dupont.com/content/dam/dupont/amer/us/en/water-solutions/public/documents/en/45-D01504-en.pdf; last checked on 29.07.2020.
170. http://www.purewateroccasional.net/wtisilica.html; last checked on 29.07.2020.
171. Wang, F.; Tarabara, V. V., Pore blocking mechanisms during early stages of membrane fouling by colloids. *Journal of Colloid and Interface Science* **2008,** *328*, 464-469.
172. Rosalam, S., *Membrane Technology for Water and Wastewater Treatment in Rural Regions*. IGI Global: Hershey, PA, USA, **2020**; p 1-354.
173. Abdelrasoul, A.; Doan, H.; Lohi, A.; Cheng, C.-H., Mass Transfer Mechanisms and Transport Resistances in Membrane Separation Process. In *Mass Transfer - Advancement in Process Modelling*, **2015**.
174. https://www.researchgate.net/figure/SEM-of-gypsum-crystals-in-the-presence-of-SDS_fig7_8944592; last checked on 29.07.2020.
175. Schneider, J. Beitrag zur Wirkungsweise von Verzögerern beim Abbinden von Stuckgipsen. PhD thesis, Technische Universität Bergakademie Freiberg, **2010**.
176. Bacchin, P.; Aimar, P.; Field, R. W., Critical and sustainable fluxes: Theory, experiments and applications. *Journal of Membrane Science* **2006,** *281*, 42-69.
177. May, P., Concentration polarization enabled hydrogel coating of desalination membranes using crosslinkable zwitterionic polymeric building blocks, Dissertation, University Duisburg-Essen, **2020**.
178. Daumann, K., Zwitterionische und vernetzbare Copolymer-Bausteine für Antifouling-Beschichtungen, Dissertation, University Duisburg-Essen, **2018**.
179. G. Caneba, Free-Radical Retrograde-Precipitation Polymerization (FRRPP): Novel Concepts, Processes, Materials, and Energy Aspects, Springer Verlag, Berlin Heidelberg, **2010**.
180. R. Kaushal, I. L. Medintz, Methods in Bioengineering: Nanoscale Bioengineering and Nanomedicine, 1st ed., Artech House, New York, **2009**.
181. Martín N, Giacalone F. Fullerene polymers: synthesis, properties and applications, Weinheim: Wiley-VCH, **2009**.
182. G. E. Totten, C. E. Bates and N. A. Clinton, Handbook of Quenchants and Quenching Technology, pp. 239-289. ASM International, Materials Park, OH, **1993**.
183. https://www.researchgate.net/figure/Classification-of-non-Newtonian-fluids_fig10_258387572; last checked on 29.07.2020.
184. D. M. Teegarden, Polymer chemistry: Introduction to an indispensable science, NSTA Press/Virginia, **2004**.
185. Akbari, S.; Mahmood, S.M.; Ghaedi, H.; Al-Hajri, S. A New Empirical Model for Viscosity of Sulfonated Polyacrylamide Polymers. *Polymers* **2019**, *11*, 1046.
186. Yang, H.; Zheng, Q.; Cheng, R., New insight into “polyelectrolyte effect”. *Colloids and Surfaces A: Physicochemical and Engineering Aspects* **2012,** *407*, 1-8.
187. Vrijenhoek, E. M.; Hong, S.; Elimelech, M., Influence of membrane surface properties on initial rate of colloidal fouling of reverse osmosis and nanofiltration membranes. *Journal of Membrane Science* **2001,** *188*, 115-128.

188. Huang, S.; Ras, R. H. A.; Tian, X., Antifouling membranes for oily wastewater treatment: Interplay between wetting and membrane fouling. *Current Opinion in Colloid & Interface Science* **2018,** *36*, 90-109.
189. Bengani, P.; Kou, Y.; Asatekin, A., Zwitterionic copolymer self-assembly for fouling resistant, high flux membranes with size-based small molecule selectivity. *Journal of Membrane Science* **2015,** *493*, 755-765.
190. Wu, J.; Lin, W.; Wang, Z.; Chen, S.; Chang, Y., Investigation of the Hydration of Nonfouling Material Poly(sulfobetaine methacrylate) by Low-Field Nuclear Magnetic Resonance. *Langmuir* **2012,** *28*, 7436-7441.
191. Terpilowski, K.; Hołysz, L.; Rymuszka, D.; Banach, R., Comparison of contact angle measurement methods of liquids on metal alloys. *Annales UMCS, Chemia* **2016,** *71*, 89.
192. https://www.nanoscience.com/techniques/tensiometry/advancing-and-receding-contact-angles/#what; last checked on 29.07.2020.
193. Li, Q.; Pan, X.; Hou, C.; Jin, Y.; Dai, H.; Wang, H.; Zhao, X.; Liu, X., Exploring the dependence of bulk properties on surface chemistries and microstructures of commercially composite RO membranes by novel characterization approaches. *Desalination* **2012,** *292*, 9-18.
194. Koutsou, C.; Karabelas, A.; Kostoglou, M., Fluid Dynamics and Mass Transfer in Spacer-Filled Membrane Channels: Effect of Uniform Channel-Gap Reduction Due to Fouling. *Fluids* **2018,** *3*.
195. Haidari, A. H.; Heijman, S. G. J.; van der Meer, W. G. J., Optimal design of spacers in reverse osmosis. *Separation and Purification Technology* **2018,** *192*, 441-456.
196. Koutsou, C. P.; Yiantsios, S. G.; Karabelas, A. J., Numerical simulation of the flow in a plane-channel containing a periodic array of cylindrical turbulence promoters. *Journal of Membrane Science* **2004,** *231*, 81-90.
197. Pellerin, E.; Michelitsch, E.; Darcovich, K.; Lin, S.; Tam, C. M., Turbulent transport in membrane modules by CFD simulation in two dimensions. *Journal of Membrane Science* **1995,** *100*, 139-153.
198. Avlonitis, S.; Hanbury, W. T.; Boudinar, M. B., Spiral wound modules performance an analytical solution: Part II. *Desalination* **1993,** *89*, 227-246.
199. Ranade, V. V.; Kumar, A., Fluid dynamics of spacer filled rectangular and curvilinear channels. *Journal of Membrane Science* **2006,** *271*, 1-15.
200. Feron, P.; Solt, G. S., The influence of separators on hydrodynamics and mass transfer in narrow cells: Flow visualisation. *Desalination* **1991,** *84*, 137-152.
201. Le, N. L.; Ulbricht, M.; Nunes, S. P., How Do Polyethylene Glycol and Poly(sulfobetaine) Hydrogel Layers on Ultrafiltration Membranes Minimize Fouling and Stay Stable in Cleaning Chemicals? *Industrial & Engineering Chemistry Research* **2017,** *56*, 6785-6795.
202. Schönemann, E.; Laschewsky, A.; Rosenhahn, A., Exploring the Long-Term Hydrolytic Behavior of Zwitterionic Polymethacrylates and Polymethacrylamides. *Polymers* **2018,** *10*, 639.
203. Yang, Z.; Guo, H.; Tang, C. Y., The upper bound of thin-film composite (TFC) polyamide membranes for desalination. *Journal of Membrane Science* **2019,** *590*, 117297.
204. Lee, J.; Woo, Y. C.; Kim, H.-S., Effect of driving pressure and recovery rate on the performance of nanofiltration and reverse osmosis membranes for the treatment of the effluent from MBR. *Desalination and water treatment* **2015,** *54*, 3589-3595.
205. Peña, N.; Gallego, S.; del Vigo, F.; Chesters, S. P., Evaluating impact of fouling on reverse osmosis membranes performance. *Desalination and Water Treatment* **2013,** *51*, 958-968.

8 Appendix

8.1 Additional figures and tables

Surface characterization of commercial RO membranes via ATR-FTIR spectroscopy

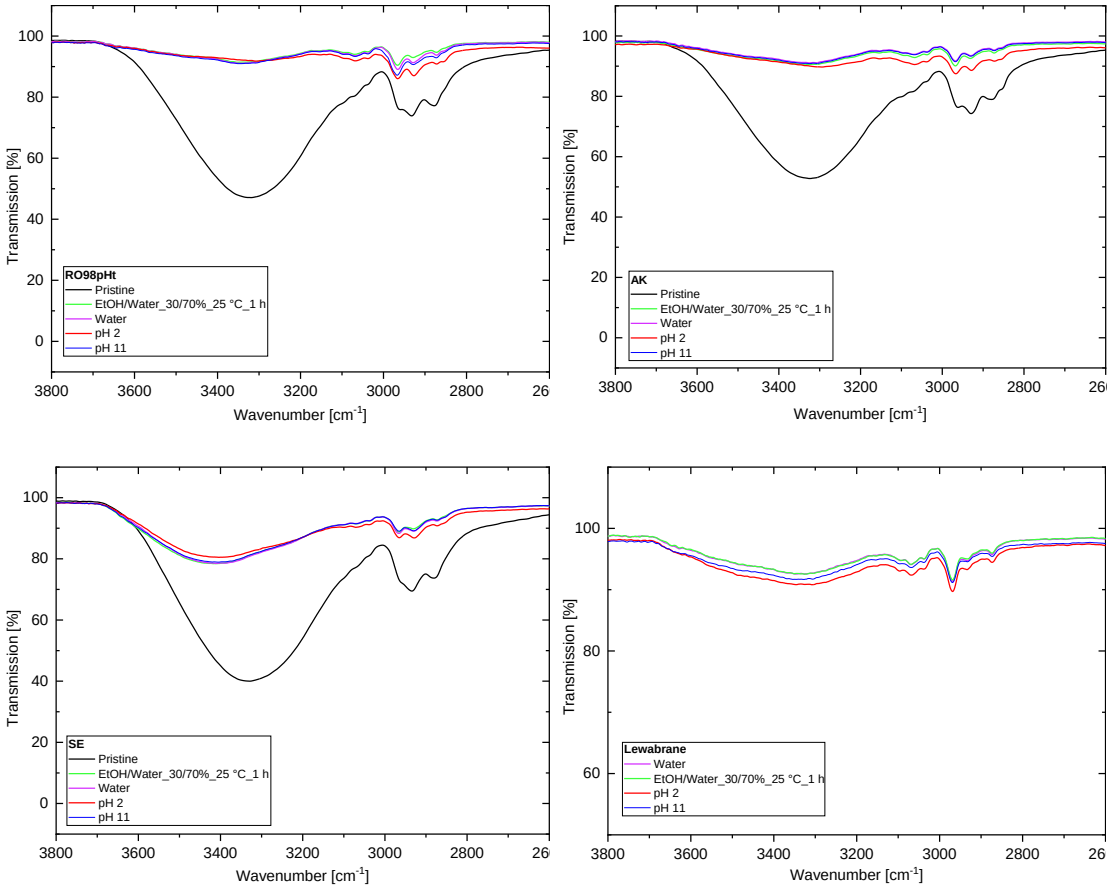

Figure 125: IR spectra of pristine and washed membranes using different washing solutions. **(a)** RO98pHt, **(b)** AK, **(c)** SE and **(d)** Lewabrane (since Lewabrane was supplied in water, no distinct OH group can be observed).

Determination of OLC from rheological measurements

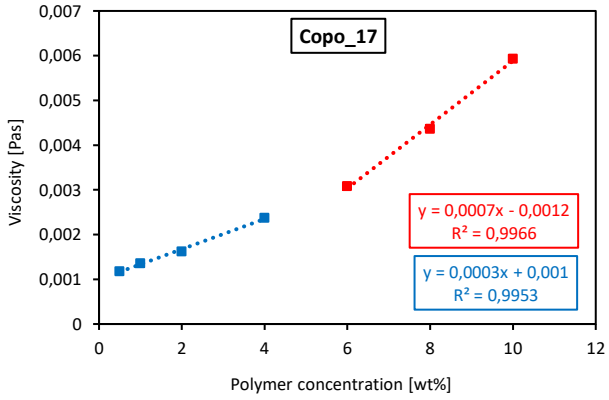

Figure 126: Viscosity vs. polymer concentration for Copo_17 for determination of OLC.

Characterization of cationic surface linker via ATR-FTIR spectroscopy and zeta potential measurement

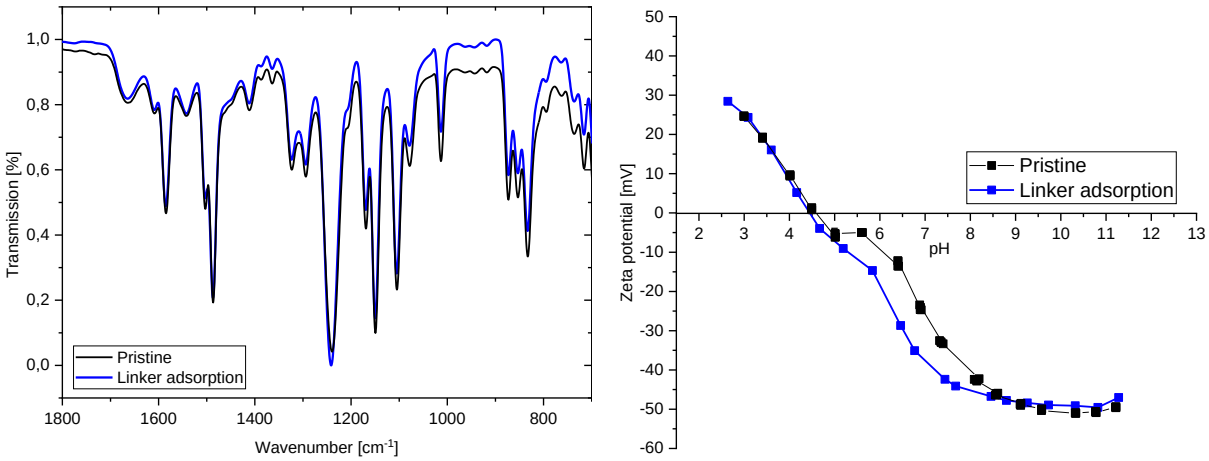

Figure 127: (a) IR spectra and **(b)** zeta potential of BW30 membrane adsorbed with the cationic surface linker.

Characterization of the element TW30 2521 after destructive opening via SEM

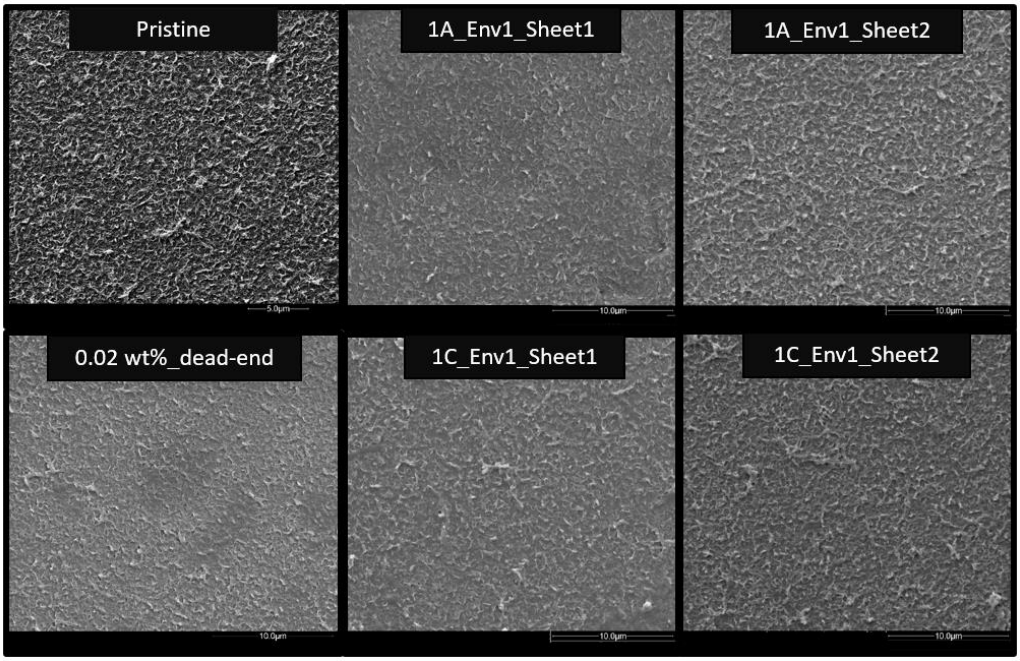

Figure 128: SEM images of the module TW30 2521 after destructive opening depending on the position along the width of the module (inner side = position 1).

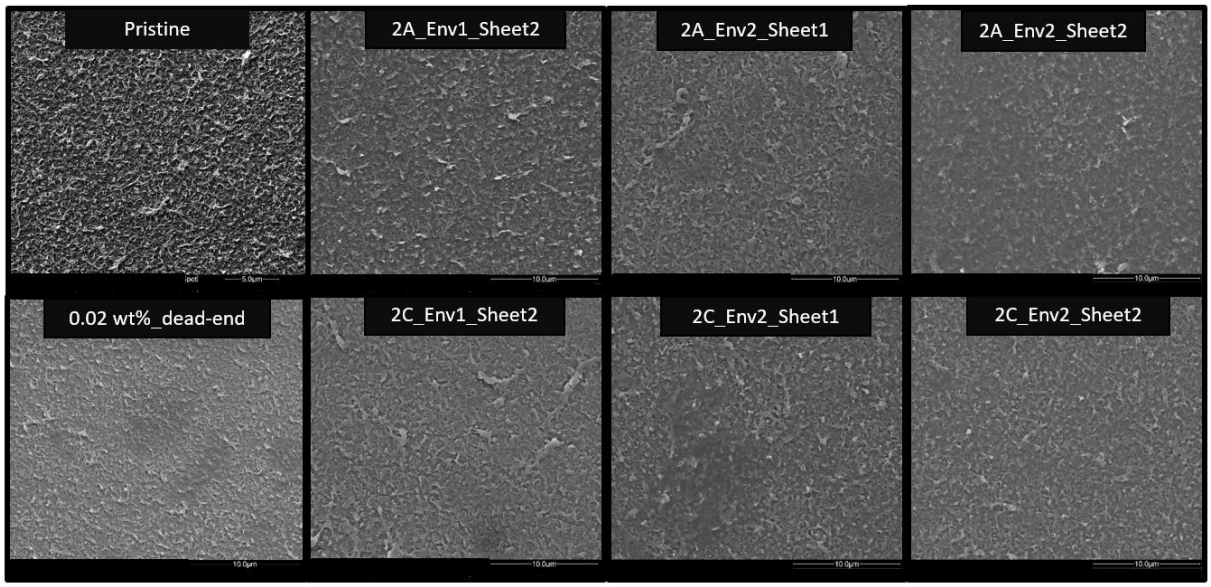

Figure 129: SEM images of the module TW30 2521 after destructive opening depending on the position along the width of the module (centre = position 2).

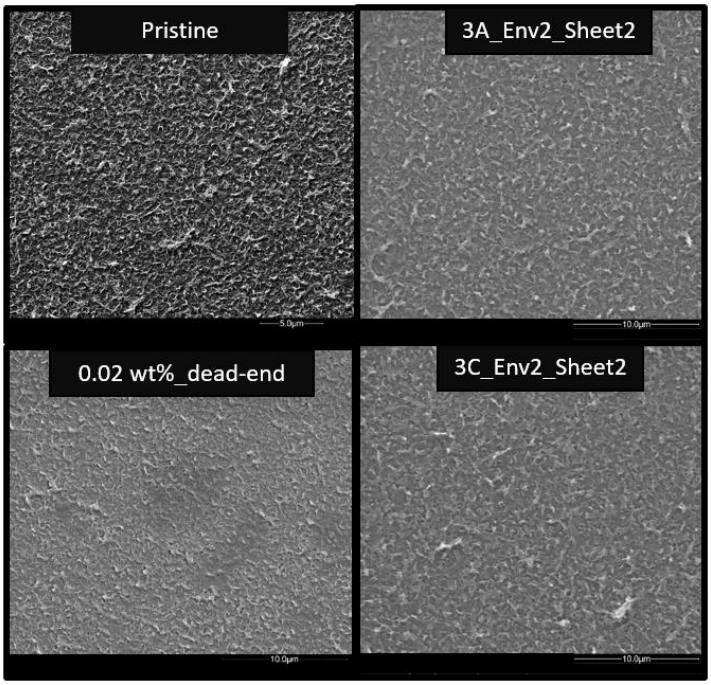

Figure 130: SEM images of the module TW30 2521 after destructive opening depending on the position along the width of the module (outer side = position 3).

Characterization of the elements BW30 4040 after field tests and autopsy – Methylene blue test of membrane leaves

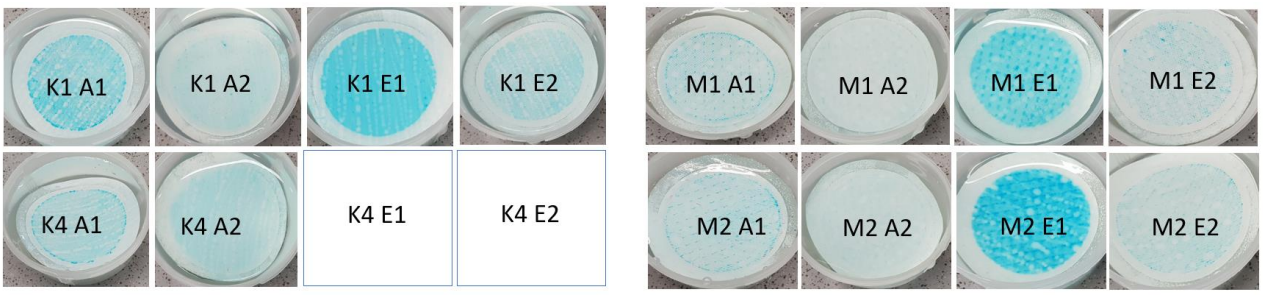

Figure 131: Autopsy of modules BW30 4040 after field tests: In addition to the comparison of the modules (conventional (K) vs. modified (M)), the results from the feed side were compared with those from the opposite side (A1 vs. E1). Two positions per side were also examined (A1 vs. A2 and E1 vs. E2). In total, 4 positions per module were analyzed. MBT of RO conv (left) and RO mod (right) after autopsy for all four positions each module.

8.2 Publications

In the context of this thesis the following student qualification thesis were written:

Rabia Mutlu & Seden Caglar „Untersuchung des Foulingverhaltens der verschiedenen Kühlwässer auf Umkehrosmosemembranen mittels Photometrie und Massenspektrometrie“, Analytikarbeit, **2018.**

Didem Denizer „Rheologische Untersuchung der Gelierungsreaktion von vernetzbaren zwitterionischen Makromolekülen“, Analytikarbeit, **2019.**

Nikolai Adler, „Untersuchung des Foulingverhaltens von modifizierten RO-Membranen mittels Photometrie und Gaschromatographie“, Analytikarbeit, **2019.**

Nikolai Adler „Untersuchung der Stabilität von hydrogelbeschichteten RO-Membranen und deren Antifouling-Eigenschaften hinsichtlich ölhaltigem Wasser“, Vertiefungsarbeit, **2019.**

Ingo Schwarzrock „Herstellung einer Antifouling-Beschichtung für Umkehrosmose-membranen durch konzentrationspolarisationsinduzierte Click Reaktion zu einem Hydrogel“, Masterarbeit, **2019.**

Oral and Poster Presentations on international conferences

November 2018, Aachen	S. Laghmari, M. Ulbricht Oral presentation of Ph.D. results, 17th Aachener Membran Kolloquium (AMK)
May 2018, Prague	S. Laghmari, M. Ulbricht Oral presentation of Ph.D. results, Membrane and Electromembrane Processes (MELPRO)

April 2018, Warsaw	S. Laghmari, M. Ulbricht Poster presentation of Ph.D. results, 7th, European Young Engineers Conference (EYEC)
February 2018, Munich	S. Laghmari, M. Ulbricht Poster presentation of Ph.D. results, ProcessNet: Fluidverfahrenstechnik, Membrantechnik und Mischvorgänge
June 2017, Lund	S. Laghmari, M. Ulbricht Poster presentation of Ph.D. results, 34th EMS Summer School on Membranes in Biorefineries

BMBF events

December 2016, Frankfurt a.M.	WavE Kick-off meeting
April 2018, Frankfurt a.M.	WavE Status seminar
December 2019, Berlin	WavE Closing event

Awards

Best poster award of “ProcessNet Fluidverfahrenstechnik, Membrantechnik und Mischvorgänge, 2018 Munich.

8.3 Curriculum Vitae

For data protection reasons, the curriculum vitae is not included in the online version.